Post-transcriptional and Post-translational Mechanisms of Autophagy Regulation

by

Vikramjit Lahiri

A dissertation submitted in partial fulfillment
of the requirements for the degree of
Doctor of Philosophy
(Molecular, Cellular and Developmental Biology)
in the University of Michigan
2022

Doctoral Committee:

Professor Daniel J. Klionsky, Chair
Associate Professor Laura Buttitta
Professor Lois S. Weisman
Professor Haoxing Xu

Vikramjit Lahiri

vlahiri@umich.edu

ORCID iD: 0000-0002-7066-094X

© Vikramjit Lahiri 2022

Dedication

This thesis is dedicated to my parents and brother whose sacrifices made this possible

Acknowledgements

I would like to acknowledge my advisor Professor Daniel J. Klionsky for his guidance throughout the last five years. Ours has been more than a student-advisor relation – he has been my mentor, my advocate and most importantly a guide whose philosophy inspired me and whose ideals I share. I would also like to acknowledge the Klionsky laboratory and all of the many members that have been a part of it during my tenure in the lab. I would especially like to thank Zhiyuan Yao for introducing me to the lab, Damian Gatica Mizala for being a very helpful lab senior, and Zhangyuan Yin for asking the hardest questions. I would also like to thank Shree Padma Metur and Wayne Hawkins for being wonderful junior colleagues. I would like to thank Hana Popelka and Aileen Ariosa for their wisdom with proteins. Finally, I would like to thank Megan Moore for making my final semester at U of M and the Klionsky lab so fulfilling.

I would like to thank my thesis committee members – Professors Haoxing Xu, Lois Weisman and Laura Buttitta. Professor Xu has always been very encouraging of my endeavors and efforts – both for my research and for my participation in the journal club courses that he led. Professor Weisman was one of the first professors I interacted with during my doctoral studies at the U of M and her insightful reasoning and astute attention to scientific detail has greatly influenced how I have conducted scientific research. Professor Buttitta is perhaps the person I have known the longest in Michigan and she has been a mentor since my undergraduate years. Her quiet determination and fierce scientific intellect continue to inspire me.

I would like to acknowledge all the professors/lecturers/graduate student instructors at U of M who have shared their knowledge with me. It has been a pleasure learning from them. In particular, I would like to thank Professor Kenneth Cadigan, who I rotated with and whose scientific acumen and insight provided for excellent instruction as I embarked on my graduate studies. I would also like to acknowledge my students during my two semesters as a graduate student instructor. Teaching them was a wonderfully fulfilling experience that helped me learn and grow immensely as a person.

No amount of gratitude would be enough for the administrative staff at LSI who supported me during my doctoral studies. I could not have done it without all their support and would particularly like to thank Natalie Bartolacci, Alyson Carter and Anna Schork for keeping my best interests in their hearts. Similarly, I owe my thanks to MCDB administrators Mary Carr, Diane Durfy and Stella Bublitz for keeping me up to date with my departmental duties. I would also like to thank Chair of Graduate Studies Lyle Simmons and former Chair John Schiefelbein for their guidance.

I would not have survived this foreign land of long, harsh winters had it not been for my chosen Ann Arbor family who number too many to name. However, I would be doing injustice if I did not mention Partha Dutta, Sai Srinivas, Rishav Mitra, Bidisha Paul, Subhechha Roy, Aneesh Lahiri, Varsha Venkatarangan, Janakraj Bhattarai, Bineet Kumar Dash, Abhraneel Sarma and Noah Meurs – who have been the best friends anyone could ever ask for.

Finally, my family – my brother Sheeladitya Lahiri, sister Aritri Lahiri, and my parents Geeti Lahiri and Sumanta Lahiri, my grandmother Mamata Bhattacharya and my late grandparents Deepali Lahiri, Pratip Kumar Lahiri, Kiran Prakash Bhattacharya – this PhD is as much yours as it is mine.

Table of Contents

List of Tables

List of Figures

Abstract

Macroautophagy (hereafter, autophagy) is a conserved catabolic process of cellular recycling essential for maintaining metabolic homeostasis. Autophagy allows for the selective or non-selective sequestration of cytoplasmic components in phagophores that mature to form double-membrane autophagosomes. This is followed by the delivery of the cargo-containing autophagosome to the degradative organelle for cargo breakdown. Selective autophagy plays a crucial role in removing damaged/superfluous cellular components. Non-selective autophagy targets random segments of the cytoplasm to the degradative organelle primarily in response to nutrient deficiency. During acute starvation, cells lack a supply of building blocks for synthesizing essential macromolecules. To prevent a collapse of cellular function, autophagy is upregulated in response to starvation via metabolic signals that integrate nutritional cues. This allows for the degradation of pre-existing macromolecules such as proteins, from the cytoplasmic portions delivered by autophagy, and the subsequent release of simple metabolites such as amino acids as breakdown products. These are then transported out of the organelle and into the cytoplasm by dedicated transporter proteins, allowing for new macromolecular synthesis. This makes autophagy a critical pathway in helping cells combat starvation. These roles of autophagy, its interaction with metabolism, where both influence each other, and the regulatory processes involved have been discussed in Chapter 1. A detailed description of the mechanisms of selective autophagy has been discussed in Chapter 4.

The autophagy pathway involves multiple steps that are completed by the concerted action of numerous proteins. Therefore, simpler systems such as the baker's yeast

Saccharomyces cerevisiae are critical to understanding this pathway, especially because most components and mechanism of the machinery are conserved. Even in yeast, over 40 proteins are involved in autophagy highlighting the complexity of the pathway. Additionally, the function of these proteins must be exquisitely regulated to ensure timely autophagy induction and execution while preventing excess self-degradation which could be lethal. In Chapters 2 and 3 I discuss two regulatory mechanisms in yeast.

In Chapter 2, I discuss how autophagy is regulated in yeast in response to two distinct nutritional challenges: nitrogen starvation and amino acid starvation. I find that autophagy is more highly upregulated during nitrogen starvation relative to amino acid starvation and that this regulation occurs at the post-transcriptional level. I focus on the protein kinase – Atg1 – involved in autophagy induction and find that nitrogen starvation differentially promotes Atg1 expression whereas *ATG1* transcription remains comparable between the two conditions. I then explore the mechanism of post-transcriptional upregulation of Atg1 during nitrogen starvation and find that the kinase Rad53 and the RNA-binding protein Ded1 are responsible for promoting facile Atg1 production during nitrogen starvation. Finally, I show that ULK1, a mammalian homolog of Atg1, is similarly post-transcriptionally regulated by DDX3, the mammalian homolog of Ded1 – highlighting the conservation of this mechanism.

A second component of the autophagy pathway – the lipid kinase Vps34 – is my focus for Chapter 3. I show that while Vps34 activity is essential for autophagy, hyperactivation of Vps34 reduces autophagy flux. I confirm that this effect is not due to transcriptional regulation because *ATG* gene expression is not affected by Vps34 hyperactivation. Indeed, I find that Vps34 blocks the fusion of the autophagosome with the vacuole.

In summary, this thesis portrays mechanisms of autophagy regulation in yeast and provides clues regarding how differential regulation occurs during distinct nutritional challenges.

Chapter 1 : An Introduction to Autophagy and Metabolism

(This chapter has been adapted from *Lahiri et al., Cell Metabolism, 2019)*

Autophagy is an evolutionarily conserved lysosome- or vacuole-dependent catabolic pathway in eukaryotes. Autophagy functions basally for cellular quality control and is induced to act as an alternative source of basic metabolites during nutrient deprivation. These functions of autophagy are intimately connected to the regulation of metabolism, and the metabolic status of the cell in turn controls the nature and extent of autophagic induction. In this chapter, I highlight the co-regulation of autophagy and metabolism with a special focus on selective autophagy that, along with bulk autophagy, plays a central role in regulating and rewiring metabolic circuits. I outline the metabolic signals that activate these pathways, the mechanisms involved, and the downstream effects and implications while recognizing yet unanswered questions. I also discuss the role of autophagy in the development and maintenance of adipose tissue, an emerging player in systemic metabolic homeostasis, and describe what is currently known about the complex relationship between autophagy and cancer.

1.1 Overview of the role of autophagy in cellular homeostasis

Autophagy is a highly conserved eukaryotic pathway for maintaining cellular homeostasis through the degradation of superfluous and/or damaged intracellular materials. Autophagy can be either selective or non-selective. Non-selective autophagy describes the random engulfment and subsequent degradation of cytoplasmic material such as proteins and/or organelles (Dikic and Elazar, 2018). This process occurs continuously at a low, basal level facilitating the turnover and recycling of cytoplasmic contents but is also upregulated under

conditions of nutrient deprivation. During starvation, degradation by non-selective autophagy provides simple macromolecules that can be utilized for essential anabolic synthesis. In addition, several forms of selective macroautophagy are now recognized, revealing a dynamic role of autophagy in cellular metabolism (Mizushima and Komatsu, 2011). Discriminant selection of autophagic cargo allows for the removal of dysfunctional/superfluous organelles as well as the generation of specific nutrients in response to environmental changes, thereby promoting cell survival and organismal health. Among other roles, selective autophagy allows the cell to adapt to lipid imbalance, glucose scarcity, amino acid deprivation, and iron shortage, and also facilitates cellular remodeling to accommodate major shifts in metabolism (Gatica et al., 2018).

Due to its diverse roles in maintaining metabolic homeostasis, autophagy plays a major role in general metabolic health and organismal development; autophagic imbalance has been linked to several mammalian pathologies including diabetes (Marasco and Linnemann, 2018), neurodegeneration (Frake et al., 2015) and cancer (Galluzzi et al., 2015). Autophagy-deficient mouse embryos die within a day of birth (Kuma et al., 2004), and adult mice induced to be autophagy-deficient die within 24 h of starvation due to hypoglycemia. Even when grown with sufficient food, these autophagy-deficient adults die in less than three months due to increased susceptibility to infection and neurodegeneration (Karsli-Uzunbas et al., 2014). Autophagy in mouse hypothalamic neurons regulates food intake and organismal energetics (Kaushik et al., 2011). Autophagy may also regulate circadian metabolic cycles by degrading core circadian proteins such as CRY1 (Toledo et al., 2018). A recent study in mice revealed the potential benefits of basal autophagy upregulation. Upregulated autophagy increases median lifespan by 12% and decreases susceptibility to age-related diseases such as cancer (Fernandez et al., 2018). These studies highlight a central role for autophagy in metabolic maintenance. This review will

describe the various autophagic mechanisms that cells employ to combat metabolic perturbations and will touch on how these responses are important for systemic metabolism in health and disease.

1.2 Mechanisms of autophagy

The general mechanism of autophagy can be summarized as cargo deposition in the lysosome/vacuole, followed by cargo degradation by hydrolytic enzymes, and efflux of the resulting breakdown products into the cytosol. However, autophagy may be classified based on the mechanism of cargo entry:

1.2.1 Macroautophagy

Macroautophagy (hereafter referred to as autophagy) begins with the initiation of the double-membrane phagophore by the ULK complex. The ULK complex is comprised of ULK1 (Atg1 in yeast) or ULK2, and several interacting proteins: ATG13, RB1CC1 and ATG101. ULK1 phosphorylates several components of the PIK3C3/VPS34 kinase complex that contains, in addition to PIK3C3/VPS34, PIK3R4/VPS15, BECN1, NRBF2 and other regulatory proteins such as ATG14, AMBRA1, SH3GLB1, RUBCN or UVRAG (Kihara et al., 2001; Itakura et al., 2008; Youle and van der Bliek, 2012). Phosphorylation of ATG14, BECN1, and/or AMBRA1 by ULK1 promotes PIK3C3/VPS34 activation and, in some cases, recruitment to the endoplasmic reticulum (ER) (Di Bartolomeo et al., 2010; Russell et al., 2013; Park et al., 2016a; Park et al., 2018). In mammals, activated PIK3C3/VPS34 produces local pools of phosphatidylinositol-3-phosphate (PtdIns3P) that define the region of phagophore initiation. One model suggests that PtdIns3P at the ER promotes the formation of omegasomes that act as sites of phagophore initiation (Ktistakis and Tooze, 2016). Subsequently, and possibly after detachment of the

omegasome from the ER, membrane recruited from diverse sources including the ER, Golgi apparatus, plasma membrane and recycling endosomes (Axe et al., 2008; Knaevelsrud et al., 2013) feeds the expanding phagophore by a still poorly understood mechanism involving ATG9-containing vesicles. In contrast, a recent model proposes that phagophores evolve from RAB11A-enriched recycling endosomes. According to this model, RAB11A, along with PtdIns3P, plays a determining role in the recruitment of the early autophagy machinery. This suggests that recycling endosomes are primary platforms from which phagophores originate while the ER may contribute secondarily (Puri et al., 2018). A contribution of RAB11A-containing recycling endosomes to autophagosome formation in response to viral infection has also been identified (Kuroki et al., 2018). In yeast, phagophore initiation occurs at the cytoplasmic phagophore assembly site (PAS). Here it is thought that tethering of Atg9-containing vesicles by the Atg1 kinase complex drives phagophore formation (Orsi et al., 2012).

Two essential ubiquitin-like conjugation systems drive autophagy. This machinery functions to covalently conjugate Atg8 (in yeast) and Atg8-family proteins (in mammals) to the phagophore membrane. The ubiquitin-like ATG12 protein is conjugated to ATG5 via the E1-like enzyme ATG7 and the E2-like enzyme ATG10. After processing by the protease, ATG4, Atg8-family proteins undergo conjugation to phosphatidylethanolamine (PE). This process, known as Atg8 lipidation, is mediated by the E1-like ATG7 and E2-like ATG3 enzymes, and the role of an E3-like ligase is filled by a complex between ATG12–ATG5 and ATG16L1 (Feng et al., 2014) (Figure 1). Mammalian Atg8-family proteins are split into two subfamilies: the MAP1LC3/LC3 family and the GABARAP family (Yu et al., 2018). Lipidation of Atg8/Atg8-family proteins allow for attachment to the phagophore where they recruit proteins containing an LC3-interacting region (LIR). Some LIR-containing proteins facilitate phagophore expansion and

closure while others act as receptors, conveying cargo specificity to the growing phagophore. Several autophagy proteins are recruited to the expanding phagophore through PtdIns3P-interacting motifs such as FYVE and PX domains. One such protein is WIPI2 that binds ATG16L1, recruiting the ATG12–ATG5-ATG16L1 complex to the phagophore (Dooley et al., 2014). Phagophore expansion concludes in closure around the cargo at which point the vesicle is called an autophagosome. The autophagy protein machinery bound to the exterior membrane of the autophagosome dissociates prior to fusion with the lysosome. While the outer membrane of the autophagosome fuses with the lysosomal/vacuolar membrane, the inner membrane and enclosed contents are degraded by resident hydrolases to generate simple biomolecules such as glucose and amino acids that are released into the cytosol via lysosomal/vacuolar membrane transporters (Figure 1).

Several proteins involved in autophagy possess non-autophagy related functions as well (Cadwell and Debnath, 2018; Subramani and Malhotra, 2013). This includes the Atg8-family protein LC3, which modulates immune responses and inflammation by a process known as LC3-associated phagocytosis (Cunha et al., 2018; Martinez et al., 2015). ATG5, another essential autophagy protein promotes exosome formation by regulating the acidification of multivesicular bodies (MVBs) by uncoupling the V1V0-ATPase (Guo et al., 2017). However, direct metabolic roles for these functions have not been established yet and they will not be discussed further in this text.

Figure 1: The molecular machinery of macroautophagy

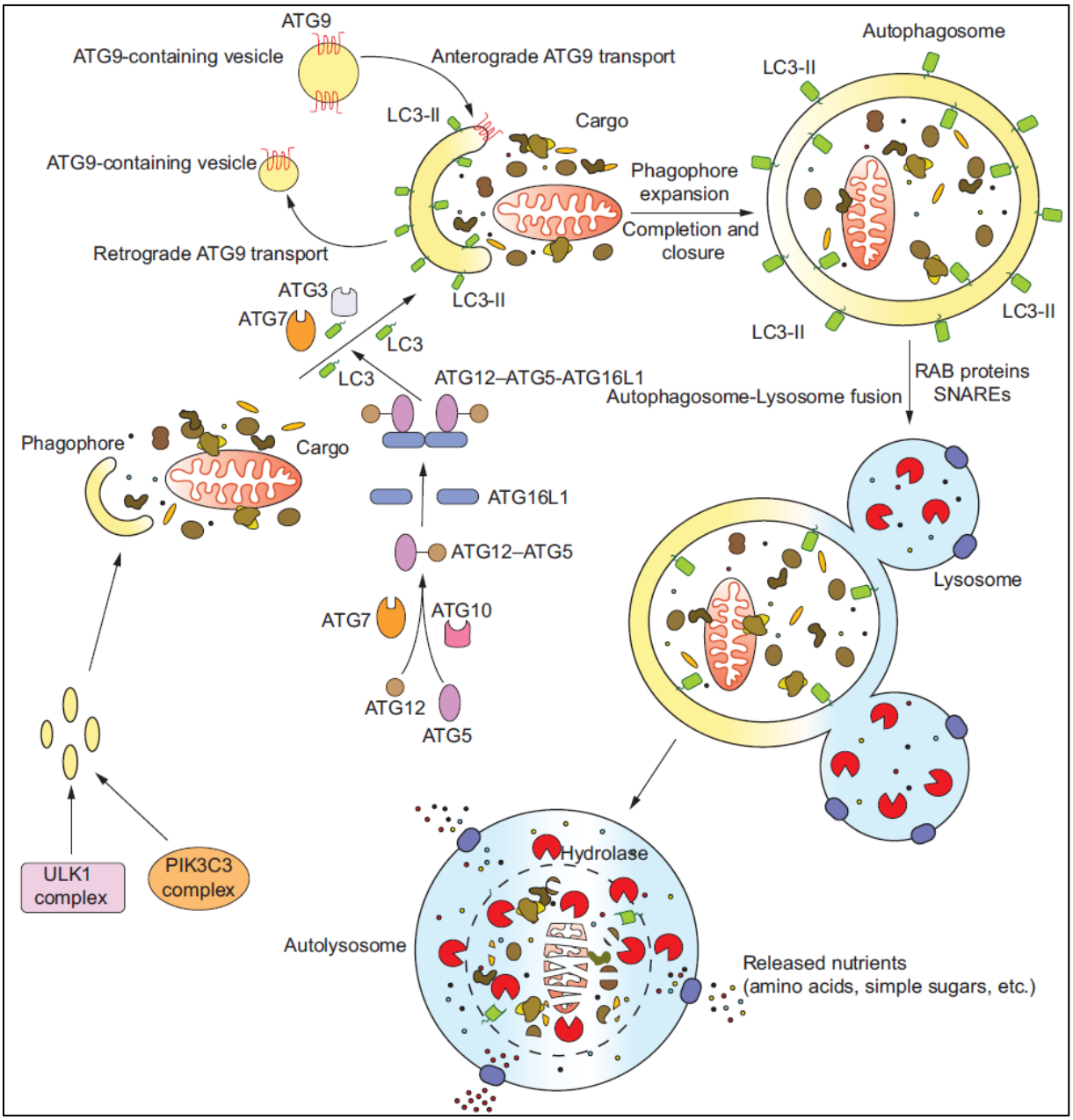

Figure 1. The molecular machinery of macroautophagy. The hallmark of macroautophagy is the double membrane autophagosome that forms by the de novo assembly of membrane from various sources. The process begins with the formation of the phagophore, a process initiated by the ULK1 and PIK3C3/VPS34 complexes. Expansion of the phagophore occurs via the continued recruitment of membrane vesicles by ATG9 as well as the conjugation of LC3 to the phagophore membrane (to form LC3-II). LC3 conjugation involves a two-step ubiquitin-like conjugation pathway involving ATG7, ATG10, ATG3, ATG12, ATG5 and ATG16L1 (refer to text for details). The phagophore expands around the cargo, finally closing to form a cargo-containing autophagosome. The autophagosome subsequently fuses with lysosome(s) by the concerted action of RAB and SNARE proteins to form the autolysosome. Lysosomal hydrolases degrade the inner autophagosomal membrane and the enclosed cargo. The breakdown products, simple macromolecules such as amino acids, are subsequently transported out in the cytoplasm by lysosomal transporters for reuse.

1.2.2 Microautophagy

Microautophagy describes the process in which autophagic cargo in the cytoplasm enters the lysosome (or endosome)/vacuole following a protrusion or invagination and inward pinching of the lysosomal (or endosomal)/vacuolar membrane. This results in the formation of a lumenal vesicle surrounding the cargo that is degraded along with its contents (Li et al., 2012). Microautophagy can be non-selective, incorporating cytoplasm randomly, or highly specific as is the case in micropexophagy, the selective degradation of peroxisomes by their direct sequestration into the lysosome (Oku and Sakai, 2016) (Figure 2A).

1.2.3 Chaperone-mediated autophagy

Chaperone-mediated autophagy (CMA) describes the HSPA8/Hsc70-dependent selective degradation of substrate proteins with an exposed KFERQ-like motif. Post-translational modifications (PTMs) allow for a great deal of diversification and regulation of the KFERQ-binding motif. For instance, a phosphorylated serine, threonine, or tyrosine can serve the role of a negatively charged amino acid in the binding motif (Kaushik and Cuervo, 2016). Similarly, acetylated lysine was recently shown to complete the CMA binding motif by acting as a pseudo-glutamine (Bonhoure et al., 2017). Additionally, PTMs at sites beyond the KFERQ motif can regulate recognition by determining whether the KFERQ motif is exposed. The dependence of some CMA motifs on PTM for completion allows the subset of CMA substrate proteins to change drastically in response to cellular conditions. Binding of the HSPA8 chaperone and associated co-chaperones to a substrate protein is followed by its lysosome targeting. Here, docking of the HSPA8-substrate complex to the lysosomal membrane is mediated by interaction with the cytoplasmic tail of the lysosomal transmembrane protein LAMP2A. At the time of HSPA8-substrate binding, LAMP2A is either monomeric or homodimeric, but soon after

binding, HSPA8 dissociates and LAMP2A multimerizes to form a mature translocation complex. HSP90 (heat shock protein 90) stabilizes LAMP2A from within the lysosomal lumen, and interactions between GFAP (glial fibrillary acidic protein) and EEF1A/EF1α (eukaryotic translation elongation factor 1 alpha 1) regulate the rate of translocation complex assembly and disassembly (Bandyopadhyay et al., 2008; Bandyopadhyay et al., 2010). The substrate protein is unfolded and translocated into the lysosomal lumen via the multimeric LAMP2A complex where it is rapidly degraded by proteases (Figure 2B).

Approximately 40% of proteins in the mammalian proteome contain a canonical KFERQ-like motif and several more contain PTM-inducible motifs (Kaushik and Cuervo, 2018), indicating that CMA may be a major intracellular protein degradation pathway. Indeed, this is validated by studies showing that the selective blockage of CMA leads to the upregulation of other degradative pathways such as macroautophagy as well as increased proteasomal activity (Massey et al., 2006; Schneider et al., 2015). Conversely, cells upregulate CMA when macroautophagy is selectively inhibited, highlighting that there is crosstalk between these pathways (Kaushik et al., 2008).

Figure 2: Other mechanisms of self-eating: Chaperone-mediated autophagy (CMA) and microautophagy

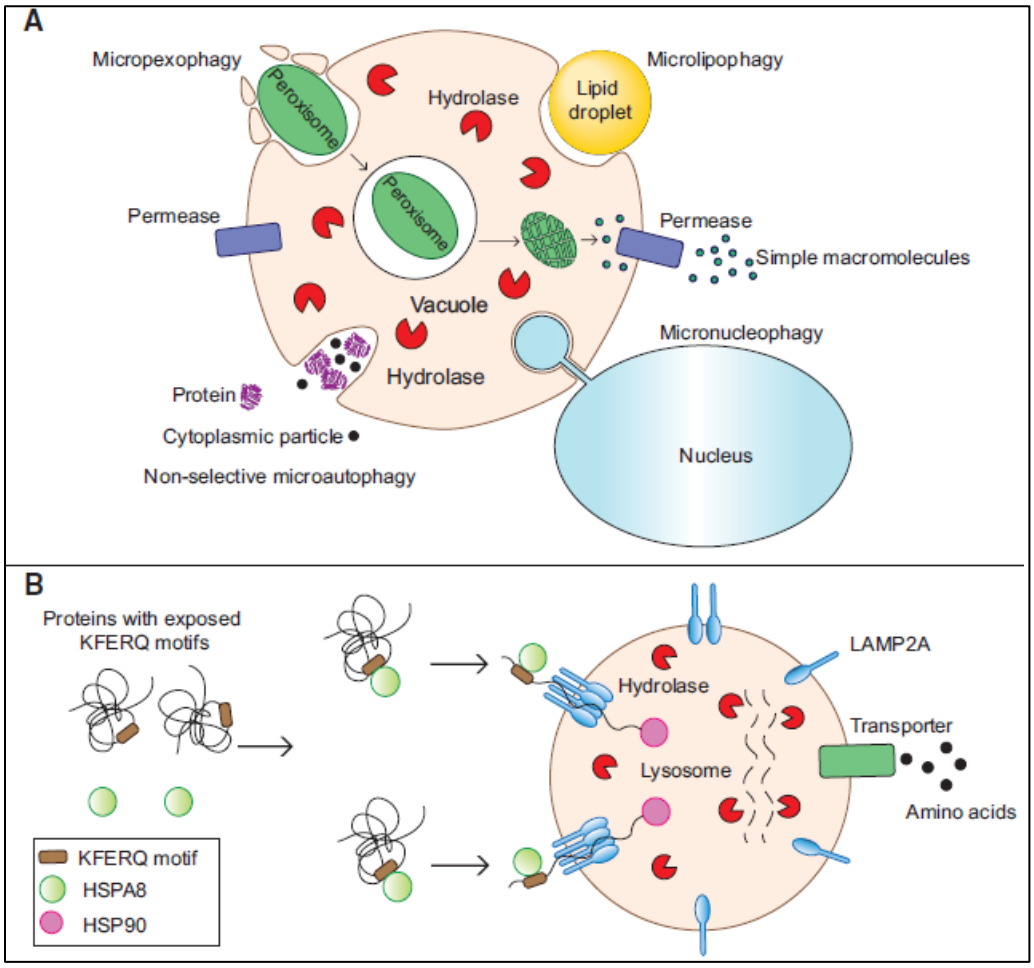

Figure 2. Other mechanisms of self-eating: Chaperone-mediated autophagy (CMA) and microautophagy. (A) In yeast, microautophagy involves the sequestration of cargo by the protrusion/invagination of the vacuolar membrane followed by an inward scission leading to the formation of a cargo-containing lumenal vesicle. This vesicle is subsequently degraded by vacuolar hydrolases releasing simple breakdown products. Microautophagy can be non-selective, degrading cytosolic components randomly, or selective, specifically degrading lipid droplets (microlipophagy) or peroxisomes (macropexophagy). Another selective microautophagic process, not discussed in the text, is the piecemeal microautophagy of the nucleus (PMN; also called micronucleophagy) which degrades portions of the nucleus. (B) CMA is a lysosome-dependent protein degradation pathway that requires the cytosolic chaperone HSPA8/HSC70. Proteins with an exposed KFERQ or KFERQ-like motif are recognized and bound by HSPA8. The complex then locates to the lysosomal membrane where the multimerization of LAMP2A allows the formation of a conduit for the delivery of the protein into the lysosomal lumen, a process facilitated by the lumenal chaperone HSP90. Lysosomal hydrolases break down the protein releasing amino acids which are transported into the cytosol.

1.3 Cellular sensors integrate autophagy with cellular metabolic status

In mammals, starvation for 24-48 h induces autophagy in nearly all nucleated cells. However, circulating amino acid and glucose levels are relatively stable during this period due to the activity of homeostatic circuits involving the breakdown of systemic reserves (Galluzzi et al., 2014). Consequently, intracellular nutrient availability for most cells is highly dependent on factors influencing nutrient uptake from the extracellular milieu. Cellular nutrient uptake is modulated by a plethora of cytokines and hormones, with INS (insulin) and IGF1 (insulin like growth factor 1) being critical reporters of the fed state. GCG (glucagon) and epinephrine play a major role in conveying a fasting status through the GCG and ADRB/β-adrenergic receptors, respectively. Upon activation, these two guanosine-protein-coupled receptors (GPCRs) stimulate cAMP production. cAMP modulates autophagy via PRKA/PKA (protein kinase cAMP-dependent), MTOR (mechanistic target of rapamycin kinase), and the MAPK (mitogen-activated protein kinase) signaling cascade, although the exact mechanisms are yet to be defined (Lizaso et al., 2013; Wauson et al., 2014; Franco et al., 2017). While cAMP generally promotes autophagy through PRKA, studies indicate that the RAPGEF3/EPAC1 branch of cAMP signaling may reduce autophagosome biogenesis and autophagic flux in neurons (Williams et al., 2008) or during invasion by certain pathogens (Mestre and Colombo, 2012). Understandably given its major role in eukaryotic cell signaling, multiple MAPK pathways are intertwined with autophagy including the MAPK/JNK (Haberzettl and Hill, 2013), MAPK/ERK (Martinez-Lopez and Singh, 2014) and MAPK/p38 (He et al., 2018) pathways.

At the cellular level, starvation decreases the abundance of key nutrients such as glucose and amino acids, which eventually induces a decrease in downstream metabolites including TCA cycle intermediates. Importantly, a reduced supply of glucose and amino acids lowers the

"energy charge" of the cell—the relative abundance of ATP in comparison to ADP and AMP. AMP kinase (AMPK) plays a major role in upregulating autophagy primarily, although not exclusively, in response to reduced energy charge. Another key regulator of autophagy, MTOR complex 1 (MTORC1), is highly responsive to intracellular amino acid levels (Figure 3).

1.3.1 AMPK

AMPK is activated in response to energy charge and, to a lesser extent, nutrient status of the cell. Significant AMPK activation requires its phosphorylation by upstream kinases, principally STK11 (Woods et al., 2003). Binding of AMP stabilizes the phosphorylation status of AMPK and imparts an allosteric effect, both of which are required for full AMPK activation. ADP too can bind AMPK but only serves to preserve phosphorylation status (Xiao et al., 2007; Xiao et al., 2011; Chen et al., 2012). ATP can competitively bind AMPK, making this protein highly responsive to cellular energy availability. AMPK also responds to the glucose concentration independent of energy charge (Zhang et al., 2013; Zhang et al., 2014; Zhang et al., 2017). CAMKK (calcium/calmodulin dependent protein kinase kinase) activates AMPK by phosphorylating the same site as STK11; however, CAMKK activation is sensitive to intracellular Ca^{2+} concentration, thus coupling AMPK activation to extracellular signals that induce changes in cellular Ca^{2+} levels as well (Hoyer-Hansen et al., 2007). A novel and elegant mechanism of autophagy regulation involving AMPK has recently been proposed. During glucose starvation, AMPK phosphorylates ACSS2 (acetyl-CoA synthetase short chain family member 2) exposing a nuclear localization signal. Once imported to the nucleus, ACSS2 binds to TFEB and translocates to the promoter region of lysosome biosynthesis and autophagy genes. Here, ACSS2 locally generates acetyl-CoA that is used for histone H3 acetylation, enhancing gene expression and promoting autophagy (Li et al., 2017) (Figure 3).

A large role of AMPK in activating autophagy is the inhibition of MTORC1 through direct phosphorylation of its RPTOR subunit as well as via the activating phosphorylation of the MTORC1 inhibitor TSC2 (TSC complex subunit 2) (Inoki et al., 2006; Gwinn et al., 2008). Inhibition of MTORC1 simultaneously inhibits cellular anabolism and strongly induces autophagy. AMPK also phosphorylates BECN1 and PIK3C3/VPS34 subunits stimulating autophagic functions of PIK3C3/VPS34 kinase complexes and inhibiting non-autophagic functions, respectively (He et al., 2013; Kim et al., 2013). Finally, autophagy is upregulated by activating phosphorylation of ULK1 by AMPK (Figure 3). Other specialized AMPK signaling outputs have been reviewed elsewhere (Mihaylova and Shaw, 2011; Hardie et al., 2016). It is, however, interesting to note that increase in lifespan through dietary restriction in *C. elegans* occurs through AMPK activation highlighting the role of AMPK as a metabolic sensor (Weir et al., 2017).

1.3.2 MTORC1

The activity of MTORC1 is tied to cellular amino acid levels through several sensors that directly or indirectly modulate the activity of RRAG GTPases. RRAG complexes are responsible for recruiting MTORC1 to the lysosomal membrane, a necessary step in MTORC1 functionality (Sancak et al., 2008) (Sancak et al., 2010). MTORC1-associated amino acid sensors include the SESN- (Chantranupong et al., 2014; Wolfson et al., 2016) and CASTOR- (Chantranupong et al., 2016) family proteins, which, in response to cytosolic leucine and arginine, respectively, modulate RRAG activity through the GTPase activating proteins GATOR1 and GATOR2 (Bar-Peled et al., 2013; Panchaud et al., 2013). MTORC1 may also sense leucine indirectly, in a cell-type specific manner, through its metabolic product acetyl-CoA. Abundance of leucine leads to increased acetyl-CoA levels which activate MTORC1 through acetylation of the

RPTOR/RAPTOR regulatory subunit (Son et al., 2019). MTORC1 is activated by lysosomal lumenal arginine through an association between the Ragulator complex and SLC38A9 (Jung et al., 2015; Wyant et al., 2017).

The protein SAMTOR is described as a link between MTORC1 activity and intracellular methionine levels (Gu et al., 2017). A role of FLCN-FNIP in amino acid signaling to MTORC1 is emerging but remains to be fully elucidated (Meng and Ferguson, 2018). Interestingly, RRAG activation is also sensitive to glucose starvation, tying MTORC1 activation to intracellular glucose levels (Efeyan et al., 2013). Additionally, HK2 (hexokinase 2), which regulates a rate-limiting step in glycolysis, inhibits MTORC1 through direct interaction in the absence of glucose (Roberts et al., 2014). MTORC1 activity is coupled to growth factors through a signaling cascade originating from INSR (insulin receptor). Ligand binding to INSR activates PIK3C (phosphatidylinositol-4,5-bisphosphate 3-kinase) that activates AKT/PKB. AKT phosphorylates the MTORC1 inhibitor TSC1/2, causing its dissociation from the lysosomal membrane-bound RHEB GTPase and subsequent MTORC1 activation (Gingras et al., 1998; Bhaskar and Hay, 2007; Menon et al., 2014) (Figure 3). A role of amino acids in TSC1/2 deactivation has also been proposed but is controversial (Demetriades et al., 2014).

MTORC1 acts to suppress autophagy in nutrient-replete conditions by several mechanisms. One such mechanism is the inhibitory phosphorylation of the ULK complex, which hinders ULK1 autophosphorylation and AMPK-dependent ULK1 phosphorylation (Kim et al., 2011). MTORC1 inhibits the PIK3C3/VPS34 kinase complex through phosphorylation of the regulatory subunits ATG14, AMBRA1, or UVRAG (Nazio et al., 2013; Yuan et al., 2013; Kim et al., 2015). MTORC1-mediated repression of autophagy also occurs via the phosphorylation of TFEB (transcription factor EB). Nuclear TFEB raises the catabolic capacity of the cell by

upregulating both autophagy and lysosome biosynthesis (Figure 3). Phosphorylation of TFEB by MTORC1 leads to its disabling, cytosolic retention (Martina et al., 2012). In addition, phosphorylation of TFEB targets it for ubiquitination leading to proteasomal degradation (Sha et al., 2017)

1.3.3 Metabolite sensors

Glucose and amino acid depletion have indirect metabolic consequences that modulate autophagy. Amino acid starvation leads to the accumulation of uncharged tRNA that activates EIF2AK4/GCN2. EIF2AK4 phosphorylates EIF2S1/EIF2α (eukaryotic initiation factor 2 subunit alpha), reducing global translation but promoting the translation of ATF4 (activating transcription factor 4) that then transcriptionally activates numerous stress-responsive genes including some involved in autophagy (Deval et al., 2009; Ye et al., 2010; B'Chir et al., 2013) (Figure 3). Recently, GORASP2/GRASP55, a structural protein responsible for Golgi stacking and reassembly, was proposed as an intracellular glucose sensor. During glucose abundance, GORASP2 is O-GlcNAcylated, a PTM that is rapidly lost upon glucose starvation. De-O-GlcNAcylated GORASP2 is targeted to autophagosomes where it interacts with the lipidated form of LC3 (LC3-II) and subsequently with LAMP2 on the lysosomal membrane to promote autophagosome-lysosome fusion (Zhang et al., 2018).

Several groups have demonstrated that autophagy may be induced by the administration of free fatty acids (FFAs) - both saturated and unsaturated. The mechanism of autophagy induction differs between these two classes with saturated FFAs activating PIK3C3/VPS34 kinase complexes through AMPK, MAPK8/JNK1, and EIF2AK2/PKR (Komiya et al., 2010; Shen et al., 2012; Niso-Santano et al., 2015). Although fatty acids are energy-rich nutrients, their abundance can be an indicator of starvation; an early response to starvation is the mobilization of

fatty acids from intracellular stores. However, whether the intracellular generation of free fatty acids mediates the activation of autophagy by itself or in conjunction with other metabolites in vivo is yet to be established.

β-oxidation of FFAs in mitochondria feeds the TCA cycle by generating acetyl CoA. Under severe, prolonged starvation, free fatty acid stores dwindle, and acetyl CoA levels begin to drop due to consumption from several cellular processes. Without acetyl-CoA, acetylases lack an acetyl group donor, resulting in a shift in the proteome toward the deacetylated state. This favors both the transcriptional expression of pro-autophagic genes and the derepression of existing autophagic proteins (Eisenberg et al., 2014; Marino et al., 2014). Additionally, without acetyl-CoA to feed the TCA cycle, regeneration of NADH slows, shifting the cellular equilibrium toward the oxidized form, NAD^+. Increased NAD^+ levels activate SIRTs (sirtuins), a family of NAD^+-dependent class III histone deacetylases. SIRTs induce autophagy through multiple mechanisms including the activation of FOXO (forkhead box protein O) transcription factors and core autophagy genes such as ATG5 and ATG7 (Lee et al., 2008; Hariharan et al., 2010) (Figure 3). Under some circumstances, cells combat diminishing acetyl-CoA levels by converting amino acids to TCA cycle intermediates such as α-ketoglutarate. This conversion, however, results in the production of ammonia which also induces autophagy, likely through the activation of AMPK and the unfolded protein response (Harder et al., 2014).

1.3.4 Metabolite sensors

Hypoxia may induce autophagy via several mechanisms. Initially, hypoxia results in reduced ATP production, and thus, reduced energy charge, activating AMPK. Another major link between hypoxia and autophagy is the transcription factor complex HIF-1. HIF1A/HIF1α, a critical HIF-1 subunit, is ubiquitinated under normoxia, resulting in its degradation by CMA.

During oxygen deprivation, HIF1A is not ubiquitinated, allowing HIF-1 to mount a cellular hypoxic response (Hubbi et al., 2013; Ferreira et al., 2015). Once activated, HIF-1 promotes autophagosome assembly (Bellot et al., 2009; Zhao et al., 2012) (Figure 3). Additionally, HIF-1 appears to crosstalk with MTORC1 and MTORC2 (Hudson et al., 2002; Brugarolas et al., 2004). Hypoxia is also linked to autophagy though the generation of reactive oxygen species (ROS) (Scherz-Shouval et al., 2007; Chen et al., 2009).

Figure 3: An intricate network of regulatory components and signaling pathways influence autophagy in response to cellular metabolic status

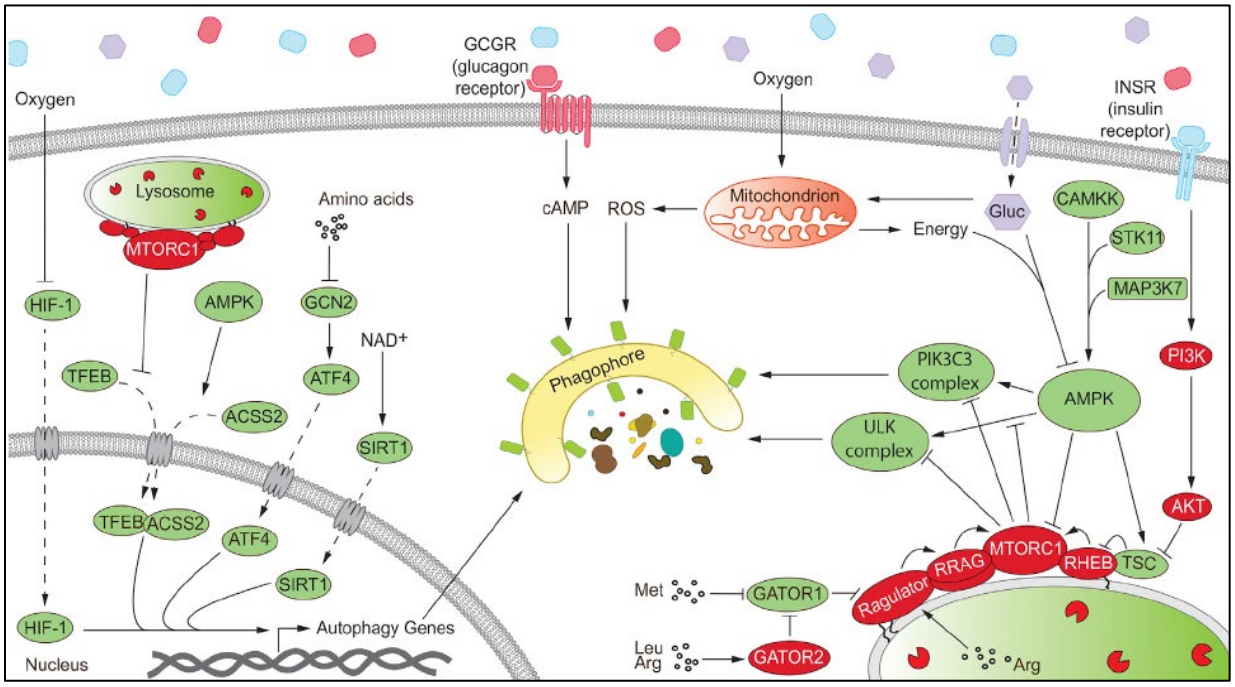

Figure 3. An intricate network of regulatory components and signaling pathways influence autophagy in response to cellular metabolic status. Autophagy is regulated at multiple levels by cellular components that respond to specific or general metabolic cues. Several proteins and protein complexes such as ATF4, HIF-1, SIRT1 and TFEB modulate the expression of autophagy-related genes at the transcriptional level. These pathways are sensitive to the abundance of amino acids, oxygen availability, the reduction status of the cellular NAD pool and activation status of MTORC1 and AMPK. Expression of autophagy genes leads to autophagy induction, depicted as an expanding phagophore. Glucagon signals a fasted organismal status and upregulates autophagy through cAMP-dependent pathways. Glucose fuels oxidative phosphorylation in mitochondria, providing energy in the form of ATP but also generating ROS that indirectly upregulate autophagy. Low cellular energy charge activates AMPK in a process that requires upstream kinases such as CAMKK and STK11. AMPK promotes autophagy by activating the autophagy-initiating ULK1 and PIK3C3/VPS34 complexes as well as inhibiting MTORC1 function. MTORC1 inhibits autophagy when recruited to the lysosome and activated. MTORC1 recruitment and activation occurs in response to the presence of both growth factors such as INS/insulin and an abundance of amino acids in the cytosol and lysosomal lumen. While INS signaling occurs through the PI3K-AKT-TSC axis, leading to the activation of the small GTPase RHEB, amino acid sufficiency is conveyed through the Ragulator complex that impinges on the small GTPases known as RRAGs. The RRAG complex represents a heterodimer between RRAGA (or B) and RRAGC (or D). Activated MTORC1 inhibits the ULK1 and PIK3C3/VPS34 complexes to downregulate autophagy (Refer to text for details).

1.4 Autophagy promotes the availability of specific nutrients/metabolites

The tremendous flexibility in the process of cargo capture and degradation allows bulk autophagy to make a wide range of metabolites available for cellular utilization. At the other end of the spectrum is selective autophagy that can mobilize specific metabolites as a response to specific cellular requirements. Selective autophagy regulates organellar and metabolic homeostasis by promoting the removal of dysfunctional/superfluous organelles downstream of metabolic cues. This involves the selective sequestration of specific cargo by a receptor that links cargo with LC3-II on the expanding phagophore. These receptors can be bona fide cargo-localized proteins or ubiquitin-binding proteins that also bind LC3-II (Figure 4A). In this section, I explore important selective autophagy pathways, the mechanisms involved and the metabolic consequences.

1.4.1 Ribophagy recycles superfluous protein synthetic machinery

Ribosomal RNA (rRNA) constitutes up to 80% of total RNA in a eukaryotic cell (Warner, 1999). The abundance of ribosomes, especially in actively growing cells, makes them a valuable pool of potentially mobilizable nucleic acids and amino acids. Selective autophagic degradation of ribosomes (ribophagy) was first described in yeast (Kraft et al., 2008; Ossareh-Nazari et al., 2010) but has since been found in mammals as well. Autophagic degradation of ribosomes also occurs as a part of other selective autophagic pathways such as mitophagy and lysophagy (An and Harper, 2018). The ribophagy receptor remained elusive in mammalian cells until recently, when NUFIP1 was identified as an autophagy receptor capable of binding both ribosomes and Atg8-family members (Wyant et al., 2018) (Figure 4A). Deletion of NUFIP1 exclusively prevents the normal decline in ribosomes under starvation conditions or upon MTORC1 inhibition; cells lacking functional NUFIP1 are also more susceptible to starvation-

induced stress. Further, large fluctuations in ribosomal levels coincide with normal diurnal cycles in mice, suggesting a yet unappreciated role for targeted degradation of ribosomes in mammalian metabolism (Sinturel et al., 2017)

1.4.2 Lipid droplets are mobilized by the coordinated activation of lipolysis and lipophagy

Intracellular fats are stored in the form of LDs that are composed of a core of neutral lipid esters wrapped within a single layer of phospholipids and surrounded by a coat of structural proteins. Structural proteins, particularly PLINs (perilipins), not only shield the LD from the cytosol but also regulate the accessibility of lipogenic and lipolytic enzymes (Singh and Cuervo, 2012). LDs are dynamic metabolic stations (Greenberg et al., 2011) that interact and mediate lipid transfer with mitochondria (Rambold et al., 2015; Benador et al., 2018) and possibly other organelles such as the ER (Ozeki et al., 2005) and endosomes (Liu et al., 2007). Further, the hydrophobic nature of the LD allows it to bind and/or sequester proteins (Prevost et al., 2018). However, the most critical metabolic function of LDs is their role as mobilizable energy stores. LD catabolism can be initiated downstream of two distinct stimuli: nutrient deprivation and acute lipid overload.

LDs may be catabolized by cytosolic lipases such as PNPLA2/ATGL and LIPE/HSL (lipase E, hormone sensitive type) (Zimmermann et al., 2004). LDs may also be degraded in the lysosome via an autophagy-dependent process known as lipophagy. Although a vacuole-dependent, autophagy-independent LD utilization mechanism has been proposed in yeast (Ouahoud et al., 2018), lipophagy is the major pathway for bulk LD-degradation in eukaryotes. Autophagy-incompetent cultured hepatocytes challenged with fatty acid overload exhibit increased triglyceride accumulation, as do hepatocytes in the autophagy-deficient mouse liver on a high-fat diet (Singh et al., 2009a). This provides a basis for metabolic disorders such as

Wolman's disease (Patrick and Lake, 1969) and cholesterol ester storage disease (CESD) (Burke and Schubert, 1972) that manifest due to deficiency of LIP (lipase, lysosomal acid type). Lipophagy is a critical metabolic pathway in neurons (Kaushik et al., 2011), brown adipose tissue (Martinez-Lopez et al., 2016) and macrophage foam cells (Ouimet et al., 2011; Lizaso et al., 2013). Basal levels of lipophagy are also required to prevent the excessive buildup of LDs (Lim et al., 2014). Although after sustained starvation there appears to be a specific sequestration of LDs within autophagosomes, an LD-specific autophagy receptor is yet to identified. Degradation of triglycerides and other lipids provides FFAs that can be metabolized through β-oxidation. TFEB, upregulated during nutrient deprivation (Settembre et al., 2013), is involved in the transcriptional upregulation of PPARGC1A (PPARG coactivator 1 alpha) and PPAR (peroxisome proliferator activated receptor) (Ghosh and Pahan, 2016), two master regulators of lipid catabolic processes, thereby connecting FFA generation to their subsequent utilization.

A proposed mechanism for selective incorporation suggests that nascent autophagosomes may form on the surface of the LD and then grow to sequester the LD partially, finally sealing off to form mature autophagosomes (Singh et al., 2009a; Singh and Cuervo, 2012) (Figure 4B). Interestingly, the lipidated form of LC3 was reported to be present on the LD surface (Shibata et al., 2009). Multiple RAB proteins also localize to the LD surface, some of which may play a role in regulating lipophagy. β-adrenergic stimulation promotes lipophagy in a RAB7-dependent manner (Lizaso et al., 2013). RAB7 may play an essential role during starvation-induced lipophagy by promoting the recruitment of lysosomes and multivesicular bodies (Schroeder et al., 2015). RAB10 colocalizes with autophagy proteins on the LD surface, and its ablation causes hepatocellular LD accumulation (Li et al., 2016).

The prevailing model of LD utilization suggests that LD catabolism occurs via a synergistic activation of lipolysis and lipophagy that promotes swift mobilization of lipid stores (Schulze et al., 2017). Both mechanisms require the removal of LD-associated PLINs by CMA. PLIN2 (perilipin 2) and PLIN3 are CMA substrates, and their degradation is upregulated after starvation, facilitated by the phosphorylation of PLIN2 by AMPK (Kaushik and Cuervo, 2015). The degradation of PLIN2 and PLIN3 allows both lipolytic enzymes and autophagy machinery access to the LD core. In the liver, PNPLA2 positively regulates lipophagy via the activation of SIRT1 (Lee et al., 2008; Sathyanarayan et al., 2017), indicating that lipolytic stimuli that activate PNPLA2 concomitantly promote lipophagy (Khan et al., 2015). PNPLA2 possesses a LIR motif and binds LC3 (Martinez-Lopez et al., 2016), an interaction critical for its LD localization.

In addition to macrolipophagy, the direct microautophagic uptake of LDs into the lysosome has also been proposed as a means of LD breakdown. In Saccharomyces cerevisiae, microlipophagy—the direct uptake of lipid droplets into the vacuole—is distinct from selective macroautophagic pathways (van Zutphen et al., 2014) and has been identified to function as a response pathway to chronic lipid imbalance (Vevea et al., 2015).

1.4.3 Glycophagy works in concert with glycogenolysis to supply glucose

Glycogen, a branched polysaccharide, is an important contributor to glucose homeostasis. In mammals, excess circulating glucose is taken up by the liver and skeletal muscle and stored as glycogen. During periods of glucose scarcity, hormonally regulated glycogen degradation releases glucose. Glycogenolysis in skeletal muscle produces glucose that is predominantly utilized locally for sustaining muscle contraction. In contrast, glycogen breakdown in the liver, as a response to lowered blood glucose, leads to increased circulating glucose for systemic utilization (Mandl and Banhegyi, 2018). There are two principal pathways of glycogen

catabolism: cytosolic glycogen undergoes a phosphorylytic degradation initiated by PYG (glycogen phosphorylase), whereas the glycogen present in the autophagic vacuole is hydrolyzed by the lysosomal enzyme GAA (glucosidase alpha, acid). The lysosomal targeting of glycogen is mediated selectively by glycophagy.

Glycophagy may rapidly provide glucose for immediate metabolic requirements while pathways such as gluconeogenesis are activated (Kuma et al., 2004; Kondomerkos et al., 2005). At the cellular level, glycophagy is regulated by the cAMP and MTOR pathways (Zhao et al., 2018). While not all glycophagy is selective, STBD1 (starch binding domain 1) has been identified as the receptor that selectively targets the glycogen particle for degradation. STBD1 binds to glycogen via a C-terminal glycan-binding domain and links it to the phagophore by its interaction with GABARAPL1 using an N-terminal LIR (Jiang et al., 2010; Jiang et al., 2011). The N terminus of STBD1 also contains a hydrophobic region that may independently mediate targeting to the phagophore.

In cardiac muscle, glycophagy is important for maintaining energy homeostasis. In the rodent heart, the pattern of STBD1 expression during fed and fasted states is sex specific as is the susceptibility to diabetic cardiomyopathy due to glycogen mishandling (Reichelt et al., 2013; Mellor et al., 2014). In Drosophila, autophagy is an efficient form of glycogen degradation in the skeletal muscle (Zirin et al., 2013). However, the specific role of glycophagy in most tissues in mammals is yet to be determined. The current consensus is that glycophagy works in concert with cytosolic glycogenolysis to orchestrate glucose metabolism. Unlike the phosphorylytic glycogenolysis, glycophagy produces non-phopshorylated glucose that can be utilized more rapidly. In mice, fast-twitch muscles that contain more glycogen deposits upregulate autophagy more than slow-twitch muscles that have lower glycogen supplies (Mizushima et al., 2004; Kaur

and Debnath, 2015). The two pathways might also differ in terms of the glycogen substrate, and an attractive hypothesis is that glycophagy may preferentially target aberrantly branched glycogen particles for degradation (Mandl and Banhegyi, 2018). The importance of glycophagy is highlighted by the lysosomal storage disorder Pompe Disease that occurs due to the deficiency of GAA. The infantile disease presents as progressively lethal skeletal myopathy, respiratory and cardiac defects. The root cause lies in dysfunctional lysosomes where the degradation of glycogen is impaired, leading to energy deficiency in cardiac and skeletal muscle. Therapeutic intervention with the supplementary administration of recombinant human GAA has proven to be promising (Kishnani et al., 2007).

1.4.4 Ferritinophagy regulates iron availability

Iron, an essential micronutrient, is a cofactor for several enzymes and proteins. Iron-dependent heme synthesis in erythrocytes is critical for oxygen transport in mammals. Cytochromes utilize iron as a cofactor. Iron is also involved in the quenching of ROS as a part of antioxidative enzymes such as CAT (catalase) (Pantopoulos et al., 2012). Within the cell, iron is incorporated into the iron-sequestering protein ferritin (Zhao and Enns, 2012) Ferritin is a cage-like protein composed of multiple light (FTL) and heavy (FTH1) chain subunits surrounding a micelle of hydrated iron (Crichton, 1971; Lawson et al., 1991). The sequestration of iron is essential because free iron is prone to cycles of oxidation and reduction, producing detrimental ROS.

Equally important, however, is the regulated release of iron when needed. When the bioavailable iron level is low, it is replenished by ferritinophagy—the selective autophagic degradation of ferritin (Santana-Codina and Mancias, 2018). Lysosomal degradation of ferritin in response to iron depletion is autophagy-dependent in several cell types (Asano et al., 2011;

Kishi-Itakura et al., 2014). The mechanism of selection, however, was unclear. Recently, NCOA4 (nuclear receptor coactivator 4) was identified as the cargo receptor that binds ferritin (Mancias et al., 2014), providing a basis for the selectivity. Inhibition of autophagy flux leads to an accumulation of NCOA4, confirming its identity as an autophagy substrate (Dowdle et al., 2014). NCOA4 binds the FTH1 subunit of ferritin (Mancias et al., 2015). Interestingly, although NCOA4 associates with multiple Atg8-family proteins in vitro, it does not possess a canonical LIR motif as seen with other autophagy receptors. It is possible that NCOA4 utilizes non-canonical LIR motifs (von Muhlinen et al., 2012). Recently, an ESCRT-dependent pathway that utilizes several autophagy proteins but not the Atg8-family, has also been proposed as a lysosomal targeting mechanism for the NCOA4-FTH1 complex (Goodwin et al., 2017).

The cellular level of NCOA4 is appropriately maintained to ensure regulated ferritinophagy. An iron-dependent interaction between NCOA4 and the E3 ubiquitin ligase HERC2 promotes the ubiquitination and degradation of NCOA4 when iron is abundant. When iron concentrations fall, NCOA4 is released and is available for binding and targeting ferritin for degradation (Mancias et al., 2015) (Figure 4C). The importance of NCOA4 in iron metabolism is highlighted by the massive accumulation of iron seen in several tissues of ncoa4-/- mice, especially splenic macrophages that function to reutilize iron from phagocytosed erythrocytes (Dowdle et al., 2014). ncoa4-null mice are also predisposed to anemia and sensitive to increased dietary intake of iron (Bellelli et al., 2016). Similarly, knockdown of ncoa4 leads to deficiencies in erythropoiesis in zebrafish (Mancias et al., 2015). NCOA4 also regulates the terminal differentiation of human erythroblasts (Gao et al., 2017). Further investigations will reveal other developmental and metabolic roles of this selective autophagy pathway.

Figure 4: Selective autophagy as a modulator of metabolic homeostasis

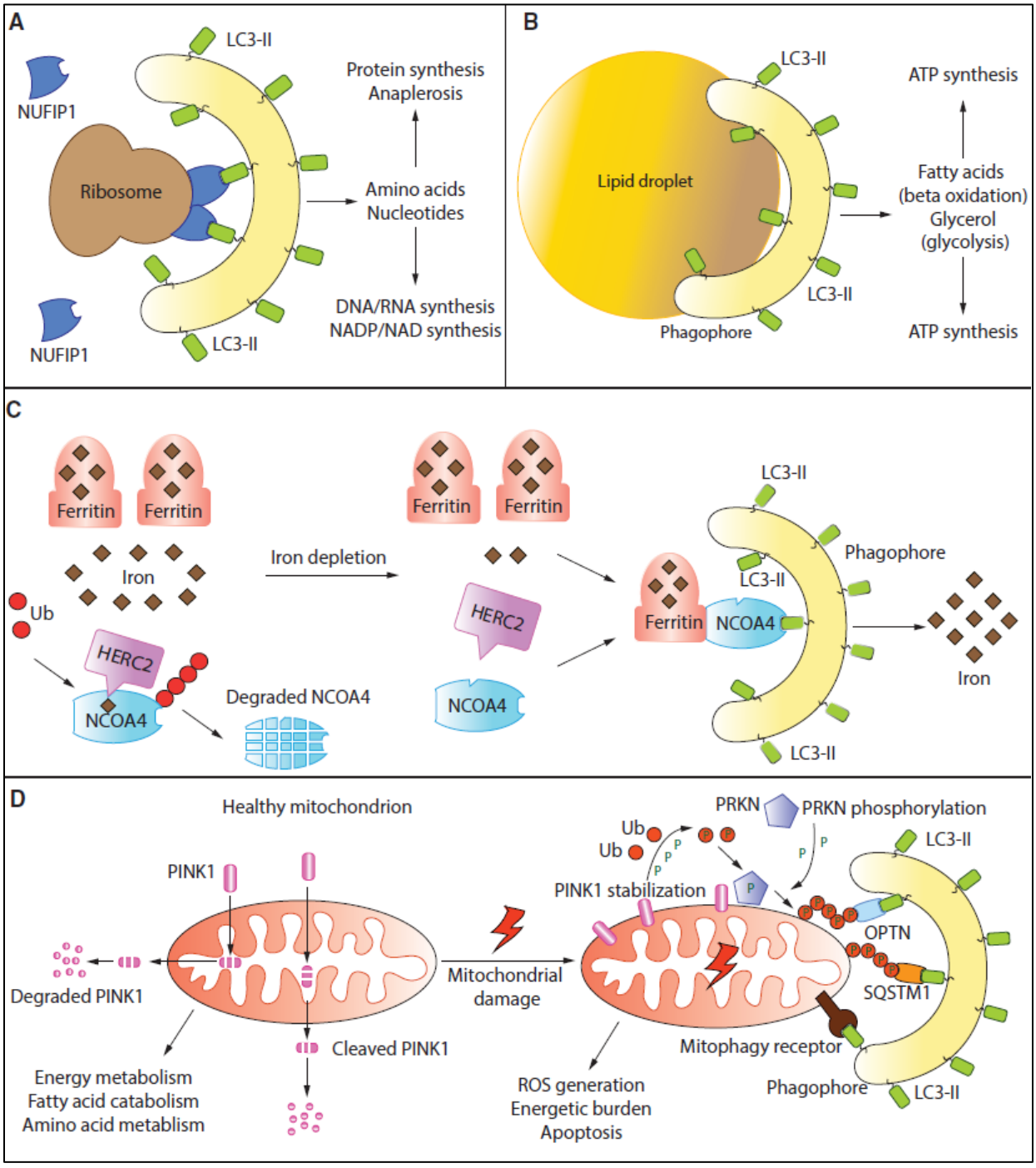

Figure 4. Selective autophagy as a modulator of metabolic homeostasis. Selective autophagy removes dysfunctional/superfluous organelles downstream of metabolic cues. It also provides a source of raw material for several metabolic processes and pathways. Selective autophagy involves the sequestration of specific cargo by a LIR-containing receptor that links the cargo with LC3-II (see text for details). An example in (A) shows the selective targeting of ribosomes to the mitochondria by the ribophagy receptor NUFIP1. Designated receptors have not yet been identified for all types of selective autophagy. Selective uptake of lipid droplets (B) may simply occur by the formation and expansion of the phagophore on the surface of the droplet. (C) Ferritinophagy allows the iron-dependent regulation of ferritin degradation. NCOA4 is the receptor that targets the iron-storing protein ferritin to LC3-II. Under conditions of iron-sufficiency, NCOA4 is ubiquitinated by HERC2 via an iron-dependent interaction, leading to NCOA4 degradation. When the cellular levels of free iron decline, this interaction is weakened allowing NCOA4 to target ferritin to the phagophore. The degradation of ferritin releases free iron. (D) Healthy mitochondria are the principal source of cellular ATP and regulate multiple metabolic circuits. Damaged mitochondria, that are detrimental, are removed by mitophagy. In the PINK1-PRKN-dependent pathway of mitophagy, the kinase PINK1 which is imported and cleaved in healthy mitochondria, and subsequently targeted for cytosolic degradation, is stabilized on the outer mitochondrial membrane (OMM). PINK1 phosphorylates ubiquitin and the E3 ubiquitin ligase PRKN promoting large-scale ubiquitination of mitochondrial OMM proteins. Ubiquitinated proteins are recognized by ubiquitin-binding autophagy receptors such as OPTN and SQSTM1 which also bind LC3-II, promoting mitochondrial degradation (refer to text for details). Mitophagy may also be orchestrated by OMM and inner mitochondrial membrane

(IMM) proteins that directly bind LC3-II and function as mitophagy receptors (refer to text for details).

1.5 Autophagy maintains the metabolic circuit

1.5.1 Mitophagy and pexophagy influence aerobic metabolism

3.1 Mitophagy and pexophagy influence aerobic metabolism

Mitochondria maintain cellular metabolism by providing ATP and regulating calcium availability. However, dysfunctional mitochondria generate ROS that not only damage cellular membranes and DNA but also lead to futile ATP consumption (Lemasters, 2014). Furthermore, severely damaged mitochondria release pro-apoptotic molecules that lead to cell death (Wang and Youle, 2009). Mitochondrial quality control is consequently a strictly regulated process. Mitochondrial maintenance is highly dynamic involving mitochondrial biogenesis, fusion, fission, and clearance (Mishra and Chan, 2016). In fact, a common mechanism to revive dysfunctional mitochondria involves fusion with healthy mitochondria (Nakada et al., 2001) (Youle and van der Bliek, 2012). Mitochondrial stress also activates mitochondria-to-nucleus signaling that promotes cellular responses such as the ATFS-1-dependent mitochondrial unfolded protein response (UPRmt) (Zhao et al., 2002; Haynes et al., 2010; Nargund et al., 2012; Melber and Haynes, 2018) and the recently identified Pdr3-dependent mitochondrial compromised protein response (mitoCPR; Weidberg and Amon, 2018).

Mitochondria that are terminally damaged are removed through a process of selective autophagy called mitophagy. Mitophagy occurs at a low, basal level to continuously replace dysfunctional mitochondria, and a stronger mitophagy response may be evoked by increased mitochondrial insult. Metabolically active tissues use mitochondrial function extensively to meet their energy demands and have high basal levels of mitophagy (McWilliams et al., 2018) to facilitate mitochondrial turnover.

The mechanisms of mitophagy have been examined in several organisms. In *S. cerevisiae*, the outer mitochondrial membrane (OMM) protein Atg32 is the mitophagy receptor (Kanki et al., 2009). BNIP3L/NIX, an OMM protein acts as the mitophagy receptor in mitochondrial clearance during erythrocyte differentiation (Sandoval et al., 2008). Mitophagy is also induced under hypoxic conditions, where cells rely on anaerobic glycolysis, rendering mitochondria superfluous. FUNDC1 is a mitophagy receptor mediating hypoxia-dependent mitochondrial clearance (Liu et al., 2012). The IMM protein PHB2 (prohibitin 2) is a novel IMM-localized mitophagy receptor that is required for the clearance of paternal mitochondria in *C. elegans* (Wei et al., 2017).

The best-characterized pathway for mitophagy is the PINK1-PRKN pathway that responds to the loss of mitochondrial membrane potential. Membrane depolarization prevents the mitochondrial import of PINK1 and stabilizes it on the outer membrane (Kondapalli et al., 2012). PINK1 phosphorylates several substrates including ubiquitin and the E3 ligase PRKN which sets in motion a feed-forward loop that promotes large scale ubiquitination of mitochondrial membrane proteins (Koyano et al., 2014; Kane et al., 2014; Pickrell and Youle, 2015). Heavily ubiquitinated mitochondria are recognized by ubiquitin-binding autophagy receptors such as SQSTM1 and OPTN that also bind LC3, thereby linking mitochondria with phagophores (Geisler et al., 2010) (Figure 4D). However, most studies concerning the PINK1-PRKN pathway utilize the context of acute dissipation of mitochondrial membrane potential, precluding the identification of subtle pathways that are likely to be critical during pathophysiology (Gatica et al., 2018). A study showed that the phosphorylation of ubiquitin by PINK1 is sufficient to induce low-amplitude mitophagy, without the need for PRKN activity (Lazarou et al., 2015).

Another PRKN-independent pathway for mitophagy that involves the recruitment of E3 ligase component RBX1 by SQSTM1, has been proposed to mitigate non-alcoholic fatty liver disease (Yamada et al., 2018). Additionally, mitophagy is independent of PINK1 in several metabolically active tissues in mice (McWilliams et al., 2018). A recent investigation concerning the in vivo relevance of PINK1 and PRKN has revealed that PINK1 and PRKN-dependent mitophagy might be critical in modulating STING1-dependent innate immune responses to mitochondrial damage. The accumulation of mitochondrial damage leads to mitochondrial disruption which promotes inflammation. When subjected to acute or chronic mitochondrial stress, the levels of pro-inflammatory cytokines are significantly higher in mice lacking PINK1 or PRKN, indicating that these proteins likely play a critical role in limiting inflammation by mediating the timely removal of damaged mitochondria (Sliter et al., 2018).

The PINK1- and PRKN-dependent generation of mitochondria-derived vesicles (MDVs) removes localized, damaged portions of mitochondria (McLelland et al., 2016; Sugiura et al., 2014). Recently, piecemeal mitophagy, a process similar to MDV generation but with distinct cargo, was proposed to maintain basal mitochondrial homeostasis (Le Guerroue et al., 2017). Both mitophagy and MDV formation require mitochondrial fission that presumably performs two functions in this context: 1) It isolates portions of mitochondria that are damaged or disengages defective mitochondria from the mitochondrial reticular network; 2) it reduces the size of the cargo (mitochondria), promoting efficient sequestration. Consequently, mitochondrial damage and mitophagy are associated with reduced mitochondrial fusion and increased fission.

The peroxisome, involved in purine catabolism and the oxidation of fatty acids, is another important site for oxidative metabolism. The β-oxidation of very long chain FAs, branched chain FAs and the α-oxidation of phytanic acid exclusively occur in the peroxisome (Cho et al., 2018).

The peroxisome produces ROS and reactive nitrogen species such as nitric oxide that are important regulators of cellular signal transduction pathways. Conversely, to quench these reactive species peroxisomes also produce antioxidant enzymes such as CAT (Bonekamp et al., 2009). Increased peroxisomal activity is promoted by increased peroxisomal protein synthesis by the transcriptional regulator PPARA (Pawlak et al., 2015). Conversely, peroxisomes can be selectively targeted for clearance by pexophagy when they are no longer beneficial.

Methylotrophic yeasts such as *Komagataella phaffii/Pichia pastoris* highlight pexophagy-mediated metabolic switching. The oxidation of methanol to formaldehyde, the first step in methanol metabolism, occurs exclusively in the peroxisome. *K. phaffii/P. pastoris* maintains numerous peroxisomes when grown in methanol as the sole carbon source (van der Klei et al., 2006). When transferred from methanol to ethanol, peroxisomes are degraded by macropexophagy, whereas transfer to glucose results in micropexophagy (Tuttle and Dunn, 1995). In *S. cerevisiae*, the mechanism of selectivity for macropexophagy has been partly elucidated. ScAtg36 is the pexophagy receptor that links the peroxisomal membrane protein (PMP) Pex3 to both Atg11, the selective autophagy scaffold/adaptor protein, and Atg8 on the phagophore (Motley et al., 2012). In *K. phaffii/P. pastoris* PpAtg30 is the selective receptor that interacts with PpPex3 and PpPex14 (Farre et al., 2008) (Farre et al., 2013). As with mitophagy, macropexophagy is also promoted by peroxisomal fission (Mao et al., 2014).

In mammals, pexophagy occurs downstream of the ubiquitination of PMPs (Kim et al., 2008). Initially, PEX3 was identified as a ubiquitination substrate responsible for pexophagy induction but was subsequently found to be dispensable for pexophagy (Yamashita et al., 2014). Other PMPs, PEX5 and ABCD3/PMP70, are ubiquitinated by a mechanism involving the E3 ubiquitin ligase PEX2 and play important roles in pexophagy (Sargent et al., 2016) (Zhang et al.,

2015). Ubiquitinated proteins are recognized by SQSTM1 and NBR1, linking peroxisomes to the phagophore. Consequently, the depletion of SQSTM1 strongly inhibits pexophagy, whereas the exogenous expression of NBR1 strongly stimulates this process (Deosaran et al., 2013; Kim et al., 2008). PEX14 also mediates pexophagy under starvation conditions. Interestingly, PEX14 can directly interact with LC3 and, in complex with NBR1, promote peroxisome sequestration (Jiang et al., 2015). However, whether the ubiquitination of certain PMPs accelerates pexophagy or whether bulk ubiquitination of several PMPs acts as the 'eat-me' signal is not yet defined.

1.5.2 Autophagy regulates the levels of metabolic enzymes

Autophagy can influence energetics by directing the degradation of specific metabolic enzymes (Madrigal-Matute and Cuervo, 2016). Because of its selective nature, CMA is an important component of this regulatory mechanism. The regulation of the M2 splice isoform of the glycolytic enzyme PKM/PKM2 (pyruvate kinase M1/2) by CMA serves as an elegant example. M2 is the embryonic isoform of the enzyme while the M1 isoform is expressed ubiquitously in adult tissues. The preferential expression of M2 over M1 promotes rapid cell proliferation, a mechanism designed for the growth of embryonic cells, but also utilized by lung cancer cells (Christofk et al., 2008). M2 has a lower affinity for its substrate phosphoenolpyruvate than M1. M2 can also be acetylated under glucose sufficiency, which promotes its CMA-mediated degradation (Lv et al., 2011). Both factors combine to reduce the conversion of phosphoenolpyruvate to pyruvate, consequently reducing glycolytic flux. When abundant glucose is available, this mechanism allows for the accumulation of glycolytic intermediates for anabolic synthesis, a requirement of rapidly proliferating cells. Consistent with this, allografts of M1-expressing cells form smaller tumors than those of M2-expressing cells.

CMA regulates the cellular abundance of several metabolic enzymes and is a critical player in maintaining metabolic homeostasis (Kaushik and Cuervo, 2018). A study using tissue-specific *lamp2a* KO in the mouse liver demonstrated that over 40% of CMA substrates are metabolic enzymes. These include a number of glycolytic enzymes as well as enzymes involved in triglyceride and steroid synthesis. Expectedly, the selective blockage of CMA in these mice leads to a drastic alteration in both lipid and carbohydrate metabolism and associated systemic changes such as reduced adipose tissue content, lowered body weight, increased energy expenditure and compromised responses to nutritional challenges such as starvation and lipid overload (Schneider et al., 2014). The loss of hepatic CMA also leads to a pronounced disruption of proteostasis with aging (Schneider et al., 2015). CMA may influence metabolic outcomes indirectly as well by regulating the levels of stress-responsive proteins such as HIF1A (Hubbi et al., 2013).

Identified in *S. cerevisiae*, the targeting of Fas (fatty acid synthase) for vacuolar degradation is a novel example of autophagy selectively degrading a single protein complex. Fas is a large enzymatic complex (Lomakin et al., 2007) that is preferentially delivered to the vacuole in an autophagy-dependent manner during nitrogen starvation. This requires interaction with Atg8 as well as the activity of Vac8 and Snx4/Atg24, two proteins involved in selective autophagy in yeast. Fas degradation during nitrogen starvation may serve to prevent the channeling of metabolic fuel for non-essential anabolic reactions because low Fas activity promotes cell viability (Shpilka et al., 2015) during starvation. Whether other protein complexes are also preferentially targeted by autophagy under similar or different conditions will be an interesting avenue for further exploration.

1.5.3 Autophagy is involved in proteostasis

The endoplasmic reticulum (ER) is the major cellular calcium store but also facilitates sterol synthesis and the folding and targeting of secretory pathway proteins. The ER houses chaperones, and the reducing environment allows disulfide bond formation (Bravo et al., 2013). The accumulation of unfolded proteins within the ER (Ron and Walter, 2007) causes ER stress. In haematopoietic cells, tunicamycin-induced ER stress engineers major metabolic alterations including glucose uptake and utilization followed by mitochondrial activation, which increase cellular oxygen consumption and overall ATP synthesis (Wang et al., 2011). ER stress is also associated with obesity, especially in the context of metabolic inflammation-induced dysfunction of the adipose tissue (Shan et al., 2017). Reduced protein secretion is another symptom of ER stress, altering the concentration of hormones and enzymes in circulation. ER stress is mitigated by the unfolded protein response that reduces general protein translation, upregulates proteasomal degradation, increases chaperone synthesis and promotes ER expansion (Araki and Nagata, 2011). Recovery from ER stress occurs via the removal of dilated ER subdomains by a process of selective autophagy known as reticulophagy (Smith et al., 2018).

In yeast, Atg39 and Atg40 are the receptors for ER sequestration (Mochida et al., 2015), whereas in mammals RETREG1/FAM134B was the first identified reticulophagy receptor (Khaminets et al., 2015). These ER-resident proteins function similarly to known autophagy receptors and interact with Atg8-family proteins. RETREG1-dependent reticulophagy maintains the volume and structure of the ER, but the role of reticulophagy in recovery from ER stress was highlighted by the identification of a second reticulophagy receptor, CCPG1 (cell cycle progression 1) (Smith et al., 2018). Loss of RETREG1 causes sensory neuropathy in mice, whereas CCPG1 hypomorphic mice show impaired pancreatic proteostasis and exhibit a loss of

polarization in the cells of the exocrine pancreas, underscoring the importance of reticulophagy. Sequestration of ER subdomains may also occur downstream of microbial infection and help resolve cellular stress (Moretti et al., 2017).

Aggregated proteins in the cytoplasm act as ATP sinks by consuming chaperone activity. Several proteins, such as amyloid-β and HTT are prone to aggregation, and these aggregates may promote apoptosis or necrosis (Stefani and Dobson, 2003). Aggrephagy—the selective degradation of protein aggregates—plays a pivotal role in removing toxic aggregates. The CUE domain-containing proteins Cue5 in yeast and its mammalian homolog TOLLIP, simultaneously bind to polyQ aggregates and Atg8-family proteins to promote aggregate-clearance (Lu et al., 2014a; Lu et al., 2014b). The ubiquitination of aggregated proteins plays an important role in their autophagy-dependent removal by recruiting autophagy receptors SQSTM1, NBR1 and OPTN (Kim et al., 2008; Pankiv et al., 2007; Kirkin et al., 2009). The SQSTM1-dependent degradation of aggregates also requires WDFY3/ALFY (Clausen et al., 2010), which acts as a scaffold for aggrephagy by binding lipids and proteins on the autophagosome (Filimonenko et al., 2010; Lystad et al., 2014). Another protein, WDR81, specifically interacts with LC3C and promotes aggrephagy (Liu et al., 2017b). Ubiquitin-mediated aggrephagy raises the question of substrate choice between autophagy and the ubiquitin-proteasome system. Several factors have been proposed to contribute to selectivity, including receptor oligomerization around the substrate, size of aggregates, the lysine residues used for linkage as well as the length and nature of the ubiquitin chain (Korolchuk et al., 2010; Lu et al., 2017; Verhoef et al., 2002).

Unlike conventionally secreted proteins, the yeast mating-factor is transported directly from the cytosol across the plasma membrane by an ABC transporter (Kuchler et al., 1989). The demonstration that IL1B/IL-1β, a mammalian cytokine, lacks a signal sequence (Rubartelli et al.,

1990), initiated further interest in unconventional forms of protein secretion. An acyl-CoA binding protein known as AcbA in Dictyostelium and Acb1 in *S. cerevisiae* is secreted unconventionally (Duran et al., 2010; Manjithaya et al., 2010) with the secretion of this protein being dependent on autophagosome formation. However, these autophagosomes do not fuse with the lysosome/vacuole but rather with the plasma membrane. The secretion of leaderless peptides via autophagosomes is known as secretory autophagy (Ponpuak et al., 2015). The autophagy-mediated secretion of lysozyme occurs in intestinal Paneth cells in response to Salmonella infection. Secreted lysozyme confers protection from the invading pathogen (Bel et al., 2017). However, the metabolic consequences of autophagy-dependent secretion have not been clarified yet.

1.6 Autophagy influences metabolism during development and disease

In this section, I first highlight how autophagy influences systemic metabolism by regulating the development of adipose tissue. Adipose tissue works in concert with another primary metabolic modulator, the liver, to maintain metabolic homeostasis under conditions of nutrient deprivation. Autophagy is critical for the execution of hepatic functions—a subject of several excellent reviews (Ueno and Komatsu, 2017; Schneider et al., 2014; Madrigal-Matute and Cuervo, 2016). The dynamic and enigmatic role of autophagy in the pathogenesis and progression of cancer will be the focus of the second part of this section.

1.6.1 Autophagy in physiology: Adipogenesis and adipocyte maintenance

Adipocytes are specialized mammalian cells that preserve energy in the form of LDs and constitute the adipose tissue. Adipose tissue performs a range of metabolic, protective, and endocrine functions and serves as a source of secreted factors such as TNF/TNFα and

CFD/adipsin. Adipocytes can be white, brown or beige, with particular adipocytes serving specific functions (Rosen and Spiegelman, 2014; Zwick et al., 2018). Adipocyte differentiation is autophagy dependent. Autophagy is induced during adipogenesis in primary MEF cells, and the ablation of autophagy halts the differentiation program at an early stage. These undifferentiated cells show higher levels of apoptosis. Consequently, *atg5*$^{-/-}$ neonatal mouse pups show reduced subcutaneous fat deposits (Baerga et al., 2009).

Brown adipose tissue (BAT), constituted by mitochondria-rich, multilocular brown adipocytes, is primarily a heat-generating organ. Brown adipocytes express high levels of UCP1 (uncoupling protein 1) that uncouples mitochondrial electron transport from ATP synthesis. In these specialized adipocytes, LDs are metabolized to free fatty acids for β-oxidation and the ensuing mitochondrial electron transport builds up a proton gradient that is dissipated as heat (Fedorenko et al., 2012). BAT is, therefore, responsible for cold and diet-induced thermogenesis. Autophagy plays a critical role in the differentiation of brown adipocytes from MYF5+ progenitors. Autophagy inhibition in MYF5^{+} cells leads to impaired BAT differentiation and function in both pups and adult mice, highlighting the importance of autophagy in BAT differentiation during the entire lifespan. These mice also exhibit glucose intolerance, although defective skeletal muscle development contributes to that phenotype (Martinez-Lopez et al., 2013). A role for mitophagy in BAT maintenance has also recently been described. Mitophagy is induced in brown adipocytes during cold-induced thermogenesis in response to UCP1-mediated mitochondrial stress. This is coupled to mitochondrial biogenesis and serves a quality control function required for the preservation of BAT function (Lu et al., 2018b).

White adipose tissue (WAT), consisting of unilocular white adipocytes that contain few mitochondria, serves as the primary energy reserve in the body; LDs from white adipocytes are

mobilized as fuel during nutrient deprivation. WAT is also an endocrine organ involved in the secretion of the appetite-regulating hormone LEP (leptin) (Kajimura, 2017), making it an important hub for metabolic regulation. Autophagy also plays an instrumental role in WAT differentiation. Adipocyte-specific *atg7* knockout mice exhibit dramatically reduced body weight, as a direct consequence of reduced white adipose tissue mass. White adipocytes in the mutants are multilocular, show smaller lipid droplets, increased cytoplasm and a greater number of mitochondria. However, the mutants do not express markers of brown adipocytes, indicating that differentiation has not been rewired along a different fate. Consistent with the increase in mitochondria, these mice exhibit increased β-oxidation, reduced lipolysis, lower serum fatty acid levels and increased insulin sensitivity. Overall, these mice remain lean irrespective of diet (Zhang et al., 2009; Singh et al., 2009b). Mitochondrial abundance is a critical difference between white and brown adipocytes, and the 'browning' of WAT is associated with an increase in mitochondrial number. One of the factors that could promote this change is a reduction in mitophagy; recent report suggests that PRKN-mediated mitophagy is indeed downregulated during the process (Taylor and Gottlieb, 2017). Therefore, autophagy plays an instrumental role in maintaining the balance of WAT and BAT.

Beige adipocytes are an inducible form of thermogenic fat cells that reside within WAT. Brown and beige adipocytes share several morphological characteristics such as multilocular lipid droplets and numerous mitochondria but are developmentally distinct (Harms and Seale, 2013). Beige adipocytes express high levels of UCP1 and emerge upon thermogenic stimulation. However, upon withdrawal of stimulation, beige cells revert to a non-thermogenic, white-adipocyte like state and lose UCP1 expression. This reversion occurs without the appearance of an intermediate cell type and is prompted by autophagy-dependent mitochondrial clearance. The

genetic deletion of *Atg5* or *Atg12* or the inhibition of lysosomal degradation using chloroquine in beige adipocytes promotes UCP1 retention and the maintenance of other beige-cell properties. Mitophagy induction during beige-to-white transition occurs through the cAMP-PRKA pathway (Altshuler-Keylin et al., 2016) and mitophagy in these cells is dependent on PRKN but not the UCP1-mediated loss of mitochondrial membrane potential (Lu et al., 2018a). Mice with prolonged maintenance of beige adipocytes exhibit decreased susceptibility to diet-induced obesity and insulin resistance (Altshuler-Keylin et al., 2016), indicating intriguing therapeutic avenues for these diseases.

1.6.2 Autophagy in pathology: The role of autophagy in cancer metabolism

As with normal cells, autophagy is an important regulator of metabolism in cancer cells (Kimmelman and White, 2017). The role of autophagy in cancer is dynamic and context dependent (Amaravadi et al., 2016). Inhibition of autophagy in mice by mosaic deletion of *Atg5* or *Atg7* promotes the development of liver neoplasms (Takamura et al., 2011; Inami et al., 2011). However, these neoplasms do not proceed to malignancy. In contrast, mice with monoallelic loss of *Becn1*, where autophagy is diminished but not absent, develop malignant tumors (Qu et al., 2003; Yue et al., 2003). Initiation of tumors in the case of partial BECN1 loss may not be solely due to decreased autophagy but also due to secondary effects on tumor-suppressors such as TP53/p53 (Liu et al., 2011); however, autophagy is critical for the sustenance of these tumors. These observations and others, coupled with infrequent mutations of core autophagy genes in human cancers (Lebovitz et al., 2015) indicate that autophagy may be important for tumor progression.

1.6.3 Autophagy in tumor-suppression: Helping cells protect themselves

In non-malignant cells autophagy is tumor-suppressive (Rybstein et al., 2018) and protects the cell from organellar dysfunction, protein-aggregation, redox imbalance, pathogens that possess transforming ability (Nakagawa et al., 2004) and genome destabilizers such as micronuclei and fragmented chromatin (Bartsch et al., 2017). Several genomic changes that compromise autophagy drive oncogenesis. The activation of the MTORC1-activating kinase AKT1 reduces autophagy and occurs frequently in cancers (Yi and Lauring, 2016). Oncogenic mutations in TP53 that prevent its nuclear localization suppress autophagy because cytoplasmic TP53 inhibits ULK1 activation (Morselli et al., 2011). Mutations in U2AF1 (U2 small nuclear RNA auxiliary factor 1) that lead to aberrant *ATG7* mRNA processing (Park et al., 2016b) are common in haematopoietic malignancies (Damm et al., 2012). The chromosomal translocation of *BRD4* to the *NUTM1/NUT* locus causes an aggressive squamous cell carcinoma. BRD4 and the BRD4-NUTM1 fusion protein were recently identified as transcriptional inhibitors of autophagy. Autophagy-deficient cells exhibit increased sensitivity to mitochondrial damage and ER stress, resulting in genomic instability and aneuploidy (Mathew et al., 2007) as well as reduced oncogene-induced senescence (Dou et al., 2015).

1.6.4 Autophagy drives tumor formation: Helping meet the metabolic needs of tumors

Once oncogenic transformation occurs, the role of autophagy switches, and tumors utilize autophagy as a cytoprotective mechanism (Rybstein et al., 2018). A large spectrum of tumors upregulate autophagy, a phenomenon associated with poor prognosis (Lazova et al., 2012). Autophagy fulfills the increased demands for energy and anabolism in rapidly proliferating cancer cells, producing simple biomolecules that can be used as energy sources or building blocks (Figure 5). Glycolytic flux is dependent on autophagy in genetically engineered mouse

models (Wei et al., 2011; Lock et al., 2011). An acute systemic ablation of *Atg7* revealed the importance of autophagy in physiological glucose homeostasis and lung tumor maintenance (Karsli-Uzunbas et al., 2014). Pancreatic ductal adenocarcinoma (PDAC), an aggressive cancer of the exocrine pancreas, exhibits MiT/TFE-family-dependent transcriptional upregulation of autophagy and lysosomal genes. The inhibition of TFE3 in PDAC decreases the pool of available metabolites, including lipids and nucleotides but particularly amino acids, highlighting the importance of autophagy in replenishing metabolic substrates (Perera et al., 2015). It is not surprising, therefore, that certain cancers such as pancreatic cancer show increased levels of basal autophagy (Yang et al., 2011). Glioblastomas and lung cancers also show a reliance on AMPK for maintenance of bioenergetics and tumor growth (Chhipa et al., 2018; Eichner et al., 2018). Additionally, AMPK-dependent upregulation of autophagy may be a mechanism of therapeutic resistance (Shteingauz et al., 2018). Indeed, inhibition of autophagy increases tumor sensitization to apoptosis (Fitzwalter et al., 2018).

The specific metabolic requirements characteristic of tumors can be met by selective autophagy (Guo et al., 2013; Strohecker et al., 2013). Malignant cells also use selective autophagy as a quality control pathway to limit organellar dysfunction that detrimentally affects tumor growth (White, 2015). Even in the hypoxic regions of tumors, mitochondrial oxidative phosphorylation generates a significant amount of ATP. The upregulation of oxidative phosphorylation may be a resistance mechanism to metformin in breast cancer (Lord et al., 2018). Conversely, damaged mitochondria promote apoptosis. Mitophagy removes damaged mitochondria, thereby regulating aerobic metabolism and preventing apoptotic signals and ROS-induced damage (Guo et al., 2011; Strohecker et al., 2013; Strohecker and White, 2014).

Recently, mitophagy has been implicated in the maintenance of the cancer stem cell population in hepatocellular carcinoma (Liu et al., 2017a).

1.6.5 Autophagy in the tumor stroma: A helping hand

The metabolic role of autophagy within tumors includes not just its role in the transformed cells themselves but expands to the metabolic rewiring of the tumor microenvironment. The tumor microenvironment (stroma), including associated fibroblasts and immune cells acts as a major source of metabolic fuel for cancer cells (Gouirand et al., 2018). The role of the stroma in providing key metabolites such as glutamine (a carbon donor for nucleotide synthesis and other anaplerotic reactions), lactate (a substrate for the TCA cycle) and free fatty acids has been investigated (Yang et al., 2016; Sonveaux et al., 2008; Wen et al., 2017; Romero et al., 2015). Recent findings also indicate that the functions of the stroma, in concert with the mutated KRAS oncogene, may influence the epigenome and metabolome of the PDAC cells (Sherman et al., 2017).

PDAC forms a highly dense, nutrient-poor and oxygen-limiting tumor (Adamska et al., 2017). PDAC survival and growth is reliant on metabolic support from stroma-associated pancreatic stellate cells (PSCs) that provide PDACs with alanine. Alanine, secreted by the PSCs, is converted into pyruvate that can then enter the TCA cycle and oxidative phosphorylation (Sousa et al., 2016). This not only allows for increased ATP production within the PDAC cells but also makes more glucose available for amino acid or nucleotide biosynthesis. PDACs induce autophagy in PSCs leading to protein degradation that releases alanine as one of the end products (Figure 5). Consequently, autophagy-deficient PSCs do not secrete alanine. PDAC cells, cultured with conditioned medium from PSCs, grow more robustly and show higher levels of oxygen consumption than those cultured without conditioned medium, indicating the importance of the

secreted alanine. However, conditioned medium from autophagy-deficient PSCs cannot promote growth of PDAC cells. Consistent with this finding, PSCs were found to have increased autophagy in the context of PDAC but not in acute pancreatitis, and the inhibition of autophagy in PSCs is detrimental to tumor growth in transplantation models (Endo et al., 2017).

Autophagy has also been implicated in promoting tumor growth by maintaining circulating arginine levels (Poillet-Perez et al., 2018). Although arginine is non-essential, arginine deficiency is detrimental to several tumor types that downregulate ASS1—an enzyme required for the de novo synthesis of arginine, using aspartate as a substrate. Downregulation of ASS1 is a metabolic switch adapted by these tumors to prevent the channeling of aspartate into arginine synthesis, instead using it for pyrimidine biosynthesis (Rabinovich et al., 2015), especially since aspartate is a limiting metabolite in hypoxic regions of tumors (Garcia-Bermudez et al., 2018). Conditional, systemic or liver-specific autophagy ablation leads to liver stress and increased release of the arginine-degrading enzyme ARG1 (arginase 1). Consequently, serum arginine levels are lowered leading to arginine deficiency and growth inhibition in tumors (Poillet-Perez et al., 2018).

Figure 5: Autophagy in tumor cells and the stroma sustains tumor progression

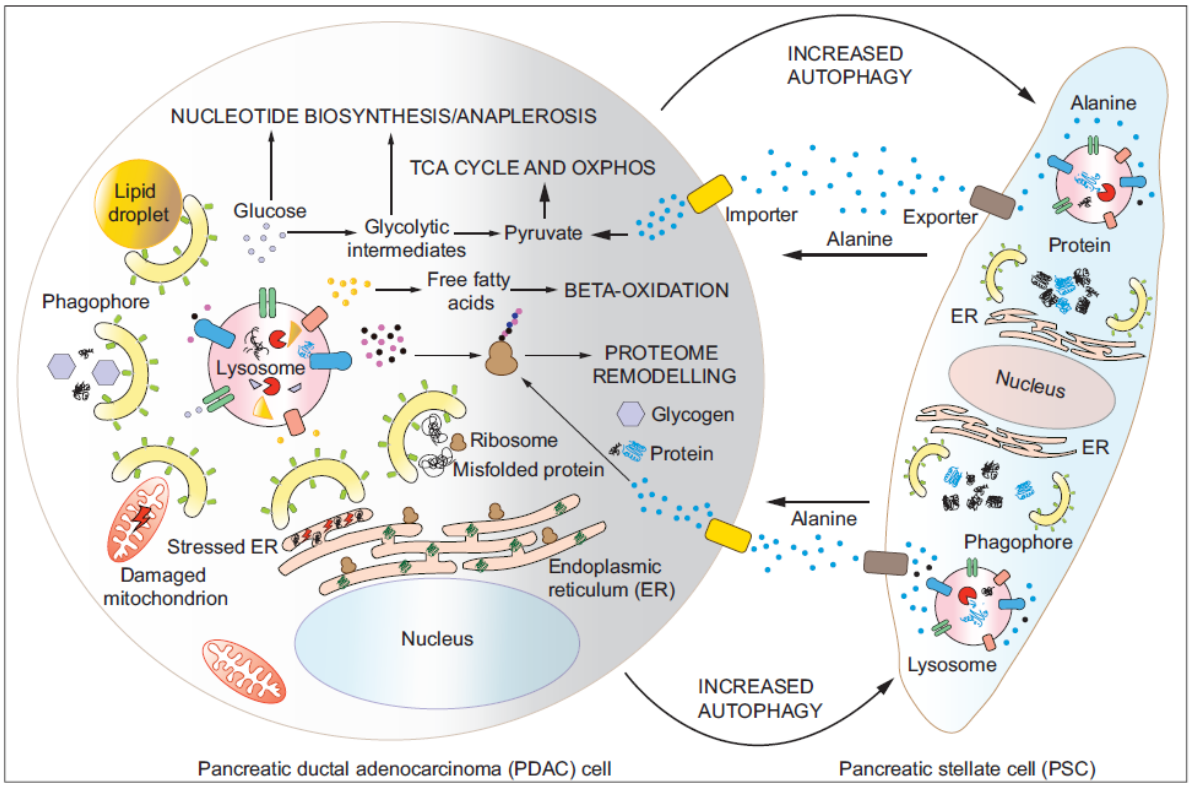

Figure 5. Autophagy in tumor cells and the stroma sustains tumor progression. Autophagy is a pro-tumorigenic pathway in transformed cells, helping them survive. Within cancer cells, autophagy removes detrimentally damaged mitochondria and helps relieve ER stress. Autophagy is also responsible for the removal of toxic, misfolded proteins. The recycling of proteins, lipid droplets, glycogen and ribosomes by autophagy promotes energy metabolism and anabolic synthesis by providing substrates for metabolic pathways. In addition, certain cancer cells like pancreatic ductal adenocarcinoma (PDAC) cells induce autophagy in neighboring stromal cells, pancreatic stellate cells (PSCs) in the case of PDAC. The degradation of proteins by autophagy in PSCs promotes alanine production and secretion. PDACs import alanine, which may be channeled into protein synthesis or, more importantly, be converted to pyruvate. This allows an external source for pyruvate and subsequent mitochondrial energy production, thereby allowing PDACs to utilize glycolytic intermediates for nucleotide synthesis and anaplerotic reactions that fuel growth (see text for details)

1.7 Conclusions and perspectives

Macroautophagy, microautophagy and CMA regulate metabolic decisions and energy flux at multiple nodes, making self-digestion an integral part of cellular energetics. Consequently, there has been increasing interest in developing tools/drugs targeting these pathways to rectify pathological states that are directly or indirectly related to altered metabolism. However, this is not trivial given the ubiquitous role of autophagy in physiological homeostasis and the increasing recognition of non-autophagy related roles of autophagy-related proteins. The ideal therapeutic approach would specifically target autophagy-related functions of these components in a manner that allows for controlled changes in self-digestion. This will require further exploration of the basic autophagic mechanisms including answers to some of the outstanding questions highlighted in this text.

One such intriguing area is the mechanism of mitophagy induction and progression in different mammalian cell types under physiological (not experimental) conditions, including the relevance of PINK1-PRKN and other parallel pathways. Another important issue to be mindful of is that a significant portion of our understanding of autophagy in mammals stems from studies in knockout mouse models where autophagy is completely abolished. This approach brings with it undesired off-target effects including possible unaccounted cellular damage and death. Instead, the use of hypomorphic alleles could provide a more accurate elucidation of autophagic mechanisms that would be instrumental in enabling the successful application of autophagy modulation as a therapeutic intervention for metabolism-related diseases.

1.8 References

Adamska, A., Domenichini, A., and Falasca, M. (2017). Pancreatic Ductal Adenocarcinoma: Current and Evolving Therapies. Int J Mol Sci 18.

Altshuler-Keylin, S., Shinoda, K., Hasegawa, Y., Ikeda, K., Hong, H., Kang, Q., Yang, Y., Perera, R.M., Debnath, J., and Kajimura, S. (2016). Beige Adipocyte Maintenance Is Regulated by Autophagy-Induced Mitochondrial Clearance. Cell Metab 24, 402-419.

Amaravadi, R., Kimmelman, A.C., and White, E. (2016). Recent insights into the function of autophagy in cancer. Genes Dev 30, 1913-1930.

An, H., and Harper, J.W. (2018). Systematic analysis of ribophagy in human cells reveals bystander flux during selective autophagy. Nat Cell Biol 20, 135-143.

Araki, K., and Nagata, K. (2011). Protein folding and quality control in the ER. Cold Spring Harb Perspect Biol 3, a007526.

Asano, T., Komatsu, M., Yamaguchi-Iwai, Y., Ishikawa, F., Mizushima, N., and Iwai, K. (2011). Distinct mechanisms of ferritin delivery to lysosomes in iron-depleted and iron-replete cells. Mol Cell Biol 31, 2040-2052.

Axe, E.L., Walker, S.A., Manifava, M., Chandra, P., Roderick, H.L., Habermann, A., Griffiths, G., and Ktistakis, N.T. (2008). Autophagosome formation from membrane compartments enriched in phosphatidylinositol 3-phosphate and dynamically connected to the endoplasmic reticulum. J Cell Biol 182, 685-701.

B'Chir, W., Maurin, A.C., Carraro, V., Averous, J., Jousse, C., Muranishi, Y., Parry, L., Stepien, G., Fafournoux, P., and Bruhat, A. (2013). The eIF2alpha/ATF4 pathway is essential for stress-induced autophagy gene expression. Nucleic Acids Res 41, 7683-7699.

Baerga, R., Zhang, Y., Chen, P.H., Goldman, S., and Jin, S. (2009). Targeted deletion of autophagy-related 5 (atg5) impairs adipogenesis in a cellular model and in mice. Autophagy 5, 1118-1130.

Bandyopadhyay, U., Kaushik, S., Varticovski, L., and Cuervo, A.M. (2008). The chaperone-mediated autophagy receptor organizes in dynamic protein complexes at the lysosomal membrane. Mol Cell Biol 28, 5747-5763.

Bandyopadhyay, U., Sridhar, S., Kaushik, S., Kiffin, R., and Cuervo, A.M. (2010). Identification of regulators of chaperone-mediated autophagy. Mol Cell 39, 535-547.

Bar-Peled, L., Chantranupong, L., Cherniack, A.D., Chen, W.W., Ottina, K.A., Grabiner, B.C., Spear, E.D., Carter, S.L., Meyerson, M., and Sabatini, D.M. (2013). A Tumor suppressor complex with GAP activity for the Rag GTPases that signal amino acid sufficiency to mTORC1. Science 340, 1100-1106.

Bartsch, K., Knittler, K., Borowski, C., Rudnik, S., Damme, M., Aden, K., Spehlmann, M.E., Frey, N., Saftig, P., Chalaris, A., et al. (2017). Absence of RNase H2 triggers generation of immunogenic micronuclei removed by autophagy. Hum Mol Genet 26, 3960-3972.

Bel, S., Pendse, M., Wang, Y., Li, Y., Ruhn, K.A., Hassell, B., Leal, T., Winter, S.E., Xavier, R.J., and Hooper, L.V. (2017). Paneth cells secrete lysozyme via secretory autophagy during bacterial infection of the intestine. Science 357, 1047-1052.

Bellelli, R., Federico, G., Matte, A., Colecchia, D., Iolascon, A., Chiariello, M., Santoro, M., De Franceschi, L., and Carlomagno, F. (2016). NCOA4 Deficiency Impairs Systemic Iron Homeostasis. Cell Rep 14, 411-421.

Bellot, G., Garcia-Medina, R., Gounon, P., Chiche, J., Roux, D., Pouyssegur, J., and Mazure, N.M. (2009). Hypoxia-induced autophagy is mediated through hypoxia-inducible factor induction of BNIP3 and BNIP3L via their BH3 domains. Mol Cell Biol 29, 2570-2581.

Benador, I.Y., Veliova, M., Mahdaviani, K., Petcherski, A., Wikstrom, J.D., Assali, E.A., Acin-Perez, R., Shum, M., Oliveira, M.F., Cinti, S., et al. (2018). Mitochondria Bound to Lipid Droplets Have Unique Bioenergetics, Composition, and Dynamics that Support Lipid Droplet Expansion. Cell Metab 27, 869-885 e866.

Bhaskar, P.T., and Hay, N. (2007). The two TORCs and Akt. Dev Cell 12, 487-502.

Bonekamp, N.A., Volkl, A., Fahimi, H.D., and Schrader, M. (2009). Reactive oxygen species and peroxisomes: struggling for balance. Biofactors 35, 346-355.

Bonhoure, A., Vallentin, A., Martin, M., Senff-Ribeiro, A., Amson, R., Telerman, A., and Vidal, M. (2017). Acetylation of translationally controlled tumor protein promotes its degradation through chaperone-mediated autophagy. Eur J Cell Biol 96, 83-98.

Bravo, R., Parra, V., Gatica, D., Rodriguez, A.E., Torrealba, N., Paredes, F., Wang, Z.V., Zorzano, A., Hill, J.A., Jaimovich, E., et al. (2013). Endoplasmic reticulum and the unfolded protein response: dynamics and metabolic integration. Int Rev Cell Mol Biol 301, 215-290.

Brugarolas, J., Lei, K., Hurley, R.L., Manning, B.D., Reiling, J.H., Hafen, E., Witters, L.A., Ellisen, L.W., and Kaelin, W.G., Jr. (2004). Regulation of mTOR function in response to hypoxia by REDD1 and the TSC1/TSC2 tumor suppressor complex. Genes Dev 18, 2893-2904.

Burke, J.A., and Schubert, W.K. (1972). Deficient activity of hepatic acid lipase in cholesterol ester storage disease. Science 176, 309-310.

Cadwell, K., and Debnath, J. (2018). Beyond self-eating: The control of nonautophagic functions and signaling pathways by autophagy-related proteins. J Cell Biol 217, 813-822.

Chantranupong, L., Scaria, S.M., Saxton, R.A., Gygi, M.P., Shen, K., Wyant, G.A., Wang, T., Harper, J.W., Gygi, S.P., and Sabatini, D.M. (2016). The CASTOR Proteins Are Arginine Sensors for the mTORC1 Pathway. Cell 165, 153-164.

Chantranupong, L., Wolfson, R.L., Orozco, J.M., Saxton, R.A., Scaria, S.M., Bar-Peled, L., Spooner, E., Isasa, M., Gygi, S.P., and Sabatini, D.M. (2014). The Sestrins interact with GATOR2 to negatively regulate the amino-acid-sensing pathway upstream of mTORC1. Cell Rep 9, 1-8.

Chen, L., Wang, J., Zhang, Y.Y., Yan, S.F., Neumann, D., Schlattner, U., Wang, Z.X., and Wu, J.W. (2012). AMP-activated protein kinase undergoes nucleotide-dependent conformational changes. Nat Struct Mol Biol 19, 716-718.

Chen, Y., Azad, M.B., and Gibson, S.B. (2009). Superoxide is the major reactive oxygen species regulating autophagy. Cell Death Differ 16, 1040-1052.

Chhipa, R.R., Fan, Q., Anderson, J., Muraleedharan, R., Huang, Y., Ciraolo, G., Chen, X., Waclaw, R., Chow, L.M., Khuchua, Z., et al. (2018). AMP kinase promotes glioblastoma bioenergetics and tumour growth. Nat Cell Biol 20, 823-835.

Cho, D.H., Kim, Y.S., Jo, D.S., Choe, S.K., and Jo, E.K. (2018). Pexophagy: Molecular Mechanisms and Implications for Health and Diseases. Mol Cells 41, 55-64.

Christofk, H.R., Vander Heiden, M.G., Harris, M.H., Ramanathan, A., Gerszten, R.E., Wei, R., Fleming, M.D., Schreiber, S.L., and Cantley, L.C. (2008). The M2 splice isoform of pyruvate kinase is important for cancer metabolism and tumour growth. Nature 452, 230-233.

Clausen, T.H., Lamark, T., Isakson, P., Finley, K., Larsen, K.B., Brech, A., Overvatn, A., Stenmark, H., Bjorkoy, G., Simonsen, A., et al. (2010). p62/SQSTM1 and ALFY interact to facilitate the formation of p62 bodies/ALIS and their degradation by autophagy. Autophagy 6, 330-344.

Crichton, R.R. (1971). Ferritin: structure, synthesis and function. N Engl J Med 284, 1413-1422.

Cunha, L.D., Yang, M., Carter, R., Guy, C., Harris, L., Crawford, J.C., Quarato, G., Boada-Romero, E., Kalkavan, H., Johnson, M.D.L., et al. (2018). LC3-Associated Phagocytosis in Myeloid Cells Promotes Tumor Immune Tolerance. Cell 175, 429-441 e416.

Damm, F., Kosmider, O., Gelsi-Boyer, V., Renneville, A., Carbuccia, N., Hidalgo-Curtis, C., Della Valle, V., Couronne, L., Scourzic, L., Chesnais, V., et al. (2012). Mutations affecting mRNA splicing define distinct clinical phenotypes and correlate with patient outcome in myelodysplastic syndromes. Blood 119, 3211-3218.

Demetriades, C., Doumpas, N., and Teleman, A.A. (2014). Regulation of TORC1 in response to amino acid starvation via lysosomal recruitment of TSC2. Cell 156, 786-799.

Deosaran, E., Larsen, K.B., Hua, R., Sargent, G., Wang, Y., Kim, S., Lamark, T., Jauregui, M., Law, K., Lippincott-Schwartz, J., et al. (2013). NBR1 acts as an autophagy receptor for peroxisomes. J Cell Sci 126, 939-952.

Deval, C., Chaveroux, C., Maurin, A.C., Cherasse, Y., Parry, L., Carraro, V., Milenkovic, D., Ferrara, M., Bruhat, A., Jousse, C., et al. (2009). Amino acid limitation regulates the expression of genes involved in several specific biological processes through GCN2-dependent and GCN2-independent pathways. FEBS J 276, 707-718.

Di Bartolomeo, S., Corazzari, M., Nazio, F., Oliverio, S., Lisi, G., Antonioli, M., Pagliarini, V., Matteoni, S., Fuoco, C., Giunta, L., et al. (2010). The dynamic interaction of AMBRA1 with the dynein motor complex regulates mammalian autophagy. J Cell Biol 191, 155-168.

Dikic, I., and Elazar, Z. (2018). Mechanism and medical implications of mammalian autophagy. Nat Rev Mol Cell Biol 19, 349-364.

Dooley, H.C., Razi, M., Polson, H.E., Girardin, S.E., Wilson, M.I., and Tooze, S.A. (2014). WIPI2 links LC3 conjugation with PI3P, autophagosome formation, and pathogen clearance by recruiting Atg12-5-16L1. Mol Cell 55, 238-252.

Dou, Z., Xu, C., Donahue, G., Shimi, T., Pan, J.A., Zhu, J., Ivanov, A., Capell, B.C., Drake, A.M., Shah, P.P., et al. (2015). Autophagy mediates degradation of nuclear lamina. Nature 527, 105-109.

Dowdle, W.E., Nyfeler, B., Nagel, J., Elling, R.A., Liu, S., Triantafellow, E., Menon, S., Wang, Z., Honda, A., Pardee, G., et al. (2014). Selective VPS34 inhibitor blocks autophagy and uncovers a role for NCOA4 in ferritin degradation and iron homeostasis in vivo. Nat Cell Biol 16, 1069-1079.

Duran, J.M., Anjard, C., Stefan, C., Loomis, W.F., and Malhotra, V. (2010). Unconventional secretion of Acb1 is mediated by autophagosomes. J Cell Biol 188, 527-536.

Efeyan, A., Zoncu, R., Chang, S., Gumper, I., Snitkin, H., Wolfson, R.L., Kirak, O., Sabatini, D.D., and Sabatini, D.M. (2013). Regulation of mTORC1 by the Rag GTPases is necessary for neonatal autophagy and survival. Nature 493, 679-683.

Eichner, L.J., Brun, S.N., Herzig, S., Young, N.P., Curtis, S.D., Shackelford, D.B., Shokhirev, M.N., Leblanc, M., Vera, L.I., Hutchins, A., et al. (2018). Genetic Analysis Reveals AMPK

Is Required to Support Tumor Growth in Murine Kras-Dependent Lung Cancer Models. Cell Metab.

Eisenberg, T., Schroeder, S., Andryushkova, A., Pendl, T., Kuttner, V., Bhukel, A., Marino, G., Pietrocola, F., Harger, A., Zimmermann, A., et al. (2014). Nucleocytosolic depletion of the energy metabolite acetyl-coenzyme a stimulates autophagy and prolongs lifespan. Cell Metab 19, 431-444.

Endo, S., Nakata, K., Ohuchida, K., Takesue, S., Nakayama, H., Abe, T., Koikawa, K., Okumura, T., Sada, M., Horioka, K., et al. (2017). Autophagy Is Required for Activation of Pancreatic Stellate Cells, Associated With Pancreatic Cancer Progression and Promotes Growth of Pancreatic Tumors in Mice. Gastroenterology 152, 1492-1506 e1424.

Farre, J.C., Burkenroad, A., Burnett, S.F., and Subramani, S. (2013). Phosphorylation of mitophagy and pexophagy receptors coordinates their interaction with Atg8 and Atg11. EMBO Rep 14, 441-449.

Farre, J.C., Manjithaya, R., Mathewson, R.D., and Subramani, S. (2008). PpAtg30 tags peroxisomes for turnover by selective autophagy. Dev Cell 14, 365-376.

Fedorenko, A., Lishko, P.V., and Kirichok, Y. (2012). Mechanism of fatty-acid-dependent UCP1 uncoupling in brown fat mitochondria. Cell 151, 400-413.

Feng, Y., He, D., Yao, Z., and Klionsky, D.J. (2014). The machinery of macroautophagy. Cell Res 24, 24-41.

Fernandez, A.F., Sebti, S., Wei, Y., Zou, Z., Shi, M., McMillan, K.L., He, C., Ting, T., Liu, Y., Chiang, W.C., et al. (2018). Disruption of the beclin 1-BCL2 autophagy regulatory complex promotes longevity in mice. Nature 558, 136-140.

Ferreira, J.V., Soares, A.R., Ramalho, J.S., Pereira, P., and Girao, H. (2015). K63 linked ubiquitin chain formation is a signal for HIF1A degradation by Chaperone-Mediated Autophagy. Sci Rep 5, 10210.

Filimonenko, M., Isakson, P., Finley, K.D., Anderson, M., Jeong, H., Melia, T.J., Bartlett, B.J., Myers, K.M., Birkeland, H.C., Lamark, T., et al. (2010). The selective macroautophagic degradation of aggregated proteins requires the PI3P-binding protein Alfy. Mol Cell 38, 265-279.

Fitzwalter, B.E., Towers, C.G., Sullivan, K.D., Andrysik, Z., Hoh, M., Ludwig, M., O'Prey, J., Ryan, K.M., Espinosa, J.M., Morgan, M.J., et al. (2018). Autophagy Inhibition Mediates Apoptosis Sensitization in Cancer Therapy by Relieving FOXO3a Turnover. Dev Cell 44, 555-565 e553.

Frake, R.A., Ricketts, T., Menzies, F.M., and Rubinsztein, D.C. (2015). Autophagy and neurodegeneration. J Clin Invest 125, 65-74.

Franco, R., Martinez-Pinilla, E., Navarro, G., and Zamarbide, M. (2017). Potential of GPCRs to modulate MAPK and mTOR pathways in Alzheimer's disease. Prog Neurobiol 149-150, 21-38.

Galluzzi, L., Pietrocola, F., Bravo-San Pedro, J.M., Amaravadi, R.K., Baehrecke, E.H., Cecconi, F., Codogno, P., Debnath, J., Gewirtz, D.A., Karantza, V., et al. (2015). Autophagy in malignant transformation and cancer progression. EMBO J 34, 856-880.

Galluzzi, L., Pietrocola, F., Levine, B., and Kroemer, G. (2014). Metabolic control of autophagy. Cell 159, 1263-1276.

Gao, X., Lee, H.Y., Li, W., Platt, R.J., Barrasa, M.I., Ma, Q., Elmes, R.R., Rosenfeld, M.G., and Lodish, H.F. (2017). Thyroid hormone receptor beta and NCOA4 regulate terminal erythrocyte differentiation. Proc Natl Acad Sci U S A 114, 10107-10112.

Garcia-Bermudez, J., Baudrier, L., La, K., Zhu, X.G., Fidelin, J., Sviderskiy, V.O., Papagiannakopoulos, T., Molina, H., Snuderl, M., Lewis, C.A., et al. (2018). Aspartate is a limiting metabolite for cancer cell proliferation under hypoxia and in tumours. Nat Cell Biol 20, 775-781.

Gatica, D., Lahiri, V., and Klionsky, D.J. (2018). Cargo recognition and degradation by selective autophagy. Nat Cell Biol 20, 233-242.

Geisler, S., Holmstrom, K.M., Skujat, D., Fiesel, F.C., Rothfuss, O.C., Kahle, P.J., and Springer, W. (2010). PINK1/Parkin-mediated mitophagy is dependent on VDAC1 and p62/SQSTM1. Nat Cell Biol 12, 119-131.

Ghosh, A., and Pahan, K. (2016). PPARalpha in lysosomal biogenesis: A perspective. Pharmacol Res 103, 144-148.

Gingras, A.C., Kennedy, S.G., O'Leary, M.A., Sonenberg, N., and Hay, N. (1998). 4E-BP1, a repressor of mRNA translation, is phosphorylated and inactivated by the Akt(PKB) signaling pathway. Genes Dev 12, 502-513.

Goodwin, J.M., Dowdle, W.E., DeJesus, R., Wang, Z., Bergman, P., Kobylarz, M., Lindeman, A., Xavier, R.J., McAllister, G., Nyfeler, B., et al. (2017). Autophagy-Independent Lysosomal Targeting Regulated by ULK1/2-FIP200 and ATG9. Cell Rep 20, 2341-2356.

Gouirand, V., Guillaumond, F., and Vasseur, S. (2018). Influence of the Tumor Microenvironment on Cancer Cells Metabolic Reprogramming. Front Oncol 8, 117.

Greenberg, A.S., Coleman, R.A., Kraemer, F.B., McManaman, J.L., Obin, M.S., Puri, V., Yan, Q.W., Miyoshi, H., and Mashek, D.G. (2011). The role of lipid droplets in metabolic disease in rodents and humans. J Clin Invest 121, 2102-2110.

Gu, X., Orozco, J.M., Saxton, R.A., Condon, K.J., Liu, G.Y., Krawczyk, P.A., Scaria, S.M., Harper, J.W., Gygi, S.P., and Sabatini, D.M. (2017). SAMTOR is an S-adenosylmethionine sensor for the mTORC1 pathway. Science 358, 813-818.

Guo, H., Chitiprolu, M., Roncevic, L., Javalet, C., Hemming, F.J., Trung, M.T., Meng, L., Latreille, E., Tanese de Souza, C., McCulloch, D., et al. (2017). Atg5 Disassociates the V1V0-ATPase to Promote Exosome Production and Tumor Metastasis Independent of Canonical Macroautophagy. Dev Cell 43, 716-730 e717.

Guo, J.Y., Chen, H.Y., Mathew, R., Fan, J., Strohecker, A.M., Karsli-Uzunbas, G., Kamphorst, J.J., Chen, G., Lemons, J.M., Karantza, V., et al. (2011). Activated Ras requires autophagy to maintain oxidative metabolism and tumorigenesis. Genes Dev 25, 460-470.

Guo, J.Y., Karsli-Uzunbas, G., Mathew, R., Aisner, S.C., Kamphorst, J.J., Strohecker, A.M., Chen, G., Price, S., Lu, W., Teng, X., et al. (2013). Autophagy suppresses progression of K-ras-induced lung tumors to oncocytomas and maintains lipid homeostasis. Genes Dev 27, 1447-1461.

Gwinn, D.M., Shackelford, D.B., Egan, D.F., Mihaylova, M.M., Mery, A., Vasquez, D.S., Turk, B.E., and Shaw, R.J. (2008). AMPK phosphorylation of raptor mediates a metabolic checkpoint. Mol Cell 30, 214-226.

Haberzettl, P., and Hill, B.G. (2013). Oxidized lipids activate autophagy in a JNK-dependent manner by stimulating the endoplasmic reticulum stress response. Redox Biol 1, 56-64.

Harder, L.M., Bunkenborg, J., and Andersen, J.S. (2014). Inducing autophagy: a comparative phosphoproteomic study of the cellular response to ammonia and rapamycin. Autophagy 10, 339-355.

Hardie, D.G., Schaffer, B.E., and Brunet, A. (2016). AMPK: An Energy-Sensing Pathway with Multiple Inputs and Outputs. Trends Cell Biol 26, 190-201.

Hariharan, N., Maejima, Y., Nakae, J., Paik, J., Depinho, R.A., and Sadoshima, J. (2010). Deacetylation of FoxO by Sirt1 Plays an Essential Role in Mediating Starvation-Induced Autophagy in Cardiac Myocytes. Circ Res 107, 1470-1482.

Harms, M., and Seale, P. (2013). Brown and beige fat: development, function and therapeutic potential. Nat Med 19, 1252-1263.

Haynes, C.M., Yang, Y., Blais, S.P., Neubert, T.A., and Ron, D. (2010). The matrix peptide exporter HAF-1 signals a mitochondrial UPR by activating the transcription factor ZC376.7 in C. elegans. Mol Cell 37, 529-540.

He, C., Zhu, H., Li, H., Zou, M.H., and Xie, Z. (2013). Dissociation of Bcl-2-Beclin1 complex by activated AMPK enhances cardiac autophagy and protects against cardiomyocyte apoptosis in diabetes. Diabetes 62, 1270-1281.

He, Y., She, H., Zhang, T., Xu, H., Cheng, L., Yepes, M., Zhao, Y., and Mao, Z. (2018). p38 MAPK inhibits autophagy and promotes microglial inflammatory responses by phosphorylating ULK1. J Cell Biol 217, 315-328.

Hoyer-Hansen, M., Bastholm, L., Szyniarowski, P., Campanella, M., Szabadkai, G., Farkas, T., Bianchi, K., Fehrenbacher, N., Elling, F., Rizzuto, R., et al. (2007). Control of macroautophagy by calcium, calmodulin-dependent kinase kinase-beta, and Bcl-2. Mol Cell 25, 193-205.

Hubbi, M.E., Hu, H., Kshitiz, Ahmed, I., Levchenko, A., and Semenza, G.L. (2013). Chaperone-mediated autophagy targets hypoxia-inducible factor-1alpha (HIF-1alpha) for lysosomal degradation. J Biol Chem 288, 10703-10714.

Hudson, C.C., Liu, M., Chiang, G.G., Otterness, D.M., Loomis, D.C., Kaper, F., Giaccia, A.J., and Abraham, R.T. (2002). Regulation of hypoxia-inducible factor 1alpha expression and function by the mammalian target of rapamycin. Mol Cell Biol 22, 7004-7014.

Inami, Y., Waguri, S., Sakamoto, A., Kouno, T., Nakada, K., Hino, O., Watanabe, S., Ando, J., Iwadate, M., Yamamoto, M., et al. (2011). Persistent activation of Nrf2 through p62 in hepatocellular carcinoma cells. J Cell Biol 193, 275-284.

Inoki, K., Ouyang, H., Zhu, T., Lindvall, C., Wang, Y., Zhang, X., Yang, Q., Bennett, C., Harada, Y., Stankunas, K., et al. (2006). TSC2 integrates Wnt and energy signals via a coordinated phosphorylation by AMPK and GSK3 to regulate cell growth. Cell 126, 955-968.

Itakura, E., Kishi, C., Inoue, K., and Mizushima, N. (2008). Beclin 1 forms two distinct phosphatidylinositol 3-kinase complexes with mammalian Atg14 and UVRAG. Mol Biol Cell 19, 5360-5372.

Jiang, L., Hara-Kuge, S., Yamashita, S., and Fujiki, Y. (2015). Peroxin Pex14p is the key component for coordinated autophagic degradation of mammalian peroxisomes by direct binding to LC3-II. Genes Cells 20, 36-49.

Jiang, S., Heller, B., Tagliabracci, V.S., Zhai, L., Irimia, J.M., DePaoli-Roach, A.A., Wells, C.D., Skurat, A.V., and Roach, P.J. (2010). Starch binding domain-containing protein 1/genethonin 1 is a novel participant in glycogen metabolism. J Biol Chem 285, 34960-34971.

Jiang, S., Wells, C.D., and Roach, P.J. (2011). Starch-binding domain-containing protein 1 (Stbd1) and glycogen metabolism: Identification of the Atg8 family interacting motif (AIM) in Stbd1 required for interaction with GABARAPL1. Biochem Biophys Res Commun 413, 420-425.

Jung, J., Genau, H.M., and Behrends, C. (2015). Amino Acid-Dependent mTORC1 Regulation by the Lysosomal Membrane Protein SLC38A9. Mol Cell Biol 35, 2479-2494.
Kajimura, S. (2017). Adipose tissue in 2016: Advances in the understanding of adipose tissue biology. Nat Rev Endocrinol 13, 69-70.
Kane, L.A., Lazarou, M., Fogel, A.I., Li, Y., Yamano, K., Sarraf, S.A., Banerjee, S., and Youle, R.J. (2014). PINK1 phosphorylates ubiquitin to activate Parkin E3 ubiquitin ligase activity. J Cell Biol 205, 143-153.
Kanki, T., Wang, K., Cao, Y., Baba, M., and Klionsky, D.J. (2009). Atg32 is a mitochondrial protein that confers selectivity during mitophagy. Dev Cell 17, 98-109.
Karsli-Uzunbas, G., Guo, J.Y., Price, S., Teng, X., Laddha, S.V., Khor, S., Kalaany, N.Y., Jacks, T., Chan, C.S., Rabinowitz, J.D., et al. (2014). Autophagy is required for glucose homeostasis and lung tumor maintenance. Cancer Discov 4, 914-927.
Kaur, J., and Debnath, J. (2015). Autophagy at the crossroads of catabolism and anabolism. Nat Rev Mol Cell Biol 16, 461-472.
Kaushik, S., and Cuervo, A.M. (2015). Degradation of lipid droplet-associated proteins by chaperone-mediated autophagy facilitates lipolysis. Nat Cell Biol 17, 759-770.
Kaushik, S., and Cuervo, A.M. (2016). AMPK-dependent phosphorylation of lipid droplet protein PLIN2 triggers its degradation by CMA. Autophagy 12, 432-438.
Kaushik, S., and Cuervo, A.M. (2018). The coming of age of chaperone-mediated autophagy. Nat Rev Mol Cell Biol 19, 365-381.
Kaushik, S., Massey, A.C., Mizushima, N., and Cuervo, A.M. (2008). Constitutive activation of chaperone-mediated autophagy in cells with impaired macroautophagy. Mol Biol Cell 19, 2179-2192.
Kaushik, S., Rodriguez-Navarro, J.A., Arias, E., Kiffin, R., Sahu, S., Schwartz, G.J., Cuervo, A.M., and Singh, R. (2011). Autophagy in hypothalamic AgRP neurons regulates food intake and energy balance. Cell Metab 14, 173-183.
Khaminets, A., Heinrich, T., Mari, M., Grumati, P., Huebner, A.K., Akutsu, M., Liebmann, L., Stolz, A., Nietzsche, S., Koch, N., et al. (2015). Regulation of endoplasmic reticulum turnover by selective autophagy. Nature 522, 354-358.
Khan, S.A., Sathyanarayan, A., Mashek, M.T., Ong, K.T., Wollaston-Hayden, E.E., and Mashek, D.G. (2015). ATGL-catalyzed lipolysis regulates SIRT1 to control PGC-1alpha/PPAR-alpha signaling. Diabetes 64, 418-426.
Kihara, A., Noda, T., Ishihara, N., and Ohsumi, Y. (2001). Two distinct Vps34 phosphatidylinositol 3-kinase complexes function in autophagy and carboxypeptidase Y sorting in Saccharomyces cerevisiae. J Cell Biol 152, 519-530.
Kim, J., Kim, Y.C., Fang, C., Russell, R.C., Kim, J.H., Fan, W., Liu, R., Zhong, Q., and Guan, K.L. (2013). Differential regulation of distinct Vps34 complexes by AMPK in nutrient stress and autophagy. Cell 152, 290-303.
Kim, J., Kundu, M., Viollet, B., and Guan, K.L. (2011). AMPK and mTOR regulate autophagy through direct phosphorylation of Ulk1. Nat Cell Biol 13, 132-141.
Kim, P.K., Hailey, D.W., Mullen, R.T., and Lippincott-Schwartz, J. (2008). Ubiquitin signals autophagic degradation of cytosolic proteins and peroxisomes. Proc Natl Acad Sci U S A 105, 20567-20574.
Kim, Y.M., Jung, C.H., Seo, M., Kim, E.K., Park, J.M., Bae, S.S., and Kim, D.H. (2015). mTORC1 phosphorylates UVRAG to negatively regulate autophagosome and endosome maturation. Mol Cell 57, 207-218.

Kimmelman, A.C., and White, E. (2017). Autophagy and Tumor Metabolism. Cell Metab 25, 1037-1043.
Kirkin, V., Lamark, T., Sou, Y.S., Bjorkoy, G., Nunn, J.L., Bruun, J.A., Shvets, E., McEwan, D.G., Clausen, T.H., Wild, P., et al. (2009). A role for NBR1 in autophagosomal degradation of ubiquitinated substrates. Mol Cell 33, 505-516.
Kishi-Itakura, C., Koyama-Honda, I., Itakura, E., and Mizushima, N. (2014). Ultrastructural analysis of autophagosome organization using mammalian autophagy-deficient cells. J Cell Sci 127, 4089-4102.
Kishnani, P.S., Corzo, D., Nicolino, M., Byrne, B., Mandel, H., Hwu, W.L., Leslie, N., Levine, J., Spencer, C., McDonald, M., et al. (2007). Recombinant human acid [alpha]-glucosidase: major clinical benefits in infantile-onset Pompe disease. Neurology 68, 99-109.
Knaevelsrud, H., Soreng, K., Raiborg, C., Haberg, K., Rasmuson, F., Brech, A., Liestol, K., Rusten, T.E., Stenmark, H., Neufeld, T.P., et al. (2013). Membrane remodeling by the PX-BAR protein SNX18 promotes autophagosome formation. J Cell Biol 202, 331-349.
Komiya, K., Uchida, T., Ueno, T., Koike, M., Abe, H., Hirose, T., Kawamori, R., Uchiyama, Y., Kominami, E., Fujitani, Y., et al. (2010). Free fatty acids stimulate autophagy in pancreatic beta-cells via JNK pathway. Biochem Biophys Res Commun 401, 561-567.
Kondapalli, C., Kazlauskaite, A., Zhang, N., Woodroof, H.I., Campbell, D.G., Gourlay, R., Burchell, L., Walden, H., Macartney, T.J., Deak, M., et al. (2012). PINK1 is activated by mitochondrial membrane potential depolarization and stimulates Parkin E3 ligase activity by phosphorylating Serine 65. Open Biol 2, 120080.
Kondomerkos, D.J., Kalamidas, S.A., Kotoulas, O.B., and Hann, A.C. (2005). Glycogen autophagy in the liver and heart of newborn rats. The effects of glucagon, adrenalin or rapamycin. Histol Histopathol 20, 689-696.
Korolchuk, V.I., Menzies, F.M., and Rubinsztein, D.C. (2010). Mechanisms of cross-talk between the ubiquitin-proteasome and autophagy-lysosome systems. FEBS Lett 584, 1393-1398.
Koyano, F., Okatsu, K., Kosako, H., Tamura, Y., Go, E., Kimura, M., Kimura, Y., Tsuchiya, H., Yoshihara, H., Hirokawa, T., et al. (2014). Ubiquitin is phosphorylated by PINK1 to activate parkin. Nature 510, 162-166.
Kraft, C., Deplazes, A., Sohrmann, M., and Peter, M. (2008). Mature ribosomes are selectively degraded upon starvation by an autophagy pathway requiring the Ubp3p/Bre5p ubiquitin protease. Nat Cell Biol 10, 602-610.
Ktistakis, N.T., and Tooze, S.A. (2016). Digesting the Expanding Mechanisms of Autophagy. Trends Cell Biol 26, 624-635.
Kuchler, K., Sterne, R.E., and Thorner, J. (1989). Saccharomyces cerevisiae STE6 gene product: a novel pathway for protein export in eukaryotic cells. EMBO J 8, 3973-3984.
Kuma, A., Hatano, M., Matsui, M., Yamamoto, A., Nakaya, H., Yoshimori, T., Ohsumi, Y., Tokuhisa, T., and Mizushima, N. (2004). The role of autophagy during the early neonatal starvation period. Nature 432, 1032-1036.
Kuroki, T., Osari, S., Nagata, K., and Kawaguchi, A. (2018). Influenza A Virus NS1 Protein Suppresses JNK1-Dependent Autophagosome Formation Mediated by Rab11a Recycling Endosomes. Front Microbiol 9, 3120.
Lawson, D.M., Artymiuk, P.J., Yewdall, S.J., Smith, J.M., Livingstone, J.C., Treffry, A., Luzzago, A., Levi, S., Arosio, P., Cesareni, G., et al. (1991). Solving the structure of human H ferritin by genetically engineering intermolecular crystal contacts. Nature 349, 541-544.

Lazarou, M., Sliter, D.A., Kane, L.A., Sarraf, S.A., Wang, C., Burman, J.L., Sideris, D.P., Fogel, A.I., and Youle, R.J. (2015). The ubiquitin kinase PINK1 recruits autophagy receptors to induce mitophagy. Nature 524, 309-314.

Lazova, R., Camp, R.L., Klump, V., Siddiqui, S.F., Amaravadi, R.K., and Pawelek, J.M. (2012). Punctate LC3B expression is a common feature of solid tumors and associated with proliferation, metastasis, and poor outcome. Clin Cancer Res 18, 370-379.

Le Guerroue, F., Eck, F., Jung, J., Starzetz, T., Mittelbronn, M., Kaulich, M., and Behrends, C. (2017). Autophagosomal Content Profiling Reveals an LC3C-Dependent Piecemeal Mitophagy Pathway. Mol Cell 68, 786-796 e786.

Lebovitz, C.B., Robertson, A.G., Goya, R., Jones, S.J., Morin, R.D., Marra, M.A., and Gorski, S.M. (2015). Cross-cancer profiling of molecular alterations within the human autophagy interaction network. Autophagy 11, 1668-1687.

Lee, I.H., Cao, L., Mostoslavsky, R., Lombard, D.B., Liu, J., Bruns, N.E., Tsokos, M., Alt, F.W., and Finkel, T. (2008). A role for the NAD-dependent deacetylase Sirt1 in the regulation of autophagy. Proc Natl Acad Sci U S A 105, 3374-3379.

Lemasters, J.J. (2014). Variants of mitochondrial autophagy: Types 1 and 2 mitophagy and micromitophagy (Type 3). Redox Biol 2, 749-754.

Li, W.W., Li, J., and Bao, J.K. (2012). Microautophagy: lesser-known self-eating. Cell Mol Life Sci 69, 1125-1136.

Li, X., Yu, W., Qian, X., Xia, Y., Zheng, Y., Lee, J.H., Li, W., Lyu, J., Rao, G., Zhang, X., et al. (2017). Nucleus-Translocated ACSS2 Promotes Gene Transcription for Lysosomal Biogenesis and Autophagy. Mol Cell 66, 684-697 e689.

Li, Z., Schulze, R.J., Weller, S.G., Krueger, E.W., Schott, M.B., Zhang, X., Casey, C.A., Liu, J., Stockli, J., James, D.E., et al. (2016). A novel Rab10-EHBP1-EHD2 complex essential for the autophagic engulfment of lipid droplets. Sci Adv 2, e1601470.

Lim, Y.M., Lim, H., Hur, K.Y., Quan, W., Lee, H.Y., Cheon, H., Ryu, D., Koo, S.H., Kim, H.L., Kim, J., et al. (2014). Systemic autophagy insufficiency compromises adaptation to metabolic stress and facilitates progression from obesity to diabetes. Nat Commun 5, 4934.

Liu, J., Xia, H., Kim, M., Xu, L., Li, Y., Zhang, L., Cai, Y., Norberg, H.V., Zhang, T., Furuya, T., et al. (2011). Beclin1 controls the levels of p53 by regulating the deubiquitination activity of USP10 and USP13. Cell 147, 223-234.

Liu, K., Lee, J., Kim, J.Y., Wang, L., Tian, Y., Chan, S.T., Cho, C., Machida, K., Chen, D., and Ou, J.J. (2017a). Mitophagy Controls the Activities of Tumor Suppressor p53 to Regulate Hepatic Cancer Stem Cells. Mol Cell 68, 281-292 e285.

Liu, L., Feng, D., Chen, G., Chen, M., Zheng, Q., Song, P., Ma, Q., Zhu, C., Wang, R., Qi, W., et al. (2012). Mitochondrial outer-membrane protein FUNDC1 mediates hypoxia-induced mitophagy in mammalian cells. Nat Cell Biol 14, 177-185.

Liu, P., Bartz, R., Zehmer, J.K., Ying, Y.S., Zhu, M., Serrero, G., and Anderson, R.G. (2007). Rab-regulated interaction of early endosomes with lipid droplets. Biochim Biophys Acta 1773, 784-793.

Liu, X., Li, Y., Wang, X., Xing, R., Liu, K., Gan, Q., Tang, C., Gao, Z., Jian, Y., Luo, S., et al. (2017b). The BEACH-containing protein WDR81 coordinates p62 and LC3C to promote aggrephagy. J Cell Biol 216, 1301-1320.

Lizaso, A., Tan, K.T., and Lee, Y.H. (2013). beta-adrenergic receptor-stimulated lipolysis requires the RAB7-mediated autolysosomal lipid degradation. Autophagy 9, 1228-1243.

Lock, R., Roy, S., Kenific, C.M., Su, J.S., Salas, E., Ronen, S.M., and Debnath, J. (2011). Autophagy facilitates glycolysis during Ras-mediated oncogenic transformation. Mol Biol Cell 22, 165-178.

Lomakin, I.B., Xiong, Y., and Steitz, T.A. (2007). The crystal structure of yeast fatty acid synthase, a cellular machine with eight active sites working together. Cell 129, 319-332.

Lord, S.R., Cheng, W.C., Liu, D., Gaude, E., Haider, S., Metcalf, T., Patel, N., Teoh, E.J., Gleeson, F., Bradley, K., et al. (2018). Integrated Pharmacodynamic Analysis Identifies Two Metabolic Adaption Pathways to Metformin in Breast Cancer. Cell Metab 28, 679-688 e674.

Lu, K., den Brave, F., and Jentsch, S. (2017). Receptor oligomerization guides pathway choice between proteasomal and autophagic degradation. Nat Cell Biol 19, 732-739.

Lu, K., Psakhye, I., and Jentsch, S. (2014a). Autophagic clearance of polyQ proteins mediated by ubiquitin-Atg8 adaptors of the conserved CUET protein family. Cell 158, 549-563.

Lu, K., Psakhye, I., and Jentsch, S. (2014b). A new class of ubiquitin-Atg8 receptors involved in selective autophagy and polyQ protein clearance. Autophagy 10, 2381-2382.

Lu, X., Altshuler-Keylin, S., Wang, Q., Chen, Y., Henrique Sponton, C., Ikeda, K., Maretich, P., Yoneshiro, T., and Kajimura, S. (2018a). Mitophagy controls beige adipocyte maintenance through a Parkin-dependent and UCP1-independent mechanism. Sci Signal 11.

Lu, Y., Fujioka, H., Joshi, D., Li, Q., Sangwung, P., Hsieh, P., Zhu, J., Torio, J., Sweet, D., Wang, L., et al. (2018b). Mitophagy is required for brown adipose tissue mitochondrial homeostasis during cold challenge. Sci Rep 8, 8251.

Lv, L., Li, D., Zhao, D., Lin, R., Chu, Y., Zhang, H., Zha, Z., Liu, Y., Li, Z., Xu, Y., et al. (2011). Acetylation targets the M2 isoform of pyruvate kinase for degradation through chaperone-mediated autophagy and promotes tumor growth. Mol Cell 42, 719-730.

Lystad, A.H., Ichimura, Y., Takagi, K., Yang, Y., Pankiv, S., Kanegae, Y., Kageyama, S., Suzuki, M., Saito, I., Mizushima, T., et al. (2014). Structural determinants in GABARAP required for the selective binding and recruitment of ALFY to LC3B-positive structures. EMBO Rep 15, 557-565.

Madrigal-Matute, J., and Cuervo, A.M. (2016). Regulation of Liver Metabolism by Autophagy. Gastroenterology 150, 328-339.

Mancias, J.D., Pontano Vaites, L., Nissim, S., Biancur, D.E., Kim, A.J., Wang, X., Liu, Y., Goessling, W., Kimmelman, A.C., and Harper, J.W. (2015). Ferritinophagy via NCOA4 is required for erythropoiesis and is regulated by iron dependent HERC2-mediated proteolysis. Elife 4.

Mancias, J.D., Wang, X., Gygi, S.P., Harper, J.W., and Kimmelman, A.C. (2014). Quantitative proteomics identifies NCOA4 as the cargo receptor mediating ferritinophagy. Nature 509, 105-109.

Mandl, J., and Banhegyi, G. (2018). The ER - Glycogen Particle - Phagophore Triangle: A Hub Connecting Glycogenolysis and Glycophagy? Pathol Oncol Res 24, 821-826.

Manjithaya, R., Anjard, C., Loomis, W.F., and Subramani, S. (2010). Unconventional secretion of Pichia pastoris Acb1 is dependent on GRASP protein, peroxisomal functions, and autophagosome formation. J Cell Biol 188, 537-546.

Mao, K., Liu, X., Feng, Y., and Klionsky, D.J. (2014). The progression of peroxisomal degradation through autophagy requires peroxisomal division. Autophagy 10, 652-661.

Marasco, M.R., and Linnemann, A.K. (2018). beta-Cell Autophagy in Diabetes Pathogenesis. Endocrinology 159, 2127-2141.

Marino, G., Pietrocola, F., Eisenberg, T., Kong, Y., Malik, S.A., Andryushkova, A., Schroeder, S., Pendl, T., Harger, A., Niso-Santano, M., et al. (2014). Regulation of autophagy by cytosolic acetyl-coenzyme A. Mol Cell 53, 710-725.

Martina, J.A., Chen, Y., Gucek, M., and Puertollano, R. (2012). MTORC1 functions as a transcriptional regulator of autophagy by preventing nuclear transport of TFEB. Autophagy 8, 903-914.

Martinez-Lopez, N., Athonvarangkul, D., Sahu, S., Coletto, L., Zong, H., Bastie, C.C., Pessin, J.E., Schwartz, G.J., and Singh, R. (2013). Autophagy in Myf5+ progenitors regulates energy and glucose homeostasis through control of brown fat and skeletal muscle development. EMBO Rep 14, 795-803.

Martinez-Lopez, N., Garcia-Macia, M., Sahu, S., Athonvarangkul, D., Liebling, E., Merlo, P., Cecconi, F., Schwartz, G.J., and Singh, R. (2016). Autophagy in the CNS and Periphery Coordinate Lipophagy and Lipolysis in the Brown Adipose Tissue and Liver. Cell Metab 23, 113-127.

Martinez-Lopez, N., and Singh, R. (2014). ATGs: Scaffolds for MAPK/ERK signaling. Autophagy 10, 535-537.

Martinez, J., Malireddi, R.K., Lu, Q., Cunha, L.D., Pelletier, S., Gingras, S., Orchard, R., Guan, J.L., Tan, H., Peng, J., et al. (2015). Molecular characterization of LC3-associated phagocytosis reveals distinct roles for Rubicon, NOX2 and autophagy proteins. Nat Cell Biol 17, 893-906.

Massey, A.C., Kaushik, S., Sovak, G., Kiffin, R., and Cuervo, A.M. (2006). Consequences of the selective blockage of chaperone-mediated autophagy. Proc Natl Acad Sci U S A 103, 5805-5810.

Mathew, R., Kongara, S., Beaudoin, B., Karp, C.M., Bray, K., Degenhardt, K., Chen, G., Jin, S., and White, E. (2007). Autophagy suppresses tumor progression by limiting chromosomal instability. Genes Dev 21, 1367-1381.

McLelland, G.L., Lee, S.A., McBride, H.M., and Fon, E.A. (2016). Syntaxin-17 delivers PINK1/parkin-dependent mitochondrial vesicles to the endolysosomal system. J Cell Biol 214, 275-291.

McWilliams, T.G., Prescott, A.R., Montava-Garriga, L., Ball, G., Singh, F., Barini, E., Muqit, M.M.K., Brooks, S.P., and Ganley, I.G. (2018). Basal Mitophagy Occurs Independently of PINK1 in Mouse Tissues of High Metabolic Demand. Cell Metab 27, 439-449 e435.

Melber, A., and Haynes, C.M. (2018). UPR(mt) regulation and output: a stress response mediated by mitochondrial-nuclear communication. Cell Res 28, 281-295.

Mellor, K.M., Varma, U., Stapleton, D.I., and Delbridge, L.M. (2014). Cardiomyocyte glycophagy is regulated by insulin and exposure to high extracellular glucose. Am J Physiol Heart Circ Physiol 306, H1240-1245.

Meng, J., and Ferguson, S.M. (2018). GATOR1-dependent recruitment of FLCN-FNIP to lysosomes coordinates Rag GTPase heterodimer nucleotide status in response to amino acids. J Cell Biol 217, 2765-2776.

Menon, S., Dibble, C.C., Talbott, G., Hoxhaj, G., Valvezan, A.J., Takahashi, H., Cantley, L.C., and Manning, B.D. (2014). Spatial control of the TSC complex integrates insulin and nutrient regulation of mTORC1 at the lysosome. Cell 156, 771-785.

Mestre, M.B., and Colombo, M.I. (2012). cAMP and EPAC are key players in the regulation of the signal transduction pathway involved in the alpha-hemolysin autophagic response. PLoS Pathog 8, e1002664.

Mihaylova, M.M., and Shaw, R.J. (2011). The AMPK signalling pathway coordinates cell growth, autophagy and metabolism. Nat Cell Biol 13, 1016-1023.
Mishra, P., and Chan, D.C. (2016). Metabolic regulation of mitochondrial dynamics. J Cell Biol 212, 379-387.
Mizushima, N., and Komatsu, M. (2011). Autophagy: renovation of cells and tissues. Cell 147, 728-741.
Mizushima, N., Yamamoto, A., Matsui, M., Yoshimori, T., and Ohsumi, Y. (2004). In vivo analysis of autophagy in response to nutrient starvation using transgenic mice expressing a fluorescent autophagosome marker. Mol Biol Cell 15, 1101-1111.
Mochida, K., Oikawa, Y., Kimura, Y., Kirisako, H., Hirano, H., Ohsumi, Y., and Nakatogawa, H. (2015). Receptor-mediated selective autophagy degrades the endoplasmic reticulum and the nucleus. Nature 522, 359-362.
Moretti, J., Roy, S., Bozec, D., Martinez, J., Chapman, J.R., Ueberheide, B., Lamming, D.W., Chen, Z.J., Horng, T., Yeretssian, G., et al. (2017). STING Senses Microbial Viability to Orchestrate Stress-Mediated Autophagy of the Endoplasmic Reticulum. Cell 171, 809-823 e813.
Morselli, E., Shen, S., Ruckenstuhl, C., Bauer, M.A., Marino, G., Galluzzi, L., Criollo, A., Michaud, M., Maiuri, M.C., Chano, T., et al. (2011). p53 inhibits autophagy by interacting with the human ortholog of yeast Atg17, RB1CC1/FIP200. Cell Cycle 10, 2763-2769.
Motley, A.M., Nuttall, J.M., and Hettema, E.H. (2012). Pex3-anchored Atg36 tags peroxisomes for degradation in Saccharomyces cerevisiae. EMBO J 31, 2852-2868.
Nakada, K., Inoue, K., Ono, T., Isobe, K., Ogura, A., Goto, Y.I., Nonaka, I., and Hayashi, J.I. (2001). Inter-mitochondrial complementation: Mitochondria-specific system preventing mice from expression of disease phenotypes by mutant mtDNA. Nat Med 7, 934-940.
Nakagawa, I., Amano, A., Mizushima, N., Yamamoto, A., Yamaguchi, H., Kamimoto, T., Nara, A., Funao, J., Nakata, M., Tsuda, K., et al. (2004). Autophagy defends cells against invading group A Streptococcus. Science 306, 1037-1040.
Nargund, A.M., Pellegrino, M.W., Fiorese, C.J., Baker, B.M., and Haynes, C.M. (2012). Mitochondrial import efficiency of ATFS-1 regulates mitochondrial UPR activation. Science 337, 587-590.
Nazio, F., Strappazzon, F., Antonioli, M., Bielli, P., Cianfanelli, V., Bordi, M., Gretzmeier, C., Dengjel, J., Piacentini, M., Fimia, G.M., et al. (2013). mTOR inhibits autophagy by controlling ULK1 ubiquitylation, self-association and function through AMBRA1 and TRAF6. Nat Cell Biol 15, 406-416.
Niso-Santano, M., Malik, S.A., Pietrocola, F., Bravo-San Pedro, J.M., Marino, G., Cianfanelli, V., Ben-Younes, A., Troncoso, R., Markaki, M., Sica, V., et al. (2015). Unsaturated fatty acids induce non-canonical autophagy. EMBO J 34, 1025-1041.
Oku, M., and Sakai, Y. (2016). Pexophagy in yeasts. Biochim Biophys Acta 1863, 992-998.
Orsi, A., Razi, M., Dooley, H.C., Robinson, D., Weston, A.E., Collinson, L.M., and Tooze, S.A. (2012). Dynamic and transient interactions of Atg9 with autophagosomes, but not membrane integration, are required for autophagy. Mol Biol Cell 23, 1860-1873.
Ossareh-Nazari, B., Bonizec, M., Cohen, M., Dokudovskaya, S., Delalande, F., Schaeffer, C., Van Dorsselaer, A., and Dargemont, C. (2010). Cdc48 and Ufd3, new partners of the ubiquitin protease Ubp3, are required for ribophagy. EMBO Rep 11, 548-554.

Ouahoud, S., Fiet, M.D., Martinez-Montanes, F., Ejsing, C.S., Kuss, O., Roden, M., and Markgraf, D.F. (2018). Lipid droplet consumption is functionally coupled to vacuole homeostasis independent of lipophagy. J Cell Sci 131.

Ouimet, M., Franklin, V., Mak, E., Liao, X., Tabas, I., and Marcel, Y.L. (2011). Autophagy regulates cholesterol efflux from macrophage foam cells via lysosomal acid lipase. Cell Metab 13, 655-667.

Ozeki, S., Cheng, J., Tauchi-Sato, K., Hatano, N., Taniguchi, H., and Fujimoto, T. (2005). Rab18 localizes to lipid droplets and induces their close apposition to the endoplasmic reticulum-derived membrane. J Cell Sci 118, 2601-2611.

Panchaud, N., Peli-Gulli, M.P., and De Virgilio, C. (2013). Amino acid deprivation inhibits TORC1 through a GTPase-activating protein complex for the Rag family GTPase Gtr1. Sci Signal 6, ra42.

Pankiv, S., Clausen, T.H., Lamark, T., Brech, A., Bruun, J.A., Outzen, H., Overvatn, A., Bjorkoy, G., and Johansen, T. (2007). p62/SQSTM1 binds directly to Atg8/LC3 to facilitate degradation of ubiquitinated protein aggregates by autophagy. J Biol Chem 282, 24131-24145.

Pantopoulos, K., Porwal, S.K., Tartakoff, A., and Devireddy, L. (2012). Mechanisms of mammalian iron homeostasis. Biochemistry 51, 5705-5724.

Park, J.M., Jung, C.H., Seo, M., Otto, N.M., Grunwald, D., Kim, K.H., Moriarity, B., Kim, Y.M., Starker, C., Nho, R.S., et al. (2016a). The ULK1 complex mediates MTORC1 signaling to the autophagy initiation machinery via binding and phosphorylating ATG14. Autophagy 12, 547-564.

Park, J.M., Seo, M., Jung, C.H., Grunwald, D., Stone, M., Otto, N.M., Toso, E., Ahn, Y., Kyba, M., Griffin, T.J., et al. (2018). ULK1 phosphorylates Ser30 of BECN1 in association with ATG14 to stimulate autophagy induction. Autophagy 14, 584-597.

Park, S.M., Ou, J., Chamberlain, L., Simone, T.M., Yang, H., Virbasius, C.M., Ali, A.M., Zhu, L.J., Mukherjee, S., Raza, A., et al. (2016b). U2AF35(S34F) Promotes Transformation by Directing Aberrant ATG7 Pre-mRNA 3' End Formation. Mol Cell 62, 479-490.

Patrick, A.D., and Lake, B.D. (1969). Deficiency of an acid lipase in Wolman's disease. Nature 222, 1067-1068.

Pawlak, M., Lefebvre, P., and Staels, B. (2015). Molecular mechanism of PPARalpha action and its impact on lipid metabolism, inflammation and fibrosis in non-alcoholic fatty liver disease. J Hepatol 62, 720-733.

Perera, R.M., Stoykova, S., Nicolay, B.N., Ross, K.N., Fitamant, J., Boukhali, M., Lengrand, J., Deshpande, V., Selig, M.K., Ferrone, C.R., et al. (2015). Transcriptional control of autophagy-lysosome function drives pancreatic cancer metabolism. Nature 524, 361-365.

Pickrell, A.M., and Youle, R.J. (2015). The roles of PINK1, parkin, and mitochondrial fidelity in Parkinson's disease. Neuron 85, 257-273.

Poillet-Perez, L., Xie, X., Zhan, L., Yang, Y., Sharp, D.W., Hu, Z.S., Su, X., Maganti, A., Jiang, C., Lu, W., et al. (2018). Autophagy maintains tumour growth through circulating arginine. Nature 563, 569-573.

Ponpuak, M., Mandell, M.A., Kimura, T., Chauhan, S., Cleyrat, C., and Deretic, V. (2015). Secretory autophagy. Curr Opin Cell Biol 35, 106-116.

Prevost, C., Sharp, M.E., Kory, N., Lin, Q., Voth, G.A., Farese, R.V., Jr., and Walther, T.C. (2018). Mechanism and Determinants of Amphipathic Helix-Containing Protein Targeting to Lipid Droplets. Dev Cell 44, 73-86 e74.

Puri, C., Vicinanza, M., Ashkenazi, A., Gratian, M.J., Zhang, Q., Bento, C.F., Renna, M., Menzies, F.M., and Rubinsztein, D.C. (2018). The RAB11A-Positive Compartment Is a Primary Platform for Autophagosome Assembly Mediated by WIPI2 Recognition of PI3P-RAB11A. Dev Cell 45, 114-131 e118.

Qu, X., Yu, J., Bhagat, G., Furuya, N., Hibshoosh, H., Troxel, A., Rosen, J., Eskelinen, E.L., Mizushima, N., Ohsumi, Y., et al. (2003). Promotion of tumorigenesis by heterozygous disruption of the beclin 1 autophagy gene. J Clin Invest 112, 1809-1820.

Rabinovich, S., Adler, L., Yizhak, K., Sarver, A., Silberman, A., Agron, S., Stettner, N., Sun, Q., Brandis, A., Helbling, D., et al. (2015). Diversion of aspartate in ASS1-deficient tumours fosters de novo pyrimidine synthesis. Nature 527, 379-383.

Rabinowitz, J.D., and White, E. (2010). Autophagy and metabolism. Science 330, 1344-1348.

Rambold, A.S., Cohen, S., and Lippincott-Schwartz, J. (2015). Fatty acid trafficking in starved cells: regulation by lipid droplet lipolysis, autophagy, and mitochondrial fusion dynamics. Dev Cell 32, 678-692.

Reichelt, M.E., Mellor, K.M., Curl, C.L., Stapleton, D., and Delbridge, L.M. (2013). Myocardial glycophagy - a specific glycogen handling response to metabolic stress is accentuated in the female heart. J Mol Cell Cardiol 65, 67-75.

Roberts, D.J., Tan-Sah, V.P., Ding, E.Y., Smith, J.M., and Miyamoto, S. (2014). Hexokinase-II positively regulates glucose starvation-induced autophagy through TORC1 inhibition. Mol Cell 53, 521-533.

Romero, I.L., Mukherjee, A., Kenny, H.A., Litchfield, L.M., and Lengyel, E. (2015). Molecular pathways: trafficking of metabolic resources in the tumor microenvironment. Clin Cancer Res 21, 680-686.

Ron, D., and Walter, P. (2007). Signal integration in the endoplasmic reticulum unfolded protein response. Nat Rev Mol Cell Biol 8, 519-529.

Rosen, E.D., and Spiegelman, B.M. (2014). What we talk about when we talk about fat. Cell 156, 20-44.

Rubartelli, A., Cozzolino, F., Talio, M., and Sitia, R. (1990). A novel secretory pathway for interleukin-1 beta, a protein lacking a signal sequence. EMBO J 9, 1503-1510.

Russell, R.C., Tian, Y., Yuan, H., Park, H.W., Chang, Y.Y., Kim, J., Kim, H., Neufeld, T.P., Dillin, A., and Guan, K.L. (2013). ULK1 induces autophagy by phosphorylating Beclin-1 and activating VPS34 lipid kinase. Nat Cell Biol 15, 741-750.

Rybstein, M.D., Bravo-San Pedro, J.M., Kroemer, G., and Galluzzi, L. (2018). The autophagic network and cancer. Nat Cell Biol 20, 243-251.

Sancak, Y., Bar-Peled, L., Zoncu, R., Markhard, A.L., Nada, S., and Sabatini, D.M. (2010). Ragulator-Rag complex targets mTORC1 to the lysosomal surface and is necessary for its activation by amino acids. Cell 141, 290-303.

Sancak, Y., Peterson, T.R., Shaul, Y.D., Lindquist, R.A., Thoreen, C.C., Bar-Peled, L., and Sabatini, D.M. (2008). The Rag GTPases bind raptor and mediate amino acid signaling to mTORC1. Science 320, 1496-1501.

Sandoval, H., Thiagarajan, P., Dasgupta, S.K., Schumacher, A., Prchal, J.T., Chen, M., and Wang, J. (2008). Essential role for Nix in autophagic maturation of erythroid cells. Nature 454, 232-235.

Santana-Codina, N., and Mancias, J.D. (2018). The Role of NCOA4-Mediated Ferritinophagy in Health and Disease. Pharmaceuticals (Basel) 11.

Sargent, G., van Zutphen, T., Shatseva, T., Zhang, L., Di Giovanni, V., Bandsma, R., and Kim, P.K. (2016). PEX2 is the E3 ubiquitin ligase required for pexophagy during starvation. J Cell Biol 214, 677-690.

Sathyanarayan, A., Mashek, M.T., and Mashek, D.G. (2017). ATGL Promotes Autophagy/Lipophagy via SIRT1 to Control Hepatic Lipid Droplet Catabolism. Cell Rep 19, 1-9.

Scherz-Shouval, R., Shvets, E., Fass, E., Shorer, H., Gil, L., and Elazar, Z. (2007). Reactive oxygen species are essential for autophagy and specifically regulate the activity of Atg4. EMBO J 26, 1749-1760.

Schneider, J.L., Suh, Y., and Cuervo, A.M. (2014). Deficient chaperone-mediated autophagy in liver leads to metabolic dysregulation. Cell Metab 20, 417-432.

Schneider, J.L., Villarroya, J., Diaz-Carretero, A., Patel, B., Urbanska, A.M., Thi, M.M., Villarroya, F., Santambrogio, L., and Cuervo, A.M. (2015). Loss of hepatic chaperone-mediated autophagy accelerates proteostasis failure in aging. Aging Cell 14, 249-264.

Schroeder, B., Schulze, R.J., Weller, S.G., Sletten, A.C., Casey, C.A., and McNiven, M.A. (2015). The small GTPase Rab7 as a central regulator of hepatocellular lipophagy. Hepatology 61, 1896-1907.

Schulze, R.J., Sathyanarayan, A., and Mashek, D.G. (2017). Breaking fat: The regulation and mechanisms of lipophagy. Biochim Biophys Acta Mol Cell Biol Lipids 1862, 1178-1187.

Settembre, C., De Cegli, R., Mansueto, G., Saha, P.K., Vetrini, F., Visvikis, O., Huynh, T., Carissimo, A., Palmer, D., Klisch, T.J., et al. (2013). TFEB controls cellular lipid metabolism through a starvation-induced autoregulatory loop. Nat Cell Biol 15, 647-658.

Sha, Y., Rao, L., Settembre, C., Ballabio, A., and Eissa, N.T. (2017). STUB1 regulates TFEB-induced autophagy-lysosome pathway. EMBO J 36, 2544-2552.

Shan, B., Wang, X., Wu, Y., Xu, C., Xia, Z., Dai, J., Shao, M., Zhao, F., He, S., Yang, L., et al. (2017). The metabolic ER stress sensor IRE1alpha suppresses alternative activation of macrophages and impairs energy expenditure in obesity. Nat Immunol 18, 519-529.

Shen, S., Niso-Santano, M., Adjemian, S., Takehara, T., Malik, S.A., Minoux, H., Souquere, S., Marino, G., Lachkar, S., Senovilla, L., et al. (2012). Cytoplasmic STAT3 represses autophagy by inhibiting PKR activity. Mol Cell 48, 667-680.

Sherman, M.H., Yu, R.T., Tseng, T.W., Sousa, C.M., Liu, S., Truitt, M.L., He, N., Ding, N., Liddle, C., Atkins, A.R., et al. (2017). Stromal cues regulate the pancreatic cancer epigenome and metabolome. Proc Natl Acad Sci U S A 114, 1129-1134.

Shibata, M., Yoshimura, K., Furuya, N., Koike, M., Ueno, T., Komatsu, M., Arai, H., Tanaka, K., Kominami, E., and Uchiyama, Y. (2009). The MAP1-LC3 conjugation system is involved in lipid droplet formation. Biochem Biophys Res Commun 382, 419-423.

Shpilka, T., Welter, E., Borovsky, N., Amar, N., Shimron, F., Peleg, Y., and Elazar, Z. (2015). Fatty acid synthase is preferentially degraded by autophagy upon nitrogen starvation in yeast. Proc Natl Acad Sci U S A 112, 1434-1439.

Shteingauz, A., Porat, Y., Voloshin, T., Schneiderman, R.S., Munster, M., Zeevi, E., Kaynan, N., Gotlib, K., Giladi, M., Kirson, E.D., et al. (2018). AMPK-dependent autophagy upregulation serves as a survival mechanism in response to Tumor Treating Fields (TTFields). Cell Death Dis 9, 1074.

Singh, R., and Cuervo, A.M. (2012). Lipophagy: connecting autophagy and lipid metabolism. Int J Cell Biol 2012, 282041.

Singh, R., Kaushik, S., Wang, Y., Xiang, Y., Novak, I., Komatsu, M., Tanaka, K., Cuervo, A.M., and Czaja, M.J. (2009a). Autophagy regulates lipid metabolism. Nature 458, 1131-1135.

Singh, R., Xiang, Y., Wang, Y., Baikati, K., Cuervo, A.M., Luu, Y.K., Tang, Y., Pessin, J.E., Schwartz, G.J., and Czaja, M.J. (2009b). Autophagy regulates adipose mass and differentiation in mice. J Clin Invest 119, 3329-3339.

Sinturel, F., Gerber, A., Mauvoisin, D., Wang, J., Gatfield, D., Stubblefield, J.J., Green, C.B., Gachon, F., and Schibler, U. (2017). Diurnal Oscillations in Liver Mass and Cell Size Accompany Ribosome Assembly Cycles. Cell 169, 651-663 e614.

Sliter, D.A., Martinez, J., Hao, L., Chen, X., Sun, N., Fischer, T.D., Burman, J.L., Li, Y., Zhang, Z., Narendra, D.P., et al. (2018). Parkin and PINK1 mitigate STING-induced inflammation. Nature 561, 258-262.

Smith, M.D., Harley, M.E., Kemp, A.J., Wills, J., Lee, M., Arends, M., von Kriegsheim, A., Behrends, C., and Wilkinson, S. (2018). CCPG1 Is a Non-canonical Autophagy Cargo Receptor Essential for ER-Phagy and Pancreatic ER Proteostasis. Dev Cell 44, 217-232 e211.

Son, S.M., Park, S.J., Lee, H., Siddiqi, F., Lee, J.E., Menzies, F.M., and Rubinsztein, D.C. (2019). Leucine Signals to mTORC1 via Its Metabolite Acetyl-Coenzyme A. Cell Metab 29, 192-201 e197.

Sonveaux, P., Vegran, F., Schroeder, T., Wergin, M.C., Verrax, J., Rabbani, Z.N., De Saedeleer, C.J., Kennedy, K.M., Diepart, C., Jordan, B.F., et al. (2008). Targeting lactate-fueled respiration selectively kills hypoxic tumor cells in mice. J Clin Invest 118, 3930-3942.

Sousa, C.M., Biancur, D.E., Wang, X., Halbrook, C.J., Sherman, M.H., Zhang, L., Kremer, D., Hwang, R.F., Witkiewicz, A.K., Ying, H., et al. (2016). Pancreatic stellate cells support tumour metabolism through autophagic alanine secretion. Nature 536, 479-483.

Stefani, M., and Dobson, C.M. (2003). Protein aggregation and aggregate toxicity: new insights into protein folding, misfolding diseases and biological evolution. J Mol Med (Berl) 81, 678-699.

Strohecker, A.M., Guo, J.Y., Karsli-Uzunbas, G., Price, S.M., Chen, G.J., Mathew, R., McMahon, M., and White, E. (2013). Autophagy sustains mitochondrial glutamine metabolism and growth of BrafV600E-driven lung tumors. Cancer Discov 3, 1272-1285.

Strohecker, A.M., and White, E. (2014). Targeting mitochondrial metabolism by inhibiting autophagy in BRAF-driven cancers. Cancer Discov 4, 766-772.

Subramani, S., and Malhotra, V. (2013). Non-autophagic roles of autophagy-related proteins. EMBO Rep 14, 143-151.

Sugiura, A., McLelland, G.L., Fon, E.A., and McBride, H.M. (2014). A new pathway for mitochondrial quality control: mitochondrial-derived vesicles. EMBO J 33, 2142-2156.

Takamura, A., Komatsu, M., Hara, T., Sakamoto, A., Kishi, C., Waguri, S., Eishi, Y., Hino, O., Tanaka, K., and Mizushima, N. (2011). Autophagy-deficient mice develop multiple liver tumors. Genes Dev 25, 795-800.

Taylor, D., and Gottlieb, R.A. (2017). Parkin-mediated mitophagy is downregulated in browning of white adipose tissue. Obesity (Silver Spring) 25, 704-712.

Toledo, M., Batista-Gonzalez, A., Merheb, E., Aoun, M.L., Tarabra, E., Feng, D., Sarparanta, J., Merlo, P., Botre, F., Schwartz, G.J., et al. (2018). Autophagy Regulates the Liver Clock and Glucose Metabolism by Degrading CRY1. Cell Metab 28, 268-281 e264.

Tsukamoto, S., Kuma, A., Murakami, M., Kishi, C., Yamamoto, A., and Mizushima, N. (2008). Autophagy is essential for preimplantation development of mouse embryos. Science 321, 117-120.

Tuttle, D.L., and Dunn, W.A., Jr. (1995). Divergent modes of autophagy in the methylotrophic yeast Pichia pastoris. J Cell Sci 108 (Pt 1), 25-35.

Ueno, T., and Komatsu, M. (2017). Autophagy in the liver: functions in health and disease. Nat Rev Gastroenterol Hepatol 14, 170-184.

van der Klei, I.J., Yurimoto, H., Sakai, Y., and Veenhuis, M. (2006). The significance of peroxisomes in methanol metabolism in methylotrophic yeast. Biochim Biophys Acta 1763, 1453-1462.

van Zutphen, T., Todde, V., de Boer, R., Kreim, M., Hofbauer, H.F., Wolinski, H., Veenhuis, M., van der Klei, I.J., and Kohlwein, S.D. (2014). Lipid droplet autophagy in the yeast Saccharomyces cerevisiae. Mol Biol Cell 25, 290-301.

Verhoef, L.G., Lindsten, K., Masucci, M.G., and Dantuma, N.P. (2002). Aggregate formation inhibits proteasomal degradation of polyglutamine proteins. Hum Mol Genet 11, 2689-2700.

Vevea, J.D., Garcia, E.J., Chan, R.B., Zhou, B., Schultz, M., Di Paolo, G., McCaffery, J.M., and Pon, L.A. (2015). Role for Lipid Droplet Biogenesis and Microlipophagy in Adaptation to Lipid Imbalance in Yeast. Dev Cell 35, 584-599.

von Muhlinen, N., Akutsu, M., Ravenhill, B.J., Foeglein, A., Bloor, S., Rutherford, T.J., Freund, S.M., Komander, D., and Randow, F. (2012). LC3C, bound selectively by a noncanonical LIR motif in NDP52, is required for antibacterial autophagy. Mol Cell 48, 329-342.

Wang, C., and Youle, R.J. (2009). The role of mitochondria in apoptosis*. Annu Rev Genet 43, 95-118.

Wang, X., Eno, C.O., Altman, B.J., Zhu, Y., Zhao, G., Olberding, K.E., Rathmell, J.C., and Li, C. (2011). ER stress modulates cellular metabolism. Biochem J 435, 285-296.

Warner, J.R. (1999). The economics of ribosome biosynthesis in yeast. Trends Biochem Sci 24, 437-440.

Wauson, E.M., Dbouk, H.A., Ghosh, A.B., and Cobb, M.H. (2014). G protein-coupled receptors and the regulation of autophagy. Trends Endocrinol Metab 25, 274-282.

Wei, H., Wei, S., Gan, B., Peng, X., Zou, W., and Guan, J.L. (2011). Suppression of autophagy by FIP200 deletion inhibits mammary tumorigenesis. Genes Dev 25, 1510-1527.

Wei, Y., Chiang, W.C., Sumpter, R., Jr., Mishra, P., and Levine, B. (2017). Prohibitin 2 Is an Inner Mitochondrial Membrane Mitophagy Receptor. Cell 168, 224-238 e210.

Weidberg, H., and Amon, A. (2018). MitoCPR-A surveillance pathway that protects mitochondria in response to protein import stress. Science 360.

Weir, H.J., Yao, P., Huynh, F.K., Escoubas, C.C., Goncalves, R.L., Burkewitz, K., Laboy, R., Hirschey, M.D., and Mair, W.B. (2017). Dietary Restriction and AMPK Increase Lifespan via Mitochondrial Network and Peroxisome Remodeling. Cell Metab 26, 884-896 e885.

Wen, Y.A., Xing, X., Harris, J.W., Zaytseva, Y.Y., Mitov, M.I., Napier, D.L., Weiss, H.L., Mark Evers, B., and Gao, T. (2017). Adipocytes activate mitochondrial fatty acid oxidation and autophagy to promote tumor growth in colon cancer. Cell Death Dis 8, e2593.

White, E. (2015). The role for autophagy in cancer. J Clin Invest 125, 42-46.

Williams, A., Sarkar, S., Cuddon, P., Ttofi, E.K., Saiki, S., Siddiqi, F.H., Jahreiss, L., Fleming, A., Pask, D., Goldsmith, P., et al. (2008). Novel targets for Huntington's disease in an mTOR-independent autophagy pathway. Nat Chem Biol 4, 295-305.

Wolfson, R.L., Chantranupong, L., Saxton, R.A., Shen, K., Scaria, S.M., Cantor, J.R., and Sabatini, D.M. (2016). Sestrin2 is a leucine sensor for the mTORC1 pathway. Science 351, 43-48.

Woods, A., Johnstone, S.R., Dickerson, K., Leiper, F.C., Fryer, L.G., Neumann, D., Schlattner, U., Wallimann, T., Carlson, M., and Carling, D. (2003). LKB1 is the upstream kinase in the AMP-activated protein kinase cascade. Curr Biol 13, 2004-2008.

Wyant, G.A., Abu-Remaileh, M., Frenkel, E.M., Laqtom, N.N., Dharamdasani, V., Lewis, C.A., Chan, S.H., Heinze, I., Ori, A., and Sabatini, D.M. (2018). NUFIP1 is a ribosome receptor for starvation-induced ribophagy. Science 360, 751-758.

Wyant, G.A., Abu-Remaileh, M., Wolfson, R.L., Chen, W.W., Freinkman, E., Danai, L.V., Vander Heiden, M.G., and Sabatini, D.M. (2017). mTORC1 Activator SLC38A9 Is Required to Efflux Essential Amino Acids from Lysosomes and Use Protein as a Nutrient. Cell 171, 642-654 e612.

Xiao, B., Heath, R., Saiu, P., Leiper, F.C., Leone, P., Jing, C., Walker, P.A., Haire, L., Eccleston, J.F., Davis, C.T., et al. (2007). Structural basis for AMP binding to mammalian AMP-activated protein kinase. Nature 449, 496-500.

Xiao, B., Sanders, M.J., Underwood, E., Heath, R., Mayer, F.V., Carmena, D., Jing, C., Walker, P.A., Eccleston, J.F., Haire, L.F., et al. (2011). Structure of mammalian AMPK and its regulation by ADP. Nature 472, 230-233.

Yamada, T., Murata, D., Adachi, Y., Itoh, K., Kameoka, S., Igarashi, A., Kato, T., Araki, Y., Huganir, R.L., Dawson, T.M., et al. (2018). Mitochondrial Stasis Reveals p62-Mediated Ubiquitination in Parkin-Independent Mitophagy and Mitigates Nonalcoholic Fatty Liver Disease. Cell Metab 28, 588-604 e585.

Yamashita, S., Abe, K., Tatemichi, Y., and Fujiki, Y. (2014). The membrane peroxin PEX3 induces peroxisome-ubiquitination-linked pexophagy. Autophagy 10, 1549-1564.

Yang, L., Achreja, A., Yeung, T.L., Mangala, L.S., Jiang, D., Han, C., Baddour, J., Marini, J.C., Ni, J., Nakahara, R., et al. (2016). Targeting Stromal Glutamine Synthetase in Tumors Disrupts Tumor Microenvironment-Regulated Cancer Cell Growth. Cell Metab 24, 685-700.

Yang, S., Wang, X., Contino, G., Liesa, M., Sahin, E., Ying, H., Bause, A., Li, Y., Stommel, J.M., Dell'antonio, G., et al. (2011). Pancreatic cancers require autophagy for tumor growth. Genes Dev 25, 717-729.

Ye, J., Kumanova, M., Hart, L.S., Sloane, K., Zhang, H., De Panis, D.N., Bobrovnikova-Marjon, E., Diehl, J.A., Ron, D., and Koumenis, C. (2010). The GCN2-ATF4 pathway is critical for tumour cell survival and proliferation in response to nutrient deprivation. EMBO J 29, 2082-2096.

Yi, K.H., and Lauring, J. (2016). Recurrent AKT mutations in human cancers: functional consequences and effects on drug sensitivity. Oncotarget 7, 4241-4251.

Yoshii, S.R., Kuma, A., Akashi, T., Hara, T., Yamamoto, A., Kurikawa, Y., Itakura, E., Tsukamoto, S., Shitara, H., Eishi, Y., et al. (2016). Systemic Analysis of Atg5-Null Mice Rescued from Neonatal Lethality by Transgenic ATG5 Expression in Neurons. Dev Cell 39, 116-130.

Youle, R.J., and van der Bliek, A.M. (2012). Mitochondrial fission, fusion, and stress. Science 337, 1062-1065.

Yu, L., Chen, Y., and Tooze, S.A. (2018). Autophagy pathway: Cellular and molecular mechanisms. Autophagy 14, 207-215.

Yuan, H.X., Russell, R.C., and Guan, K.L. (2013). Regulation of PIK3C3/VPS34 complexes by MTOR in nutrient stress-induced autophagy. Autophagy 9, 1983-1995.

Yue, Z., Jin, S., Yang, C., Levine, A.J., and Heintz, N. (2003). Beclin 1, an autophagy gene essential for early embryonic development, is a haploinsufficient tumor suppressor. Proc Natl Acad Sci U S A 100, 15077-15082.

Zhang, C.S., Hawley, S.A., Zong, Y., Li, M., Wang, Z., Gray, A., Ma, T., Cui, J., Feng, J.W., Zhu, M., et al. (2017). Fructose-1,6-bisphosphate and aldolase mediate glucose sensing by AMPK. Nature 548, 112-116.

Zhang, C.S., Jiang, B., Li, M., Zhu, M., Peng, Y., Zhang, Y.L., Wu, Y.Q., Li, T.Y., Liang, Y., Lu, Z., et al. (2014). The lysosomal v-ATPase-Ragulator complex is a common activator for AMPK and mTORC1, acting as a switch between catabolism and anabolism. Cell Metab 20, 526-540.

Zhang, J., Tripathi, D.N., Jing, J., Alexander, A., Kim, J., Powell, R.T., Dere, R., Tait-Mulder, J., Lee, J.H., Paull, T.T., et al. (2015). ATM functions at the peroxisome to induce pexophagy in response to ROS. Nat Cell Biol 17, 1259-1269.

Zhang, X., Wang, L., Lak, B., Li, J., Jokitalo, E., and Wang, Y. (2018). GRASP55 Senses Glucose Deprivation through O-GlcNAcylation to Promote Autophagosome-Lysosome Fusion. Dev Cell 45, 245-261 e246.

Zhang, Y., Goldman, S., Baerga, R., Zhao, Y., Komatsu, M., and Jin, S. (2009). Adipose-specific deletion of autophagy-related gene 7 (atg7) in mice reveals a role in adipogenesis. Proc Natl Acad Sci U S A 106, 19860-19865.

Zhang, Y.L., Guo, H., Zhang, C.S., Lin, S.Y., Yin, Z., Peng, Y., Luo, H., Shi, Y., Lian, G., Zhang, C., et al. (2013). AMP as a low-energy charge signal autonomously initiates assembly of AXIN-AMPK-LKB1 complex for AMPK activation. Cell Metab 18, 546-555.

Zhao, H., Tang, M., Liu, M., and Chen, L. (2018). Glycophagy: An emerging target in pathology. Clin Chim Acta 484, 298-303.

Zhao, N., and Enns, C.A. (2012). Iron transport machinery of human cells: players and their interactions. Curr Top Membr 69, 67-93.

Zhao, Q., Wang, J., Levichkin, I.V., Stasinopoulos, S., Ryan, M.T., and Hoogenraad, N.J. (2002). A mitochondrial specific stress response in mammalian cells. EMBO J 21, 4411-4419.

Zhao, Y., Chen, G., Zhang, W., Xu, N., Zhu, J.Y., Jia, J., Sun, Z.J., Wang, Y.N., and Zhao, Y.F. (2012). Autophagy regulates hypoxia-induced osteoclastogenesis through the HIF-1alpha/BNIP3 signaling pathway. J Cell Physiol 227, 639-648.

Zimmermann, R., Strauss, J.G., Haemmerle, G., Schoiswohl, G., Birner-Gruenberger, R., Riederer, M., Lass, A., Neuberger, G., Eisenhaber, F., Hermetter, A., et al. (2004). Fat mobilization in adipose tissue is promoted by adipose triglyceride lipase. Science 306, 1383-1386.

Zirin, J., Nieuwenhuis, J., and Perrimon, N. (2013). Role of autophagy in glycogen breakdown and its relevance to chloroquine myopathy. PLoS Biol 11, e1001708.

Zwick, R.K., Guerrero-Juarez, C.F., Horsley, V., and Plikus, M.V. (2018). Anatomical, Physiological, and Functional Diversity of Adipose Tissue. Cell Metab 27, 68-83.

Chapter 2 : Mechanism of Regulation of Macroautophagy During Distinct Nutrient Stress

(This chapter has been adapted from *Lahiri et al., Autophagy, 2021)*

Macroautophagy/autophagy is a highly conserved nutrient-recycling pathway that eukaryotes utilize to combat diverse stresses including nutrient depletion. Dysregulation of autophagy disrupts cellular homeostasis leading to starvation susceptibility in yeast and disease development in humans. In yeast, the robust autophagy response to starvation is controlled by the upregulation of *ATG* genes, via regulatory processes involving multiple levels of gene expression. Despite the identification of several regulators through genetic studies, the predominant mechanism of regulation modulating the autophagy response to subtle differences in nutrient status remains undefined. In this chapter, we report the unexpected finding that subtle changes in nutrient availability can cause large differences in autophagy flux, governed by hitherto unknown post-transcriptional regulatory mechanisms affecting the expression of the key autophagy inducing kinase Atg1 (ULK1/ULK2 in mammals). We have identified two novel post-transcriptional regulators of ATG1 expression, the kinase Rad53 and the RNA-binding protein Ded1 (DDX3 in mammals). Furthermore, we show that DDX3 regulates ULK1 expression post-transcriptionally, establishing mechanistic conservation and highlighting the power of yeast biology in uncovering regulatory mechanisms that can inform therapeutic approaches.

2.1 Introduction

Macroautophagy (hereafter, autophagy) is a nutrient-recycling pathway conserved among eukaryotes (Gatica et al., 2018). The hallmark of autophagy is the de novo synthesis of a transient membranous structure which expands to form the double-membrane autophagosome (Chang et al., 2021; Melia et al., 2020). Autophagy occurs basally to maintain homeostasis but is induced in response to various cues, including nutrient-depletion; this type of stress promotes the nonselective sequestration of cytoplasm leading to its subsequent engulfment within the lumen of autophagosomes (Corona Velazquez and Jackson, 2018; Nakatogawa, 2020). Autophagosomes subsequently fuse with the lysosomes or vacuole, to promote cargo degradation leading to the generation of simple metabolites that, upon efflux back into the cytosol, act as an alternative source of nutrients (Liu et al., 2021; May et al., 2020; White et al., 2015). The ability to provide nutrients makes autophagy a critical survival pathway in cancer cells (Amaravadi et al., 2016; White, 2015). Mutant KRAS-driven pancreatic cancers require autophagy-derived nutrients for survival (Guo et al., 2011; Lock et al., 2011; Mulcahy Levy and Thorburn, 2020). In pancreatic ductal adenocarcinoma, pancreatic stellate cells, present in the tumor microenvironment, upregulate autophagy to generate alanine, which is supplied to the tumor cells to meet their metabolic requirements. (Fu et al., 2018; Sousa et al., 2016). The identification of autophagy inhibitors has, therefore, gained importance as a therapeutic tool (Amaravadi et al., 2019; Mulcahy Levy and Thorburn, 2020).

Autophagy inhibition for therapeutic purposes needs to be nuanced because a complete block of autophagy compromises survival (Karsli-Uzunbas et al., 2014; Mizushima and Levine, 2020). This necessitates the need to understand the subtle aspects of autophagy regulation. Even in a simple eukaryote – the budding yeast *Saccharomyces cerevisiae* – the autophagy pathway is

complex and requires the concerted activity of several Atg (autophagy-related) proteins (Feng et al., 2014; Yin et al., 2016). Because autophagy is initiated in response to stresses such as nutrient depletion, the induction of *ATG* gene expression contrasts with that of most other genes. In yeast and mammalian cells, starvation leads to the activation of several pathways that suppress general transcription and translation but promotes that of *ATG* genes (Gross and Graef, 2020; Kim et al., 2011; Russell et al., 2014). Furthermore, because it is primarily a degradative process, the cell needs to fine-tune autophagy to meet cellular requirements while preventing unnecessary breakdown of the cytoplasm. The expression of *ATG* genes is, therefore, subject to a complex regulatory network that acts at transcriptional, post-transcriptional and translational levels (Abildgaard et al., 2020; Delorme-Axford and Klionsky, 2018; Lahiri et al., 2019). Additionally, Atg protein function is extensively regulated by post-translational modifications allowing for the exquisite regulation of autophagy in response to starvation (McEwan and Dikic, 2011; Xie et al., 2015).

Previous investigations, focused on genetically modulating the transcription of individual *ATG* genes, demonstrated that *ATG8* (Xie et al., 2008) and *ATG9* (Jin et al., 2014) expression levels are directly correlated with the size and frequency of autophagosome formation respectively. However, whether these mechanisms are the predominant physiological response to different nutritional challenges remains untested. Here, we study how autophagy is modulated in response to subtle differences in nutrient availability. We do so by comparing autophagy flux during nitrogen and amino acid starvation – two related but distinct starvation conditions – and show that modulation of autophagy under these conditions occurs primarily via post-transcriptional regulation of *ATG* gene expression, particularly that of *ATG1*. Atg1 (ULK1/ULK2 in mammals) is a Ser/Thr kinase that is critical in the initiation of autophagy and

the activation of Atg9 function through phosphorylation. We explore regulation of *ATG1* expression under these conditions and identify the kinase Rad53, as a post-transcriptional regulator of starvation-induced autophagy. Furthermore, we have identified a second novel regulator of *ATG1* expression, the RNA-helicase Ded1. We show that Ded1 directly binds to the 5'-UTR of *ATG1* preferentially during nitrogen starvation, where it likely functions to resolve secondary structures in the *ATG1* mRNA to facilitate efficient translation (Sen et al., 2019; Sen et al., 2015). In agreement with this, we show that the loss of Ded1 leads to a greater reduction in Atg1 expression and autophagy during nitrogen starvation relative to amino acid starvation. Crucially, this mode of regulation is conserved – DDX3 (the mammalian homolog of Ded1) positively regulates ULK1 expression post-transcriptionally to promote autophagy in mammalian cells. Consistently, knockdown of DDX3 leads to a reduction in, but not a complete block of, autophagy, thereby making this protein with previously characterized pro-tumorigenic functions (Botlagunta et al., 2008; Chen et al., 2015; Wilky et al., 2016) an attractive candidate for therapeutic exploration.

2.2 Results

2.2.1 Differential autophagy flux during distinct nutrient stresses is not determined by ATG transcription

In yeast, autophagy is initiated in response to loss of nutrient availability (Cebollero and Reggiori, 2009). However, how different starvation stresses differentially modulate regulators to influence autophagy flux is unclear. To shed light on these mechanisms, we investigated the effect of differential nutrient availability on autophagy regulation by comparing complete nitrogen starvation with amino acid starvation (Conrad et al., 2014). Yeast cells subjected to nitrogen starvation were starved of organic nitrogen and limited for inorganic nitrogen, whereas

amino-acid starved cells were deprived only of amino acids. We chose these two conditions for our study because despite being similar stresses overall, they represent the subtle differences that are frequently associated with divergence from homeostasis that promotes physiological responses. Additionally, while these two conditions have been studied in yeast (Ecker et al., 2010), this is, to the best of our knowledge, the first large-scale comparison of the autophagy response between these conditions, thus providing the potential for novel discoveries. The transcription factor Gcn4 is a master regulator of gene expression in response to general amino acid deprivation (Natarajan et al., 2001). Cytoplasmic dearth of amino acids activates the eIF2 kinase Gcn2 which promotes the efficient translation of Gcn4 (Dever et al., 1992). Because both nitrogen and amino acid starvation lead to an amino acid deficit, the expression of Gcn4 was increased to very similar levels in cells subjected to either nitrogen starvation ("–N") or amino acid starvation ("–A") treatment compared to those grown in the nutrient-rich YPD medium ("+") (Figure 6A and 6B), highlighting the similar nature of both conditions.

To compare autophagy flux between these starvation treatments, we utilized the GFP-Atg8 processing assay as an end-point measurement. We found that nitrogen starvation led to the robust activation of autophagy flux with the autophagy response being significantly lower with amino acid starvation (Figure 6C and 6D). This finding was corroborated by the prApe1 maturation assay for autophagy flux (Huang et al., 2014), which measures the autophagy-dependent maturation of precursor aminopeptidase I (prApe1; Figures 7A and 7B). To assess the long-term effect of both starvation treatments, we carried out a longer time-course analysis using the Pho8Δ60 activity assay as an end-point measurement (Klionsky, 2007). Extended nitrogen starvation elicited a significantly stronger autophagy response compared to extended amino acid

starvation (Figure 6E) while both starvation treatments showed increased autophagy relative to nutrient-rich conditions.

We then sought to directly examine the characteristics—frequency and size—of autophagosome formation under these starvation conditions (Backues et al., 2014). Autophagosomes were monitored by the accumulation of autophagic bodies (ABs; the single-membrane vesicle generated by fusion of an autophagosome with a vacuole) within the vacuole lumen of yeast cells lacking the major vacuolar protease Pep4 (to prevent autophagic body degradation) and Vps4 (to block the accumulation of multivesicular bodies). Consistent with biochemical assays, transmission electron microscopy (TEM) analyses revealed that ABs were more numerous in cells subjected to nitrogen starvation compared to amino acid starvation (Figure 6F and 6G). In addition, ABs in nitrogen-starved cells were significantly larger than in amino-acid starved cells (Figures 6F and 7C). Because the SEY6210 strain, used as the parent for constructing strains for autophagy flux analysis, is an auxotroph, we confirmed the autophagy responses to nitrogen and amino acid starvation using the prototrophic strain CEN.PK (Kummel et al., 2010). Consistent with the autophagy phenotype in SEY6210, we found that nitrogen starvation led to increased Atg8-lipidation. Furthermore, this difference was aggravated upon treatment with the protease inhibitor PMSF, confirming that reduced flux was not responsible for the increased abundance of lipidated Atg8. (Figure 7D).

Autophagy in yeast is robustly regulated by transcriptional control (Backues et al., 2012; Bernard et al., 2015b; Delorme-Axford and Klionsky, 2018; Jin et al., 2014; Jin and Klionsky, 2014), so we hypothesized a differential *ATG* transcriptome under these starvation conditions. We tested our hypothesis by carrying out RNA-sequencing analysis for both sets of treatments. For high-confidence identification of DEGs (differentially expressed genes), we used the

following significance parameters: 2-fold enrichment with an associated $p < 0.05$ cut-off. Contrary to our expectations, the core *ATG* genes were not identified among the DEGs (Figure 6H), with the majority of DEGs involved in translation and metabolism (Figure 7E). *ATG31* was the only core autophagy gene along with *ATG32* and *ATG39*, involved in mitophagy (Kanki et al., 2009) and reticulophagy (Mochida et al., 2015), respectively, differentially expressed with higher expression in nitrogen starvation (Figures 7F and 7G, and data not shown). We confirmed that the transcriptional response did not vary with time by measuring the transcriptional upregulation of two genes crucial to the induction of autophagy: *ATG1* (Mizushima, 2010) and *ATG9* (Matoba et al., 2020). At both 1 h and 6 h post-starvation, nitrogen and amino acid starvation elicited similar levels of transcriptional response for both *ATG1* (Figures 6I and 6J) and *ATG9* (Figures 7H and 7I) consistent with our findings from the RNA-sequencing experiments. Taken together, these data suggest that differential autophagy flux during nitrogen and amino acid starvation is not due to differential transcriptional activation of *ATG* genes.

Figure 6: Differential autophagy flux during distinct nutrient stresses is not determined by ATG transcription

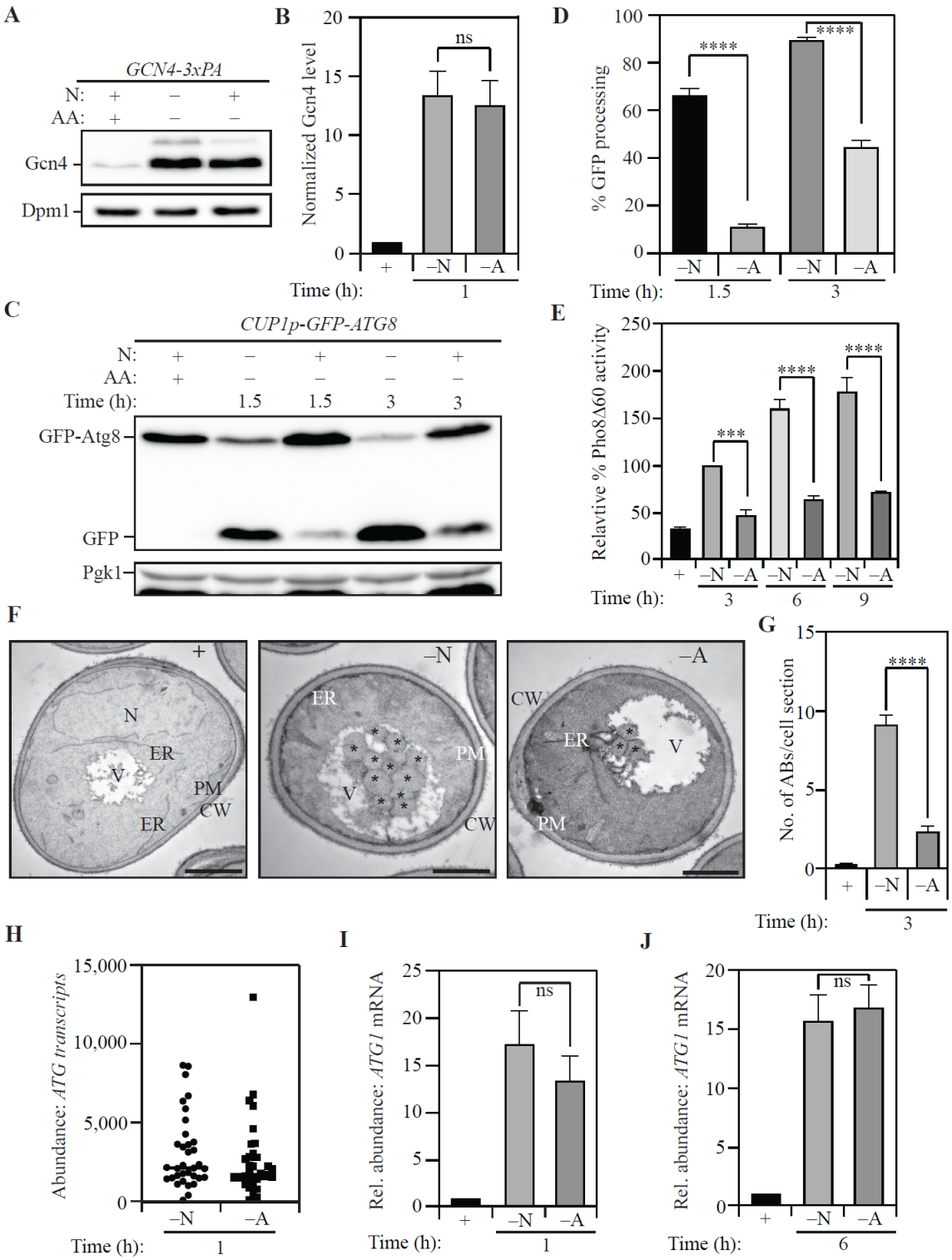

Figure 6. Differential autophagy flux during distinct nutrient stresses is not determined by *ATG* transcription. (A) Gcn4 expression is upregulated during both nitrogen and amino acid starvation: WT (SEY6210) cells with C-terminally 3x-PA tagged Gcn4 were harvested in nutrient-replete conditions or after starvation for the indicated time and examined by western blot. Gcn4 was detected using the anti-PA antibody and Dpm1 was used as a loading control. (B) Densitometric analysis for (A) from three independent biological replicates. (C) The GFP-Atg8 processing assay demonstrates increased autophagy flux during nitrogen starvation relative to amino acid starvation: WT (WLY176) cells with integrated *CUP1p-GFP-ATG8* were harvested in nutrient-replete conditions or after starvation for the indicated times and assessed by western blot. The appearance of free GFP indicates autophagy flux. Pgk1 was used as a loading control. (D) Densitometric analysis of (C) from three independent biological replicates. (E) Autophagy flux is higher during nitrogen starvation compared to amino acid starvation as assessed by the Pho8Δ60 assay: WT (WLY176) cells were harvested in nutrient-replete conditions or after starvation for the indicated times and Pho8Δ60 enzyme activity was measured by colorimetry. An increase in Pho8Δ60 activity indicates increased autophagic flux. Data from three independent biological replicates. (F) Autophagosome formation is more frequent during nitrogen starvation compared to amino acid starvation: WT (SEY6210) *pep4*Δ *vps4*Δ cells were harvested in nutrient-replete conditions or after starvation for 3 h. The cells were fixed, stained and ultrastructural analysis was used to visualize the number of ABs. Scale bar: 1 μm. (G) Quantification of the number of ABs from 100 randomly selected cell profiles from two independent biological replicates. (H) RNA-Sequencing reveals similar abundance of *ATG* transcripts during nitrogen and amino acid starvation: DESeq2 analysis of *ATG* transcriptome

during nitrogen and amino acid starvation. The plot represents the mean of three independent biological replicates from WT (SEY6210) cells. (I) and (J) There is a similar abundance of *ATG1* transcript in cells subjected to nitrogen or amino acid starvation: qRT-PCR detection of *ATG1* mRNA in WT (SEY6210) cells after 1 h (I) or 6 h (J) of starvation. *ALG9* was used as a reference gene for normalization. Data from three independent biological replicates. Data in (B), (D), (E), (G), (H), (I) and (J) represent mean ± SEM from the indicated number of replicates. Statistical analysis for (B), (G), (I) and (J) was carried out using unpaired Student's t-test while (D) and (E) were analyzed using one-way analysis of variance (ANOVA). Multiple comparisons were carried out using Tukey's multiple comparisons test. *$p < 0.05$, **$p < 0.005$, ***$p < 0.001$, ****$p < 0.0001$ ns: not significant.

Figure 7: Differential autophagy flux during distinct nutrient stresses is not determined by ATG transcription

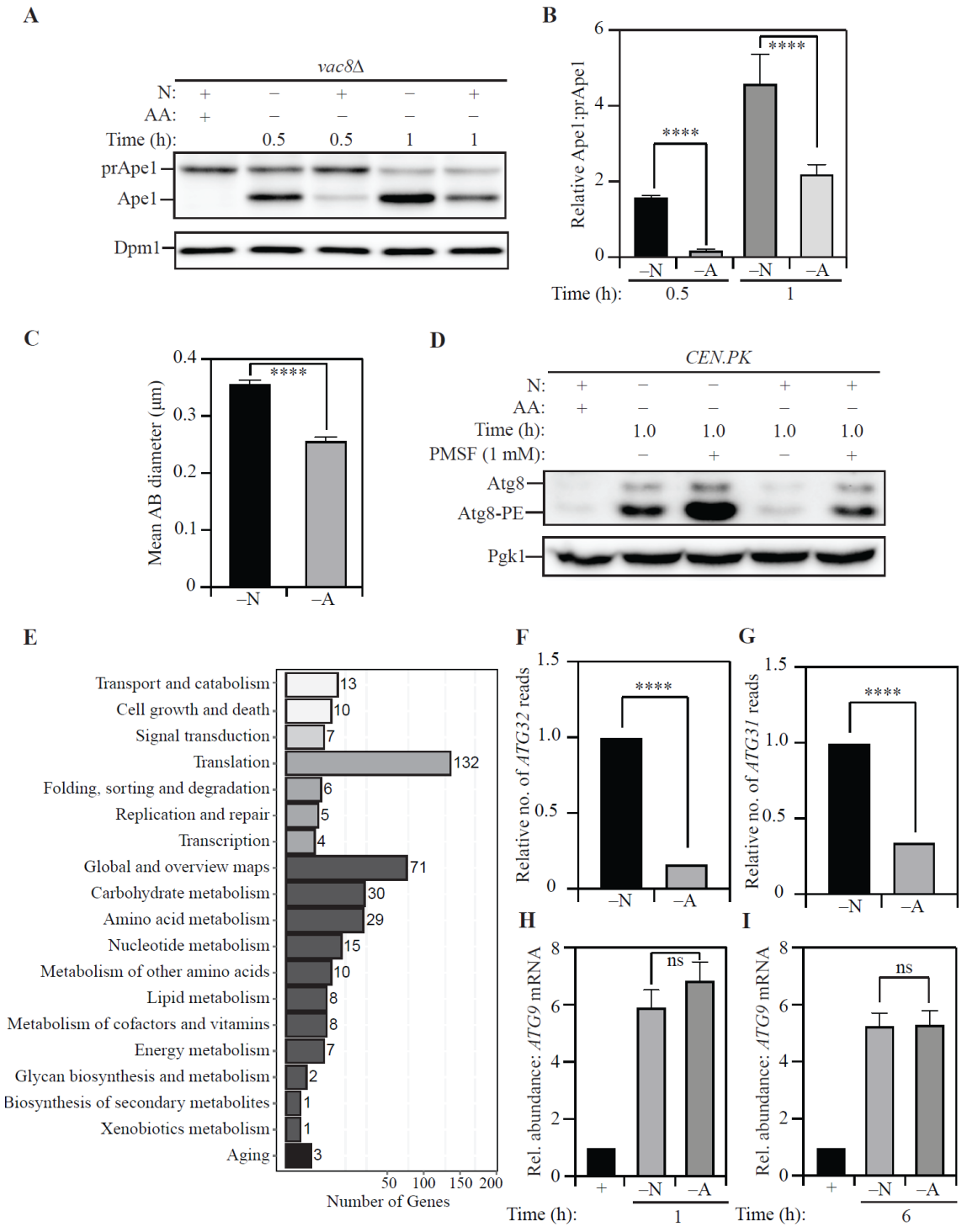

Figure 7. Differential autophagy flux during distinct nutrient stresses is not determined by *ATG* transcription. (**A**) Higher autophagy flux during nitrogen starvation compared to amino acid starvation, demonstrated by the precursor Ape1 (prApe1) maturation assay: SEY6210 *vac8*Δ cells were harvested in nutrient-replete conditions or after starvation for the indicated times. Conversion of prApe1 to Ape1 indicates autophagy flux. Dpm1 was used as a loading control (**B**) Densitometric analysis of (A) from three independent biological replicates. (**C**) The size of autophagosomes is larger during nitrogen starvation relative to amino acid starvation: Quantification of the diameter of autophagic bodies from SEY6210 *pep4*Δ *vps4*Δ cells starved for nitrogen or amino acids. Data from 100 cell profiles per condition across two independent biological replicates. (**D**) Elevated Atg8-lipidation in nitrogen starvation relative to amino acid starvation in the absence and presence of the serine protease inhibitor PMSF: CEN.PK cells were harvested in nutrient-replete conditions or after starvation for the indicated times. Pgk1 was used as a loading control. (**E**) Identified DEGs were grouped according to cellular function. (**F and G**) Abundance of *ATG32* and *ATG31* transcripts is significantly lower in amino acid starvation relative to nitrogen starvation as determined by RNA-Sequencing. Data represent the mean of three independent biological replicates. (**H and I**) Transcriptional upregulation of *ATG9* is similar during nitrogen and amino acid starvation: qRT-PCR-based detection of *ATG9* mRNA in WT (SEY6210) cells after 1 h (H) or 6 h (I) of starvation. *ALG9* was used as a reference gene for normalization. Data are from three independent biological replicates. Data in (B), (C), (H) and (I) represent mean ± SEM from indicated number of replicates. Statistical analysis for (B) was carried out using one-way analysis of variance (ANOVA) while (C), (H) and (I) were analyzed using an unpaired Student's t-test. Data in (F) and (G) represent mean from indicated number of

replicates. Statistical analysis for (F) and (G) was carried out using one-way analysis of variance (ANOVA). Multiple comparisons were carried out using Tukey's multiple comparisons test. *$p < 0.05$, **$p < 0.005$, ***$p < 0.001$, ****$p < 0.0001$ ns: not significant. Related to Figure 6.

2.2.2 Post-transcriptional activation of ATG gene expression is a critical node determining autophagy during nitrogen starvation

The induction of autophagy upon starvation depends on the synthesis of key Atg proteins. For example, Atg1, which is critical for the initiation of autophagy, is robustly synthesized in response to starvation (Yin et al., 2019). Because *ATG* transcription was not differentially affected we investigated differential expression of Atg proteins that could contribute to the differential autophagy flux. To this end, we compared the proteome of cells subjected to nitrogen starvation and amino acid starvation using stable isotope labelling with amino acids in culture (SILAC) (Figure 9A) (Deng et al., 2019). SILAC analysis revealed that several Atg proteins were differentially expressed, with increased expression in nitrogen starvation (Figure 8A). The proteins with the largest and most consistent differential expression were Atg1 and Atg9 (Figure 8A). The expression of Atg9, a protein responsible for lipid delivery and transfer for phagophore formation (Matoba et al., 2020), was ~45% lower in amino acid starvation compared to in nitrogen starvation. We confirmed this observation with immunoblotting for endogenous Atg9 protein and, consistent with our SILAC analysis, found a ~50% reduction in amino acid starvation relative to nitrogen starvation (Figure 9B and 9C). This outcome is consistent with previous findings that suggest Atg9 levels are directly correlated with the frequency of autophagosome formation (Jin et al., 2014).

In our SILAC analysis, amino-acid starved cells showed an ~50% reduction in Atg1 expression compared to nitrogen-starved cells. In contrast, other components of the Atg1 complex such as Atg13 and Atg17 did not exhibit significant differential expression, prompting us to focus on Atg1. We confirmed differential Atg1 expression by examining endogenous Atg1 levels by immunoblotting. In agreement with our SILAC data, Atg1 levels were found to be 50%

lower during amino acid starvation compared to nitrogen starvation at 2 h (Figures 8B and 9D) and ~65% lower at 6 h post-starvation (Figures 8C and 8D). A similar response was observed in the prototrophic CEN.PK strain where nitrogen starvation led to elevated Atg1 expression relative to amino acid starvation (Figure 9E). Taken together, these data suggest that post-transcriptional control is a critical node in the regulation of *ATG* gene expression that contributes to differential responses in autophagy flux. To rule out the possibility that *ATG* mRNA transcription is generally increased in response to any type of nutrient depletion, we compared the transcriptional induction of *ATG1* and *ATG9* during glucose starvation, which fails to significantly stimulate autophagy (Lang et al., 2014). Expectedly, we found no transcriptional response for either *ATG1* (Figure 8E) or *ATG9* (Figure 9F), consistent with autophagy flux not being significantly induced, as assessed by the Pho8Δ60 assay (Figure 8F).

To investigate the mechanism of differential regulation further, we focused on *ATG1*, because Atg1 is responsible for autophagy initiation and regulating Atg9 activity through phosphorylation. We compared the stability of *ATG1* mRNA in nitrogen starvation to that in amino acid starvation, to confirm that reduced protein expression during amino acid starvation is not due to mRNA instability. We induced *ATG1* transcription with a pulse of nitrogen starvation, following which we treated the cells with the transcriptional inhibitor 1,10-phenanthroline (Gatica et al., 2019). Cells were then either allowed to recover in rich medium (YPD) or starved in nitrogen starvation or amino acid starvation medium to monitor *ATG1* mRNA stability (Figure 9G). While recovery in YPD ("+" in Figure 8G) led to a significant reduction in the levels of *ATG1* mRNA, there was no decrease in either nitrogen starvation ("–N") or amino acid starvation ("–A") media highlighting that *ATG1* mRNA was similarly stable under both conditions. Furthermore, to rule out the possibility that the difference in Atg1 levels is due to

post-translational instability of the corresponding proteins during amino acid starvation, we used a cycloheximide chase assay. Because Atg1 levels are low during growing conditions and Atg1 is synthesized in response to starvation, we took advantage of constitutive Atg1 expression when measuring Atg1 stability. A strain expressing Atg1 from a *CUP1* promoter was treated with cycloheximide and Atg1 protein level was followed by immunoblotting after 2, 4 and 6 h of treatment (Figure 9H). We found no significant difference in the stability of Atg1 protein between nitrogen and amino acid starvation (Figures 8H and 8I). Taken together, these findings further suggest that a post-transcriptional mechanism promotes the translation of *ATG1* mRNA during nitrogen starvation.

Figure 8: Post-transcriptional activation of ATG gene expression is a critical node determining autophagy during nitrogen starvation

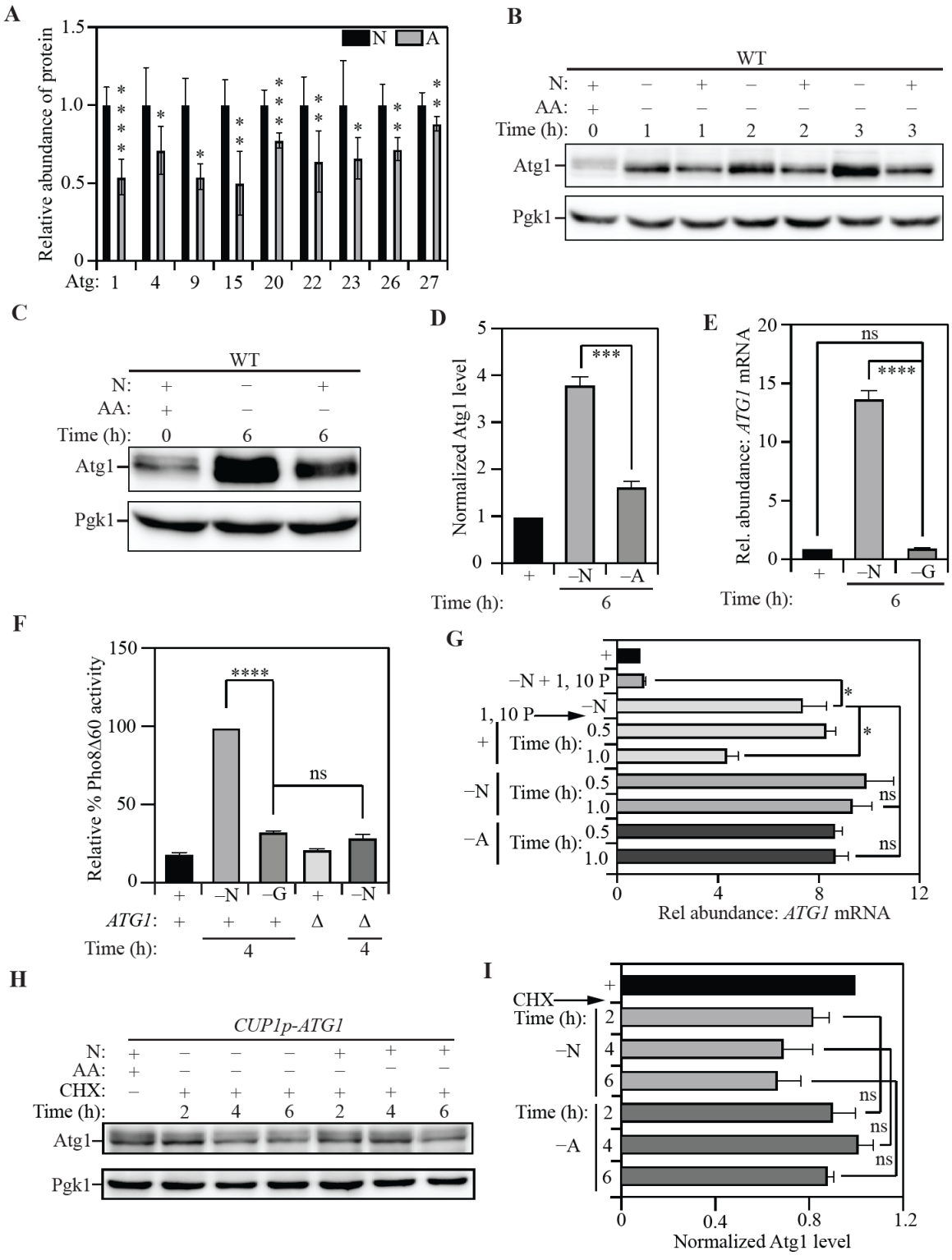

Figure 8. Post-transcriptional activation of *ATG* gene expression is a critical node determining autophagy during nitrogen starvation. (A) The Atg proteome is significantly different during nitrogen starvation compared to amino acid starvation: Triplex-SILAC labeling was used to compare the Atg protein abundance between nutrient-replete, nitrogen starvation and amino-acid starvation conditions in SEY6210 *arg4*Δ cells using LC-MS/MS. The plot shows the levels of differentially expressed Atg proteins during amino acid starvation (gray bars) relative to nitrogen starvation (black bars). Individual proteins were normalized to the total protein input. Data from at least three independent biological replicates. Significant differences are highlighted. (B) and (C) Atg1 levels increase substantially more during nitrogen versus amino acid starvation. WT (SEY6210) cells were harvested in nutrient-replete conditions or after starvation for the indicated times and protein levels analyzed by western blot. Pgk1 was used as a loading control. (D) Densitometric analysis of (C) from three independent biological replicates. (E) Transcriptional upregulation of *ATG1* occurs during nitrogen, but not glucose, starvation: qRT-PCR detection of *ATG1* mRNA in WT (SEY6210) cells after 1 h of starvation. *ALG9* was used as a reference gene for normalization. Data from three independent biological replicates. (F) Autophagy flux is upregulated during nitrogen, but not glucose, starvation: WT (WLY176) cells were harvested in nutrient-replete conditions or after starvation for the indicated times and Pho8Δ60 enzyme activity was measured by colorimetry. An increase in Pho8Δ60 activity indicates increased autophagic flux. Negative control: SEY6210 *atg1*Δ cells. Data from three independent biological replicates. (G) *ATG1* mRNA is stable under conditions of nitrogen and amino acid starvation: WT (SEY6210) cells were pulsed with nitrogen starvation to induce *ATG1* transcription and/or treated with the transcriptional inhibitor 1,10-phenanthroline (1,10 P)

to stop transcription. Cells were then kept in nitrogen-starvation medium or transferred to nutrient-replete medium or amino acid starvation for the indicated times. At each time point *ATG1* mRNA abundance was measured by qRT-PCR. *ALG9* was used as the reference gene for normalization. Data are from three independent biological replicates. (H) and (I) Atg1 protein is not preferentially degraded during amino acid starvation relative to nitrogen starvation: WT (SEY6210) cells harboring a centromeric *CUP1p-ATG1* (constitutive Atg1 expression) plasmid were grown in nutrient-replete conditions and treated with cycloheximide (CHX). Following treatment, cells were transferred to nitrogen or amino acid starvation medium and harvested at the indicated time points. Atg1 abundance was measured by western blot. Pgk1 was used as a loading control (H). Data from three independent biological replicates (I). Data in (A), (D), (E), (F), (G) and (I) represent mean ± SEM from indicated number of replicates. Statistical analysis for (A) and (D) was carried out using unpaired Student's t-test while (E), (F), (G) and (I) were analyzed using one-way analysis of variance (ANOVA). Multiple comparisons were carried out using Tukey's multiple comparisons test. *$p < 0.05$, **$p < 0.005$, ***$p < 0.001$, ****$p < 0.0001$ ns: not significant.

Figure 9: Post-transcriptional activation of ATG gene expression is a critical node determining autophagy during nitrogen starvation

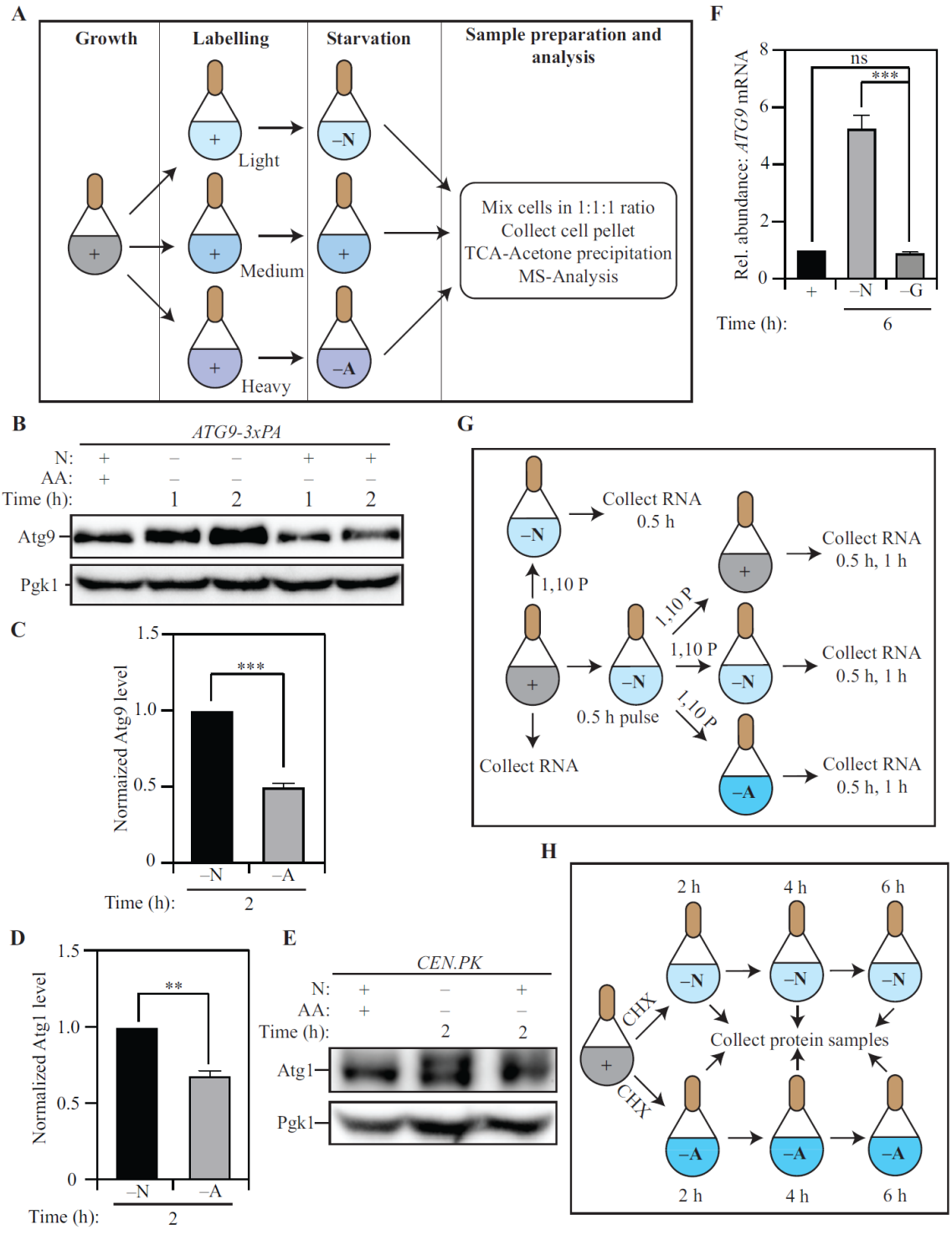

Figure 9. Post-transcriptional activation of *ATG* gene expression is a critical node determining autophagy during nitrogen starvation. (**A**) Scheme of the triplex SILAC experiment. "Light", "Medium" and "Heavy" refer to the nature of arginine and lysine isotopes present in the media. Across different biological replicates, the nature of the medium used for growing cells for each treatment (nutrient-replete, nitrogen starvation or amino acid starvation) was alternated. (**B**) Atg9 levels are higher during nitrogen starvation compared to amino acid starvation: WT (SEY6210) cells were harvested in nutrient-replete conditions or after starvation for the indicated times and Atg9 protein levels were assessed by western blot. Pgk1 was used as a loading control. (**C**) Densitometric analysis of (B) from three independent biological replicates. (**D**) Densitometric analysis of Atg1 levels in WT cells after 2 h of nitrogen or amino acid starvation (from Figure 8B) from three independent biological replicates. (**E**) Atg1 levels increase substantially more during nitrogen versus amino acid starvation: CEN.PK cells were harvested in nutrient-replete conditions or after starvation for the indicated times and protein levels analyzed by western blot. Pgk1 was used as a loading control. (**F**) Transcriptional upregulation of *ATG9* mRNA occurs during nitrogen, but not glucose, starvation: qRT-PCR-based detection of *ATG9* mRNA in WT cells after 1 h of starvation. *ALG9* was used as a reference gene for normalization. Data are from three independent biological replicates. (**G**) Schematic for *ATG1* mRNA stability assay by 1,10-phenanthroline (1,10 P) chase (Figure 8G). (**H**) Schematic for Atg1 stability assay by cycloheximide chase (Figures 8H and 8I). Data in (C), (D) and (F) represent mean ± SEM from indicated number of replicates. Statistical analysis for (C) and (D) was carried out using an unpaired Student's t-test while (F) was analyzed using one-way analysis of variance (ANOVA). Multiple comparisons were carried out using Tukey's

multiple comparisons test. $p < 0.05$, $^{**}p < 0.005$, $^{***}p < 0.001$, $^{****}p < 0.0001$ ns: not significant. Related to Figure 8.

2.2.3 Post-transcriptional regulation of ATG1 expression by Rad53 facilitates nitrogen starvation-induced autophagy

Higher Atg1 levels are correlated with the increased autophagy flux. To identify the molecular basis for increased Atg1 expression, we sought to identify regulators that specifically promote autophagy and Atg1 expression during nitrogen starvation. Because kinases are known to be involved in autophagy regulation (Licheva et al., 2021), we performed a screen to identify kinases that affected autophagy during nitrogen starvation. A Saccharomyces cerevisiae kinase deletion library, constructed in the BY4742 strain background, was utilized for this screen. Kinase deletion mutants were compared to wild-type BY4742 for identification of differences in autophagy flux. Autophagy flux was monitored by measuring the relative Atg8 degradation rate in the absence or presence of the serine protease inhibitor phenylmethylsulfonyl fluoride (PMSF). In brief, PMSF blocks the vacuolar degradation of Atg8 causing an increased accumulation of Atg8–PE when autophagy flux is high (Steinfeld et al., 2021). From this preliminary analysis we determined that the DNA damage response-related kinase Rad53 (Jung et al., 2019; Szyjka et al., 2008) is a potential regulator of autophagy and that the loss of Rad53 led to a 40% decrease in autophagy flux during nitrogen starvation (Figure 11A and 11B; data for other kinases not shown). Whereas Rad53 has been previously identified as a regulator of genotoxic-stress induced autophagy, its role in starvation-induced autophagy is unexplored (Eapen et al., 2017). Consistent with this finding, compared to wild-type (WT) cells, *rad53*Δ *sml1*Δ cells (deletion of *SML1* is essential for the viability of the *rad53*Δ strain) exhibited ~50% lower levels of Atg1 after nitrogen starvation, while the expression of Atg1 during amino acid starvation was not significantly affected (Figure 10A and 10B). During genotoxic stress, the regulation of autophagy by Rad53 occurs at the transcriptional level (Eapen et al., 2017). To

determine if the effect on Atg1 expression was post-transcriptional, we probed the level of *ATG1* mRNA in WT and *rad53*Δ *sml1*Δ cells using qRT-PCR and found that the steady state levels of ATG1 transcript was not affected by the deletion of *RAD53* during nitrogen starvation (Figure 10C). To investigate the effect of the *rad53*Δ *sml1*Δ deletion on autophagy flux, we used the Pho8Δ60 assay and found that while the loss of Rad53 led to a 25% reduction in autophagy during nitrogen starvation, it had no effect on autophagy during amino acid starvation (Figure 11C and 11D). Next, we utilized the accumulation of free GFP resulting from the nitrogen-starvation induced degradation of Pgi1-GFP as a marker for autophagy activity upon prolonged starvation (Liu et al., 2019). Pgi1-GFP has a longer half-life as an autophagy substrate during starvation relative to GFP-Atg8, preventing substrate exhaustion. Compared to WT cells or *sml1*Δ cells*, rad53*Δ *sml1*Δ cells showed 40% lower Pgi1-GFP processing activity (Figure 10D and 10E) after starvation, confirming that the autophagy phenotype is strictly due to the deletion of *RAD53* and not *SML1*.

Next, we utilized the differential Atg8 degradation assay to demonstrate that the kinase activity of Rad53 is responsible for its stimulatory effect on autophagy. The kinase-dead $Rad53^{K227A\ D339A}$ mutant of Rad53 (Holzen and Sclafani, 2010) exhibited a similar defect in autophagy as the *rad53*Δ *sml1*Δ strain (Figure 11E and 11F). To ensure that the autophagy phenotype of the *rad53*Δ *sml1*Δ strain is not due to chronic stress caused by the loss of Rad53, we used the auxin-inducible degron (AID) system to achieve tight temporal control of Rad53 loss (Morawska and Ulrich, 2013). Rad53-AID was degraded swiftly upon treatment with IAA (auxin) (Figure 10F; last two lanes). Compared to Rad53-AID cells treated with DMSO (vehicle), IAA-treated Rad53-AID cells showed an ~40% reduction in Atg1 expression (Figure 10F and 10G). Consistent with the results from the *rad53*Δ *sml1*Δ cells, the Pho8Δ60 activity

was reduced by ~25% in Rad53-AID cells treated with IAA, compared to those treated with DMSO (Figure 10H).

The canonical activation of Rad53 occurs downstream of the DNA damage response by the Mec1 kinase (Sweeney et al., 2005). Therefore, we tested whether Mec1 has any role in autophagy during nitrogen starvation. Accordingly, we constructed a MEC1-AID strain to probe if Mec1 plays a role in starvation-induced autophagy. IAA treatment in this strain did not result in decreased Atg1 expression (Figures 12A and 12B), or reduced autophagy flux as measured by the Pho8Δ60 activity assay (Figure 12C), compared to treatment with DMSO. This contrasts with DNA damage-induced autophagy where Mec1 is involved in autophagy regulation (Eapen et al., 2017), highlighting the fact that the role of Rad53 in nitrogen-starvation induced autophagy is distinct from its role in DNA-damage induced autophagy.

To probe selective Rad53 activation during nitrogen starvation we looked at differential phosphorylation of Rad53 between the two starvation conditions. The S175 site of Rad53 was previously identified by several large-scale phosphoproteome studies (Albuquerque et al., 2008; Chen et al., 2014), but the kinase responsible for the phosphorylation remains unclear (Schleker et al., 2010). Furthermore, a recent study demonstrated that unlike Rad53 S560, which is phosphorylated extensively in response to DNA damage, Rad53 S175 is only modestly phosphorylated, suggesting a distinct regulatory function for this site (Lanz et al., 2021). Our SILAC analysis identified S175 on Rad53 as a site that was more strongly phosphorylated during nitrogen starvation relative to amino acid starvation (Figure 10I). We reasoned that if this phosphorylation is critical for the autophagy-stimulating effect of Rad53, mutation of the residue to an alanine should dampen autophagy during nitrogen starvation. Indeed, the plasmid-based re-introduction of the phospho-dead Rad53^{S175A} mutant in a *rad53*Δ *sml1*Δ background revealed a

partial ~25% reduction in autophagy flux, as measured by the Pgi1-GFP processing assay, compared to the re-introduction of WT Rad53 (Figure 10J and 10K). This finding indicates that the S175 site is likely an important site for Rad53 activation during nitrogen starvation but may not be the sole activation site for Rad53. In-silico analysis suggested that the S175 residue is likely to be phosphorylated by a proline-directed kinase. Because the proline-directed kinase Cdc28 is known to regulate Rad53 phosphorylation (Abreu et al., 2013; Schleker et al., 2010), we examined whether Cdc28 is responsible for regulating *ATG1* expression during nitrogen-starvation induced autophagy. Treatment of a *CDC28-AID* strain with IAA led to complete loss of Cdc28 (Figure 12D; last two lanes) but had no effect on Atg1 levels (Figures 12D and 12E) or autophagy flux (Figure 12F) indicating that Cdc28 is not involved in nitrogen starvation-induced autophagy. Taken together, these data suggest that an unconventional mode of Rad53 activation promotes Atg1 expression and autophagy during nitrogen starvation.

Figure 10: Post-transcriptional regulation of ATG1 expression by Rad53 facilitates nitrogen starvation-induced autophagy

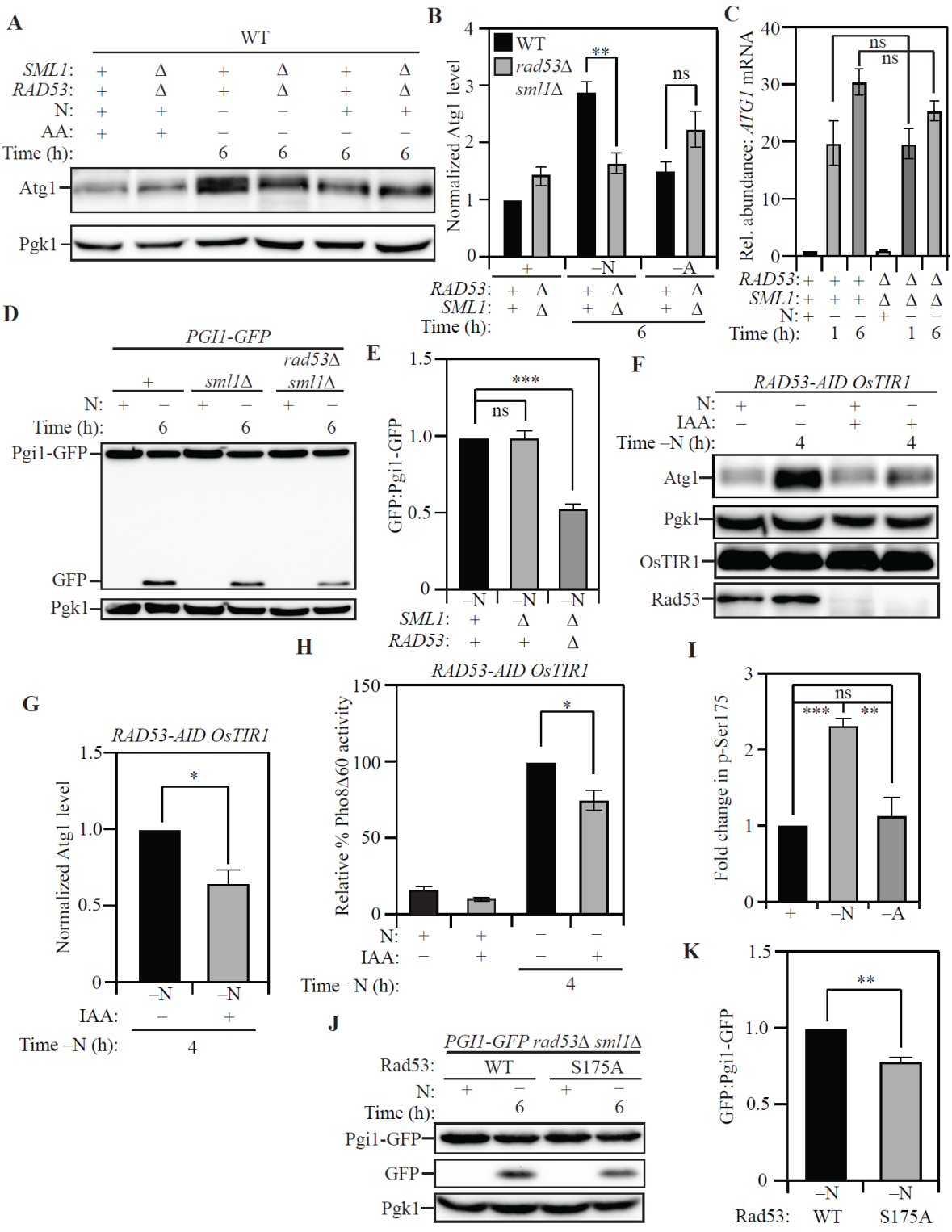

Figure 10. Post-transcriptional regulation of *ATG1* expression by Rad53 facilitates nitrogen starvation-induced autophagy. (A) Atg1 levels exhibit a significantly greater increase in WT (SEY6210) cells relative to *rad53*Δ *sml1*Δ cells upon nitrogen starvation but not upon amino acid starvation: Cells of the indicated genotypes were harvested during nutrient-replete conditions or after nitrogen or amino acid starvation for the indicated times and protein level examined by western blot. Pgk1 was used as a loading control. (B) Densitometric analyses for (A) from three independent biological replicates. (C) A similar abundance of *ATG1* transcript was detected in WT (SEY6210) and *rad53*Δ *sml1*Δ cells after nitrogen starvation: Cells of the indicated genotypes were harvested during nutrient-replete conditions or after starvation. qRT-PCR was used to determine *ATG1* transcript abundance using *ALG9* as the reference gene for normalization. Data from three independent biological replicates. (D) Autophagy flux during nitrogen starvation, assessed by the Pgi1-GFP processing assay, is reduced in *rad53*Δ *sml1*Δ cells compared to WT (SEY6210) and *sml1*Δ cells: Cells of the indicated genotypes, expressing chromosomally tagged Pgi1-GFP were harvested and examined as in (A). The appearance of free GFP indicates autophagy flux. (E) Densitometric analysis of (D) from three independent biological replicates. (F) The acute loss of Rad53 leads to a reduction in Atg1 expression during nitrogen starvation: WT (WLY176) *RAD53-AID* cells expressing the OsTIR1 ubiquitin ligase were treated with either IAA or DMSO and harvested during nutrient-replete conditions or after nitrogen starvation for the indicated times. IAA treatment activates the ligase activity and targets Rad53-AID for proteasomal degradation. Pgk1 was used as a loading control. (G) Densitometric analysis of (F) from three independent biological replicates. (H) The Pho8Δ60 assay reveals a reduction in autophagy flux during nitrogen starvation caused by the acute loss of Rad53: WT

(WLY176) *RAD53-AID OsTIR1* cells were harvested during nutrient-replete conditions or after starvation for the indicated times with or without IAA treatment, and Pho8Δ60 enzyme activity was measured by colorimetry. An increase in Pho8Δ60 activity indicates increased autophagic flux. Data are from three independent biological replicates. (I) Rad53 S175 phosphorylation levels are significantly higher in nitrogen starvation compared to amino acid starvation or nutrient-replete conditions: Phosphoproteome analysis of SEY6210 *arg4*Δ cells comparing nitrogen and amino acid starvation using triplex-SILAC labelling and LC-MS/MS analysis. The plot represents data from four independent biological replicates. (J) A phospho-dead mutation of Rad53 S175 ($Rad53^{S175A}$) reduces autophagy flux during nitrogen starvation, as examined by the Pgi1-GFP processing assay: WT (SEY6210) *rad53*Δ *sml1*Δ *PGI1-GFP* cells expressing either Rad53 or $Rad53^{S175A}$ were harvested during nutrient-replete conditions or after starvation for the indicated times. The appearance of free GFP indicates autophagy flux. Pgk1 used as loading control (K) Densitometric analysis of (J) from three independent biological replicates. Data in (B), (C), (E), (G), (H), (I) and (K) represent the mean ± SEM from the indicated number of replicates. Statistical analysis for (B), (C), (E) and (H) was carried out using one-way analysis of variance (ANOVA). (G) and (K) were analyzed using unpaired Student's t-test while (I) was analyzed using paired Student's t-test. Multiple comparisons were carried out using Tukey's multiple comparisons test. *$p < 0.05$, **$p < 0.005$, ***$p < 0.001$, ****$p < 0.0001$ ns: not significant.

Figure 11: Post-transcriptional regulation of ATG1 expression by Rad53 facilitates nitrogen starvation-induced autophagy

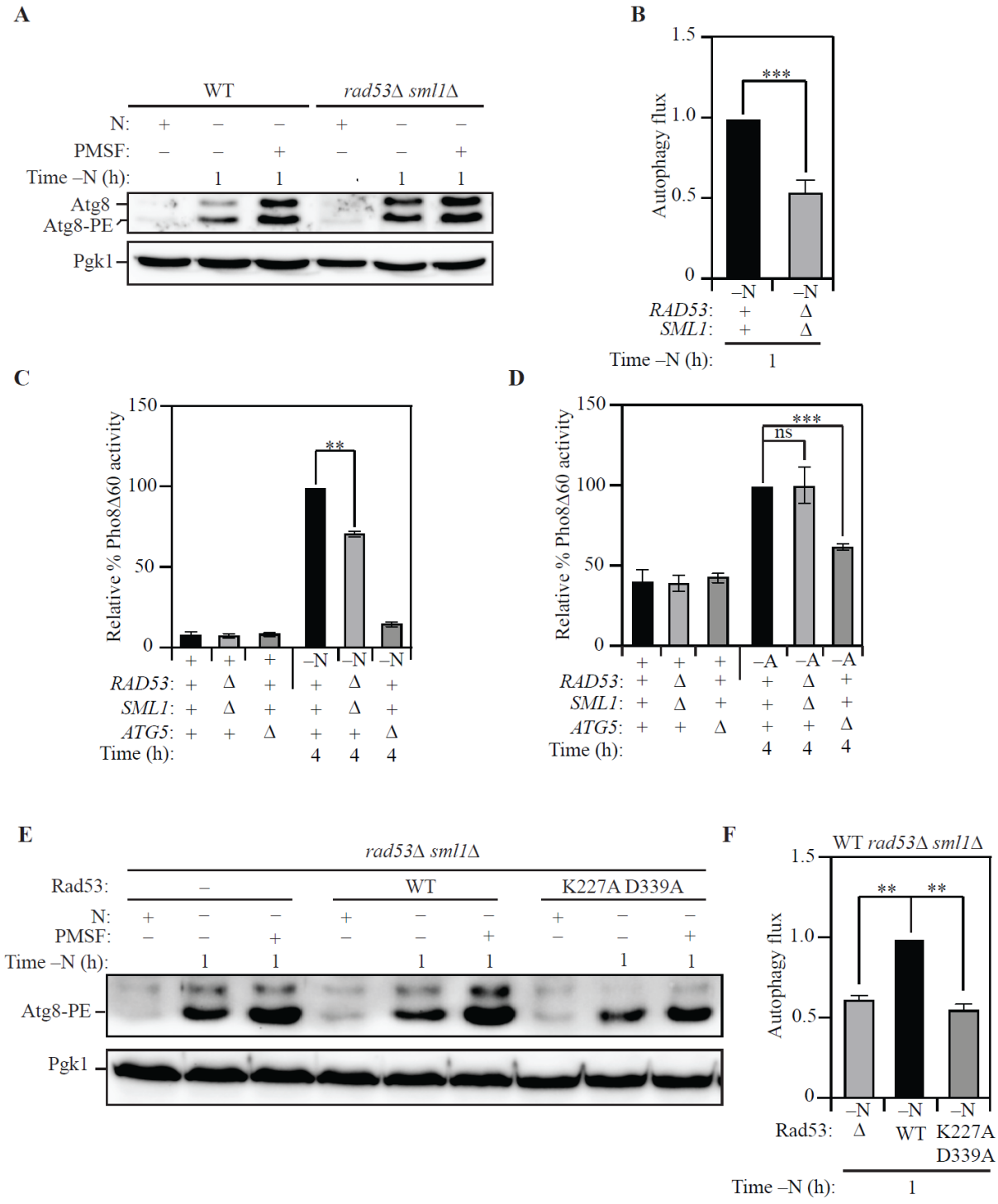

Figure 11. Post-transcriptional regulation of *ATG1* expression by Rad53 facilitates nitrogen starvation-induced autophagy. (A and B) The loss of Rad53 function reduces autophagy flux during nitrogen starvation but not amino acid starvation, as demonstrated by the Pho8Δ60 assay: WT (WLY176) and *rad53*Δ *sml1*Δ cells were harvested during nutrient-replete conditions or after nitrogen starvation (A) or amino acid starvation (B) for the indicated times. Pho8Δ60 enzyme activity was measured by colorimetry. An increase in Pho8Δ60 activity indicates increased autophagic flux. Negative control: SEY6210 *atg5*Δ cells. Data from three independent biological replicates. (**C**) The loss of Rad53 function impairs autophagy during nitrogen starvation as demonstrated by the Atg8-lipidation assay: WT (SEY6210) and *rad53*Δ *sml1*Δ cells were harvested during nutrient-replete conditions or after starvation with or without PMSF treatment. Increased Atg8–PE accumulation upon PMSF treatment (relative to no treatment control) indicates autophagy flux. (**D**) Densitometric analysis of (C) from three independent biological replicates. (**E**) Abolishing Rad53 kinase activity reduces autophagy flux during nitrogen starvation: WLY176 *rad53*Δ *sml1*Δ cells expressing either Rad53 or Rad53^{K227A,D339A} (kinase dead Rad53) from a centromeric plasmid were harvested during nutrient-replete conditions or after starvation with or without PMSF treatment. Increased Atg8–PE accumulation upon PMSF treatment (relative to the no-treatment control) indicates autophagy flux. (**F**) Densitometric analysis of (E) from three independent biological replicates. Data in (A), (B), (D) and (F) represent mean ± SEM from the indicated number of replicates. Statistical analysis for (A) and (B) was carried out using two-way analysis of variance (ANOVA) while (D) was analyzed using an unpaired Student's t-test. Statistical analysis for (F) was carried out using one-

way analysis of variance (ANOVA). Multiple comparisons were carried out using Tukey's multiple comparisons test. *$p < 0.05$, **$p < 0.005$, ***$p < 0.001$, ****$p < 0.0001$ ns: not significant. Related to Figure 10.

Figure 12: Mec1 and Cdc28 are not involved in Rad53 activation during nitrogen starvation-induced autophagy

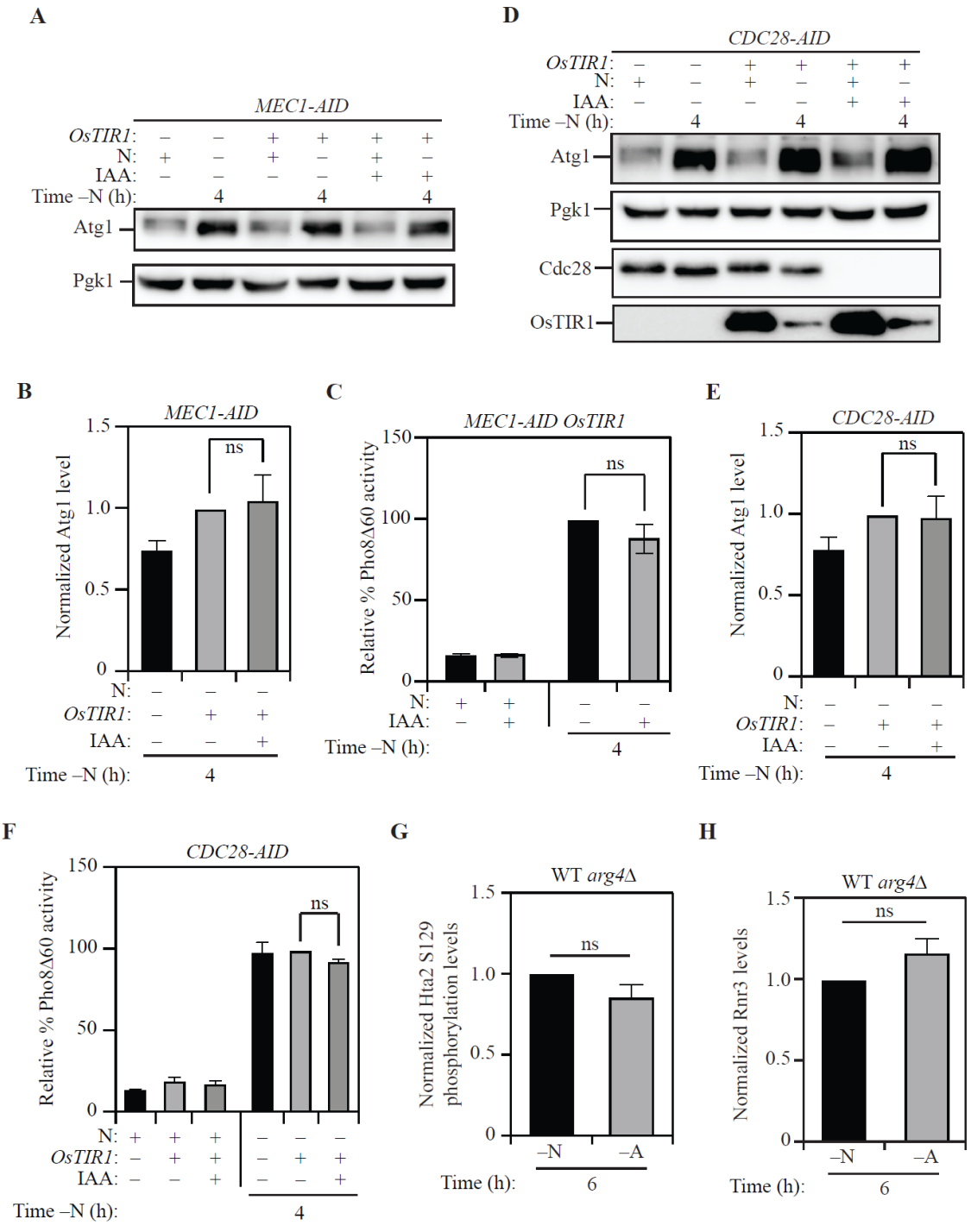

Figure 12. Mec1 and Cdc28 are not involved in Rad53 activation during nitrogen starvation-induced autophagy. Mec1 and Cdc28 are not involved in Rad53 activation during nitrogen starvation-induced autophagy. (**A**) The acute loss of Mec1 has no effect on Atg1 expression during nitrogen starvation: WT (WLY176) *CUP1p-GFP-ATG8 MEC1-AID* cells without OsTIR1 expression and WT *CUP1p-GFP-ATG8 MEC1-AID OsTIR1* cells were harvested during nutrient-replete conditions or after nitrogen starvation with or without IAA treatment. Atg1 proteins levels were examined by western blot. Pgk1 was used as a loading control. (**B**) Densitometric analysis of three independent biological replicates from (A). (**C**) The acute loss of Mec1 does not affect autophagy flux during nitrogen starvation: WLY176 *CUP1p-GFP-ATG8 MEC1-AID OsTIR1* cells were harvested as in (A) and Pho8Δ60 enzyme activity was measured by colorimetry. An increase in Pho8Δ60 activity indicates increased autophagic flux. Data from three independent biological replicates. (**D**) The acute loss of Cdc28 has no effect on Atg1 expression: WT *CUP1p-GFP-ATG8 CDC28-AID* cells without OsTIR1 expression and WT *CUP1p-GFP-ATG8 CDC28-AID OsTIR1* cells were harvested and examined as in (A). Pgk1 was used as a loading control. (**E**) Densitometric analysis of three independent biological replicates from (D). (**F**) The acute loss of Cdc28 does not affect autophagy flux during nitrogen starvation: WLY176 *CUP1p-GFP-ATG8 CDC28-AID OsTIR1* cells were harvested and measured as in (C). Data from three independent biological replicates. (**G and H**) No differential DNA damage in nitrogen starvation relative to amino acid starvation. Hta2 S129 phosphorylation levels (G) and Rnr3 levels (H) are similar during nitrogen and amino acid starvation (see text for details). Data in (B), (C), and (E-H) represent the mean ± SEM from the indicated number of replicates. Statistical analysis for (B) and (E) was carried out using one-way

analysis of variance (ANOVA). Statistical analysis for (C) and (F) was carried out using two-way analysis of variance (ANOVA). Statistical analysis for (G) and (H) was carried out using Unpaired t-test. Multiple comparisons were carried out using Tukey's multiple comparisons test. *$p < 0.05$, **$p < 0.005$, ***$p < 0.001$, ****$p < 0.0001$, ns: not significant. Related to Figure 10.

2.2.4 Ded1 binds ATG1 mRNA to promote Atg1 expression

Our results indicated that post-transcriptional mechanisms promote the expression of Atg1 during nitrogen starvation relative to amino acid starvation. Therefore, we hypothesized that the regulation occurs via an RNA-binding protein (RBP), which binds *ATG1* mRNA preferentially during nitrogen starvation and facilitates its translation. Accordingly, we carried out an unbiased preliminary screen for proteins that bind the 5'-UTR of *ATG1* which identified Ded1 in addition to several previously characterized *ATG1* mRNA-binding proteins (see Materials and Methods for details on the screen methodology).

Ded1 is an essential RNA-helicase that is involved in promoting translation initiation under nutrient-rich conditions (de la Cruz et al., 1997) that has recently been demonstrated to be a Rad53 substrate (Lao et al., 2018). Because Ded1 was identified from a single large-scale dataset, we used RNA-immunoprecipitation (RNA-IP) to verify that Ded1 binds *ATG1* mRNA in vivo during nitrogen starvation. For this purpose, we tagged Ded1 with a 3xPA-tag and affinity isolated Ded1-PA, harvested from cells subjected to nitrogen starvation, using IgG-Sepharose beads. This affinity isolation was followed by the extraction of bound RNA and detection using qRT-PCR. As a control, we used a strain where Ded1 was not epitope tagged with PA, which served as the background to eliminate non-specific isolates (Gatica et al., 2018; Liu et al., 2019). Using *PGK1* mRNA as an internal control, and normalizing detection to the untagged strain, we found that Ded1 specifically associates with the 5'-UTR of *ATG1* mRNA in vivo (Figure 13A). We validated this interaction using a reciprocal approach: we synthesized 500 bp of the 5'-UTR of *ATG1* mRNA immediately upstream of the ORF and labeled the synthesized RNA with desthiobiotin. We incubated this RNA with nitrogen-starved yeast cell lysates. Following cross-

linking and streptavidin affinity isolation, we probed the interaction between the in vitro synthesized *ATG1* 5'-UTR fragment (*ATG1* fragment) and endogenous epitope-tagged Ded1 (Ded1-PA) from nitrogen starved cell lysates by immunoblotting. Indeed, we found that Ded1-PA exhibited a 4-fold enrichment when affinity isolated with the *ATG1* fragment compared to the control RNA fragment (Figures 13B and 13C), indicating specific binding to the *ATG1* fragment.

We next tested whether Ded1 has a stimulatory role in Atg1 expression during nitrogen starvation. Because DED1 is an essential gene, we used a temperature sensitive ded1-95 strain (ded1ts) to investigate Atg1 expression at permissive (23°C) and non-permissive (35°C) temperatures relative to WT (Burckin et al., 2005). At both temperatures, the expression of Atg1 was significantly reduced in the ded1ts strain with a severe 80% reduction at the non-permissive temperature (Figure 15A and 15B). This reduction was post-transcriptional because the steady state levels of *ATG1* mRNA were essentially unchanged between the wild-type and the *ded1^{ts}* strains (Figure 15C).

Contrary to the reduction in Atg1 levels, a significant reduction was not noticed in the levels of Atg9 in the ded1ts strain, which highlights the specificity of Ded1 for *ATG1* mRNA (Figures 15D and 15E). To eliminate the possibility of the defects being caused due to chronic stress in the ded1ts strain, we generated an auxin-inducible Ded1 (*DED1-AID*) strain to temporally control the loss of Ded1. Treatment with IAA led to degradation of cellular Ded1 (Figure 13D, last lane). We used this strain to probe for differences in Atg1 expression upon Ded1 degradation. Relative to DMSO treatment, degradation of Ded1 by IAA treatment led to an 80% reduction in Atg1 expression (Figures 13D and 13E), consistent with the reduction observed in the ded1ts strain. Once again, loss of Ded1 by IAA treatment did not affect *ATG1* mRNA

levels (Figure 13F) indicating post-transcriptional regulation. To ensure that the acute loss of Ded1 did not affect general translation, we used Coomassie Brilliant Blue staining to compare total protein profiles of *DED1-AID* cells treated with or without IAA after nitrogen starvation (Figure 15F). Quantification of lane profiles indicated that there was no significant decrease in the total protein content upon IAA-mediated Ded1 degradation (Figure 15G).

Next, we tested whether the strength of the interaction between Ded1 and the 5'-UTR of the *ATG1* mRNA differed in amino acid starvation relative to nitrogen starvation. Using epitope-tagged Ded1 (Ded1-13xMYC) for RNA-IP, we investigated this interaction in cells subjected to nitrogen starvation and amino acid starvation. Consistent with our hypothesis, Ded1 binding to the 5'-UTR of the *ATG1* mRNA was reduced by ~60% in amino acid starvation relative to nitrogen starvation (Figure 13G). This was not due to reduced Ded1 expression because Ded1 levels were higher during amino acid starvation relative to nitrogen starvation (Figure 13H). This finding suggests that while a basal level of Ded1-*ATG1* mRNA interaction is present during amino acid starvation, increased Ded1 binding to the *ATG1* mRNA promotes increased Atg1 synthesis during nitrogen starvation. Indeed, when probing the levels of Atg1 after amino acid starvation in the *DED1-AID* strain, we observed an ~35% reduction in Atg1 level upon Ded1 degradation by IAA (Figures 13I and 13J), compared to the ~75% reduction observed during nitrogen starvation. This result highlights the fact that Ded1 promotes Atg1 expression preferentially during nitrogen starvation.

Finally, to investigate whether Rad53 promotes the binding of Ded1 to *ATG1* mRNA, we compared the ability of epitope-tagged Ded1 (Ded1-13xMYC) to bind the 5'-UTR of *ATG1* mRNA in WT and rad53Δ sml1Δ cells using RNA-IP. Using *PGK1* mRNA as an internal control, we determined that the ability of Ded1 to bind the 5'-UTR of *ATG1* mRNA was reduced

by 65% in a *rad53*Δ *sml1*Δ background (Figure 13K), mirroring the reduction in binding in amino-acid relative to nitrogen-starvation conditions. Taken together, these findings indicate that Ded1 binds the 5'-UTR of *ATG1* mRNA. Moreover, they also reveal that this binding preferentially occurs during nitrogen starvation and is mediated, at least in part, by Rad53.

Having determined that Ded1 regulates Atg1 expression, we investigated the role of Ded1 in autophagy. To measure the impact of Ded1 on autophagy flux, we transformed WT and *ded1*^{ts} cells with an *ATG8*-promoter driven *GFP-ATG8* plasmid and followed the appearance of free GFP after nitrogen starvation. Autophagy flux was reduced in the ded1ts strain at both permissive and non-permissive temperatures, relative to WT (Figures 15H and 15I). We confirmed this phenotype with biochemical assays utilizing the Ded1-AID strain chromosomally expressing a *CUP1* promoter-driven GFP-Atg8, where treatment with IAA led to a 70% reduction in autophagy flux compared to treatment with DMSO (Figure 14A and 14B). This was corroborated by the Pho8Δ60 activity assay, where the loss of Ded1 led to a 60% reduction in autophagy flux (Figure 14C). Mirroring its effect on Atg1 expression during amino acid starvation relative to nitrogen starvation, loss of Ded1 by IAA treatment led to a smaller (~30%) reduction in autophagy flux, as assessed by the Pho8Δ60 activity assay (Figure 14D). Next, we used a *pep4*Δ *vps4*Δ *DED1-AID* strain to directly compare autophagosome formation in the presence and absence of Ded1 (Figure 14E) after nitrogen starvation using TEM. The loss of Ded1 by IAA treatment caused a severe reduction in the number of ABs accumulated within the vacuole, indicating a lower frequency of autophagosome formation (Figures 14F and 14G). The size of the ABs was also reduced in the IAA-treated *DED1-AID* cells (Figure 14H). Taken together, these findings implicate Ded1 in the regulation of autophagy flux through the regulation of Atg1 expression (Figure 14I).

Figure 13: Ded1 binds ATG1 mRNA to promote Atg1 expression

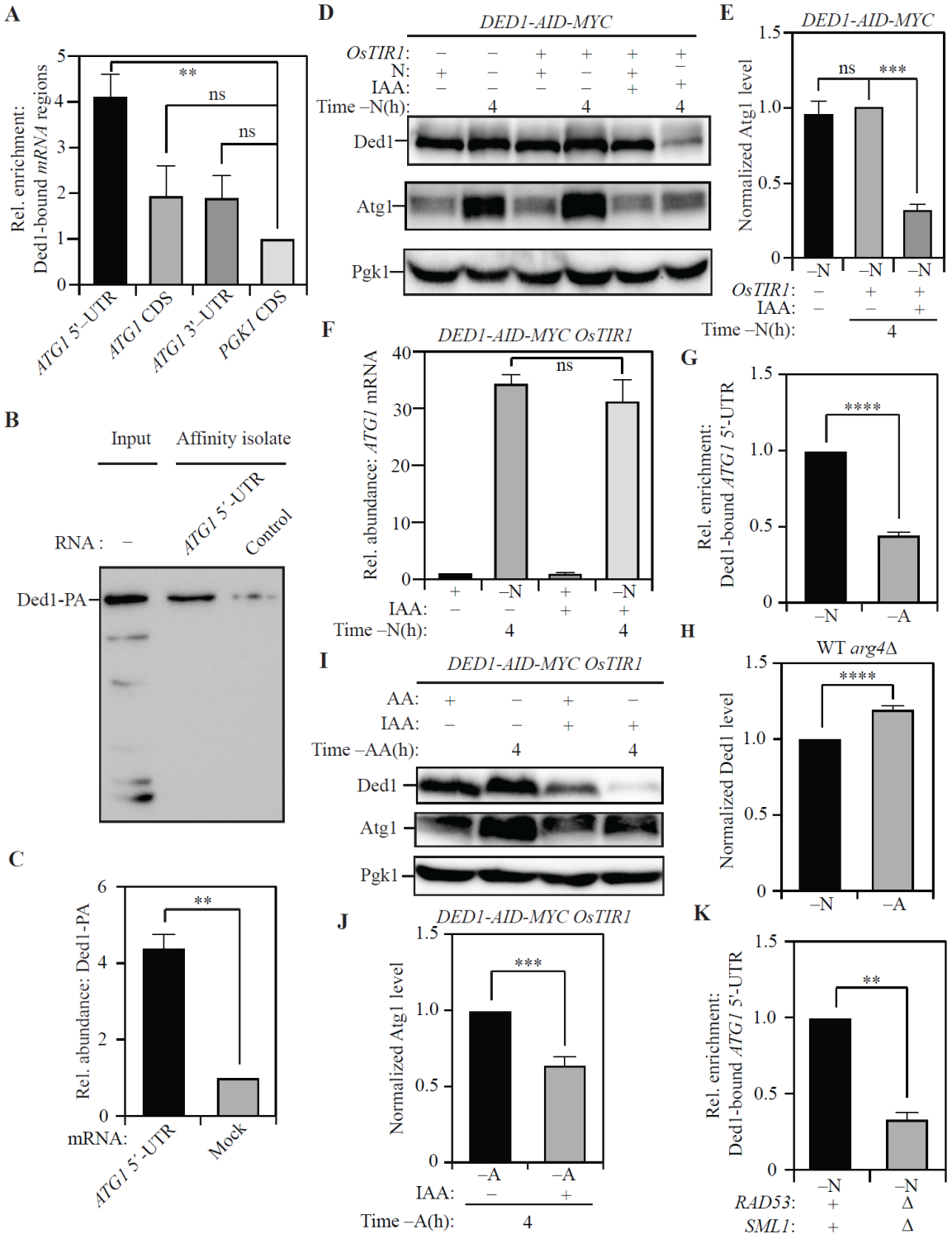

Figure 13. Ded1 binds *ATG1* mRNA to promote Atg1 expression. (A) RNA-IP analysis demonstrates Ded1 binding to the 5'-UTR of *ATG1* mRNA during nitrogen starvation: PA-tagged Ded1 was immunoprecipitated using IgG-Sepharose beads and bound RNA was amplified and detected by qRT-PCR. Specific primers were used to identify the relative enrichment of the indicated regions of the *ATG1* mRNA. Primers targeting the *PGK1* mRNA coding sequence (CDS) were used as an internal control. A strain with untagged Ded1 was used as a control for normalization. (B) In vitro RNA affinity isolation confirms interaction between Ded1 and the 5'-UTR of *ATG1* mRNA during nitrogen starvation: The sequence of bases from 500 bp upstream of the *ATG1* mRNA up to the coding sequence of *ATG1* mRNA was synthesized *in vitro* and labelled with desthibiotin (*ATG1* 5'-UTR fragment). The fragment was incubated with lysates from WT (SEY6210) Ded1-13xMYC cells. The RNA was affinity isolated using streptavidin, and Ded1 was probed by immunoblotting using anti-MYC antibody. The presence of Ded1 indicates binding to the *ATG1* 5'-UTR fragment. Mock fragment (random sequence) used as a control (C) Data for (B) from three independent biological replicates. (D) The acute loss of Ded1 leads to reduced Atg1 expression during nitrogen starvation: WT (WLY176) *CUP1p-GFP-ATG8 DED1-AID* cells without OsTIR1 expression and WT (WLY176) *CUP1p-GFP-ATG8 DED1-AID OsTIR1* cells were harvested during nutrient-replete conditions or after nitrogen starvation with or without IAA treatment and protein levels were examined by western blot. Pgk1 was used as a loading control. (E) Densitometric analysis of Atg1 levels from (D) from three independent biological replicates. (F) The acute loss of Ded1 has no effect on *ATG1* transcription during nitrogen starvation: Total RNA was isolated from WT (WLY176) *CUP1p-GFP-ATG8 DED1-AID OsTIR1* cells during nutrient-replete conditions

or after nitrogen starvation with or without IAA treatment. qRT-PCR analysis was used to measure the *ATG1* transcript level with *ALG9* as a reference gene. Data from three independent biological replicates. (G) The interaction between Ded1 and the 5'-UTR of *ATG1* mRNA is stronger during nitrogen starvation compared to amino acid starvation, as demonstrated by RNA-IP analysis. Data are representative of three independent biological replicates. (H) Ded1 levels are higher during amino acid starvation relative to nitrogen starvation: Ded1 levels were measured in WT (SEY6210) *arg4*Δ cells using SILAC and normalized to total protein input per sample. (I) The acute loss of Ded1 leads to a partial decrease in Atg1 expression during amino acid starvation: WT (WLY176) *CUP1p-GFP-ATG8 DED1-AID OsTIR1* cells were harvested during nutrient-replete conditions or after amino acid starvation with or without IAA treatment and protein levels examined by western blot. Pgk1 was used as a loading control. (J) Densitometric analysis of Atg1 levels in (I) from three independent biological replicates. (K) The interaction between Ded1 and *ATG1* mRNA is weaker in *rad53*Δ *sml1*Δ cells relative to WT (SEY6210) cells during nitrogen starvation, as demonstrated by RNA-IP analysis. Data are representative of three independent biological replicates. Data in (A), (C), (E), (F), (G), (I) and (J) represent the mean ± SEM from the indicated number of replicates. Statistical analysis for (A), (E) and (F) was carried out using one-way analysis of variance (ANOVA) while (C), (G), (I) and (J) were analyzed using unpaired Student's t-test. Multiple comparisons were carried out using Tukey's multiple comparisons test. *$p < 0.05$, **$p < 0.005$, ***$p < 0.001$, ****$p < 0.0001$ ns: not significant.

Figure 14: Ded1 regulates autophagy in yeast

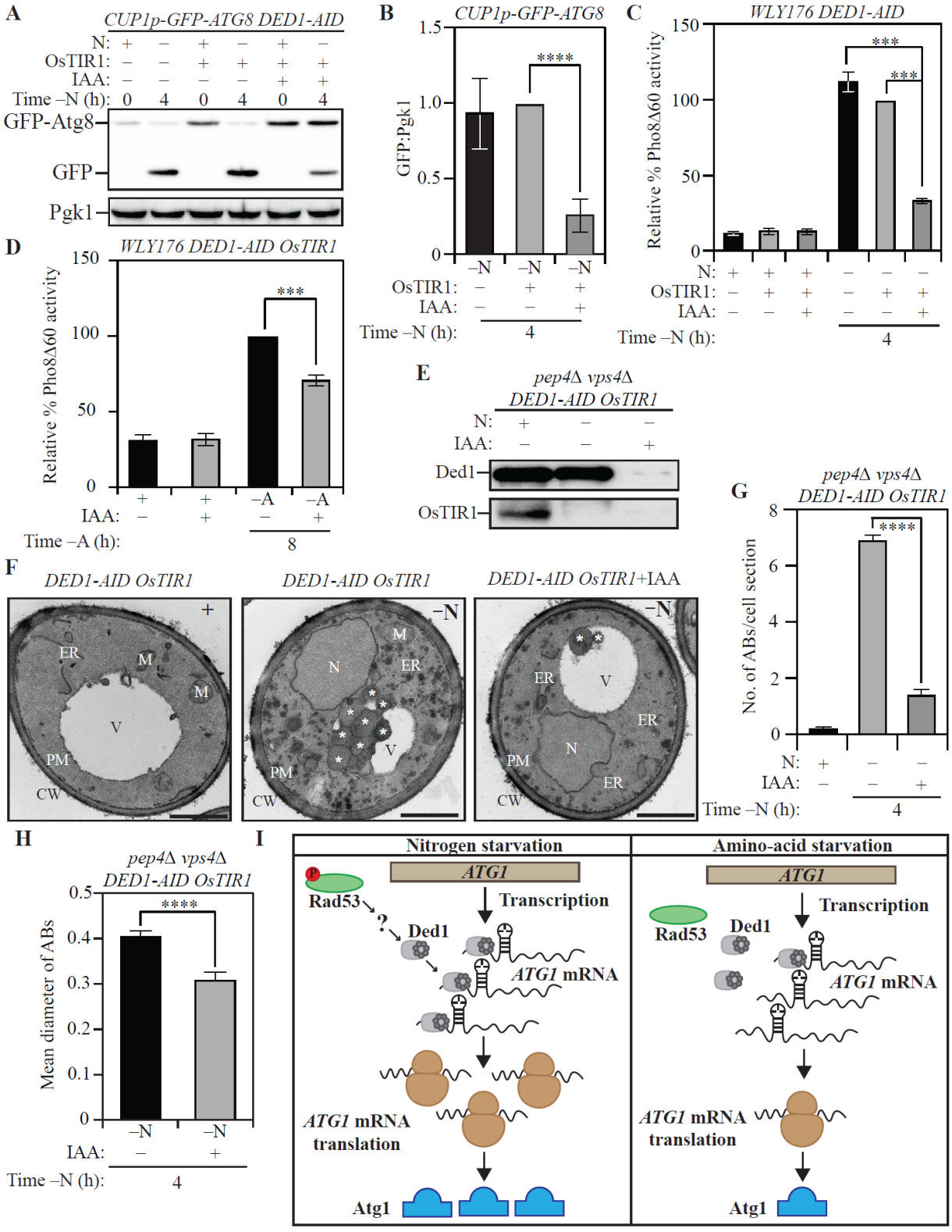

Figure 14. Ded1 regulates autophagy in yeast. (A) The acute loss of Ded1 causes a reduction in autophagy flux during nitrogen starvation as assessed by the GFP-Atg8 processing assay: WT (WLY176) *CUP1p-GFP-ATG8 DED1-AID* cells lacking OsTIR1 and WT (WLY176) *CUP1p-GFP-ATG8 DED1-AID OsTIR1* cells were harvested during nutrient-replete conditions or after nitrogen starvation with or without IAA treatment and examined by western blot. The appearance of free GFP indicates autophagy flux. (B) Densitometric analysis of (A) from three independent biological replicates. (C) and (D) The acute loss of Ded1 reduces autophagy flux significantly more during nitrogen starvation than amino acid starvation as demonstrated by the Pho8Δ60 assay: WT (WLY176) *CUP1p-GFP-ATG8 DED1-AID* cells and WT (WLY176) *CUP1p-GFP-ATG8 DED1-AID OsTIR1* cells were harvested during nutrient-replete and nitrogen starvation (C) or amino-acid starvation (D) conditions and Pho8Δ60 enzyme activity was measured by colorimetry. An increase in Pho8Δ60 activity indicates increased autophagic flux. Data are from three independent biological replicates. (E) Degradation of Ded1-AID upon IAA treatment in SEY6210 *pep4*Δ *vps4*Δ *DED1-AID OsTIR1* cells. (F), (G) and (H) Defects in autophagosome formation during nitrogen starvation due to acute loss of Ded1: (F) SEY6210 *pep4*Δ *vps4*Δ *DED1-AID OsTIR1* cells were harvested during nutrient-replete conditions or after 3-h nitrogen starvation with or without IAA treatment. The cells were fixed, stained and ultrastructural analysis was used to visualize the number and size of ABs. (G) Quantification of the number of ABs from 100 randomly selected cell profiles from two independent biological replicates. (H) Quantification of the diameter of ABs counted in (G). (I) Schematic depicting the proposed post-transcriptional regulation of *ATG1* expression that regulates autophagy differentially between nitrogen and amino acid starvation. Data in (B), (C), (D), (G) and (H) represent mean ± SEM from the indicated number of replicates. Statistical analysis was carried

out using one-way analysis of variance (ANOVA) Multiple comparisons were carried out using Tukey's multiple comparisons test. *$p < 0.05$, **$p < 0.005$, ***$p < 0.001$, ****$p < 0.0001$ ns: not significant.

Figure 15: Ded1 regulates Atg1 expression and autophagy in yeast

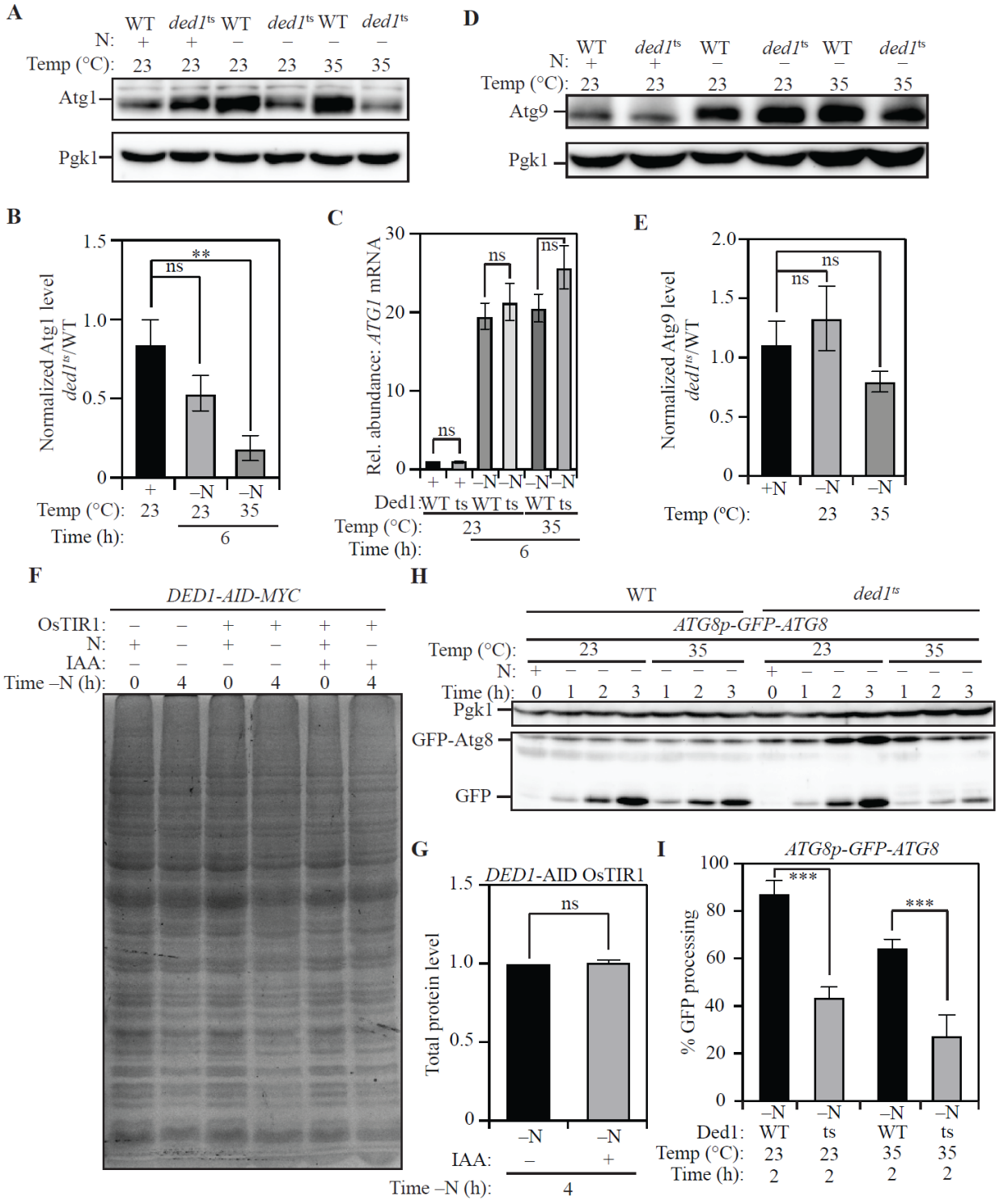

Figure 15. Ded1 regulates Atg1 expression and autophagy in yeast. (A) The loss of Ded1 activity impairs Atg1 expression during nitrogen starvation: WT (SEY6210) or *ded1*^{ts} (non-permissive temperature: 35°C) strains were harvested during nutrient-replete conditions or after nitrogen starvation at 23°C or 35°C. Atg1 levels were examined using western blot. Pgk1 was used as a loading control. (**B**) Densitometric analyses of Atg1 expression in *ded1*^{ts} relative to SEY6210 from three independent biological replicates. (**C**) The loss of Ded1 activity has no effect on *ATG1* transcription during nitrogen starvation: Strains and conditions as in (A) were used to measure the levels of *ATG1* mRNA by qRT-PCR. *ALG9* was used as a reference gene for normalization. Data from three independent biological replicates. (**D**) The loss of Ded1 activity has no effect on Atg9 expression: WT (SEY6210) or *ded1*^{ts} strains were harvested as in (A). Atg9 levels were examined using western blot. Pgk1 was used as a loading control. (**E**) Densitometric analyses of Atg9 expression in *ded1*^{ts} relative to the WT (SEY6210) from three independent biological replicates. (**F**) Total protein profile reveals that the loss of Ded1 activity does not promote changes in general translation during nitrogen starvation: WT (WLY176) *CUP1p-GFP-ATG8 DED1-AID* cells without OsTIR1 expression and WT (WLY176) *CUP1p-GFP-ATG8 DED1-AID OsTIR1* cells harvested during nutrient-replete conditions or after nitrogen starvation with or without IAA treatment. Proteins were stained using Coomassie Brilliant Blue. (**G**) Total protein quantified by densitometric analysis of five prominent bands from the total profile across three independent biological replicates. (**H**) The loss of Ded1 activity impairs autophagy flux during nitrogen starvation, assessed by the GFP-Atg8 processing assay: WT (SEY6210) or *ded1*^{ts} (non-permissive temperature: 35°C) cells were transformed with

an *ATG8p-GFP-ATG8* plasmid (expressing *ATG8* under the control of the endogenous promoter) and harvested in nutrient-replete conditions or after starvation for the indicated times at either 23°C or 35°C. Proteins were examined by western blot. The appearance of free GFP indicates autophagy flux. Pgk1 was used as a loading control. (**I**) Densitometric analysis from three independent biological replicates. Data in (B), (C), (E), (G) and (I) represent the mean ± SEM from the indicated number of replicates. Statistical analysis for (B), (C), (E) and (I) was carried out using one-way analysis of variance (ANOVA). Statistical analysis for (G) was carried out using an unpaired Student's t-test. Multiple comparisons were carried out using Tukey's multiple comparisons test. *$p < 0.05$, **$p < 0.005$, ***$p < 0.001$, ****$p < 0.0001$ ns: not significant. Related to Figures 13 and 14.

2.2.5 DDX3 regulates ULK1 expression and autophagy in mammalian cells

To examine whether the function of Ded1 is conserved, we investigated the ability of DDX3, the mammalian homolog of Ded1 (Tarn and Chang, 2009), to regulate ULK1 expression. We used the pancreatic ductal cancer-derived cell line PANC-1 as well as the fibrosarcoma-derived cell line HT-1080 to probe for a role of DDX3 in autophagy regulation. We found that stable knockdown (KD) of DDX3 led to a reduction in the level of ULK1 protein (Figure 16A) in PANC-1 cells. Crucially, the reduction in ULK1 levels occurred without reduction in the level of ULK1 mRNA (Figure 16B) indicating post-transcriptional regulation. To measure changes in autophagy caused by DDX3 KD, PANC-1 cells were treated with the MTOR inhibitor rapamycin for up to 4 h. At all the time points tested (0.5, 2 and 4 h), DDX3 KD cells (Figure 16C and 16D) showed reduced ULK1 expression (Figure 16C and 16E) and reduced LC3-lipidation ratio (LC3-II:LC3-I; Figure 16C and 16F) relative to control cells. Additionally, co-treatment with bafilomycin A_1 enhanced the LC3 lipidation ratio in both control and DDX3 KD cells, with control cells still exhibiting significantly higher levels of lipidated LC3 compared to DDX3 KD. This finding highlighted the fact that the decreased LC3 lipidation ratio in shDDX3 cells could not be attributed to accelerated autophagy flux but was caused be an overall reduction in autophagy (Klionsky et al., 2021) (Figure 16C and 16F). Finally, the increased accumulation of SQSTM1 in DDX3 KD cells relative to control cells confirmed that autophagy flux was reduced upon loss of DDX3 (Bjorkoy et al., 2009) (Figure 16C and 16G). In contrast, the level of ATG5 was unaffected upon DDX3 KD highlighting the fact that DDX3 loss did not affect general ATG gene expression (Figures 16C and 17A). The phenotypes observed in PANC-1 cells

were consistent in HT-1080 cells: stable DDX3 KD (Figures 17B and 17C) led to a reduction in ULK1 levels without alteration of *ULK1* mRNA (Figures 17B, 17D and 17E), as well as a reduction in the LC3 lipidation ratio (both with and without bafilomycin A1; Figures 17B and 17F). Similarly, DDX3 KD caused an increased accumulation of SQSTM1 following rapamycin treatment, but no further increase with bafilomycin A1, indicating a reduction in autophagy rather than accelerated flux (Figures 17B and 17G) without affecting ATG5 levels (Figures 17B and 17H). Taken together, these data indicate that DDX3 plays a selective role in modulating ULK1 expression and regulating autophagy in mammalian cells.

Figure 16: DDX3 regulates autophagy in mammalian cells

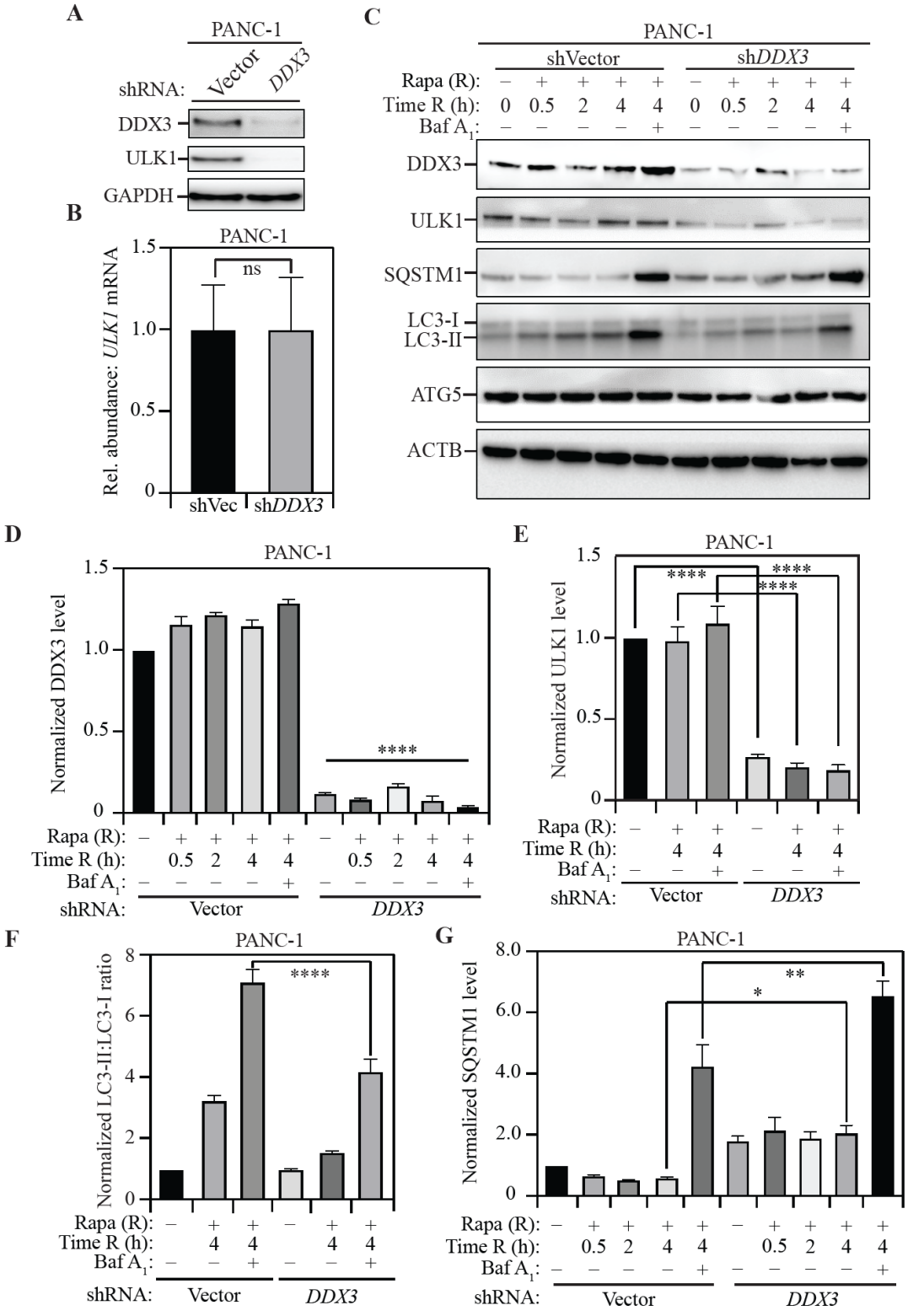

Figure 16. DDX3 regulates autophagy in mammalian cells. (A) Stable shRNA-mediated knockdown of DDX3 in PANC-1 cells: Western blotting to probe for DDX3 and ULK1 levels in cells transfected with shVector (control) or sh*DDX3*. GAPDH was used as a loading control. (B) Relative abundance of *ULK1* mRNA in sh*DDX3* cells compared to control cells. *GAPDH* was used as a reference gene. Data represent three independent biological replicates. (C) The loss of DDX3 leads to a reduction in ULK1 levels and autophagy in mammalian cells: PANC-1 cells, stably transfected with either vector shRNA (control) or shRNA targeting *DDX3*, were treated with rapamycin (Rapa; R) for the indicated times with or without co-treatment with bafilomycin A_1 (Baf A_1). A representative blot shows the levels of DDX3, ULK1, SQSTM1, LC3-I, LC3-II, and ATG5 with ACTB as a loading control, upon harvesting cells at the indicated time points after rapamycin treatment. (D) and (E) Normalized DDX3 (D) and ULK1 (E) levels at the indicated time points with the indicated treatments. Data represent three independent biological replicates. (F) Normalized LC3-II:LC3-I ratio at the indicated time points with the indicated treatments. Decreased LC3-II:LC3-I ratio in the presence of bafilomycin A_1 indicates reduced autophagy flux. Data represent three independent biological replicates. (G) Normalized SQSTM1 level at the indicated time points with the indicated treatments. Increased SQSTM1 accumulation indicates reduced autophagy flux. Data represent three independent biological replicates. Data in (B), (D), (E), (F) and (G) represent mean ± SEM from indicated number of replicates. (B) was analyzed using unpaired Student's t-test while the statistical analysis for (D), (E), (F) and (G) was carried out using one-way analysis of variance (ANOVA). Multiple comparisons were carried out using Tukey's multiple comparisons test. *$p < 0.05$, **$p < 0.005$, ***$p < 0.001$, ****$p < 0.0001$ ns: not significant.

Figure 17: DDX3 regulates autophagy in mammalian cells

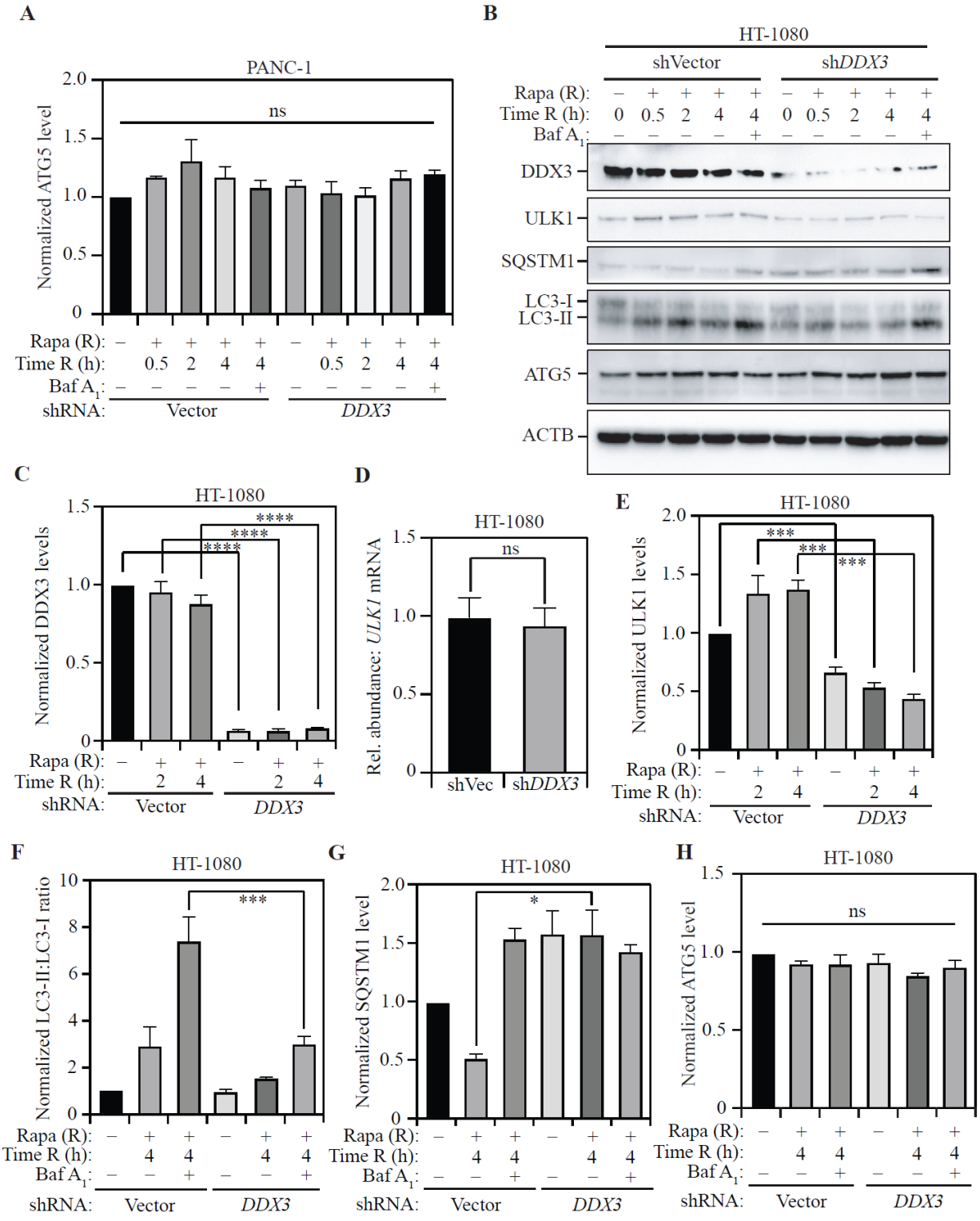

Figure 17. DDX3 regulates autophagy in mammalian cells. (A) The loss of DDX3 has no effect on ATG5 expression: PANC-1 cells, stably transfected with either vector shRNA (control) or shRNA targeting *DDX3*, were treated with rapamycin (Rapa) for the indicated times with or without co-treatment with bafilomycin A_1 (Baf A_1). Normalized ATG5 level at the indicated time points with the indicated treatments. (**B**) The loss of DDX3 impairs ULK1 expression and autophagy in mammalian cells: HT-1080 cells, stably transfected with either vector shRNA (control) or shRNA targeting *DDX3*, were treated with rapamycin for the indicated times with or without co-treatment with bafilomycin A_1. A representative blot shows the levels of DDX3, ULK1, SQSTM1, LC3-I and LC3-II, and ATG5 with ACTB as a loading control, upon harvesting cells at the indicated time points after rapamycin treatment. (**C**) Normalized DDX3 levels at the indicated time points with the indicated treatments. Data represent three independent biological replicates. (**D**) Relative abundance of *ULK1* mRNA in sh*DDX3* cells compared to control cells. *GAPDH* was used as a reference gene. Data represent three independent biological replicates. (**E**) Normalized DDX3 levels at the indicated time points with the indicated treatments. Data represent three independent biological replicates. (**F, G and H**) Normalized LC3-II:LC3-I ratio (F), normalized SQSTM1 level (G) and normalized ATG5 level (H) at the indicated time points with the indicated treatments. Decreased LC3-II:LC3-I (F) ratio in the presence of bafilomycin A_1 indicates reduced autophagy flux. An increased SQSTM1 accumulation (G) indicates reduced autophagy flux. Data represent three independent biological replicates. Data in (A), and (C-H) represent mean ± SEM from the indicated number of replicates. Statistical analysis for (A), (C), and (E-H) was carried out using one-way analysis of variance (ANOVA) while (D) was analyzed using an unpaired Student's t-test. Multiple

comparisons were carried out using Tukey's multiple comparisons test. *p < 0.05, **p < 0.005, ***p < 0.001, ****p < 0.0001 ns: not significant. Related to Figure 16.

2.3 Discussion

Autophagy is a highly complex process, and genetic studies in the model yeast system have been crucial in identifying regulators of autophagy. The expression of ATG1, which encodes the Ser/Thr kinase responsible for autophagy initiation, is subject to multiple levels of regulation. *ATG1* is transcriptionally regulated by Gcn4 (Bernard et al., 2015b), Pho23 (Jin et al., 2014) and Rph1 (Bernard et al., 2015a): Gcn4 promotes *ATG1* transcription during nitrogen starvation, whereas Pho23 and Rph1 repress transcription during nutrient-replete conditions. The cytoplasmic exoribonuclease Xrn1 regulates the stability of the *ATG1* mRNA, mediating its degradation during nutrient-replete conditions (Delorme-Axford et al., 2018). In contrast, the Pat1-Lsm complex prevents 3'-5' degradation of *ATG1* mRNA by the exosome during nitrogen starvation, thereby stabilizing the *ATG1* mRNA (Gatica et al., 2019). In nutrient-replete conditions, the RNA helicase Dhh1 associates with Dcp2 to facilitate the degradation of *ATG1* transcripts to reduce autophagy (Hu et al., 2015), while associating with Eap1 to promote *ATG1* translation and autophagy during sustained nitrogen starvation (Liu et al., 2019). Atg1 expression is enhanced during long-term nitrogen starvation by the RGG motif-containing protein Psp2, which associates with components of the translational machinery eIF4E and eIF4G2, to promote the translation of *ATG1* mRNA (Yin et al., 2019). However, several questions remain unanswered including which of these mechanisms of regulation is physiologically critical and whether there are yet unknown regulators of *ATG1* expression.

We have compared two different nutrient-starvation treatments to uncover the fact that autophagy is physiologically regulated at the level of post-transcriptional control in yeast. *ATG1* undergoes transcriptional upregulation during both amino acid starvation and nitrogen starvation but post-transcriptional mechanisms that allow facile translation of the *ATG1* mRNA occur

simultaneously only during nitrogen starvation. While the physiological rationale driving the disconnect between ATG1 transcription and translation during amino acid starvation is unclear, an attractive hypothesis is as follows: nitrogen starvation imposes a stricter nutrient stress response that warrants swift autophagy activation, but the milder amino acid starvation initiates transcriptional priming without promoting unnecessary self-consumption.

In the process of elucidating cellular mechanisms that promote autophagy during nitrogen starvation, we have uncovered the kinase Rad53 as a post-transcriptional regulator of *ATG1* expression. While Rad53 has previously been implicated in regulating autophagy transcriptionally in response to genotoxic stress (Eapen et al., 2017), a role in promoting Atg1 expression post-transcriptionally during nitrogen starvation is novel. We confirmed that there was no differential DNA damage in nitrogen starvation, relative to amino acid starvation, which would be responsible for differential Rad53 activation. Results from our SILAC analysis indicated that conventional markers for DNA damage in yeast including S129 phosphorylation of Hta2 (Downs et al., 2000) and the expression of Rnr3 (ribonucleotide reductase 3) (Tkach et al., 2012) were not significantly different between nitrogen and amino acid starvation (Figure 12G and 12H). Additionally, we found no evidence of a role for Mec1 – a key mediator of the DNA-damage response pathway that activates Rad53 – in nitrogen-starvation induced autophagy. Consistent with this novel function of Rad53, we found that a previously identified but incompletely characterized phosphorylation site on Rad53 – Ser175 – was more abundantly phosphorylated during nitrogen starvation compared to amino acid starvation. Indeed, the $Rad53^{S175A}$ mutant exhibited reduced autophagy flux during nitrogen starvation, supporting selective activation of Rad53 during nitrogen starvation. Previous studies suggest that Rad53 S175 phosphorylation is independent of DNA damage or spindle checkpoint responses and is a

proline-directed site likely to be phosphorylated by Cdc28. However, we found that Cdc28 was not involved in autophagy regulation during nitrogen starvation, indicating that Rad53 S175 phosphorylation during nitrogen starvation was not mediated by Cdc28. Our future analyses will focus on the identification of the kinase responsible for this phosphorylation.

We also identified the RNA-helicase Ded1 as a downstream effector that regulates the expression of *ATG1* mRNA. The ATG1 mRNA is a highly structured mRNA with stem-loop structures in the 5'-UTR and the 5'-UTR proximal CDS (Liu et al., 2019). We hypothesized that Ded1 would bind the 5'-UTR of *ATG1* where it would function to resolve secondary structures to promote facile translation (Sen et al., 2019; Sen et al., 2015). Using RNA-immunoprecipitation, we confirmed that Ded1 binds to the 5'-UTR of *ATG1* mRNA. Consistent with its hypothesized role in promoting *ATG1* translation during nitrogen starvation, the loss of Ded1 activity led to a reduction in Atg1 expression after nitrogen starvation, without affecting general translation. We also demonstrated that the Ded1-*ATG1* mRNA interaction is 60% lower in amino acid starvation relative to nitrogen starvation, highlighting the fact that increased Ded1 binding likely drives increased *ATG1* translation during nitrogen starvation. Ded1 has previously been identified as a Rad53 substrate (Lao et al., 2018), indicating the possibility that Ded1 is regulated differentially by Rad53 during distinct nutrient-starvation conditions. Indeed, we show that in cells lacking Rad53, the interaction between Ded1 and *ATG1* mRNA during nitrogen starvation is reduced by ~65%, consistent with the difference seen between the two starvation treatments. TEM analysis revealed a reduction in number and size of autophagosomes following nitrogen starvation in cells suffering transient loss of Ded1, indicating its importance in mediating the autophagy response.

Our study demonstrates an intriguing role for Ded1 within the landscape of regulators identified to modulate *ATG1* expression. Whereas negative regulators like Xrn1 prevent

unnecessary *ATG1* expression during nutrient-rich conditions, positive regulators such as Pat1 and Psp2 promote ATG1 expression during starvation by stabilizing *ATG1* mRNA and promoting *ATG1* mRNA translation, respectively. Dhh1 switches from a negative regulatory role to a positive regulatory role as nutrient levels diminish. However, there is a temporal delay among these processes: whereas Pat1 stabilizes *ATG1* mRNA shortly after cells are exposed to nitrogen starvation (1-2 h), the roles of Psp2 and Dhh1 in promoting *ATG1* mRNA translation occur after extended starvation (24 h). This difference suggests that another regulator is involved in promoting *ATG1* translation within this time window, and our data suggest that this regulator is Ded1. Accordingly, strong binding of Ded1 to *ATG1* mRNA promotes translation during nitrogen starvation, whereas weaker binding during amino acid starvation leads to decreased Atg1 expression. What happens to the *ATG1* transcripts during amino acid starvation is an intriguing question. It is probable that the *ATG1* mRNA are sequestered in specialized RNA-containing structures such as stress granules or P-bodies. Because stress granules and P-bodies have largely been studied in the context of glucose starvation, this will be a challenging but interesting subject of investigation for a subsequent study.

Our study also demonstrated that DDX3, the human homolog of Ded1 (Tarn and Chang, 2009), is involved in the post-transcriptional activation of ULK1 expression, highlighting a conservation of function. DDX3 is a DEAD-box protein involved in RNA metabolism (Soto-Rifo and Ohlmann, 2013), influencing several cellular pathways including cell cycle regulation (Heerma van Voss et al., 2018; Lai et al., 2010), WNT signaling (Cruciat et al., 2013; Heerma van Voss et al., 2015; Zhao et al., 2016) and apoptosis (Sun et al., 2013). DDX3 has been implicated in stimulatory roles in the development of several cancers including breast cancer, lung cancer and colorectal cancer (Ariumi, 2014; Bol et al., 2015; Botlagunta et al., 2008;

Heerma van Voss et al., 2015; Wilky et al., 2016). DDX3 knockdown reduces cell migration and metastasis highlighting the oncogenic role of DDX3 in malignant cancers (Chen et al., 2015). Using pancreatic cancer- and fibrosarcoma-derived human cell lines, we show that DDX3 is also responsible for mediating the autophagy response; cells lacking DDX3 function exhibited reduced ULK1 expression and autophagy flux as assessed by LC3-lipidation and SQSTM1 accumulation assays. In mammalian cells, ULK1 and ULK2 show some functional redundancy. It is possible that DDX3 may not regulate ULK2 expression, which may explain why we saw a limited reduction of LC3-II and partial block in autophagy in the knockdown cells. Indeed, a partial block in autophagy may be therapeutically more desirable than a complete block. Additionally, targeting ULK1 for autophagy inhibition is an approach that had already been adopted. For example, SBI-0206965, a small-molecule kinase inhibitor of ULK1, has shown promise in pre-clinical studies in cellular models of cancer (Egan et al., 2015). Therefore, targeting DDX3 function, which would compromise both autophagy-dependent and autophagy-independent tumor survival pathways, could be an attractive therapeutic avenue for treating autophagy-addicted tumors.

2.4 Materials and Methods

2.4.1 Yeast growth and starvation media

Yeast cells were cultured in YPD (Bacto-yeast extract 10 g; Bacto-peptone 20 g; 2% dextrose; double-distilled H2O to 1 L) to mid-log phase (O.D = 0.8 – 1.0) before harvesting. For SILAC experiments yeast cells were cultures in SMD (0.67% yeast nitrogen base without amino acids; 2% D-glucose; and appropriate amino acids and nucleic acid bases) with light, medium or heavy lysine and arginine. Strains of interest carrying centromeric plasmids were grown in SMD selective medium in which the appropriate amino acids and/or nucleic acid bases were omitted.

Nitrogen starvation was carried out in SD(–N) medium (0.17% yeast nitrogen base without amino acids and ammonium sulfate, with 2% glucose). Amino acid starvation was carried out in SD(-A) medium (0.67% yeast nitrogen base without amino acids; 2% D-glucose; and appropriate nucleic acid bases). If the strain of interest was a temperature-sensitive mutant, cells were grown at a permissive temperature and shifted to a nonpermissive temperature for an appropriate period before the final harvesting.

2.4.2 Protein sample preparation and Immunoblotting

For yeast samples, proteins were precipitated using 10% TCA and the cell pellet was washed with acetone and dried. Dried, precipitated cell pellets were lysed by vortexing with glass beads in MURB buffer (50 mM sodium phosphate, pH 7.0, 25 mM MES, 1% SDS [w:v], 3 M urea, 1 mM NaN3, 1% β-mercaptoethanol, 0.01% bromophenol blue) for 5 min. Lysed samples were incubated at 55°C for 15 min before being collected by centrifugation at 10,000xg for 3 min. The supernatant was used as the sample for immunoblotting. Immunoblotting was carried out with standard denaturing SDS-PAGE followed by a semi-dry transfer using Trans-Blot® SD Semi-Dry Transfer Cell (Bio-Rad). After blocking with TBST containing 5% skim milk for 1 h, the membrane was incubated overnight at 4°C with various primary antibodies (1:1000). After incubation with peroxidase-conjugated secondary antibodies (goat anti-rabbit IgG secondary antibody [Fisher, ICN55676; 1:1000]; rabbit anti-mouse IgG secondary antibody [Jackson; 1:1000]) for 1 h at room temperature, the signals were visualized by chemiluminescence using Clarity and Clarity Max ECL Western Blotting Substrates (Bio-Rad) on a ChemiDoc Touch Imaging System (Bio-Rad).

For mammalian samples, cells were lysed in 1× cell lysis buffer (Cell Signaling Technology, 9803) containing protease inhibitor (Roche, 11836153001) on ice for 10 min. After

centrifugation at 14,000 × g for 15 min at 4°C, the supernatants were collected and quantified using the BCA assay (Thermo Fisher Scientific, 23225). The 30 µg of each sample were resolved on 4–12% Criterion XT Bis–Tris gels (Bio-Rad, 3450124) in XT MES running buffer (Bio-Rad, 1610789) and transferred to PVDF membranes (Bio-Rad, 1620233) using the Trans-Blot Turbo Transfer Pack and System (Bio-Rad). After blocking with TBST containing 5% skim milk for 1 h, the membrane was incubated overnight at 4°C with various primary antibodies (1:1000). After incubation with peroxidase-conjugated secondary antibodies (goat anti-rabbit IgG secondary antibody [Cell Signaling Technology, 7074; 1:1000]; rabbit anti-goat IgG secondary antibody [Abcam, ab6741; 1:1000]) for 1 h at room temperature, the signals were visualized by chemiluminescence using SuperSignal™ West Femto Maximum Sensitivity Substrate (Thermo Fisher Scientific, 34095). We collected protein from each cell line in three biologically independent samples and mixed them together for western blot analysis. The relative intensities of the bands of western blots from three regions were automatically analyzed and normalized to a loading control using the ChemiDoc Touch Imaging System Version 1.2 (Bio-Rad).

2.4.3 RNA isolation, RNA-Sequencing, and qRT-PCR

The RNA extraction protocol and qPCR primers are published previously (Hu et al., 2015). In brief, RNA isolation was performed using the Macherey-Nagel Mini kit for RNA purification. For RNA-Sequencing, isolated RNA was frozen and submitted to BGI Genomics Inc. Transcriptome profiling was carried out using the DNBSeq™ technology and bioinformatics analysis was done using three well-established workflows: DESeq2, EBSeq and NOIseq.

For qRT-PCR using yeast cells, cDNA synthesis was carried out using random primers and the High-Capacity cDNA Reverse Transcription Kit (Applied Biosystems™). cDNA samples were analyzed using a Bio-Rad CFX Connect Real-Time System. Samples were tested in Hard-Shell

96-clear well black shell plates (Bio-Rad). The reaction mix (15 µl final volume) consisted of 7.5 µl Radiant Green Lo-ROX qPCR kit (Radiant), 0.6 µl each primer (400 nM final concentration), 1.3 µl H2O, and 5 µl of a 1:5 dilution of the cDNA preparation. The thermocycling program consisted of an initial hold at 95°C for 3 min, followed by 40 cycles of 5 s at 95°C and 25 s at 62°C. After completion, a melting curve was generated to verify PCR specificity, as well as the absence of contamination and primer dimers. The transcript abundance in samples was determined using the CFX Manager Software regression method. Relative abundance of reference mRNAs and normalization for different total RNA amounts was carried out as described previously (Hu et al., 2015).

For qRT-PCR using mammalian cells, total RNA was extracted and purified from cultured cells using the RNA extraction kit (E.Z.N.A.® HP Total RNA Kit, R6812, Omega, Biotek) according to the manufacturer's instructions. The RNA was quantified by determining absorbance at 260 nm. One microgram of total RNA from each sample was reverse transcribed into cDNA using the iScript cDNA synthesis kit (Bio-Rad, 1708890) in a volume of 20 µl; cDNA from cell samples was amplified. The qPCR was performed using 2X SYBR Green q-PCR master mix (Bimake, B21202) on the C1000 Touch Thermocycler CFX96 Real-Time System (Bio-Rad) according to the manufacturer's protocol. Analysis was performed using Bio-Rad CFX Manager software 3.1 (Bio-Rad). The gene expression was calculated via the $2^{-\Delta\Delta Ct}$ method and normalized to GAPDH. The relative concentrations of mRNA were expressed in arbitrary units based on the untreated group, which was assigned a value of 1.

2.4.4 SILAC sample preparation and LC-MS/MS analysis

Samples were prepared as described previously (Hu et al., 2019a). Briefly, dried TCA-treated cell pellets (50 mg) of each labeling were mixed and lysed in urea buffer (8 M urea, 50

mM Tris-HCl, pH 8.0). Proteins were then alkylated by treatment with 5 mM iodoacetamide for 30 min and digested by Lys-C (Lysyl Endopeptidase, WAKO Chemicals) for 4 h. The concentration of urea was diluted to 1 M and digested with trypsin (Promega) overnight. On the following day, peptides were acidified and purified by SPE using HR-X columns in combination with C18 cartridges (Macherey-Nagel). Buffers used were as follows: Buffer A, 0.1% formic acid in deionized water; Buffer B, 80% acetonitrile and 0.1% formic acid in deionized water. Elutes were frozen in liquid nitrogen and lyophilized overnight. On the third day, peptides were fractionated by HpH reversed phase chromatography (Batth et al., 2014). The dry peptide powder was suspended 5% ammonium hydroxide and fractionated using a Waters XBridge BEH130 C18 3.5 µm 4.6 × 250 mm column on an Ultimate 3000 HPLC (Thermo Scientific). Peptides were loaded with 100% HpH buffer A containing 10 mM ammonium formate in deionized water (pH 10) and fractionated by increasing acetonitrile concentration from 1% to 40% using buffer B (10 mM ammonium formate and 90% acetonitrile;pH 10) in 25 min. Ninety-six fractions were collected in a 96-deep well plate. Fractions were mixed with an interval of 12 to yield 8 final fractions. The peptides were acidified, frozen in liquid nitrogen and lyophilized overnight. On the fourth day, the dry peptides were suspended in 200 µl 80% acetonitrile with 0.1% TFA. Phosphopeptides were enriched either by TiO_2 beads (GL Sciences) manually (Zarei et al., 2016) or by Fe(III)-NTA cartridges (Agilent) automatically using the Bravo Automated Liquid Handling Platform (Agilent) (Post et al., 2017). Samples were concentrated by vacuum concentration and resuspended in 20 µL of 0.1% formic acid for LC-MS/MS analysis. The tip flow-through was stored at −80°C for proteome analysis.

LC-MS/MS measurements were performed on a QExactive (QE) Plus and HF-X mass spectrometer coupled to an EasyLC 1000 and EasyLC 1200 nanoflow-HPLC, respectively (all

Thermo Scientific). Peptides were fractionated on a fused silica HPLC-column tip (I.D. 75 µm, New Objective, self-packed with ReproSil-Pur 120 C18-AQ, 1.9 µm (Dr. Maisch) to a length of 20 cm) using a gradient of A (0.1% formic acid in water) and B (0.1% formic acid in 80% acetonitrile in water): samples were loaded with 0% B with a flow rate of 600 nL/min; peptides were separated by 5%–30% B within 85 min with a flow rate of 250 nL/min. Spray voltage was set to 2.3 kV and the ion-transfer tube temperature to 250°C; no sheath and auxiliary gas were used. Mass spectrometers were operated in the data-dependent mode; after each MS scan (mass range m/z = 370 – 1750; resolution: 70,000 for QE Plus and 120,000 for HF-X) a maximum of ten, or twelve MS/MS scans were performed using a normalized collision energy of 25%, a target value of 1,000 (QE Plus)/5,000 (HF-X) and a resolution of 17,500 for QE Plus and 30,000 for HF-X. MS raw files were analyzed using MaxQuant (version 1.6.2.10) (Cox and Mann, 2008b; Cox and Mann, 2008a) using a Uniprot full-length S. cerevisiae database (March, 2016) and common contaminants such as keratins and enzymes used for in-gel digestion as reference. Carbamidomethylcysteine was set as fixed modification and protein amino-terminal acetylation, serine-, threonine- and tyrosine- (heavy) phosphorylation, and oxidation of methionine were set as variable modifications. The MS/MS tolerance was set to 20 ppm and three missed cleavages were allowed using trypsin/P as enzyme specificity. Peptide, site, and protein FDR based on a forward-reverse database were set to 0.01, minimum peptide length was set to 7, the minimum score for modified peptides was 40, and minimum number of peptides for identification of proteins was set to one, which must be unique. The “match-between-run” option was used with a time window of 0.7 min. MaxQuant results were analyzed using Perseus (Tyanova et al., 2016).

2.4.5 Ultrastructural analysis

The sample preparation protocol for TEM analysis was adapted from a previously described protocol (Backues et al., 2014). SEY6210 *pep4*Δ *vps4*Δ or SEY6210 *pep4*Δ *vps4*Δ *DED1-AID-MYC OsTIR1-MYC* cells were cultured in YPD, with or without auxin, and 20 OD_{600} unit equivalents of cells in log phase were harvested by centrifugation at 3,000 g for 5 min at room temperature (RT). Cells were then washed once with 10 ml of distilled water. Cell pellets were subsequently resuspended in 1 ml of freshly prepared ice-cold 1.5% $KMnO_4$ (Sigma Aldrich, 223468-25G) and transferred into microcentrifuge tubes. The microcentrifuge tubes were entirely filled completely with ice-cold 1.5% $KMnO_4$ to exclude air and incubated on a slow-moving rotating wheel for 30 min at 4°C. Cells were then centrifuged at 3,000 x g for 3 min at 4°C and the supernatant discarded. Pellets were again resuspended in 1.5 ml of ice-cold 1.5% $KMnO_4$ and microcentrifuge tubes incubated on a rotating wheel overnight at 4°C. After 5 washes with 1 ml of distilled water, cells were collected by centrifugation at 5,000 x g for 3 min.

Dehydration was performed by incubating the cells in 1 ml of 10, 30, 50, 70, 90 and 95% acetone (acetone for analysis ENSURE®; MERCK, 1.00014.2500) with at least 20 min incubation at RT. Between each incubation steps, cells were collected by centrifugation at 5,000 x g for 4 min. Cells were then incubated 3 times in 1 ml of water-free acetone (dried acetone; MERCK, 1.00299.0500) for at least 20 min each time, on a slow motion rotating wheel at RT. This was followed by incubation in 33% freshly made Spurr's resin (11.8 g nonenyl succinic anhydride [Ted Pella, 18301], 8.2 g ERL 4221 epoxide resin [Ted Pella, 18306-4221], 1.9 g diglycidyl ether of poly [propylene glycol] 736 [Ted Pella, 18310], 0.2 g dimethylaminoethanol [Ted Pella, 18315]) on a slow-motion rotating wheel for at least 1 h at RT. Cells were collected by centrifugation at 5,000 x g for 5 min and the supernatants discarded. Following this, cells

were incubated in 100% Spurr's resin on a rotating wheel overnight at RT and collected by centrifugation at 5,000 x g for 5 min and the supernatant discarded. Incubation in 100% Spurr's resin was repeated for 8 h at RT and the samples transferred to conic embedding capsules (BEEM embedding capsules size 00, EMS, 70010-B). The capsules were centrifuged at 5,000 x g for 5 min and the supernatant discarded. The tubes were then topped with fresh 100% Spurr's resin and heated at 65˚C for 4 days to polymerize the resin.

Ultra-thin 55-nm sections were cut using a Leica ultramicrotome (Leica Microsystems) and collected on formvar carbon-coated 50-mesh copper grids (EMS). Cell sections were stained with a filtered lead-citrate solution (80 mM lead nitrate, 120 mM sodium citrate, pH 12) for 2 min at RT. Sections were viewed either in either a CM100bio TEM or a Talos F200i (FEI). The average number of ABs per cell section was determined by counting 100 randomly selected cell profiles over 3 grids for each analyzed condition. The average diameter of ABs was measured using the ImageJ software (Schneider et al., 2012) and examining at least 100 ABs profiles randomly selected.

2.4.6 Auxin-inducible degradation

S. cerevisiae SEY6210 cells were first transformed with the plasmid pNHK53 (ADH1p-OsTIR1-9MYC). Genes of interest (*DED1*, *RAD53*, *CDC28* and *MEC1*) was then tagged with AID-9MYC by homologous recombination. The DNA fragments used for transformation were amplified with pHIS3-AID*-9MYC (Addgene, 99524; deposited by Dr. Helle Ulrich) as the template DNA. The auxin-inducible degron refers to the 71-116 amino acids of the AT1G04250/ATIAA17 protein in plants. To deplete target protein levels, the cells were treated with 500 mM 3-indoleacetic acid (IAA/auxin; Sigma) or DMSO (vehicle) during mid-log phase growth in YPD medium for 60-90 min (depending on the protein of interest) to induce

degradation of target protein. Subsequently, samples were collected for downstream analyses: enzymatic assays, immunoblots or qRT-PCR.

2.4.7 RNA Immunoprecipitation

The RNA immunoprecipitation protocol was modified from previously published procedures (Liu et al., 2019; Selth et al., 2009). For determining Ded1-*ATG1* mRNA interaction, a Ded1-PA tagged strain and an untagged (control) strain were cultured to mid-log phase and subjected to nitrogen starvation for 4 h. Cross-linking was performed by adding formaldehyde, to a final concentration of 0.8%, and shaking slowly for 10 min at room temperature. Cross-linking was halted with glycine treatment, to a final concentration of 0.2 M, with shaking for 5 min. Cultures were then harvested, washed in PBS, and resuspended in FA lysis buffer (50 mM HEPES, pH 7.5, 150 mM NaCl, 1 mM EDTA, 1% Triton X-100 [Sigma, T8787], 0.1% sodium deoxycholate [Sigma, D6750], 0.1% SDS), containing 5 mM PMSF, 1 tablet of complete protease inhibitor cocktail (Roche, 1873580) and RNasin® PLUS RNase inhibitor (Promega/Fisher Scientific, PRN2615). Yeast cells were lysed by vortexing with glass beads (USA Scientific, 7400-2405) at 4°C, centrifuged (5000 x g, 1 min) and the supernatant was collected. Samples were sonicated at 4°C using three 15-s pulses of 45% amplitude, with 60-s pauses for cooling on ice. Sonicated samples were collected by centrifugation (10,000 x g, 10 min), and the supernatant was collected and divided into input and IP fractions. IP fractions were incubated with IgG Sepharose 6 Fast Flow beads (GE healthcare Life Sciences), overnight with shaking at 4°C, while input fractions were frozen in liquid nitrogen and left at -80°C. IP fractions were washed with FA lysis buffer several times, resuspended in RIP elution buffer (50 mM Tris-HCl, pH 7.5, 10 mM EDTA, 1% SDS) and incubated at 70°C for 10 min with intermittent vortexing. IP supernatant and input samples were collected and incubated with a combination of

Proteinase K and RNase inhibitor at 42°C for 1 h, followed by 1 h at 65°C to ensure degradation of proteins bound to RNA.

Next, the samples were treated with equal volume of acid phenol-chloroform, mixed by vortexing and centrifuged. The aqueous layer of each sample was recovered and treated with 25 ml 3 M sodium acetate, 20 mg glycogen (Roche/Sigma, 10901393001), and 625 ml ice-cold 100% ethanol to precipitate the RNA. Samples were incubated for 1 h to overnight at -80°C, following which they were centrifuged, washed with 70% ethanol, and dried for 15 min. Pellets were resuspended in 90 ml of nuclease-free water and treated with DNase (10 ml TURBO DNase buffer, 2 ml TURBO DNase [TURBO DNA-free kit; Invitrogen/Fisher Scientific, AM1907]) with 0.5 ml of RNasin® PLUS RNase inhibitor (Promega/Fisher Scientific, PRN2615). Samples were incubated for 45 min at 37°C to eliminate DNA. Following incubation, DNase was inhibited using the DNase inactivation reagent (TURBO DNA-free kit). Samples were then subjected to qRT-PCR as described in the qRT-PCR method section.

For determining Ded1-*ATG1* mRNA interaction in the WT or *rad53*Δ *sml1*Δ background, the procedure followed was the same as described in the earlier paragraph except for the following: 1) Ded1 was tagged C-terminally with 13xMYC; 2) IP fractions were incubated with MYC magnetic beads (Pierce™/Fisher Scientific, 88843) overnight with shaking at 4°C; and 3) magnetic separation was used for collecting beads during the incubation, washing and elution processes.

2.4.8 In vitro RNA interactome capture screen/mRNA IP

RNA in vitro transcription was performed as previously described (Yin et al., 2019). The linearized pUC19-ATG1-5' UTR was used as template to carry out RNA transcription using the HiScribe T7 High Yield RNA synthesis kit (NEB, E2040S). The yield of the resulting RNA was

measured using a nanodrop and the 3'-end was labelled with desthiobiotin according to manufacturer's instructions using the Pierce 3'-End desthiobiotinylation kit (Thermo Fisher Scientific, 20163). The labelled mRNA was used in the in vitro RNA immunoprecipitation.

Cell pellets were resuspended in lysis buffer (10 mM Tris-HCl, pH 7.5, 0.1 M NaCl, 30 mM $MgCl_2$, 1% Triton X-100, RNasin® PLUS RNase inhibitor [Promega/Fisher Scientific, PRN2615] and Roche complete protease inhibitor cocktail [Roche, 1873580]) and mechanically lysed using acid washed beads for 5 min at 4°C. The lysates were centrifuged at 12,000 xg for 10 min and the supernatant was collected. The affinity isolation was set up according to the manufacturer's instructions (Thermo Fisher Scientific, 20164). Protein enrichment in labeled RNA reaction was measured either using MS analysis (for preliminary screen leading to Ded1 identification) or monitored by immunoblotting (for confirming interaction between Ded1 and *ATG1*-5' UTR).

2.4.9 Mammalian cell culture, transfection, and infection

The PANC-1 (CRL-1469) and HT1080 (CCL-121) cell lines were obtained from the American Type Culture Collection. These cells were cultured in Dulbecco's modified Eagle's medium (Thermo Fisher Scientific, 11995073) supplemented with 10% heat-inactivated fetal bovine serum (Thermo Fisher Scientific, A3840001) and 1% penicillin and streptomycin (Thermo Fisher Scientific, 15070-063) at 37°C, with 95% humidity, and 5% CO2. Lentiviral particles were generated by transfection of the *DDX3* shRNA (Sigma, TRCN0000000002 and TRCN0000000003), and the 2nd generation lentiviral systems (viral packaging psPAX2 and viral envelope pMD2G) were collected, mixed with polybrene, and added into 293-T cells using Lipofectamine 2000 (Life Technologies) for transfection. Culture media were harvested 48 h

after transfection and filtered through 0.45-µm filters. Upon infection, the stable cell lines were established by selecting with 2-5 µg/ml puromycin.

2.4.10 Quantification and statistical analyses

Western blot images were quantified using Bio-Rad ImageLab software. Statistical analyses were performed using GraphPad Prism 9.1.0. Statistical significance was determined in all cases from at least 3 independent biological replicates using either Student's t test, one-way ANOVA or two-way ANOVA followed by Tukey's multiple comparisons test. Differences with a P value < 0.05 or lower were considered significant. *$p < 0.05$, **$p < 0.01$, ***$p < 0.001$. Number of independent experiments (n), statistical tests utilized, dispersion of measurements and significance are also described in the figure legends.

2.5 Acknowledgements

We would like to thank members of the Klionsky group for their constructive suggestions during the study, and BGI Americas Corp for their collaboration on the RNA-Sequencing experiment. We would like to thank Rishav Mitra for insightful comments aiding manuscript preparation. We would like to thank Subhechha Roy for help with figure preparation. This work was supported by NIGMS grant GM131919 (DJK), by the Swiss National Science Foundation and the canton and University of Fribourg (JD), ENW KLEIN-1 OCENW.KLEIN.118 (FR), ZonMW TOP 91217002 (FR), and NCI grant R01CA160417 (DT). M.M. is supported by an ALW Open Programme (ALWOP.355).

2.6 Tables

Table 1. Yeast strains used in this study.

Strain	Genotype	Reference
SEY6210	*MATα leu2-3,112 ura3-52 his3-Δ200 trp1-Δ901 suc2-Δ9 lys2-801; GAL*	[61]
VLY001	SEY6210 *GCN4-3xPA::TRP1*	This study
VLY002	WLY176 *CUP1p-GFP-ATG8::LEU2*	This study
VLY003	SEY6210 *pep4Δ::KAN*	This study
VLY004	SEY6210 *pep4Δ::KAN vps4Δ::LEU2*	This study
VLY005	SEY6210 *vac8Δ::KAN*	This study
VLY006	SEY6210 *arg4Δ::HIS*	This study
VLY007	SEY6210 *ATG9-3xPA::TRP1*	This study
VLY008	SEY6210 *atg1Δ::HIS3*	This study
VLY009	SEY6210 *sml1Δ::HIS3*	This study
VLY010	SEY6210 *sml1Δ::HIS3 rad53Δ::URA3*	This study
VLY011	SEY6210 *PGI1-GFP::TRP1*	[58]
VLY012	SEY6210 *sml1Δ::HIS3 PGI1-GFP::TRP1*	This study
VLY013	SEY6210 *sml1Δ::HIS3 rad53Δ::URA3 PGI1-GFP::TRP1*	This study
VLY014	WLY176 *RAD53-AID-MYC::HIS3*	This study
VLY015	VLY014 *pNHK53::URA3*	This study
VLY016	VLY002 *MEC1-AID-MYC::HIS3*	This study
VLY017	VLY016 *pNHK53::URA3*	This study
VLY018	VLY002 *CDC28-AID-MYC::HIS3*	This study
VLY019	VLY018 *pNHK53::URA3*	This study
VLY020	SEY6210 *DED1-3xPA::TRP1*	This study
VLY021	SEY6210 *DED1-13xMYC::HIS3*	This study
VLY022	VLY010 *DED1-13xMYC::HIS3*	This study
	ded1-95	[113]

VLY022	VLY002 *DED1-AID-MYC::HIS3*	This study
VLY023	VLY022 *pNHK53::URA3*	This study
VLY024	VLY004 *DED1-AID-MYC::HIS3*	This study
VLY025	VLY024 *pNHK53::URA3*	This study
WLY176	SEY6210 *pho13*Δ *pho8*::*pho8*Δ60	[30]

Table 2. Primers for yeast genetics.

Name	Sequence (5'-3')
GCN4 TF	AAATGAGGTTGCCAGATTAAAGAAATTAGTTGGCGAACGCCGGATCCCCGGGTTAATTAA
GCN4 TR	GAGAATGAAATAAAAAATATAAAATAAAAGGTAAATGAAAGAATTCGAGCTCGTTTAAAC
GCN4 TC	TCCACTGAAGAAGTTTCTCT
PEP4 DF	AAAGAAAAAAAAAAAGCCTAGTGACCTAGTATTTAATCCAAATAAAATTCAAACAAAAACCAAAACTAACCGGATCCCCGGGTTAATTAA
PEP4 DR	TTGTTATCTACTTATAAAAGCTCTCTAGATGGCAGAAAAGGATAGGGCGGAGAAGTAAGAAAAGTTTAGCGAATTCGAGCTCGTTTAAAC
PEP4 DC	CGTTTTCAATATCTTGAGCTCCTCAATTGTATTTG
VPS4 DF	TTGAGGACATGGAAGACAAAAATAAAGCAGCATAGAGTGCCTATAGTAGATGGGGTACAACAGCTGAAGCTTCGTACGC
VPS4 DR	TTTTTTTATTTTTTATTTTCATGTACACAAGAAATCTACATTAGCACGTTAATCAATTGAGCATAGGCCACTAGTGGATCTG
VPS4 DC	GTGTCATCTGTTGCAGTCG
VAC8 DF	CAGGAACTGAGCAAACTATAAGGGTGTTCTTTCTTCTGTACTATATATACATTTGCAACTCAGCTGAAGCTTCGTACGC
VAC8 DR	AACTTCTGAGAAGAAAATTTTGATAAAAATTATAATGCCTAGTCCCGCTTTTGAAGAAAAGCATAGGCCACTAGTGGAT
VAC8 DC	GAGCCCTTAAGGAGGACTC
ARG4 DF	GCTCAAAAGCAGGTAACTATATAACAAGACTAAGGCAAACCAGCTGAAGCTTCGTACGC

ARG4 DR	CCAGACCTGATGAAATTCTTGCGCATAACGTCGCCATCTGGCATAGGCCACTAGTGGATCTG
ARG4 DC	CAGCGGTAGATGTAAGCC
ATG9 TF	CTTGTTAAAGAGTATTACAAGAAGTCTGACGTCGGAAGACGGATCCCCGGGTTAATTAA
ATG9 TR	ATATAGTTATATTGGATGATGTACACGACACAGTCTGCCGAATTCGAGCTCGTTTAAAC
ATG9 TC	CCGAAGACCATAGCGATAAAG
ATG1 DF	ATTTGAAGCTACCCCATATTTTCAAATCTCTTTTACAACACCAGACGAGAAATTAAGAAACAGCTGAAGCTTCGTACGC
ATG1 DR	AGATACTTGAAAATATAGCAGGTCATTTGTACTTAATAAGAAAACCATATTATGCATCACGCATAGGCCACTAGTGGATCTG
ATG1 DC	TCCCCCATCAGCATCAGTTTGTG
SML1 DF	CCTTTGTGATCTTACGGTCTCACTAACCTCTCTTCAACTGCTCAATAATTTCCCGCTCAGCTGAAGCTTCGTACGC
SML1 DR	GAAAAGAACAGAACTAGTGGGAAATGGAAAGAGAAAAGAAAAGAGTATGAAAGGAACTGCATAGGCCACTAGTGGATCTG
SML1 DC	CATTGCCGTCGAACGTC
RAD53 D F	TCTTAAGCTTTAAAAGAGAGAATAGTGAGAAAAGATAGTGTTACACAACATCAACTAAAACAGCTGAAGCTTCGTACGC
RAD53 D R	GGTATCTACCATCTTCTCTCTTAAAAAGGGGCAGCATTTTCTATGGGTATTTGTCCTTGGGCATAGGCCACTAGTGGATCTG
RAD53 D C	GCTCAGCACCTACCTAAATG

RAD53 A F	GGTTAAAAGGGCAAAATTGGACCAAACCTCAAAAGGCCCCGAG AATTTGCAATTTTCGCTTCGTACGCTGCAGGTCGA
RAD53 A R	TATCTACCATCTTCTCTCTTAAAAAGGGGCAGCATTTTCTATGGG TATTTGTCCTTGGCATCGATGAATTCGAGCTCG
RAD53 A C	GCATGTATGAATCTCCGGC
MEC1 A F	AGAAGCAACATCAGAAGACAATCTAAGCAAGATGTATATTGGT TGGCTTCCATTTTGGCTTCGTACGCTGCAGGTCGA
MEC1 A R	TGCAGTGATGGTTAGATCAAGAGGAAGTTCGTCTGTTGCCGAAA ATGGTGGAAAGTCGCATCGATGAATTCGAGCTCG
MEC1 A C	CATGGAACAGGTAGATAAATTTCC
CDC28 A F	CCCTATTAACCGGATTAGCGCCAGAAGAGCAGCCATCCACCCCT ACTTCCAAGAATCACTTCGTACGCTGCAGGTCGA
CDC28 A R	AGGCTATAATGACAGTGCAGTAGCATTTGTAATATAATAGCGAA ATAGATTATAATGCCATCGATGAATTCGAGCTCG
CDC28 A C	GGACCAACCGTTAGGAGC
DED1 A F	TGGGGTAACAGCGGTGGTTCAAACAACTCTTCTTGGTGGCTTCG TACGCTGCAGGTCGA
DED1 A R	GCAGAAAACGAAGAATCCTCACCCTAGTTTGTCTGAAACATCGA TGAATTCGAGCTCG
DED1 A C	GAGCTACCGCCATTCATG
RA	TCGACCTGCAGCGTACGAAG
RD	GCGTACGAAGCTTCAGCTG
RT	TTAATTAACCCGGGGATCCG

Table 2 Legend: A, AID tagging; C, PCR-based forward detection primer; D, deletion; F, forward primer; R, reverse primer; RA, PCR-based reverse detection primer for AID tagging; RD, PCR-based reverse detection primer for deletion; RT, PCR-based reverse detection primer for tagging; T, tagging.

Table 3. **Primers for qRT-PCR.**

Name	Sequence (5'-3')
ATG1 F	ATCTAAGATGGCCGCACATATG
ATG1 R	AGGGTAGTCACCATAGGCATTC
ATG9 F	CGTACTAACAGAGTCTTTCCTTG
ATG9 R	CTAAGACACCACCCTTATTGAG
ALG9 F	CACGGATAGTGGCTTTGGTGAACAATTAC
ALG9 R	TATGATTATCTGGCAGCAGGAAAGAACTTGGG
ATG1 5'-UTR F	TAGGCCGAGGTTAATTCTAGAACG
ATG1 5'-UTR R	ATAGTACTGTTCTCTGTTTCCCCAGA
ATG1 CDS F	GAGCTTCCAATCATTTGGAGTTATTC
ATG1 CDS R	CTATTCTTTGGGCTGGATCAAATGTC
ATG1 3'-UTR F	GAGGCAGAAGATGAACCACCAAA
ATG1 3'-UTR R	GTAAAGCATTTCGAGAGTAGCATAAC
PGK1 CDS	GAAGGACAAGCGTGTCTTCATCAG
PGK1 CDS	CGTACTTGATGGTTGGCAAAGCAG
hGAPDH F	GTCTCCTCTGACTTCAACAGCG
hGAPDH R	ACCACCCTGTTGCTGTAGCCAA
hULK1 F	GCAAGGACTCTTCCTGTGACAC
hULK1 R	CCACTGCACATCAGGCTGTCTG

Table 4 Primers for shRNA-mediated knockdown.

Name	Sequence (5'-3')
DDX3F	CCGGCGGAGTGATTACGATGGCATTCTCGAGAATGCCATCGTAATCACT CCGTTTTT
DDX3R	CCGGCGTAGAATAGTCGAACAAGATCTCGAGATCTTGTTCGACTATTCT ACGTTTTT

2.7 References

Abildgaard, M.H., Brynjolfsdottir, S.H., and Frankel, L.B. (2020). The Autophagy-RNA Interplay: Degradation and Beyond. Trends Biochem Sci 45, 845-857.

Abreu, C.M., Kumar, R., Hamilton, D., Dawdy, A.W., Creavin, K., Eivers, S., Finn, K., Balsbaugh, J.L., O'Connor, R., Kiely, P.A., et al. (2013). Site-specific phosphorylation of the DNA damage response mediator rad9 by cyclin-dependent kinases regulates activation of checkpoint kinase 1. PLoS Genet 9, e1003310.

Albuquerque, C.P., Smolka, M.B., Payne, S.H., Bafna, V., Eng, J., and Zhou, H. (2008). A multidimensional chromatography technology for in-depth phosphoproteome analysis. Mol Cell Proteomics 7, 1389-1396.

Amaravadi, R., Kimmelman, A.C., and White, E. (2016). Recent insights into the function of autophagy in cancer. Genes Dev 30, 1913-1930.

Amaravadi, R.K., Kimmelman, A.C., and Debnath, J. (2019). Targeting Autophagy in Cancer: Recent Advances and Future Directions. Cancer Discov 9, 1167-1181.

Ariumi, Y. (2014). Multiple functions of DDX3 RNA helicase in gene regulation, tumorigenesis, and viral infection. Front Genet 5, 423.

Backues, S.K., Chen, D., Ruan, J., Xie, Z., and Klionsky, D.J. (2014). Estimating the size and number of autophagic bodies by electron microscopy. Autophagy 10, 155-164.

Backues, S.K., Lynch-Day, M.A., and Klionsky, D.J. (2012). The Ume6-Sin3-Rpd3 complex regulates ATG8 transcription to control autophagosome size. Autophagy 8, 1835-1836.

Batth, T.S., Francavilla, C., and Olsen, J.V. (2014). Off-line high-pH reversed-phase fractionation for in-depth phosphoproteomics. J Proteome Res 13, 6176-6186.

Bernard, A., Jin, M., Gonzalez-Rodriguez, P., Fullgrabe, J., Delorme-Axford, E., Backues, S.K., Joseph, B., and Klionsky, D.J. (2015a). Rph1/KDM4 mediates nutrient-limitation signaling that leads to the transcriptional induction of autophagy. Curr Biol 25, 546-555.

Bernard, A., Jin, M., Xu, Z., and Klionsky, D.J. (2015b). A large-scale analysis of autophagy-related gene expression identifies new regulators of autophagy. Autophagy 11, 2114-2122.

Bjorkoy, G., Lamark, T., Pankiv, S., Overvatn, A., Brech, A., and Johansen, T. (2009). Monitoring autophagic degradation of p62/SQSTM1. Methods Enzymol 452, 181-197.

Bol, G.M., Xie, M., and Raman, V. (2015). DDX3, a potential target for cancer treatment. Mol Cancer 14, 188.

Botlagunta, M., Vesuna, F., Mironchik, Y., Raman, A., Lisok, A., Winnard, P., Jr., Mukadam, S., Van Diest, P., Chen, J.H., Farabaugh, P., et al. (2008). Oncogenic role of DDX3 in breast cancer biogenesis. Oncogene 27, 3912-3922.

Burckin, T., Nagel, R., Mandel-Gutfreund, Y., Shiue, L., Clark, T.A., Chong, J.L., Chang, T.H., Squazzo, S., Hartzog, G., and Ares, M., Jr. (2005). Exploring functional relationships between components of the gene expression machinery. Nat Struct Mol Biol 12, 175-182.

Cartagena-Lirola, H., Guerini, I., Manfrini, N., Lucchini, G., and Longhese, M.P. (2008). Role of the Saccharomyces cerevisiae Rad53 checkpoint kinase in signaling double-strand breaks during the meiotic cell cycle. Mol Cell Biol 28, 4480-4493.

Cebollero, E., and Reggiori, F. (2009). Regulation of autophagy in yeast Saccharomyces cerevisiae. Biochim Biophys Acta 1793, 1413-1421.

Chang, C., Jensen, L.E., and Hurley, J.H. (2021). Autophagosome biogenesis comes out of the black box. Nat Cell Biol 23, 450-456.

Chen, E.S., Hoch, N.C., Wang, S.C., Pellicioli, A., Heierhorst, J., and Tsai, M.D. (2014). Use of Quantitative Mass Spectrometric Analysis to Elucidate the Mechanisms of Phospho-priming and Auto-activation of the Checkpoint Kinase Rad53 in Vivo. Mol Cell Proteomics 13, 551-565.

Chen, H.H., Yu, H.I., Cho, W.C., and Tarn, W.Y. (2015). DDX3 modulates cell adhesion and motility and cancer cell metastasis via Rac1-mediated signaling pathway. Oncogene 34, 2790-2800.

Conrad, M., Schothorst, J., Kankipati, H.N., Van Zeebroeck, G., Rubio-Texeira, M., and Thevelein, J.M. (2014). Nutrient sensing and signaling in the yeast Saccharomyces cerevisiae. FEMS Microbiol Rev 38, 254-299.

Corona Velazquez, A.F., and Jackson, W.T. (2018). So Many Roads: the Multifaceted Regulation of Autophagy Induction. Mol Cell Biol 38.

Cox, J., and Mann, M. (2008a). MaxQuant enables high peptide identification rates, individualized p.p.b.-range mass accuracies and proteome-wide protein quantification. Nature Biotechnology 26, 1367-1372.

Cox, J., and Mann, M. (2008b). MaxQuant enables high peptide identification rates, individualized p.p.b.-range mass accuracies and proteome-wide protein quantification. Nat Biotechnol 26, 1367-1372.

Cruciat, C.M., Dolde, C., de Groot, R.E., Ohkawara, B., Reinhard, C., Korswagen, H.C., and Niehrs, C. (2013). RNA helicase DDX3 is a regulatory subunit of casein kinase 1 in Wnt-beta-catenin signaling. Science 339, 1436-1441.

de la Cruz, J., Iost, I., Kressler, D., and Linder, P. (1997). The p20 and Ded1 proteins have antagonistic roles in eIF4E-dependent translation in Saccharomyces cerevisiae. Proc Natl Acad Sci U S A 94, 5201-5206.

Delorme-Axford, E., Abernathy, E., Lennemann, N.J., Bernard, A., Ariosa, A., Coyne, C.B., Kirkegaard, K., and Klionsky, D.J. (2018). The exoribonuclease Xrn1 is a post-transcriptional negative regulator of autophagy. Autophagy 14, 898-912.

Delorme-Axford, E., and Klionsky, D.J. (2018). Transcriptional and post-transcriptional regulation of autophagy in the yeast Saccharomyces cerevisiae. J Biol Chem 293, 5396-5403.

Deng, J., Erdjument-Bromage, H., and Neubert, T.A. (2019). Quantitative Comparison of Proteomes Using SILAC. Curr Protoc Protein Sci 95, e74.

Dever, T.E., Feng, L., Wek, R.C., Cigan, A.M., Donahue, T.F., and Hinnebusch, A.G. (1992). Phosphorylation of initiation factor 2 alpha by protein kinase GCN2 mediates gene-specific translational control of GCN4 in yeast. Cell 68, 585-596.

Downs, J.A., Lowndes, N.F., and Jackson, S.P. (2000). A role for Saccharomyces cerevisiae histone H2A in DNA repair. Nature 408, 1001-1004.

Eapen, V.V., Waterman, D.P., Bernard, A., Schiffmann, N., Sayas, E., Kamber, R., Lemos, B., Memisoglu, G., Ang, J., Mazella, A., et al. (2017). A pathway of targeted autophagy is induced by DNA damage in budding yeast. Proc Natl Acad Sci U S A 114, E1158-E1167.

Ecker, N., Mor, A., Journo, D., and Abeliovich, H. (2010). Induction of autophagic flux by amino acid deprivation is distinct from nitrogen starvation-induced macroautophagy. Autophagy 6, 879-890.

Egan, D.F., Chun, M.G., Vamos, M., Zou, H., Rong, J., Miller, C.J., Lou, H.J., Raveendra-Panickar, D., Yang, C.C., Sheffler, D.J., et al. (2015). Small Molecule Inhibition of the Autophagy Kinase ULK1 and Identification of ULK1 Substrates. Mol Cell 59, 285-297.

Feng, Y., He, D., Yao, Z., and Klionsky, D.J. (2014). The machinery of macroautophagy. Cell Res 24, 24-41.

Fu, Y., Liu, S., Zeng, S., and Shen, H. (2018). The critical roles of activated stellate cells-mediated paracrine signaling, metabolism and onco-immunology in pancreatic ductal adenocarcinoma. Mol Cancer 17, 62.

Gatica, D., Hu, G., Liu, X., Zhang, N., Williamson, P.R., and Klionsky, D.J. (2019). The Pat1-Lsm Complex Stabilizes ATG mRNA during Nitrogen Starvation-Induced Autophagy. Mol Cell 73, 314-324 e314.

Gatica, D., Lahiri, V., and Klionsky, D.J. (2018). Cargo recognition and degradation by selective autophagy. Nat Cell Biol 20, 233-242.

Gomez-Sanchez, R., Rose, J., Guimaraes, R., Mari, M., Papinski, D., Rieter, E., Geerts, W.J., Hardenberg, R., Kraft, C., Ungermann, C., et al. (2018). Atg9 establishes Atg2-dependent contact sites between the endoplasmic reticulum and phagophores. J Cell Biol 217, 2743-2763.

Gross, A.S., and Graef, M. (2020). Mechanisms of Autophagy in Metabolic Stress Response. J Mol Biol 432, 28-52.

Guo, J.Y., Chen, H.Y., Mathew, R., Fan, J., Strohecker, A.M., Karsli-Uzunbas, G., Kamphorst, J.J., Chen, G., Lemons, J.M., Karantza, V., et al. (2011). Activated Ras requires autophagy to maintain oxidative metabolism and tumorigenesis. Genes Dev 25, 460-470.

Heerma van Voss, M.R., Kammers, K., Vesuna, F., Brilliant, J., Bergman, Y., Tantravedi, S., Wu, X., Cole, R.N., Holland, A., van Diest, P.J., et al. (2018). Global Effects of DDX3 Inhibition on Cell Cycle Regulation Identified by a Combined Phosphoproteomics and Single Cell Tracking Approach. Transl Oncol 11, 755-763.

Heerma van Voss, M.R., Vesuna, F., Trumpi, K., Brilliant, J., Berlinicke, C., de Leng, W., Kranenburg, O., Offerhaus, G.J., Burger, H., van der Wall, E., et al. (2015). Identification of the DEAD box RNA helicase DDX3 as a therapeutic target in colorectal cancer. Oncotarget 6, 28312-28326.

Holzen, T.M., and Sclafani, R. (2010). Genetic interaction of RAD53 protein kinase with histones is important for DNA replication. Cell Cycle 9, 4735-4747.

Hu, G., McQuiston, T., Bernard, A., Park, Y.D., Qiu, J., Vural, A., Zhang, N., Waterman, S.R., Blewett, N.H., Myers, T.G., et al. (2015). A conserved mechanism of TOR-dependent RCK-mediated mRNA degradation regulates autophagy. Nat Cell Biol 17, 930-942.

Hu, Z., Raucci, S., Jaquenoud, M., Hatakeyama, R., Stumpe, M., Rohr, R., Reggiori, F., De Virgilio, C., and Dengjel, J. (2019a). Multilayered Control of Protein Turnover by TORC1 and Atg1. Cell Rep 28, 3486-3496 e3486.

Hu, Z., Raucci, S., Jaquenoud, M., Hatakeyama, R., Stumpe, M., Rohr, R., Reggiori, F., De Virgilio, C., and Dengjel, J. (2019b). Multilayered Control of Protein Turnover by TORC1 and Atg1. Cell Reports 28, 3486-3496.e3486.

Huang, W.P., Shintani, T., and Xie, Z. (2014). Assays for autophagy I: the Cvt pathway and nonselective autophagy. Methods Mol Biol 1163, 153-164.

Javaheri, A., Wysocki, R., Jobin-Robitaille, O., Altaf, M., Cote, J., and Kron, S.J. (2006). Yeast G1 DNA damage checkpoint regulation by H2A phosphorylation is independent of chromatin remodeling. Proc Natl Acad Sci U S A 103, 13771-13776.

Jin, M., He, D., Backues, S.K., Freeberg, M.A., Liu, X., Kim, J.K., and Klionsky, D.J. (2014). Transcriptional regulation by Pho23 modulates the frequency of autophagosome formation. Curr Biol 24, 1314-1322.
Jin, M., and Klionsky, D.J. (2014). Regulation of autophagy: modulation of the size and number of autophagosomes. FEBS Lett 588, 2457-2463.
Jung, K.W., Lee, Y., Huh, E.Y., Lee, S.C., Lim, S., and Bahn, Y.S. (2019). Rad53- and Chk1-Dependent DNA Damage Response Pathways Cooperatively Promote Fungal Pathogenesis and Modulate Antifungal Drug Susceptibility. mBio 10.
Kanki, T., Wang, K., Cao, Y., Baba, M., and Klionsky, D.J. (2009). Atg32 is a mitochondrial protein that confers selectivity during mitophagy. Dev Cell 17, 98-109.
Karsli-Uzunbas, G., Guo, J.Y., Price, S., Teng, X., Laddha, S.V., Khor, S., Kalaany, N.Y., Jacks, T., Chan, C.S., Rabinowitz, J.D., et al. (2014). Autophagy is required for glucose homeostasis and lung tumor maintenance. Cancer Discov 4, 914-927.
Kim, J., Kundu, M., Viollet, B., and Guan, K.L. (2011). AMPK and mTOR regulate autophagy through direct phosphorylation of Ulk1. Nat Cell Biol 13, 132-141.
Klionsky, D.J. (2007). Monitoring autophagy in yeast: the Pho8Delta60 assay. Methods Mol Biol 390, 363-371.
Klionsky, D.J., Abdel-Aziz, A.K., Abdelfatah, S., Abdellatif, M., Abdoli, A., Abel, S., Abeliovich, H., Abildgaard, M.H., Abudu, Y.P., Acevedo-Arozena, A., et al. (2021). Guidelines for the use and interpretation of assays for monitoring autophagy (4th edition)(1). Autophagy 17, 1-382.
Lahiri, V., Hawkins, W.D., and Klionsky, D.J. (2019). Watch What You (Self-) Eat: Autophagic Mechanisms that Modulate Metabolism. Cell Metab 29, 803-826.
Lai, M.C., Chang, W.C., Shieh, S.Y., and Tarn, W.Y. (2010). DDX3 regulates cell growth through translational control of cyclin E1. Mol Cell Biol 30, 5444-5453.
Lang, M.J., Martinez-Marquez, J.Y., Prosser, D.C., Ganser, L.R., Buelto, D., Wendland, B., and Duncan, M.C. (2014). Glucose starvation inhibits autophagy via vacuolar hydrolysis and induces plasma membrane internalization by down-regulating recycling. J Biol Chem 289, 16736-16747.
Lanz, M.C., Yugandhar, K., Gupta, S., Sanford, E.J., Faca, V.M., Vega, S., Joiner, A.M.N., Fromme, J.C., Yu, H., and Smolka, M.B. (2021). In-depth and 3-dimensional exploration of the budding yeast phosphoproteome. EMBO Rep 22, e51121.
Lao, J.P., Ulrich, K.M., Johnson, J.R., Newton, B.W., Vashisht, A.A., Wohlschlegel, J.A., Krogan, N.J., and Toczyski, D.P. (2018). The Yeast DNA Damage Checkpoint Kinase Rad53 Targets the Exoribonuclease, Xrn1. G3 (Bethesda) 8, 3931-3944.
Li, Z., Vizeacoumar, F.J., Bahr, S., Li, J., Warringer, J., Vizeacoumar, F.S., Min, R., VanderSluis, B., Bellay, J., DeVit, M. et al. (2011) Nat Biotechnol 29, 361-367.
Licheva, M., Raman, B., Kraft, C., and Reggiori, F. (2021). Phosphoregulation of the autophagy machinery by kinases and phosphatases. Autophagy, 1-20.
Liu, K., Sutter, B.M., and Tu, B.P. (2021). Autophagy sustains glutamate and aspartate synthesis in Saccharomyces cerevisiae during nitrogen starvation. Nat Commun 12, 57.
Liu, X., Yao, Z., Jin, M., Namkoong, S., Yin, Z., Lee, J.H., and Klionsky, D.J. (2019). Dhh1 promotes autophagy-related protein translation during nitrogen starvation. PLoS Biol 17, e3000219.

Lock, R., Roy, S., Kenific, C.M., Su, J.S., Salas, E., Ronen, S.M., and Debnath, J. (2011). Autophagy facilitates glycolysis during Ras-mediated oncogenic transformation. Mol Biol Cell 22, 165-178.

Matoba, K., Kotani, T., Tsutsumi, A., Tsuji, T., Mori, T., Noshiro, D., Sugita, Y., Nomura, N., Iwata, S., Ohsumi, Y., et al. (2020). Atg9 is a lipid scramblase that mediates autophagosomal membrane expansion. Nat Struct Mol Biol 27, 1185-1193.

May, A.I., Prescott, M., and Ohsumi, Y. (2020). Autophagy facilitates adaptation of budding yeast to respiratory growth by recycling serine for one-carbon metabolism. Nat Commun 11, 5052.

McEwan, D.G., and Dikic, I. (2011). The Three Musketeers of Autophagy: phosphorylation, ubiquitylation and acetylation. Trends Cell Biol 21, 195-201.

Melia, T.J., Lystad, A.H., and Simonsen, A. (2020). Autophagosome biogenesis: From membrane growth to closure. J Cell Biol 219.

Mizushima, N. (2010). The role of the Atg1/ULK1 complex in autophagy regulation. Curr Opin Cell Biol 22, 132-139.

Mizushima, N., and Levine, B. (2020). Autophagy in Human Diseases. N Engl J Med 383, 1564-1576.

Mochida, K., Oikawa, Y., Kimura, Y., Kirisako, H., Hirano, H., Ohsumi, Y., and Nakatogawa, H. (2015). Receptor-mediated selective autophagy degrades the endoplasmic reticulum and the nucleus. Nature 522, 359-362.

Morawska, M., and Ulrich, H.D. (2013). An expanded tool kit for the auxin-inducible degron system in budding yeast. Yeast 30, 341-351.

Mulcahy Levy, J.M., and Thorburn, A. (2020). Autophagy in cancer: moving from understanding mechanism to improving therapy responses in patients. Cell Death Differ 27, 843-857.

Nakatogawa, H. (2020). Mechanisms governing autophagosome biogenesis. Nat Rev Mol Cell Biol 21, 439-458.

Natarajan, K., Meyer, M.R., Jackson, B.M., Slade, D., Roberts, C., Hinnebusch, A.G., and Marton, M.J. (2001). Transcriptional profiling shows that Gcn4p is a master regulator of gene expression during amino acid starvation in yeast. Mol Cell Biol 21, 4347-4368.

Noda, T. (2017). Regulation of Autophagy through TORC1 and mTORC1. Biomolecules 7.

Papinski, D., Schuschnig, M., Reiter, W., Wilhelm, L., Barnes, C.A., Maiolica, A., Hansmann, I., Pfaffenwimmer, T., Kijanska, M., Stoffel, I., et al. (2014). Early steps in autophagy depend on direct phosphorylation of Atg9 by the Atg1 kinase. Mol Cell 53, 471-483.

Post, H., Penning, R., Fitzpatrick, M.A., Garrigues, L.B., Wu, W., MacGillavry, H.D., Hoogenraad, C.C., Heck, A.J.R., and Altelaar, A.F.M. (2017). Robust, Sensitive, and Automated Phosphopeptide Enrichment Optimized for Low Sample Amounts Applied to Primary Hippocampal Neurons. Journal of Proteome Research 16, 728-737.

Redon, C., Pilch, D.R., and Bonner, W.M. (2006). Genetic analysis of Saccharomyces cerevisiae H2A serine 129 mutant suggests a functional relationship between H2A and the sister-chromatid cohesion partners Csm3-Tof1 for the repair of topoisomerase I-induced DNA damage. Genetics 172, 67-76.

Redon, C., Pilch, D.R., Rogakou, E.P., Orr, A.H., Lowndes, N.F., and Bonner, W.M. (2003). Yeast histone 2A serine 129 is essential for the efficient repair of checkpoint-blind DNA damage. EMBO Rep 4, 678-684.

Russell, R.C., Yuan, H.X., and Guan, K.L. (2014). Autophagy regulation by nutrient signaling. Cell Res 24, 42-57.
Sawa-Makarska, J., Baumann, V., Coudevylle, N., von Bulow, S., Nogellova, V., Abert, C., Schuschnig, M., Graef, M., Hummer, G., and Martens, S. (2020). Reconstitution of autophagosome nucleation defines Atg9 vesicles as seeds for membrane formation. Science 369.
Schleker, T., Shimada, K., Sack, R., Pike, B.L., and Gasser, S.M. (2010). Cell cycle-dependent phosphorylation of Rad53 kinase by Cdc5 and Cdc28 modulates checkpoint adaptation. Cell Cycle 9, 350-363.
Schneider, C.A., Rasband, W.S., and Eliceiri, K.W. (2012). NIH Image to ImageJ: 25 years of image analysis. Nat Methods 9, 671-675.
Selth, L.A., Gilbert, C., and Svejstrup, J.Q. (2009). RNA immunoprecipitation to determine RNA-protein associations in vivo. Cold Spring Harb Protoc 2009, pdb prot5234.
Sen, N.D., Gupta, N., S, K.A., Preiss, T., Lorsch, J.R., and Hinnebusch, A.G. (2019). Functional interplay between DEAD-box RNA helicases Ded1 and Dbp1 in preinitiation complex attachment and scanning on structured mRNAs in vivo. Nucleic Acids Res 47, 8785-8806.
Sen, N.D., Zhou, F., Ingolia, N.T., and Hinnebusch, A.G. (2015). Genome-wide analysis of translational efficiency reveals distinct but overlapping functions of yeast DEAD-box RNA helicases Ded1 and eIF4A. Genome Res 25, 1196-1205.
Soto-Rifo, R., and Ohlmann, T. (2013). The role of the DEAD-box RNA helicase DDX3 in mRNA metabolism. Wiley Interdiscip Rev RNA 4, 369-385.
Sousa, C.M., Biancur, D.E., Wang, X., Halbrook, C.J., Sherman, M.H., Zhang, L., Kremer, D., Hwang, R.F., Witkiewicz, A.K., Ying, H., et al. (2016). Pancreatic stellate cells support tumour metabolism through autophagic alanine secretion. Nature 536, 479-483.
Sridharan, S., Jain, K., and Basu, A. (2011). Regulation of autophagy by kinases. Cancers (Basel) 3, 2630-2654.
Steinfeld, N., Lahiri, V., Morrison, A., Metur, S.P., Klionsky, D.J., and Weisman, L.S. (2021). Elevating PI3P drives select downstream membrane trafficking pathways. Mol Biol Cell 32, 143-156.
Sun, M., Zhou, T., Jonasch, E., and Jope, R.S. (2013). DDX3 regulates DNA damage-induced apoptosis and p53 stabilization. Biochim Biophys Acta 1833, 1489-1497.
Sweeney, F.D., Yang, F., Chi, A., Shabanowitz, J., Hunt, D.F., and Durocher, D. (2005). Saccharomyces cerevisiae Rad9 acts as a Mec1 adaptor to allow Rad53 activation. Curr Biol 15, 1364-1375.
Szyjka, S.J., Aparicio, J.G., Viggiani, C.J., Knott, S., Xu, W., Tavare, S., and Aparicio, O.M. (2008). Rad53 regulates replication fork restart after DNA damage in Saccharomyces cerevisiae. Genes Dev 22, 1906-1920.
Tang, F., Hu, P., Yang, Z., Xue, C., Gong, J., Sun, S., Shi, L., Zhang, S., Li, Z., Yang, C., et al. (2017). SBI0206965, a novel inhibitor of Ulk1, suppresses non-small cell lung cancer cell growth by modulating both autophagy and apoptosis pathways. Oncol Rep 37, 3449-3458.
Tarn, W.Y., and Chang, T.H. (2009). The current understanding of Ded1p/DDX3 homologs from yeast to human. RNA Biol 6, 17-20.
Tkach, J.M., Yimit, A., Lee, A.Y., Riffle, M., Costanzo, M., Jaschob, D., Hendry, J.A., Ou, J., Moffat, J., Boone, C., et al. (2012). Dissecting DNA damage response pathways by analysing protein localization and abundance changes during DNA replication stress. Nat Cell Biol 14, 966-976.

Tyanova, S., Temu, T., and Cox, J. (2016). The MaxQuant computational platform for mass spectrometry-based shotgun proteomics. Nature Protocols 11, 2301-2319.
White, E. (2015). The role for autophagy in cancer. J Clin Invest 125, 42-46.
White, E., Mehnert, J.M., and Chan, C.S. (2015). Autophagy, Metabolism, and Cancer. Clin Cancer Res 21, 5037-5046.
Wilky, B.A., Kim, C., McCarty, G., Montgomery, E.A., Kammers, K., DeVine, L.R., Cole, R.N., Raman, V., and Loeb, D.M. (2016). RNA helicase DDX3: a novel therapeutic target in Ewing sarcoma. Oncogene 35, 2574-2583.
Xie, Y., Kang, R., Sun, X., Zhong, M., Huang, J., Klionsky, D.J., and Tang, D. (2015). Posttranslational modification of autophagy-related proteins in macroautophagy. Autophagy 11, 28-45.
Xie, Z., Nair, U., and Klionsky, D.J. (2008). Atg8 controls phagophore expansion during autophagosome formation. Mol Biol Cell 19, 3290-3298.
Yamamoto, H., Kakuta, S., Watanabe, T.M., Kitamura, A., Sekito, T., Kondo-Kakuta, C., Ichikawa, R., Kinjo, M., and Ohsumi, Y. (2012). Atg9 vesicles are an important membrane source during early steps of autophagosome formation. J Cell Biol 198, 219-233.
Yin, Z., Liu, X., Ariosa, A., Huang, H., Jin, M., Karbstein, K., and Klionsky, D.J. (2019). Psp2, a novel regulator of autophagy that promotes autophagy-related protein translation. Cell Res 29, 994-1008.
Yin, Z., Pascual, C., and Klionsky, D.J. (2016). Autophagy: machinery and regulation. Microb Cell 3, 588-596.
Zarei, M., Sprenger, A., Rackiewicz, M., and Dengjel, J. (2016). Fast and easy phosphopeptide fractionation by combinatorial ERLIC-SCX solid-phase extraction for in-depth phosphoproteome analysis. Nature Protocols 11, 37-45.
Zhao, L., Mao, Y., Zhou, J., Zhao, Y., Cao, Y., and Chen, X. (2016). Multifunctional DDX3: dual roles in various cancer development and its related signaling pathways. Am J Cancer Res 6, 387-402.
Zheng, Y., Liu, L., Wang, Y., Xiao, S., Mai, R., Zhu, Z., and Cao, Y. (2021). Glioblastoma stem cell (GSC)-derived PD-L1-containing exosomes activates AMPK/ULK1 pathway mediated autophagy to increase temozolomide-resistance in glioblastoma. Cell Biosci 11, 63.

Chapter 3 : Hyperactivation of Vps34 Leads to Reduced Autophagy Flux by Partial Inhibition of a Late Stage of Autophagy

(This chapter has been adapted from *Steinfeld, Lahiri et al., Molecular Biology of the Cell, 2021)*

(Note: Vikramjit Lahiri contributed to the investigations on the role of Vps34 hyperactivation on autophagy)

Phosphoinositide signaling lipids are essential for several cellular processes. The requirement for a phosphoinositide is conventionally studied by depleting the corresponding lipid kinase. However, there are very few reports on the impact of elevating phosphoinositides. That phosphoinositides are dynamically elevated in response to stimuli suggests that in addition to being required, phosphoinositides drive downstream pathways. To test this hypothesis, we elevated the levels of phosphatidylinositol 3-phosphate (PtdIns3P) by generating hyperactive alleles of the yeast phosphatidylinositol 3-kinase, Vps34. We find that hyperactive Vps34 drives certain pathways, including PtdIns(3,5)P_2 synthesis and retrograde transport from the vacuole. This demonstrates that PtdIns3P is rate limiting in some pathways. Interestingly, hyperactive Vps34 does not affect ESCRT function. Thus, elevating PtdIns3P does not always increase the rate of PtdIns3P-dependent pathways. Elevating PtdIns3P can also delay a pathway. Elevating PtdIns3P slowed late steps in autophagy, in part by delaying the disassembly of autophagy proteins from mature autophagosomes as well as delaying fusion of autophagosomes with the vacuole. This latter defect is likely due to a more general defect in vacuole fusion, as assessed by changes in vacuole morphology. These studies suggest that stimulus-induced elevation of phosphoinositides provides a way for stimuli to selectively regulate downstream processes.

3.1 Introduction

Phosphoinositide (PI) lipids are signaling molecules that play critical roles in multiple cellular processes. It is assumed that generation of specific PI species on membranes recruits distinct effector proteins that regulate downstream pathways (reviewed in (Schink et al., 2016)). PI species are generated by phosphorylation at the 3-, 4-, and 5- positions of the inositol head group of phosphatidylinositol (PtdIns) and the levels of these lipids are dynamically regulated by PI lipid kinases and phosphatases in response to stimuli (Balla, 2013). For example, during hyperosmotic shock in S. cerevisiae, there is a transient 15 to 20-fold elevation in phosphatidylinositol-3,5-bisphosphate (PI[3,5]P_2; Duex et al., 2006a). Most studies of how PI lipids regulate downstream pathways use knockout or knockdown of PI kinases to deplete a specific PI lipid and thereby test the necessity for that PI species in a process (Kihara et al., 2001). However, the dynamic regulation of PI lipids suggests that in addition to being required for specific pathways, changes in PI lipids may drive downstream processes. Here, we test this hypothesis directly by manipulating the levels of phosphatidylinositol 3-phosphate (PtdIns3P), which is dynamically regulated in yeast (Duex et al., 2006a).

In yeast, the PtdIns 3-kinase, Vps34, is the sole enzyme responsible for generating PtdIns3P from PtdIns (Schu et al., 1993). Vps34 functions within two large regulatory complexes (Kihara et al., 2001). Complex I is dedicated to autophagy, and complex II is required for several trafficking pathways in the endomembrane system. The pseudokinase, Vps15, is absolutely required for Vps34 function and PtdIns3P synthesis in yeast (Stack et al., 1993). In addition to Vps34 and Vps15, both complexes contain Vps30 (BECN1 in mammalian systems), which contains a BARA domain crucial for binding the PtdIns 3-kinase complex to membranes (Huang

et al., 2012; Rostislavleva et al., 2015). Furthermore, each complex contains complex-specific protein subunits, which specify the intracellular localization of the complexes (Obara et al., 2006). Complex I includes Atg14 and Atg38 (Araki et al., 2013), whereas complex II contains Vps38 (Kihara et al., 2001).

Several PtdIns3P-dependent cellular processes have been identified in cells (Figure 18A). In yeast, synthesis of PtdIns(3,5)P_2 is achieved by phosphorylation of PtdIns3P at the 5 position (Gary et al., 1998). Thus, Vps34 mutants that do not produce PtdIns3P also do not produce PtdIns(3,5)P_2 (Dove et al., 1997). PtdIns3P is also required for multiple retrograde transport pathways. Yeast retromer functions in retrograde transport of transmembrane sorting receptors from endosomes back to the Golgi (Seaman et al., 1997; Seaman et al., 1998). The retromer requires PtdIns3P, which recruits retromer sorting nexins Vps5 and Vps17 to membranes (Burda et al., 2002). These sorting nexins contain PtdIns3P-binding PX domains as well as BAR domains (SNX-BAR; Yu and Lemmon, 2001). Recently, another SNX-BAR protein, Snx4, has been implicated in retrograde transport for retrieval of proteins from the vacuole to endosomes (Ma et al., 2017; Suzuki and Emr, 2018). PtdIns3P is required for proper Snx4 localization and is necessary for Snx4-dependent retrograde transport (Nice et al., 2002; Suzuki and Emr, 2018).

Function of the endosomal sorting complexes required for transport (ESCRT) pathway also depends on PtdIns3P. The ESCRT complex functions on both endosomes and the vacuole to target selected transmembrane proteins for degradation. The selected proteins are first ubiquitinated, which enables their recognition and binding to the ESCRT complex. Once the cargo proteins are bound, the ESCRT complex generates vesicles via inward budding into lumen of the organelle, and the cargoes are ultimately degraded in the vacuole. ESCRT-0 functions by binding ubiquitinated ESCRT client proteins and recruiting ESCRT-I to membranes. Vps34 is

required for proper localization of the ESCRT-0 subunit Vps27, which contains a PtdIns3P-binding FYVE domain (Katzmann et al., 2003). Additionally, PtdIns3P is required for fusion of vesicles with the vacuole and homotypic vacuole fusion. This is due in part to the direct binding of the SNARE Vam7 (Cheever et al., 2001; Fratti and Wickner, 2007) and the heterodimeric GEF subunits Mon1 and Ccz1 (Cabrera et al., 2014) to PtdIns3P. Moreover, Vps34-dependent generation of PtdIns3P is required for the vacuole association of many additional proteins required for vacuole fusion (Lawrence et al., 2014).

PtdIns3P is also required for autophagy. Defects in PtdIns 3-kinase complex I block autophagy in yeast (Kihara et al., 2001). Early in autophagy, PtdIns3P recruits Atg18 to the phagophore (Dove et al., 2004; Obara et al., 2008) where it interacts with Atg2 and tethers pre-autophagosomal membranes to the endoplasmic reticulum, allowing Atg2 to transport lipids to promote autophagosome biogenesis (Rieter et al., 2013; Kotani et al., 2018; Valverde et al., 2019). Following autophagosome formation, Ymr1, a myotubularin family protein and putative PtdIns3P phosphatase (Taylor et al., 2000; Parrish et al., 2004) is crucial for autophagosome fusion with the vacuole. Deletion of *YMR1* causes a failure of key autophagy machinery including Atg18 to dissociate from mature autophagosomes. This leads to accumulation of autophagosomes in the cytoplasm (Cebollero et al., 2012) and suggests that turnover of PtdIns3P is crucial for this process. PtdIns3P also has a positive role in a late step in autophagy. In vitro studies indicate that fusion of autophagosomes with the vacuole requires PtdIns3P and likely acts by recruiting the Rab GTPase Ypt7, which in turn recruits the HOPS tethering complex (Bas et al., 2018). Thus, while PtdIns3P is required for some steps in autophagy, impeding turnover of PtdIns3P inhibits the resolution of autophagosomes.

Here, we report the generation and use of hyperactive mutations in Vps34 and the discovery that PtdIns3P drives select pathways, including synthesis of PtdIns(3,5)P_2 during hyperosmotic shock and retrograde transport of Atg27. In these cases, the PtdIns3P-dependent step is rate limiting. We also show that hyperactive Vps34 does not affect ESCRT function at endosomes or on the vacuole. Thus, elevating PtdIns3P does not always increase the overall rate of a complex pathway. We also show that elevating PtdIns3P can delay a pathway. Hyperactive Vps34 does not lead to an acceleration in the induction of autophagy, but inhibits late steps in autophagy, in part via a delay in disassembly of the autophagy machinery from the surface of mature autophagosomes and also a delay in fusion of autophagosomes with the vacuole. This latter defect is likely due to a more general defect in vacuole fusion, as evidenced by an increase in the number of vacuole lobes per cell, which is consistent with a defect in homotypic vacuole fusion. Overall, our studies suggest that stimulus-induced elevation of PtdIns3P levels regulates some, but not all, PtdIns3P-dependent membrane trafficking pathways and that phosphoinositide lipids are commonly rate-limiting in pathways where they are required.

3.2 Results and Discussion

3.2.1 Generation of hyperactive Vps34 mutants

To test the hypothesis that changes in PI levels drive downstream processes, we devised a strategy for specifically elevating PtdIns3P. PtdIns3P was an attractive target because several downstream PtdIns3P-dependent processes have been identified in yeast. Additionally, the existing 4.4 Å crystal structure of the yeast PtdIns 3-kinase complex allowed us to predict amino acid changes that would increase PtdIns3P levels (Rostislavleva et al., 2015). Moreover, the crystal structure also allowed us to map the location of amino acid changes responsible for the hyperactivity of the Vps34 mutants identified in our screen.

We found that overexpression of Vps34 alone or together with Vps15 caused a modest, 13%, increase in PtdIns3P levels despite robust overexpression (Figure 19A and 19B). This result suggests either that overexpression of additional subunits of the Vps34 complex are required for increased Vps34 function or that Vps34 kinase activity is negatively regulated.

To achieve more robust elevation of PtdIns3P levels, we tested whether point mutations in Vps34 would yield a hyperactive enzyme. Vps34 activity is proposed to be regulated in part via changes in the contact of the Vps34 helical and kinase domains (HELCAT) with the Vps15 pseudokinase domain (Figure 18B) (Stjepanovic et al., 2017). In the inactive conformation, the Vps34 HELCAT domain contacts the Vps15 scaffold. During activation, the Vps34 HELCAT domain is proposed to alter its contact with Vps15 and allow Vps34 to access its PI substrate. Based on the structure of the PI 3-kinase complex, we introduced point mutations in Vps34 along its contact site with Vps15 (Figure 19C). We tested eight Vps34 point mutants and identified two mutations, R283E and A287D, that robustly increased PtdIns3P by 36 and 27%, respectively (Figure 19D).

Combining R283E and A287D, but not other mutations along the Vps34 HELCAT-Vps15 interface, elevated PtdIns3P levels by approximately 40% (Figure 19E). These two mutants are on an alpha-helix N-terminal to the helical domain of Vps34 and face Vps15 (Figure 18C). Identification of these hyperactive Vps34 mutants provides further evidence that altered contact between the Vps34 HELCAT domain and Vps15 promotes Vps34 kinase activity.

We also performed an unbiased genetic screen for hyperactive Vps34 mutants using a method similar to one used to generate hyperactive mutations in the PtdIns3P 5-kinase, Fab1 (Duex et al., 2006b; Lang et al., 2017). We generated a hypomorphic $Vps34^{K759D}$ allele, which

has a mutation in the activation loop of Vps34 and found that it lowers PtdIns3P levels to approximately 20% of wild-type Vps34. We then performed random PCR mutagenesis on the C-terminal half of $Vps34^{K759D}$ (Figure 20A). Mutagenized plasmids were tested for their ability to rescue growth in *vps34*Δ cells grown on rapamycin at 33°C. From 22 independently isolated mutants, we identified nine unique point mutations. Five of these mutations elevate PtdIns3P levels. The best of these mutations, Y501C, elevated PtdIns3P approximately 40% (Figure 18C and 20C). Interestingly, each of the five mutated residues are located on either the alpha-C helix of the Vps34 kinase domain or an adjacent helix of the helical domain (Figure 20B). Conformational changes in the alpha-C helix are critical to regulating kinase function (Taylor et al., 2015). We hypothesize these hyperactive mutants favor an active conformation of the alpha-C helix. It is not known whether these are regulatory sites on the native enzyme. We determined that combining the R283E and A287D mutant with Y501C (Vps34-EDC) elevates PtdIns3P by approximately 60%, which is higher than either mutant alone (Figure 18D). The Vps34-EDC mutant does not change Vps34 protein levels (Figure 21A and 21B), nor does it change the localization of Vps34 within the cell as measured by the amount of Envy-Vps34 that colocalizes with the vacuole (Figure 21C and 21D). This suggests that the distribution of PtdIns3P in the cell is most likely unchanged by the hyperactive mutant.

PtdIns3P is the substrate for the PtdIns3P 5-kinase, Fab1, which generates PtdIns(3,5)P_2 (Gary et al., 1998). We tested whether elevation of PtdIns3P via hyperactive Vps34 leads to an elevation of PtdIns(3,5)P_2. At basal conditions, no statistically significant increase in PtdIns(3,5)P_2 levels was detected (Figure 18E). However, when hyperosmotic shock was used to induce a transient elevation of PtdIns(3,5)P_2 (Duex et al., 2006a), the presence of hyperactive Vps34 mutants resulted in a further elevation of PtdIns(3,5)P_2 (Figure 18F). Note that while

PtdIns3P levels decrease during hyperosmotic shock, hyperactive Vps34 mutants still elevate PtdIns3P above wild-type levels (Figure 20D). Thus, hyperactive Vps34 drives elevation of PtdIns(3,5)P_2 during hyperosmotic shock. We ruled out several potential mechanisms by which hyperactive Vps34 might elevate PtdIns(3,5)P_2. We determined that hyperactive Vps34-EDC does not change the amount of Fab1-Envy that colocalizes with the vacuole (Figure 22A and 22B). Additionally, there was no change in the amount of Fab1 complex member Fig4 (Botelho et al., 2008) that colocalizes with the vacuole (Figure 22C and 22D). These results suggest that hyperactive Vps34 does not result in increased recruitment of the Fab1 complex to membranes. Moreover, the increase in PtdIns(3,5)P_2 is likely not due to inhibition of Fig4, the PtdIns(3,5)P_2 5-phosphatase (Gary et al., 2002). Catalytically dead Fig4 mutants exhibit a mild increase in PtdIns(3,5)P_2 under basal conditions, yet a decrease in PtdIns(3,5)P_2 at 10 min following hyperosmotic shock (Duex et al., 2006b; Strunk et al., 2020). Thus, the increase in PtdIns(3,5)P_2 caused by Vps34-EDC most likely occurs because of increased availability of PtdIns3P, which may provide more substrate for Fab1 and/or activate Fab1. Note that the additional PtdIns(3,5)P_2 provided during hyperosmotic shock by hyperactive Vps34-EDC does not affect the growth of yeast cells following hyperosmotic shock (Figure 22E).

Figure 18: Generation of hyperactive Vps34 mutants

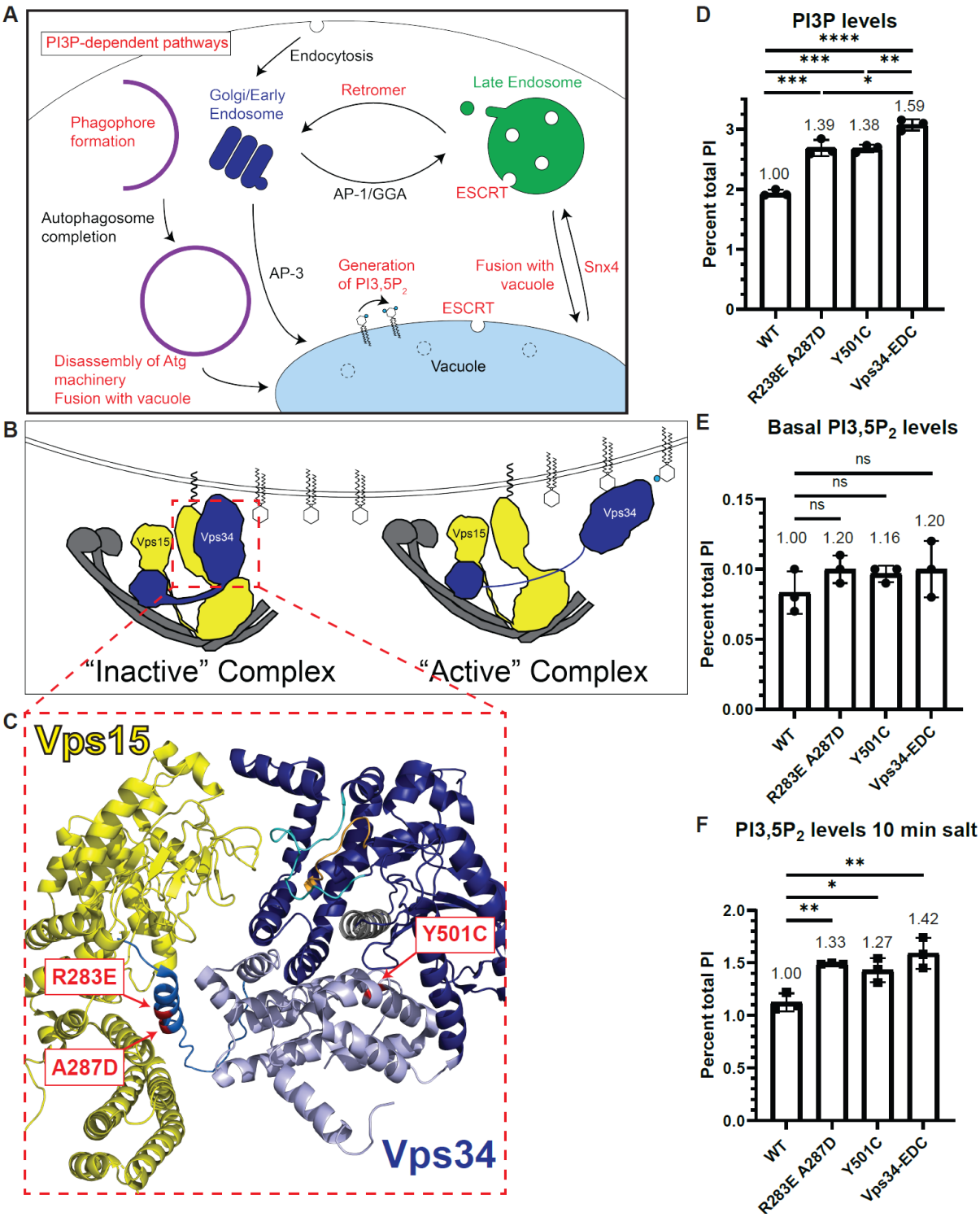

Figure 18. Generation of hyperactive Vps34 mutants.

A) Schematic indicating several PtdIns3P-dependent intracellular trafficking pathways in yeast. PI3P serves as the substrate for PtdIns(3,5)P_2. PtdIns3P is also required for Snx4-dependent retrograde transport from the vacuole and retromer-dependent retrograde transport from endosomes. ESCRT function at late endosomes and the vacuole is also dependent on PtdIns3P. Furthermore, PtdIns3P is required for phagophore formation during the initiation of autophagy and then PtdIns3P is removed prior to the disassembly of some autophagy proteins from the surface of mature autophagosomes. In addition, fusion of autophagosomes and other vesicles with the vacuole, as well as homotypic vacuole fusion (not shown), are PtdIns3P-dependent pathways.

B) Vps34 is proposed to be regulated in part via changes in contact of the Vps34 HELCAT domain with Vps15. In the inactive conformation, the Vps34 HELCAT domain contacts the Vps15 scaffold. During activation, the Vps34 HELCAT domain is proposed to alter the contact with Vps15 and allow Vps34 to access its PtdIns substrate (Stjepanovic *et al.*, 2017).

C) Crystal structure of the helical (light blue) and kinase (dark blue) domains of Vps34 and its contact with the pseudo-kinase domain of Vps15 (yellow) (Rostislavleva *et al.*, 2015). The three amino acid changes that comprise the Vps34-EDC hyperactive mutant are indicated (red). Two of these mutations, R283E and A287D, are on an alpha-helix N-terminal to the helical domain of Vps34 (neutral blue) and may hinder Vps34 HELCAT interaction with Vps15 and favor the active Vps34 conformation. The Y501C mutation is in the helical domain of Vps34 and faces the alpha-C helix (gray) of the kinase domain, nearby the activation (cyan) and catalytic (orange) loops of Vps34.

D-F) The Vps34 mutants R283E A287D and Y501C elevate PtdIns3P levels. PtdIns(3,5)P_2 levels are also elevated during hyperosmotic shock. Combining the mutants to Vps34-EDC further elevated PtdIns3P levels and PtdIns(3,5)P_2 levels. *vps34*Δ cells were transformed with a wild-type or mutant pRS416-Vps34 plasmid. PtdIns lipid levels were measured by metabolically labeling cells with myo-^{3}H-inositol for 16 h. Prior to harvest, indicated cultures were exposed to 10 min of hyperosmotic shock. PtdIns lipid head groups were separated by anion exchange and HPLC. n=3. Error bars indicate standard deviation. Unpaired t-test. ns=p>.05, *=p<.05, **=p<.01, ***=p<.001, ****=p<.0001.

Figure 19: Generation of hyperactive Vps34 mutants based on a high-resolution structure of the Vps34-Vps15-Vps30-Vps38 complex

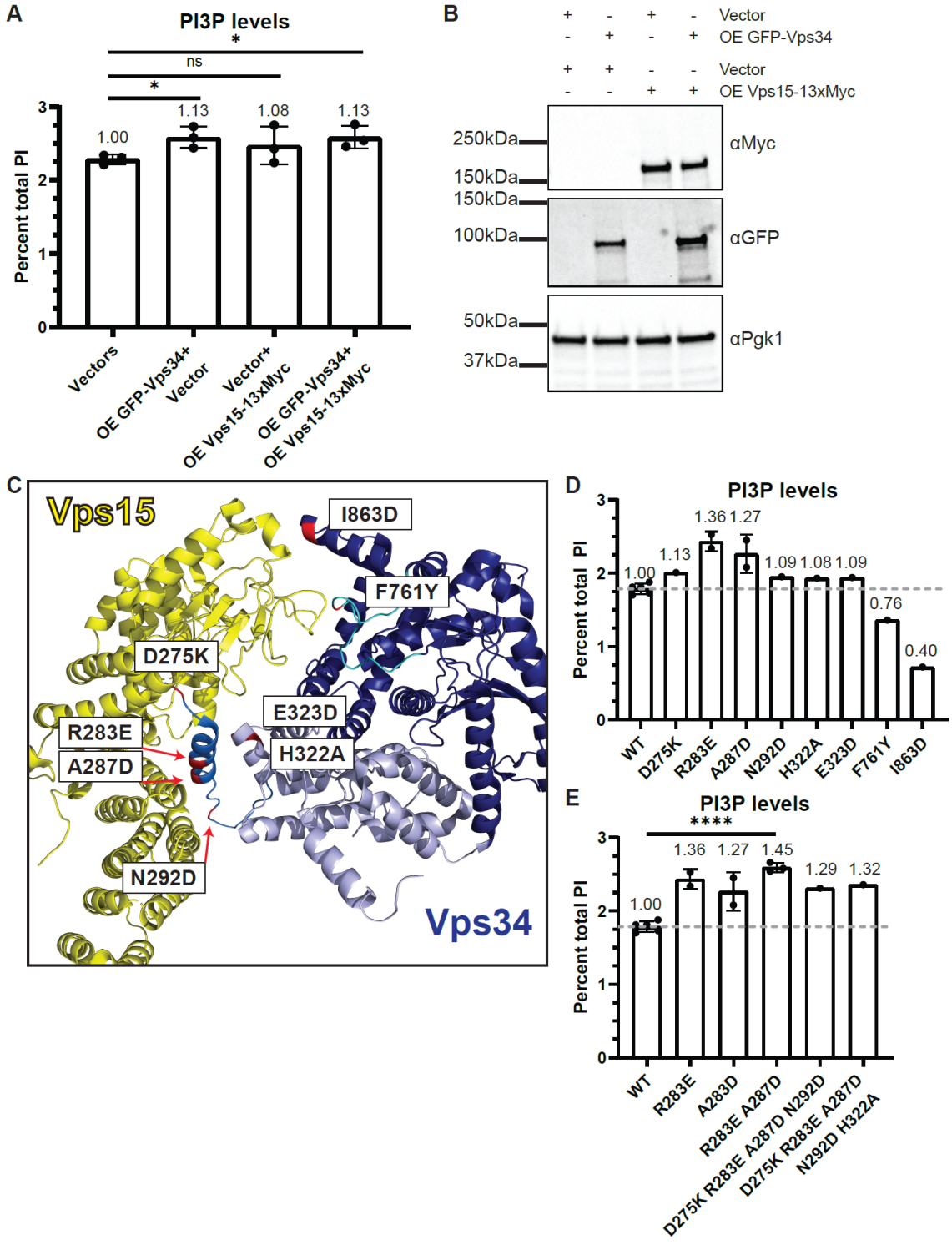

Figure 19. Generation of hyperactive Vps34 mutants based on a high-resolution structure of the Vps34-Vps15-Vps30-Vps38 complex.

A and B) Overexpression of GFP-Vps34 and Vps15-13xMyc results in a modest 13% increase in PI3P levels. Wild-type yeast cells were transformed with pRS426-GFP-Vps34, pRS425-Vps15-13xMyc, or both plasmids together. PI lipid levels were measured. In parallel, GFP-Vps34 and Vps15-13xMyc protein levels were analyzed via western blot to measure overexpression. Vps15-13xMYC was detected using anti-MYC antibody. GFP-Vps34 was detected with anti-GFP antibody. Pgk1 was used as a loading control. Representative of n=3. PI lipid levels were measured by metabolically labeling cells with myo-^{3}H-inositol for 16 h, harvesting cells, and separating PI lipid head groups by anion exchange and HPLC. n=3. Error bars indicate standard deviation. Unpaired t-test. ns=p>.05, *=p<.05.

C) Based on the crystal structure of the PtdIns 3-kinase complex and the hypothesis that altering the contact between Vps34 HELCAT (helical in light blue kinase in dark blue) and Vps15 (yellow) would activate Vps34, we tested eight point mutants (red) in Vps34 for elevated PtdIns3P levels (Rostislavleva *et al.*, 2015; Stjepanovic *et al.*, 2017). D275K, R283E, A287D, and N292D are on an alpha-helix N-terminal to the helical domain of Vps34 (neutral blue), E323D and H322A are in the helical domain, F761Y is in the activation loop (cyan), and I863D is in the kinase domain.

D and E) Of the mutants predicted to disrupt the interaction between Vps34 HELCAT and Vps15, PI3P levels are most elevated by R283E and A287D (D). Combination of R283E with A287D further elevated PtdIns3P levels (E). However, combining R283E A287D with additional

mutations did not further elevated PtdIns3P levels (E). *vps34*Δ cells were transformed with a wild-type or mutant pRS416-Vps34 plasmid. PI lipid levels were measured by metabolically labeling cells with myo-^{3}H-inositol for 16 h, harvesting cells, and separating PI lipid head groups by anion exchange and HPLC. n=5 for WT, n=2 for R283E and A287D, n=3 for R283E A287D, n=1 for the rest. WT, R283E, and A287D data points are the same in D and E. Error bars indicate standard deviation. Unpaired t-test. ****=p<.0001. Related to Figure 18.

Figure 20: Generation of hyperactive Vps34 mutants via a mutant screen

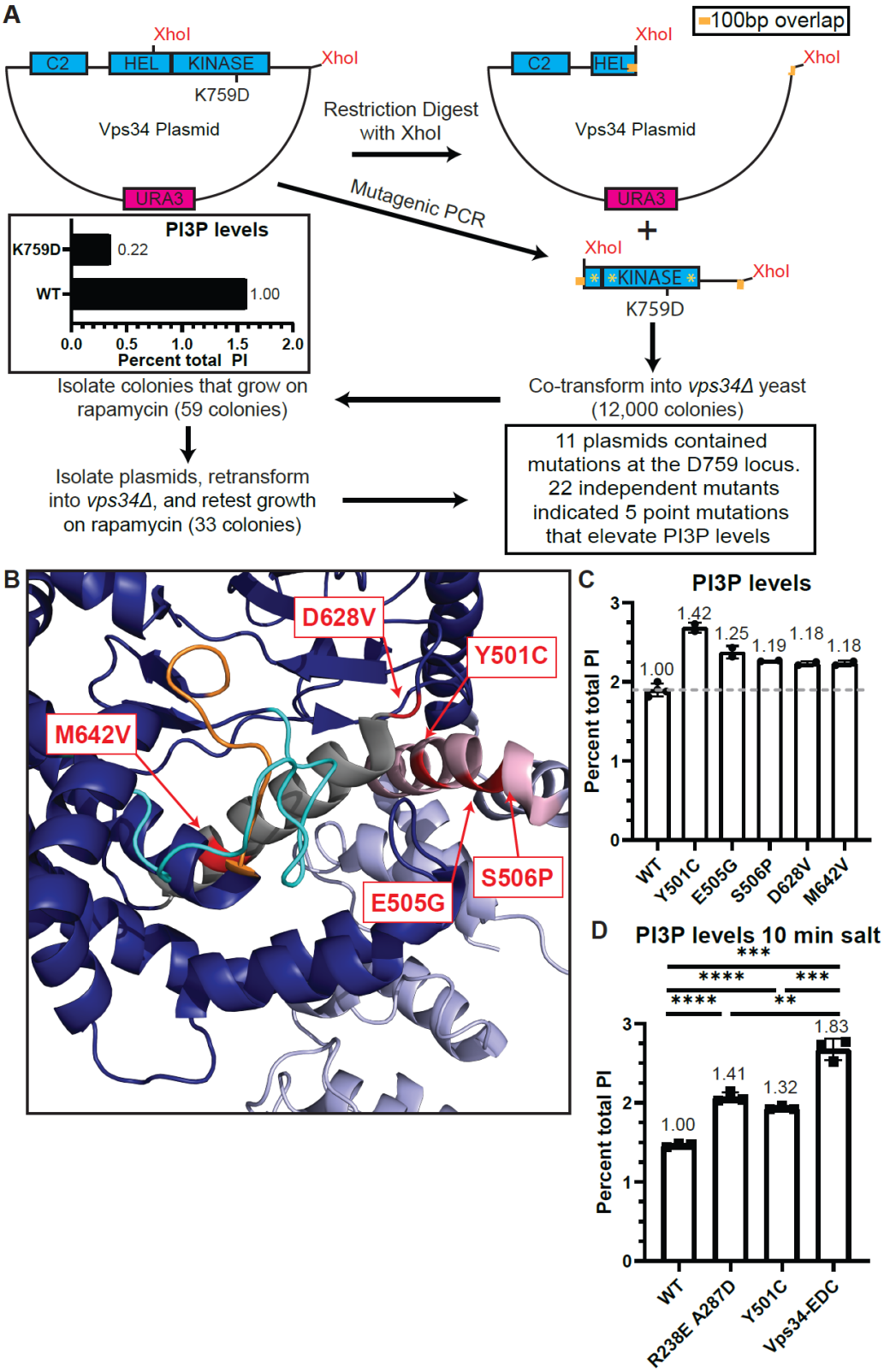

Figure 20. Generation of hyperactive Vps34 mutants via a mutant screen.

A) A screen for hyperactive mutations in Vps34 was designed to identify mutants that rescued growth of a hypomorphic Vps34 allele, $Vps34^{K759D}$, a mutation in the activation loop of Vps34 that lowers PtdIns3P levels to 22% of wild type. *vps34*Δ cells were transformed with pRS416-Vps34 or pRS416-Vps34-K759D plasmids. PI lipid levels were measured by metabolically labeling cells with myo-^{3}H-inositol for 16 h, harvesting cells, and separating PI lipid head groups by anion exchange and HPLC. n=1. The C-terminal half of Vps34 was PCR amplified using mutagenic Taq DNA polymerase and a Vps34 plasmid was cut with restriction enzyme, XhoI, to remove the region of Vps34 that was mutated. The plasmid backbone and mutated PCR fragment were co-transformed into *vps34*Δ cells. Two days following co-transformation, colonies were replica plated to plates containing 10 nM rapamycin and grown at 33°C. Mutant Vps34 plasmids were isolated from colonies that rescued growth on rapamycin at 33°C and retransformed into *vps34*Δ cells to confirm rescued growth on rapamycin at 33°C. Sanger sequencing was used to identify the mutations present in isolated plasmids. 22 independent mutants revealed nine unique point mutations. Of those nine mutations, changes at five of them were found to elevate PtdIns3P levels.

B) Crystal structure of the helical (light blue) and kinase (dark blue) domains of Vps34, indicating five residues identified in the hyperactive Vps34 mutant screen (red). M642V and D628V are at opposite ends of the alpha-C helix (gray) of the kinase domain, nearby the activation (cyan) and catalytic (orange) loops of Vps34. Y501C, E505G, and S506P face the alpha-C helix on the same side of an alpha helix in the helical domain of Vps34 (light pink).

C) Of the mutants identified in the Vps34 hyperactive mutant screen, PtdIns3P levels are most elevated by Y501C. *vps34*Δ cells were transformed with a wild-type or mutant pRS416-Vps34

plasmid. PI lipid levels were measured by metabolically labeling cells with myo-^{3}H-inositol for 16 h, harvesting cells, and separating PI lipid head groups by anion exchange and HPLC. n=4 for WT, n=2 for the rest. Error bars indicate standard deviation.

D) The Vps34 mutants R283E A287D and Y501C elevate PtdIns3P levels during hyperosmotic shock. Combining the mutants to generate Vps34-EDC further elevated PtdIns3P during hyperosmotic shock. *vps34*Δ cells were transformed with a wild-type or mutant pRS416-Vps34 plasmid. PI lipid levels were measured by metabolically labeling cells with myo-^{3}H-inositol for 16 h. Prior to harvest, indicated cultures were exposed to 10 min of hyperosmotic shock. PI lipid head groups were separated by anion exchange and HPLC. Data are from the same samples as Figure 1D-F. n=3. Error bars indicate standard deviation. Unpaired t-test. **=p<.01, ***=p<.001, ****=p<.0001. Related to Figure 18.

Figure 21: Hyperactive Vps34-EDC does not affect the protein levels or localization of Vps34

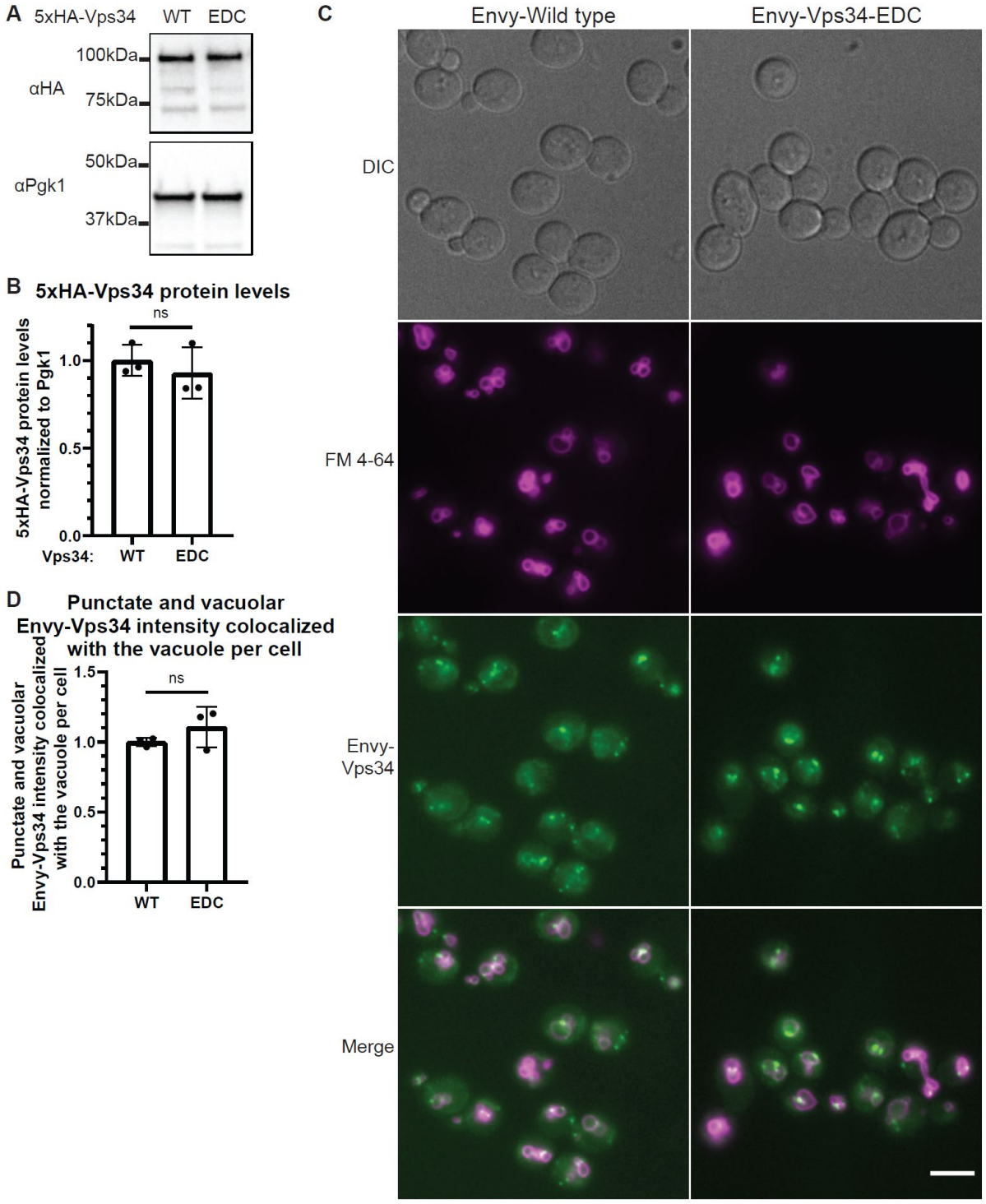

<u>Figure 21.</u> Hyperactive Vps34-EDC does not affect the protein levels or localization of Vps34.

A and B) Hyperactive Vps34-EDC does not change 5xHA-Vps34 protein levels. *vps34Δ* cells were transformed with pRS416-5xHA-Vps34 or pRS416-5xHA-Vps34-EDC. 5xHA-Vps34 protein levels were analyzed via western blot using anti-HA antibody. 5xHA-Vps34 levels were normalized to Pgk1. Levels were then normalized to wild type. Representative of n=3. Error bars indicate standard deviation. Unpaired t-test. ns=p>.05.

C and D) Hyperactive Vps34-EDC does not change the intensity of punctate and vacuolar Envy-Vps34 localized to the vacuole. *vps34*Δ cells were transformed with pRS416-Envy-Vps34 or pRS416-Envy-Vps34-EDC. After labeling with FM 4-64, cells were chased at 24°C for 3 h before imaging. DIC, differential interference contrast. Scale bar: 5 μm. The Envy-Vps34 signal that overlaps FM 4-64 was divided by the number of cells quantified. Quantification of at least 100 cells per n, n=3. The average of the wild-type samples was normalized to 1. Error bars indicate standard deviation. Unpaired t-test. ns=p>.05. Related to Figure 18.

Figure 22: Hyperactive Vps34-EDC does not affect the localization of some members of the PtdIns(3,5)P_2 kinase complex

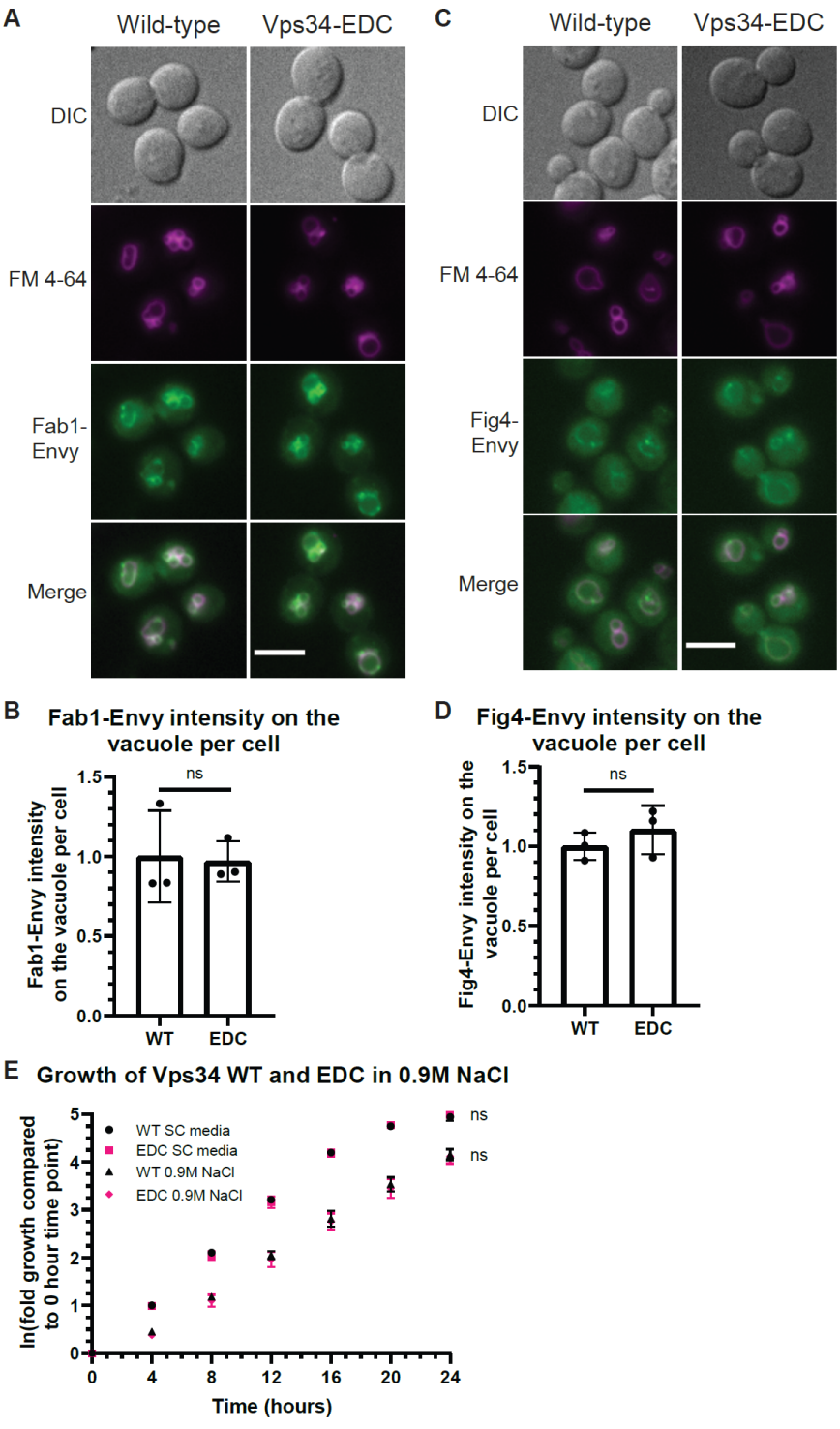

Figure 22. Hyperactive Vps34-EDC does not affect the localization of some members of the PtdIns(3,5)P_2 kinase complex.

A and B) Hyperactive Vps34-EDC does not change the localization of Fab1-Envy to the vacuole. *vps34*Δ cells were transformed with pRS416-Fab1-Envy and pRS413-Vps34 or pRS413-Vps34-EDC. After labeling with FM 4-64, cells were chased at 24°C for 3 h before imaging. DIC, differential interference contrast. Scale bar: 5 μm. The Fab1-Envy signal that overlaps FM 4-64 was divided by the number of cells quantified. Quantification of at least 100 cells per n, n=3. The average of the wild-type samples was normalized to 1. Error bars indicate standard deviation. Unpaired t-test. ns=p>.05.

C and D) Hyperactive Vps34-EDC does not change the localization of Fig4-Envy to the vacuole. *vps34*Δ cells were transformed with pRS413-Fig4-Envy and pRS416-Vps34 or pRS416-Vps34-EDC. After labeling with FM 4-64, cells were chased at 24°C for 3 h before imaging. DIC, differential interference contrast. Scale bar: 5 μm. The Fig4-Envy signal that overlaps FM 4-64 was divided by the number of cells quantified. Quantification of at least 100 cells per n, n=3. The average of the wild-type samples was normalized to 1. Error bars indicate standard deviation. Unpaired t-test. ns=p>.05.

E) Hyperactive Vps34-EDC does not affect the growth of yeast cells following hyperosmotic shock. *vps34*Δ cells were transformed with pRS416-Vps34 or pRS416-Vps34-EDC. Cells were grown to mid-log phase in SC media and then diluted to equal concentrations. An equal volume of SC media or SC media with 1.8 M NaCl was added to the culture to begin the time-course. ODs were measured immediately following the addition of SC media or SC media with 1.8 M NaCl and then every 4 hours for 24 hours. The time zero OD measurement for each sample was

normalized to 1. A natural logarithmic transformation was applied to the normalized ODs so that exponential growth is represented linearly. n=4. Error bars indicate standard deviation. Unpaired t-test between WT and EDC at each time point. ns=p>.05. Related to Figure 18.

3.2.2 Hyperactive Vps34 increases retrograde transport of Atg27

Atg27 is a cargo for PtdIns3P-dependent Snx4- and retromer-dependent retrograde transport pathways. Following its synthesis, Atg27 is delivered from the Golgi to the vacuole via the AP-3 pathway (Segarra et al., 2015). From the vacuole, Atg27 undergoes retrograde transport to endosomes in a Snx4-dependent manner (Ma et al., 2017; Suzuki and Emr, 2018). From endosomes, Atg27 undergoes retrograde transport back to the Golgi via the retromer (Suzuki and Emr, 2018). Due to the cyclic nature of its transport, changes in Atg27 localization signify changes in the rates of each of these transport steps.

We tested whether hyperactive Vps34 increases the rate of retrograde transport of Atg27 from the vacuole to endosomes and/or Golgi. In wild-type cells, Atg27-2xGFP was primarily localized to the vacuole (Figure 23A) with a few Golgi (Figure 23D) and endosomal (Figure 23F) puncta. Notably, in the presence of Vps34-EDC, Atg27-2xGFP was more punctate (Figure 23A) and fewer hyperactive Vps34-EDC cells had Atg27-2xGFP visible on the vacuole (Figure 23B). Moreover, on a per cell basis, less Atg27-2xGFP colocalized with the vacuole (Figure 23C). Blocking retrograde transport from the vacuole by deletion of *SNX4* suppressed Atg27-2xGFP traffic from the vacuole (Figure 23A-C). These results suggest that hyperactive Vps34-EDC accelerates the Snx4 and/or retromer pathways.

The loss of Atg27-2xGFP localization to the vacuole is likely not caused by impairment of the AP-3-dependent anterograde delivery of Atg27 to the vacuole. We tested the localization of another AP-3 client protein Yck3 (Sun et al., 2004) and found that it was delivered to the vacuole in the presence of Vps34-EDC (Figure 24A), indicating that Vps34-EDC does not cause a defect in AP-3 function.

We tested whether the additional Atg27-2xGFP puncta present in Vps34-EDC correspond to Golgi and/or endosomes. We found that expression of Vps34-EDC resulted in a higher percentage of the total cellular Atg27-2xGFP that colocalizes with the Golgi marker, Sec7-mCherry (Figure 23D and 23E). There was no statistically significant difference between Vps34-EDC-expressing cells compared to wild type with respect to the total cellular Atg27-2xGFP signal that colocalized with endosome marker Vps8-mCherry (Figure 23F and 23G). Accumulation of Atg27-2xGFP in the Golgi is consistent with the hypothesis that hyperactive Vps34-EDC leads to increases in both Snx4- and retromer-dependent retrograde transport of Atg27.

We tested whether deletion of the retromer subunit VPS35 suppresses the increased Atg27-2xGFP localization to the Golgi caused by Vps34-EDC. Consistent with the retromer being required for accelerated retrograde transport of Atg27, in *vps35*Δ cells, there was no difference in Atg27-2xGFP localization to the Golgi between wild-type Vps34 and Vps34-EDC (Figure 24B and 24C). However, surprisingly, *vps35*Δ cells exhibited increased localization of Atg27-2xGFP to the Golgi compared to wild-type cells. This result was unexpected since a previous study reported that Atg27 accumulates on endosomes in *vps35*Δ cells with less Atg27 on Golgi (Suzuki and Emr, 2018), which fits with the view that the retromer functions in retrograde traffic of proteins from endosomes to the Golgi. However, this previous study is complicated by the fact that experiments were performed following an hour of treatment with rapamycin. Because rapamycin inhibits protein synthesis in yeast (Barbet et al., 1996), we reasoned that rapamycin treatment may have masked a defect in AP-3-dependent anterograde delivery of Atg27 to the vacuole, leading to accumulation of Atg27 in the Golgi. However,

deletion of *VPS35* does not appear to affect AP-3 function, as another AP-3 client protein Yck3 is delivered to the vacuole in *vps35*Δ cells (Figure 24D). Thus, under basal conditions, trafficking of Atg27 in *vps35*Δ cells is more complex than previously appreciated. Together, these results suggest that in yeast, elevating PtdIns3P drives retrograde transport from the vacuole, and leaves open the possibility that retrograde traffic from endosomes to the Golgi is accelerated as well.

Figure 23: Hyperactive Vps34 increases retrograde transport of Atg27

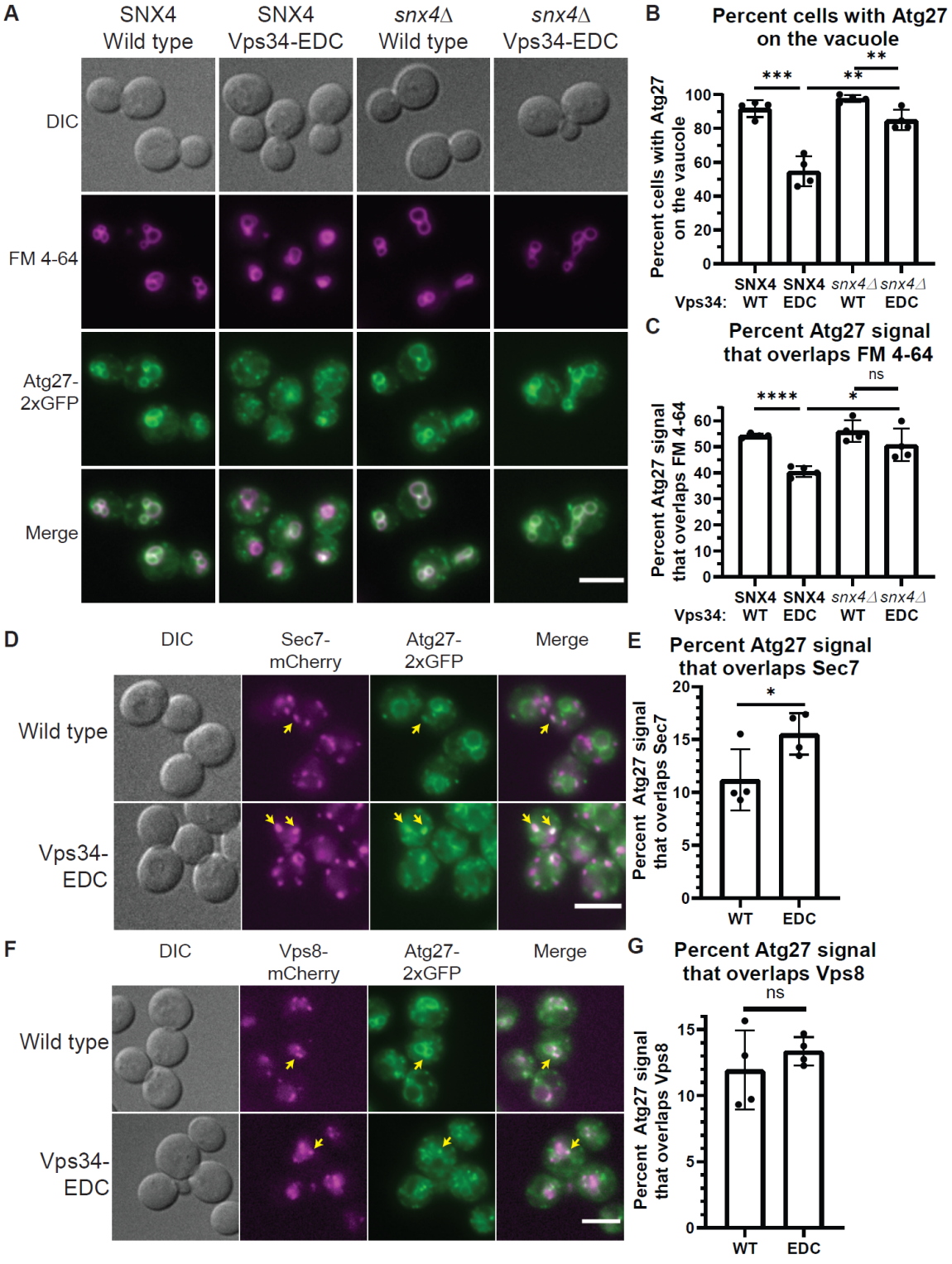

Figure 23. Hyperactive Vps34 increases retrograde transport of Atg27.

A-C) Hyperactive Vps34-EDC results in fewer cells that contain Atg27-2xGFP on the vacuole (FM 4-64, magenta) (B) and in less total Atg27-2xGFP colocalization with FM 4-64 (C). Deletion of *SNX4* results in the retention of Atg27-2xGFP on the vacuole. *vps34*Δ or *vps34*Δ *snx4*Δ cells with Atg27-2xGFP integrated at the endogenous locus were transformed with pRS416-Vps34 or pRS416-Vps34-EDC. After labeling with FM 4-64, cells were chased at 24°C for 3 h before imaging. DIC, differential interference contrast. Scale bar: 5 μm. Cells were scored as either having Atg27-2xGFP visible on the vacuole (colocalization with FM 4-64) or present only in puncta. The scorer was blinded to the genotype of the cells being quantified (B). To measure Atg27-2xGFP localization on a population basis, the Atg27-2xGFP signal that overlaps FM 4-64 was divided by total Atg27-2xGFP signal (C). Quantification of at least 40 cells per n, n=4. Error bars indicate standard deviation. Unpaired t-test. ns=p>.05, *=p<.05, **=p<.01, ***=p<.001, ****=p<.0001.

D and E) Atg27-2xGFP partially colocalizes with the trans-Golgi (Sec7-mCherry). This colocalization increases in the presence of hyperactive Vps34-EDC. *vps34*Δ cells with Atg27-2xGFP and Sec7-mCherry integrated at the endogenous loci were transformed with pRS416-Vps34 or pRS416-Vps34-EDC. DIC, differential interference contrast. Scale bar: 5 μm. Examples of Atg27-2xGFP puncta that colocalize with Sec7-mCherry are indicated by yellow arrows. The Atg27-2xGFP signal that overlaps Sec7-mCherry was divided by total Atg27-2xGFP signal. Quantification of at least 40 cells per n, n=4. Error bars indicate standard deviation. Unpaired t-test. *=p<.05.

F and G) Atg27-2xGFP partially colocalizes with endosomes (Vps8-mCherry). This colocalization is not statistically different for hyperactive Vps34-EDC compared to wild type. *vps34*Δ cells with Atg27-2xGFP and Vps8-mCherry integrated at the endogenous loci were transformed with pRS416-Vps34 or pRS416-Vps34-EDC. DIC, differential interference contrast. Scale bar: 5 μm. Examples of Atg27-2xGFP puncta that colocalize with Vps8-mCherry are indicated by yellow arrows. The Atg27-2xGFP signal that overlaps Vps8-mCherry was divided by total Atg27-2xGFP signal. Quantification of at least 40 cells per n, n=4. Error bars indicate standard deviation. Unpaired t-test. ns=p>.05.

Figure 24: Hyperactive Vps34 increases retrograde transport of Atg27

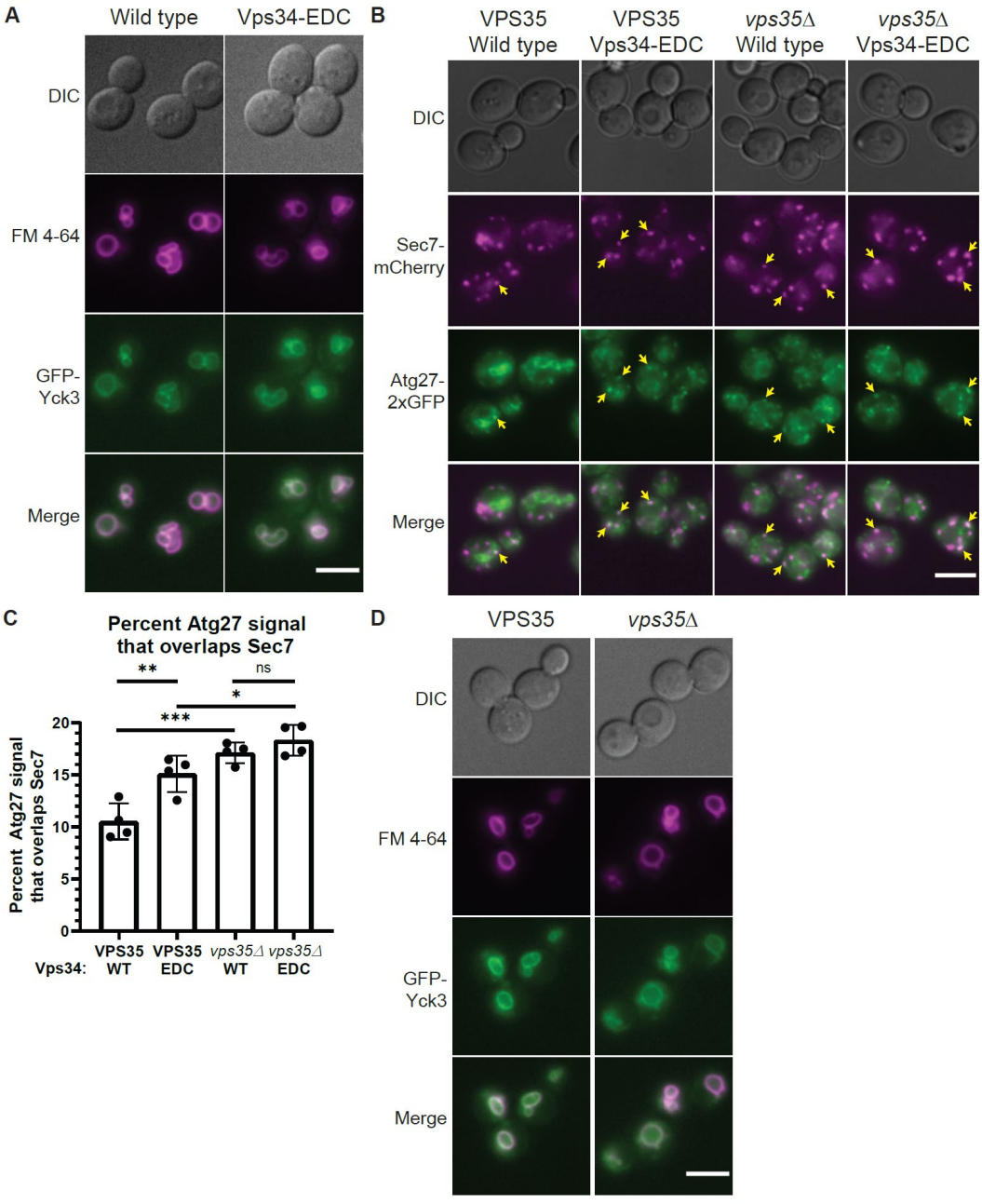

Figure 24. Hyperactive Vps34 increases retrograde transport of Atg27.

A) Hyperactive Vps34-EDC does not change the localization of the GFP-Yck3 kinase, an AP-3 client protein localized to the vacuole membrane. *vps34*Δ cells were co-transformed with pRS413-Vps34 or pRS413-Vps34-EDC and pRS416-GFP-Yck3. After labeling with FM 4-64, cells were chased at 24°C for 3 h before imaging. DIC, differential interference contrast. Scale bar: 5 μm. At least 40 cells per n, n=3.

B and C) Atg27-2xGFP partially colocalizes with the trans-Golgi (Sec7-mCherry). This colocalization increases in the presence of hyperactive Vps34-EDC. In the absence of *VPS35*, Atg27-2xGFP colocalization with the trans-Golgi is unchanged between wild type and Vps34-EDC. *vps34*Δ or *vps34*Δ *vps35*Δ cells with Atg27-2xGFP and Sec7-mCherry integrated at the endogenous loci were transformed with pRS416-Vps34 or pRS416-Vps34-EDC. DIC, differential interference contrast. Scale bar: 5 μm. Examples of Atg27-2xGFP puncta that colocalize with Sec7-mCherry are indicated by yellow arrows. The Atg27-2xGFP signal that overlaps Sec7-mCherry was divided by total Atg27-2xGFP signal. Quantification of at least 40 cells per n, n=4. Error bars indicate standard deviation. Unpaired t-test. ns=p>.05, *=p<.05, **=p<.01, ***=p<.001.

D) Deletion of *VPS35* does not change the localization of the GFP-Yck3 kinase, an AP-3 client protein localized to the vacuole membrane. Wild-type or *vps35*Δ cells were transformed with pRS416-GFP-Yck3. After labeling with FM 4-64, cells were chased at 24°C for 3 h before imaging. DIC, differential interference contrast. Scale bar: 5 μm. At least 40 cells per n, n=4. Related to Figure 23.

3.2.3 Hyperactive Vps34 does not affect ESCRT-dependent degradation of amino acid transporters Ypq1 or Mup1

ESCRT function is regulated by PI3P and plays a crucial role in trafficking select transmembrane proteins to the vacuole for degradation, including the vacuolar cationic amino acid transporter Ypq1 (Li et al., 2015; Zhu et al., 2017). Following withdrawal of lysine, Ypq1 is ubiquitinated and internalized inside the vacuole by the ESCRT machinery where it is degraded.

Using western blot analysis, we tested whether hyperactive Vps34-EDC accelerates ESCRT-dependent degradation of Ypq1 following withdrawal of lysine by measuring Ypq1-GFP levels normalized to Vph1. We found that degradation of Ypq1-GFP was not affected by Vps34-EDC (Figure 25A and 25B), suggesting that elevating PI3P does not affect ESCRT function in the degradation of Ypq1.

We also tested a second ESCRT substrate, the plasma membrane methionine transporter Mup1 (Teis et al., 2008). Mup1 accumulates on the plasma membrane when cells are starved for methionine. When methionine is reintroduced to cells, Mup1 is ubiquitinated, endocytosed, delivered to endosomes, and internalized by ESCRT into multi-vesicular bodies, which then fuse with the vacuole where Mup1 is degraded (Menant et al., 2006; Teis et al., 2008). Thus, to test ESCRT function, we measured Mup1-GFP levels normalized to Pgk1 following re-addition of methionine.

Similar to what was observed with Ypq1, there were no statistically significant differences in the rate of Mup1 degradation between wild-type and hyperactive Vps34-EDC following re-addition of methionine (Figure 25C and 25D). The half-life of Mup1-GFP

following re-addition of methionine was calculated to be 33.7 min (SEM 2.39 min) with wild-type Vps34, and 30.8 min (SEM 2.61 min) with Vps34-EDC. This experiment indicates that elevating PtdIns3P does not affect ESCRT function in the degradation of Mup1. Overall, in contrast to the retrograde transport of Atg27, elevating PtdIns3P does not accelerate ESCRT function on the vacuole or endosomes, demonstrating that elevating PtdIns3P does not always increase the overall rate of a complex pathway.

Figure 25: Hyperactive Vps34 does not affect ESCRT-dependent degradation of amino acid transporters Ypq1 or Mup1

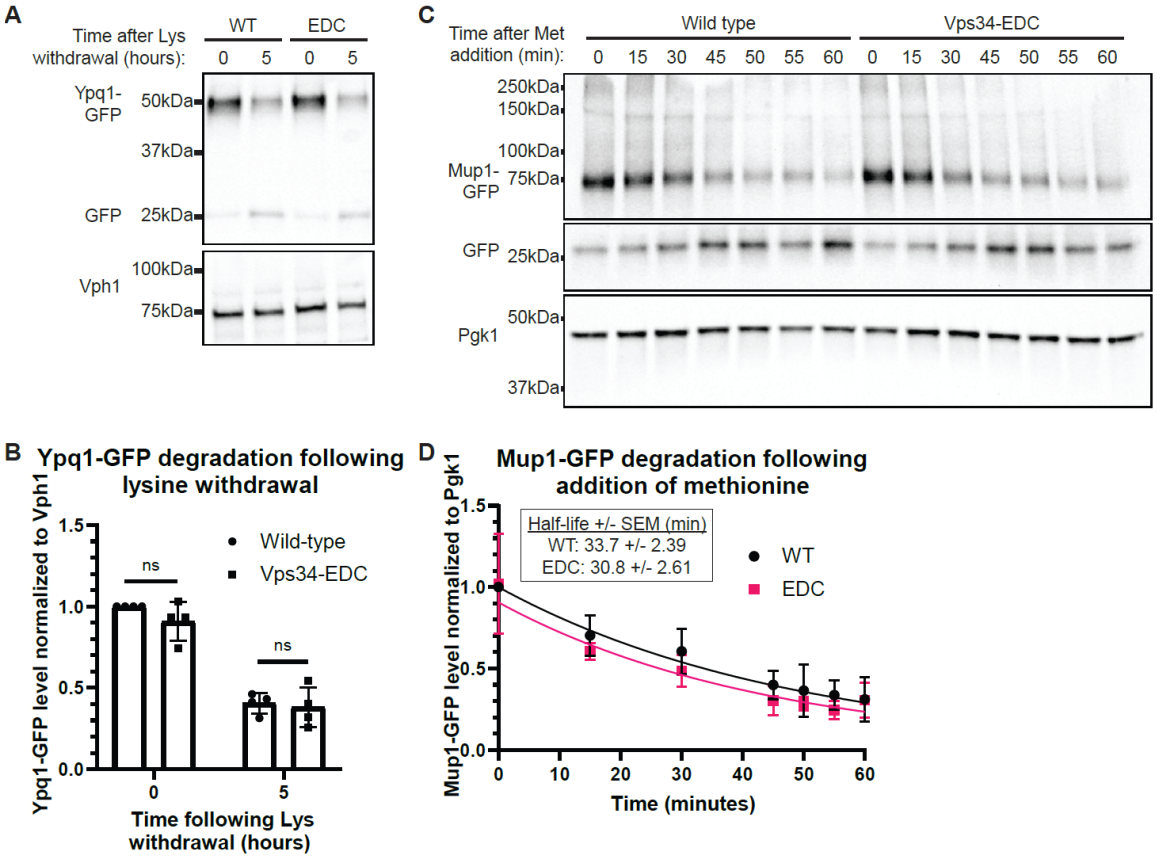

<u>Figure 25.</u> Hyperactive Vps34 does not affect ESCRT-dependent degradation of amino acid transporters Ypq1 or Mup1.

A and B) ESCRT-dependent internalization of Ypq1-GFP following the withdrawal of lysine is not statistically significantly different for hyperactive Vps34-EDC compared to wild type. *vps34Δ* cells were transformed with pRS416-Vps34 or pRS416-Vps34-EDC and pRS414-Ypq1-GFP. To induce Ypq1-GFP internalization, cells were transferred to media lacking lysine. Samples were collected at 0 and 5 h following lysine withdrawal. Ypq1-GFP protein levels were analyzed via western blot using anti-GFP antibody and were normalized to Vph1. Levels were then normalized to wild type at the zero timepoint. Representative of n=4. Error bars indicate standard deviation. Unpaired t-test. ns=p>.05.

C and D) ESCRT-dependent internalization of Mup1-GFP following the addition of methionine is not statistically significantly different for hyperactive Vps34-EDC compared to wild type. *vps34*Δ cells were transformed with pRS416-Vps34 or pRS416-Vps34-EDC and pRS414-Mup1-GFP. Cells were grown in media lacking methionine. To induce Mup1-GFP internalization, cells were transferred to media containing methionine. Samples were collected at the indicated time points following methionine addition. Mup1-GFP protein levels were analyzed via western blot using anti-GFP antibody, and normalized to Pgk1. Levels were then normalized to wild type at the zero timepoint. Representative of n=4. Error bars indicate standard deviation. The degradation rate of Mup1-GFP was determined using a linear mixed effects model. The logarithmic transformation of Mup1-GFP levels was modelled as a linear function of time and allowed to vary by genotype. Replicate-specific intercepts were included to account for residual correlation between protein levels within the same replicate. The difference in degradation rates between genotypes was not statistically significant (a 95% confidence interval of the genotype

by time interaction contained 0). The equation generated by the linear mixed effects model is plotted (D). The half-life of Mup1-GFP following re-addition of methionine was calculated to be 33.7 min (SEM 2.39 min) with wild-type Vps34, and 30.8 min (SEM 2.61 min) with Vps34-EDC.

3.2.4 Hyperactive Vps34 inhibits a late step in autophagy

PtdIns3P is involved in multiple steps of autophagy, including autophagosome biogenesis, disassembly of the autophagy machinery from the surface of mature autophagosomes, and the fusion of mature autophagosomes with the vacuole. As part of our analysis, we investigated each of these steps. A combination of autophagy induction and flux was assessed by determining the levels of lipidated Atg8 (Atg8–PE) (Klionsky et al., 2016). Atg8 (LC3 and GABARAP subfamilies in mammals) is a ubiquitin-like protein. The expression of ATG8 is strongly induced after autophagy induction, following which Atg8 is conjugated to phosphatidylethanolamine (PE), on the phagophore membrane. (Ichimura et al., 2000). Following phagophore expansion and closure, and before autophagosome-vacuole fusion, Atg8–PE on the cytoplasmic surface of the resulting autophagosome is cleaved from the membrane. The lumenal surface of the autophagosome however contains of Atg8–PE that is trapped within the autophagosome. This pool of Atg8–PE can be monitored as autophagic cargo since following fusion with the vacuole, this pool of Atg8–PE is degraded in the vacuolar lumen. Consequently, the steady-state level of Atg8–PE after autophagy induction is a function of both its generation and its degradation in the vacuole.

Treating cells with the serine protease inhibitor PMSF blocks the vacuolar degradation of Atg8–PE, facilitating the measurement of autophagy induction independent of Atg8–PE turnover. Following 1 hour of autophagy stimulation by nitrogen starvation, no difference in Atg8–PE levels could be detected between strains expressing Vps34-WT and Vps34-EDC in the presence of PMSF (Figure 26A and 26B). suggesting that the extent of autophagy induction was unchanged by hyperactive Vps34-EDC. Similarly, in the presence of PMSF, no difference in Atg8–PE levels could be detected between strains expressing Vps34-WT and Vps34-EDC at

either 15- or 30-min following nitrogen starvation (Figure 26C and 26D). These results suggest that autophagy initiation requires but is not driven by PtdIns3P.

As a second independent measure of the induction of autophagy, we investigated the transcriptional upregulation of critical autophagy genes, *ATG1*, *ATG7*, and *ATG9*, whose expression is elevated during nitrogen starvation (Delorme-Axford and Klionsky, 2018). We found no differences in mRNA levels between Vps34-WT and Vps34-EDC following 30 min of nitrogen starvation (Figure 27A), suggesting that hyperactive Vps34 does not affect the transcription of autophagy genes.

While the levels of Atg8–PE are very similar between Vps34-WT and Vps34-EDC following starvation in the presence of PMSF, comparing Atg8–PE levels in the absence of PMSF reveals that Vps34-EDC partially blocks autophagy flux autophagy. In the absence of PMSF, degradation of Atg8–PE can occur following autophagy flux. In the absence of PMSF, following 1 h of nitrogen starvation Atg8–PE protein levels were markedly lower in Vps34-WT compared to Vps34-EDC (Figure 26A and 26B). The observation that no difference in Atg8–PE levels were detected between Vps34-WT and Vps34-EDC in the presence of PMSF, but Atg8–PE is lower in Vps34-WT in the absence of PMSF, indicates that hyperactive Vps34 partially inhibits vacuolar delivery and degradation of Atg8-PE.

To further characterize the defect in a late step of autophagy, we examined the dynamics of autophagosome biogenesis using GFP-tagged Atg8 as a marker. Hyperactive Vps34-EDC results in an increased number of GFP-Atg8 puncta in cells following 30 min of nitrogen starvation (Figure 27B and 27C). This result is consistent with either an increase in the induction of autophagy and/or with the inhibition of a late step in autophagy. Using time-lapse microscopy of GFP-Atg8 puncta, we measured the lifetime of GFP-Atg8 puncta in strains expressing either

Vps34-WT or Vps34-EDC. GFP-Atg8 puncta in the presence of Vps34-WT persisted for 9 min, consistent with previous studies (Cebollero et al., 2012). In contrast, GFP-Atg8 puncta in the presence of Vps34-EDC persisted for 13.5 min (Figure 26E and 26F). These results suggest that the resolution of autophagosomes is delayed by hyperactive Vps34. Further evidence of this inhibition is observed by measuring the degradation of GFP-Atg8 via the appearance of proteolytically resistant free GFP by immunoblot analysis. Expression of hyperactive Vps34-EDC resulted in a reduction in the appearance of free GFP following 1 and 2 h of nitrogen starvation (Figure 28A and 28B), indicating a reduction in autophagy flux.

To explore whether yet higher elevation of PtdIns3P levels would further reduce autophagy flux, we enhanced the elevation of PtdIns3P by combining the Vps34-EDC mutant with a knockout of the gene encoding the putative PtdIns3P phosphatase Ymr1. We found that the Vps34-EDC *ymr1*Δ mutant elevated PI3P by 105%, compared to 53% by Vps34-EDC alone and 28% by a *ymr1*Δ mutant alone (Figure 28C). Deletion of *YMR1* in our strain background more robustly elevated PtdIns3P levels than previously reported (Parrish et al., 2004) and the increase in PtdIns3P levels caused by *ymr1* deletion was more evident in the presence of Vps34-EDC. Notably, the double Vps34-EDC *ymr1*Δ mutant inhibited autophagy flux considerably more than either mutation alone as measured by degradation of GFP-Atg8 by immunoblot analysis (Figure 28A and 28B). These results strongly indicate an inverse correlation between autophagy flux and an increase in cellular PtdIns3P. Furthermore, the turnover of PtdIns3P on autophagosomes may be critical for the successful completion of a late step in autophagy.

Prior to the fusion of mature autophagosomes with the vacuole, some autophagy proteins, including the PtdIns3P-binding protein Atg18, must be removed from the autophagosome surface (Cebollero et al., 2012). Removal of proteins from the surface of autophagosomes likely

requires depletion of PtdIns3P via the PtdIns3P phosphatase Ymr1 (Cebollero et al., 2012). Additionally, in vitro studies suggest that PtdIns3P is required for the fusion of the autophagosome with the vacuole (Bas et al., 2018). Thus, we tested whether the expression of hyperactive Vps34-EDC had an impact on the displacement of Atg18 from the autophagosome surface and/or the fusion of autophagosomes with the vacuole.

To specifically test displacement of Atg18 from the autophagosome surface independent of autophagosome-vacuole fusion, we blocked autophagosome-vacuole fusion by deleting the gene encoding the vacuolar t-SNARE Vam3 (Cebollero et al., 2012). We assessed the disassembly of Atg18 after 1 h of nitrogen starvation, by determining the percentage of GFP-Atg8-positive autophagosomes that no longer colocalized with surface Atg18-RFP. In *vam3*Δ cells, hyperactive Vps34-EDC leads to a 10% increase in the percentage of GFP-Atg8 puncta that colocalize with Atg18-RFP (Figure 28D and 28E). This result suggests that hyperactive Vps34-EDC leads to a defect in the dissociation of autophagy proteins from mature autophagosomes.

We also tested whether there was a defect in autophagosome fusion with the vacuole in a strain with wild-type Vam3. After 1 h of nitrogen starvation, we measured the percentage of GFP-Atg8-positive autophagosomes that colocalize with Atg18-RFP. In this experiment, both disassembly of Atg18-RFP from the autophagosome surface and autophagosome-vacuole fusion can occur. A defect in autophagosome-vacuole fusion will result in the persistence of GFP-Atg8 puncta that do not colocalize with Atg18-RFP and thus a decrease in the colocalization between GFP-Atg8 and Atg18-RFP. Indeed, we found that hyperactive Vps34-EDC caused a 9% decrease in the percentage of GFP-Atg8 puncta that colocalize with Atg18-RFP (Figure 28D and 28E). Note that the 10% defect in disassembly of Atg18-RFP from autophagosomes that was observed

in the *vam3*Δ cells likely also occurs in the wild-type *VAM3* strain. Thus, this result suggests that Vps34-EDC leads to approximately a 20% defect in fusion of autophagosomes with the vacuole. Additionally, the total number of GFP-Atg8 puncta observed in *vam3*Δ cells did not change between wild type and hyperactive Vps34-EDC (Figure 27D). Since autophagosomes are not turned over in *vam3*Δ cells, this result provides further evidence that hyperactive Vps34-EDC does not affect the induction of autophagy, indicating that differences in autophagy induction are not responsible for changes in the colocalization of GFP-Atg8 and Atg18-RFP. Note that Atg18 protein levels were not different between wild type and Vps34-EDC under nutrient rich conditions or following nitrogen starvation (Figure 27E and 27F).

Together, our results suggest that while hyperactive Vps34-EDC has no effect on the induction of autophagy, it results in a decrease in autophagic flux in part via defects in both disassembly of the autophagy machinery from the surface of mature autophagosomes and fusion of autophagosomes with the vacuole. However, the 10% defect in disassembly of autophagy proteins from autophagosomes and the 20% defect in autophagosome-vacuole fusion do not fully account for the observed defect in autophagic flux. Autophagic flux, as measured by Atg8–PE levels or lifetime of Atg8 puncta, or degradation of GFP-Atg8 indicated a defect in the range of 50-70%. Thus, there are likely additional steps in the resolution of autophagy that are affected by hyperactive Vps34-EDC. Interestingly, despite inhibiting autophagy, hyperactive Vps34-EDC does not affect the survival of yeast cells during long-term nitrogen starvation (Figure 27G), which suggests that Vps34-EDC cells maintain sufficient levels of autophagy function to allow for survival during chronic nitrogen starvation.

The finding that hyperactive Vps34-EDC causes a partial defect in autophagosome fusion with the vacuole, raises the possibility that there is a more global defect in fusion to the vacuole. A defect in vacuole-vacuole fusion would result in a more fragmented vacuole morphology. To assess homotypic vacuole fusion, we counted the number of vacuole lobes per cell, finding a small but significant 12% increase in vacuole lobes (Figure 29A and 29B). This difference was predominantly due to an approximately 40% decrease in the number of cells with a single vacuole (Figure 29C). While an increase in the number of vacuole lobes per cell could also be caused by an increase in vacuole fission, a modest impairment of fusion fits closely with the observed defect in autophagosome fusion with the vacuole.

Figure 26: Hyperactive Vps34 inhibits a late step in autophagy

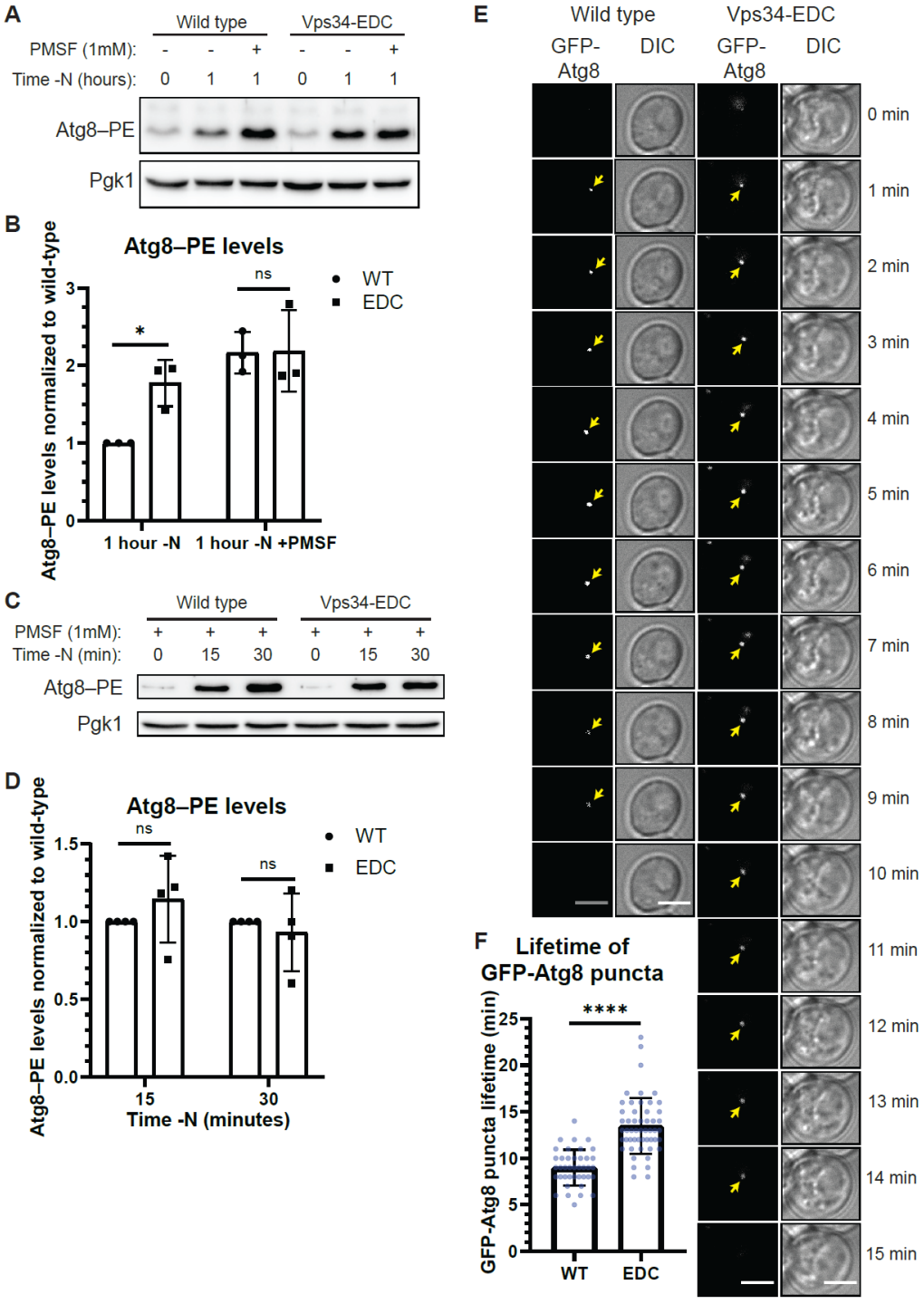

Figure 26. Hyperactive Vps34 inhibits a late step in autophagy.

A and B) Comparison of Atg8–PE protein levels in the absence and presence of PMSF, a protease inhibitor, suggests that Vps34-EDC inhibits a late step in autophagy, but does not change the rate of autophagy induction. During autophagy, the levels of Atg8–PE are determined by both covalent attachment of phosphatidylethanolamine (PE) to Atg8 and by degradation of Atg8–PE once autophagosomes fuse with the vacuole. When degradation of Atg8–PE is inhibited by the serine protease inhibitor, PMSF, there was no difference in Atg8–PE levels in Vps34-WT compared to Vps34-EDC, suggesting that autophagy induction is unchanged by Vps34-EDC. However, in the absence of PMSF, Atg8–PE protein levels are elevated by hyperactive Vps34-EDC following 1 hour of nitrogen starvation, suggesting that Vps34-EDC inhibits a late step in autophagy. *Vps34*Δ cells were transformed with pRS416-Vps34 or pRS416-Vps34-EDC. Atg8–PE protein levels were analyzed via western blot using anti-Atg8 antibody. Atg8–PE levels were normalized to Pgk1. Levels were further normalized to wild type at 1 h nitrogen starvation. Representative of n=3. Error bars indicate standard deviation. Unpaired t-test. Ns=p>.05, *=p<.05.

C and D) Following 15 and 30 min of nitrogen starvation, Atg8–PE protein levels are unchanged between hyperactive Vps34-EDC and wild type when degradation of Atg8–PE is inhibited by the protease inhibitor, PMSF. This result suggests that Vps34-EDC does not affect autophagy induction. *Vps34*Δ cells were transformed with pRS416-Vps34 or pRS416-Vps34-EDC. Atg8–PE protein levels were analyzed via western blot using anti-Atg8 antibody. Atg8–PE levels were normalized to Pgk1. Levels were further normalized to wild type at 15 and 30 min following

nitrogen starvation. Representative of n=4. Error bars indicate standard deviation. Unpaired t-test. Ns=p>.05.

E and F) Hyperactive Vps34-EDC results in an increase in the lifetime of GFP-Atg8 puncta in cells. *Vps34*Δ cells were co-transformed with pRS414-GFP-Atg8 and pRS416-Vps34 or pRS416-Vps34-EDC. Cells were imaged every min for 26 min following 30 min of nitrogen starvation. 20 z-slices that were 0.2 µm apart were acquired at each time point. Single z-slice. DIC, differential interference contrast. Scale bar: 3.5 µm. GFP-Atg8 puncta were tracked over time with the lifetime of each punctum calculated as the time between the first and last frames the puncta were visible. Only GFP-Atg8 puncta that could be followed unambiguously over their lifetime were analyzed. For wild type, n=40. For Vps34-EDC, n=52. Error bars indicate standard deviation. Unpaired t-test. ****=p<.0001.

Figure 27: Hyperactive Vps34 inhibits a late step in autophagy

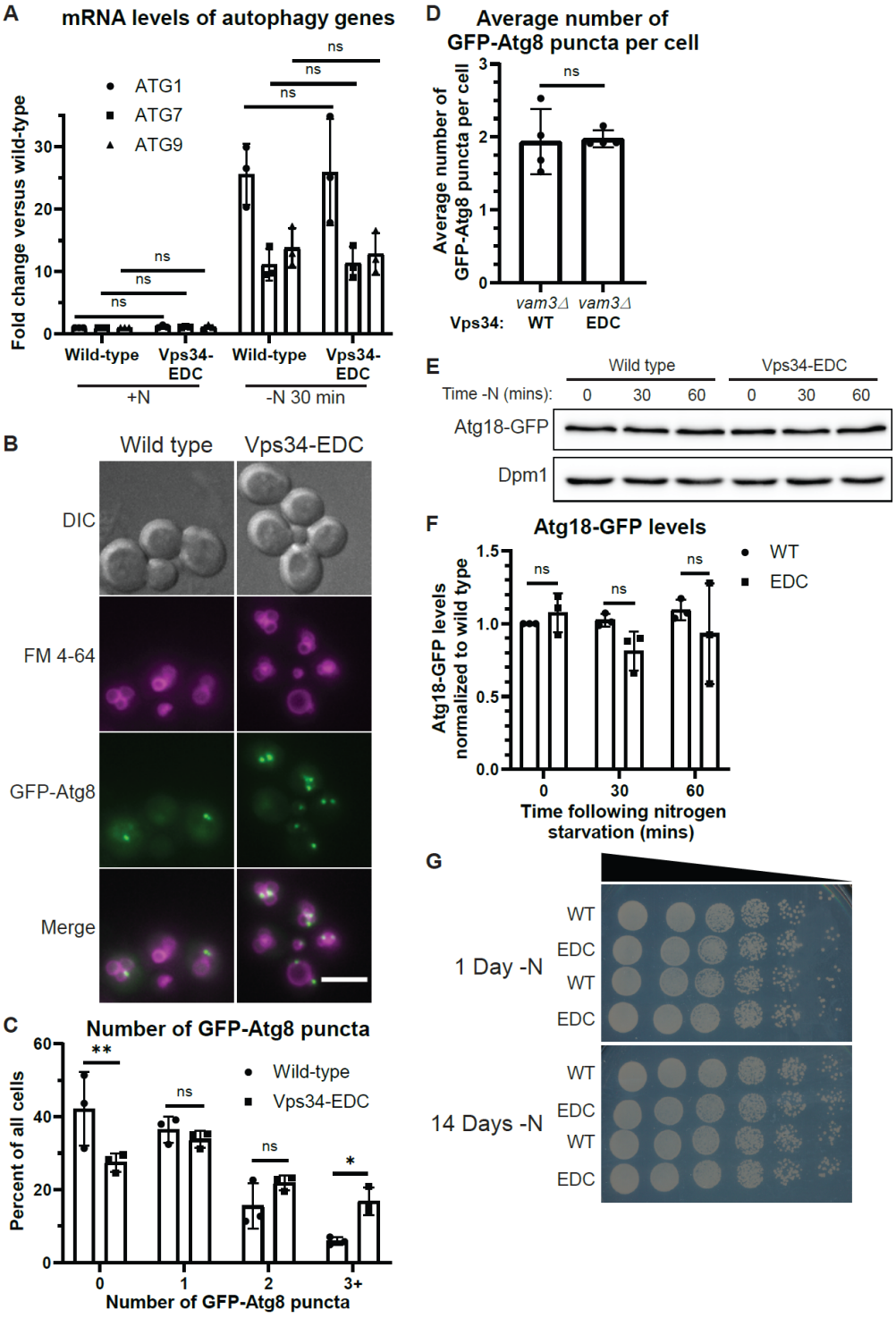

Figure 27. Hyperactive Vps34 inhibits a late step in autophagy.

A) mRNA levels of *ATG1*, *ATG7*, and ATG9 *are* unchanged between Vps34-EDC and wild type, suggesting that Vps34-EDC does not affect the transcription of select autophagy genes. *vps34*Δ cells were transformed with pRS416-Vps34 or pRS416-Vps34-EDC. *ATG1*, *ATG7*, and *ATG9* mRNA transcript levels were measured by qRT-PCR in nitrogen rich conditions and following 30 min of nitrogen starvation. mRNA levels were normalized to wild type in nitrogen rich conditions. n=3. Error bars indicate standard deviation. Unpaired t-test. ns=p>.05.

B and C) Hyperactive Vps34-EDC results in an increase in the number of GFP-Atg8 puncta in cells following 30 min of nitrogen starvation. *vps34*Δ cells were co-transformed with pRS414-GFP-Atg8 and pRS416-Vps34 or pRS416-Vps34-EDC. After labeling with FM 4-64, cells were chased at 24°C for 3 h before 9 z-slices that were 0.2 µm apart were imaged. Maximum intensity projection. DIC, differential interference contrast. Scale bar: 5 µm. GFP-Atg8 puncta were counted by a scorer who was blinded to the genotype of the cells being quantified. Quantification of at least 100 cells per n, n=3. Error bars indicate standard deviation. Two-way ANOVA and Dunnett's post-hoc test. ns=p>.05, *=p<.05, **=p<.01.

D) Hyperactive Vps34-EDC does not cause an increase in the number of GFP-Atg8 puncta in *ymr1*Δ cells after an hour of nitrogen starvation. This experiment is an alternative quantification of the experiment performed in Figure 5D and E. *vps34*Δ *vam3*Δ cells with Atg18-RFP integrated at the endogenous locus were transformed with pRS413-GFP-Atg8 and pRS416-Vps34 or pRS416-Vps34-EDC. GFP-Atg8 puncta were counted by a scorer who was blinded to the genotype of the cells being quantified. Cells without visible Atg18-RFP were excluded from

quantification. Quantification of 100 cells per n, n=4. Error bars indicate standard deviation. Unpaired t-test. ns=p>.05.

E and F) Vps34-EDC does not change Atg18-GFP protein levels at basal conditions or during nitrogen starvation. *vps34*Δ cells were co-transformed with pRS413-Vps34 or pRS413-Vps34-EDC and pRS416-Atg18-GFP. Atg18-GFP protein levels were analyzed via western blot using anti-GFP antibody. Atg18-GFP levels were normalized to Dpm1. Levels were then normalized to wild type at basal conditions. Representative of n=3. Error bars indicate standard deviation. Unpaired t-test. ns=p>.05.

G) Hyperactive Vps34-EDC does not affect the survival of yeast cells during long-term nitrogen starvation. *vps34*Δ cells were transformed with pRS416-Vps34 or pRS416-Vps34-EDC and grown to mid-log phase in SC media. Equal numbers of cells were collected and rinsed twice in nitrogen starvation media before resuspending in nitrogen starvation media. Following 1 day and 14 days of nitrogen starvation, equal volumes of culture were serially diluted 1:5 and spotted on SC plates. Plates were imaged following 3 days of yeast growth. 2 representative samples of n=4. Related to Figure 26 and 28.

Figure 28: Hyperactive Vps34 inhibits a late step in autophagy

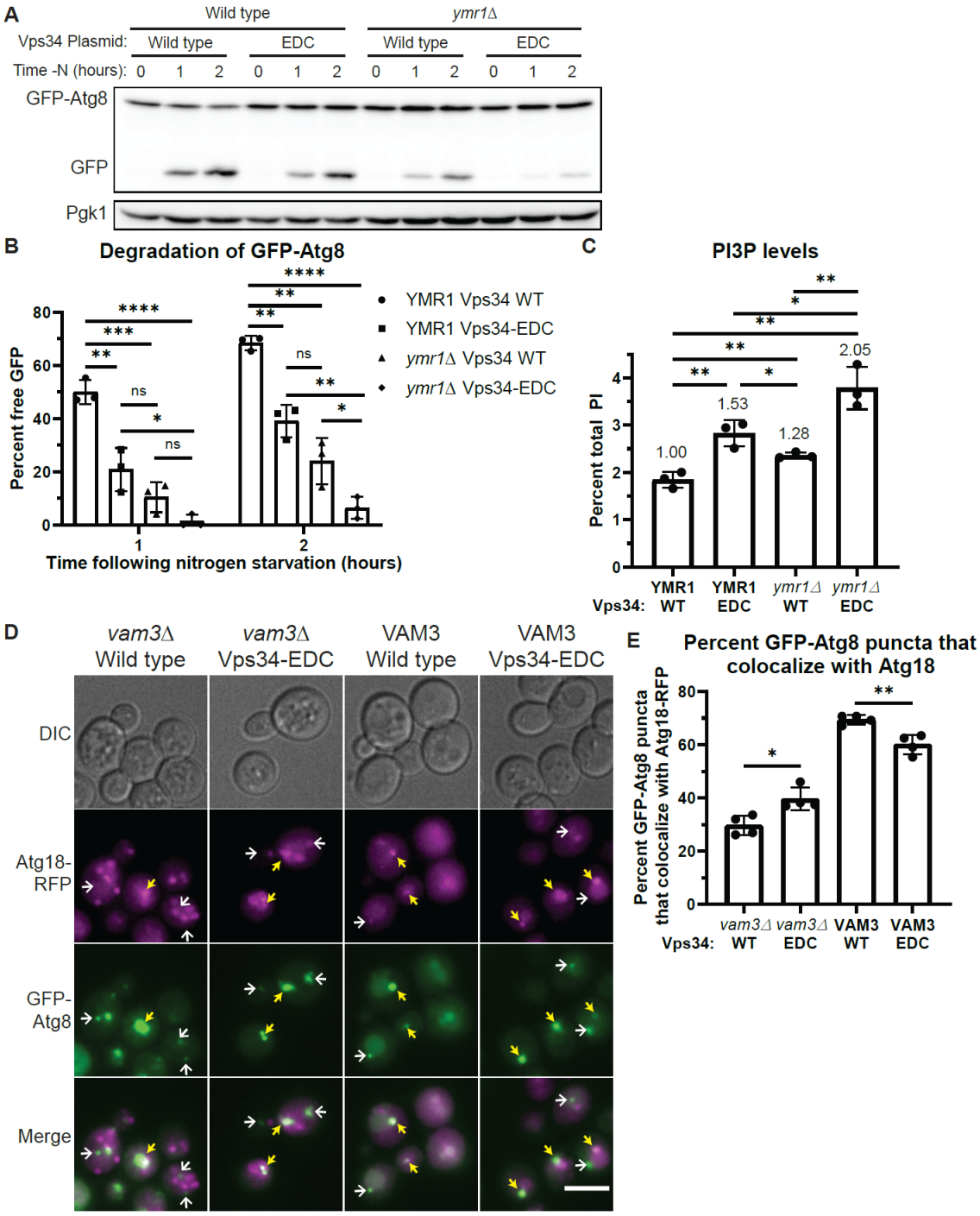

Figure 28. Hyperactive Vps34 inhibits a late step in autophagy.

A and B) The Vps34-EDC mutant or deletion of *YMR1* inhibits degradation of GFP-Atg8 following nitrogen starvation. Combining Vps34-EDC with a *ymr1* deletion further inhibits degradation of GFP-Atg8, indicating a block in autophagy flux. *vps34*Δ or *vps34*Δ *ymr1*Δ cells were co-transformed with pRS416-Vps34 or pRS416-Vps34-EDC and copper inducible pRS414-pCup1-GFP-Atg8. No exogenous copper was added during this experiment. GFP-Atg8 and GFP protein levels were analyzed via western blot using anti-GFP antibody. Free GFP levels were divided by the sum of GFP-Atg8 and free GFP and expressed as a percent. Representative of n=3. Error bars indicate standard deviation. Unpaired t-test. ns=p>.05, *=p<.05, **=p<.01, ***=p<.001, ****=p<.0001.

C) The Vps34-EDC mutant and deletion of the yeast myotubularin *YMR1*, elevated PI3P levels. Combining Vps34-EDC with *ymr1* deletion further elevated PI3P levels. *vps34*Δ or *vps34*Δ *ymr1*Δ cells were transformed with pRS416-Vps34 or pRS416-Vps34-EDC. PI lipid levels were measured by metabolically labeling cells with myo-^{3}H-inositol for 16 h, harvesting cells, and separating PI lipid head groups by anion exchange and HPLC. n=3. Error bars indicate standard deviation. Unpaired t-test. *=p<.05, **=p<.01.

D and E) Hyperactive Vps34-EDC leads to a defect in disassembly of the autophagy machinery from the surface of mature autophagosomes as well as a defect in fusion of autophagosomes with the vacuole. In the presence of Vam3, Vps34-EDC caused a small but statistically significant decrease in the percentage of GFP-Atg8 puncta that colocalize with Atg18-RFP after an hour of nitrogen starvation. This suggests that Vps34-EDC leads to a minor defect in fusion of autophagosomes with the vacuole. However, in *vam3*Δ cells where fusion of autophagosomes

with the vacuole is completely blocked, hyperactive Vps34-EDC leads to a small but statistically significant increase in the percentage of GFP-Atg8 puncta that colocalize with Atg18-RFP after an hour of nitrogen starvation. This result suggests that Vps34-EDC also leads to a minor defect in the dissociation of key autophagy machinery from mature autophagosomes. *vps34*Δ or *vps34*Δ *vam3*Δ cells with Atg18-RFP integrated at the endogenous locus were transformed with pRS413-GFP-Atg8 and pRS416-Vps34 or pRS416-Vps34-EDC. Cells were imaged after 1 h of nitrogen starvation. DIC, differential interference contrast. Scale bar: 5 μm. Individual GFP-Atg8 puncta were scored on whether or not they colocalized with Atg18-RFP puncta. The scorer was blinded to the genotype of the cells being quantified. Cells without visible Atg18-RFP were excluded from quantification. Examples of GFP-Atg8 puncta that colocalize with Atg18-RFP are indicated by yellow arrows. Examples of GFP-Atg8 puncta that do not colocalize with Atg18-RFP are indicated by white arrows. Quantification of 100 cells per n, n=4. Error bars indicate standard deviation. Unpaired t-test. **=p<.01, ****=p<.0001.

3.2.5 Hyperactive Vps34 does not inhibit general vacuolar fusion events

The finding that hyperactive Vps34-EDC causes a partial defect in autophagosome fusion with the vacuole, raises the possibility that there is a more global defect in fusion to the vacuole. A defect in vacuole-vacuole fusion would result in a more fragmented vacuole morphology. To assess homotypic vacuole fusion, we counted the number of vacuole lobes per cell, finding a small but significant 12% increase in vacuole lobes (Figure 29A-B). This difference was predominantly due to an approximately 40% decrease in the number of cells with a single vacuole (Figure 29C). While an increase in the number of vacuole lobes per cell could also be caused by an increase in vacuole fission, a modest impairment of fusion fits closely with the observed defect in autophagosome fusion with the vacuole.

Figure 29: Hyperactive Vps34-EDC may lead to a modest decrease in homotypic vacuole fusion

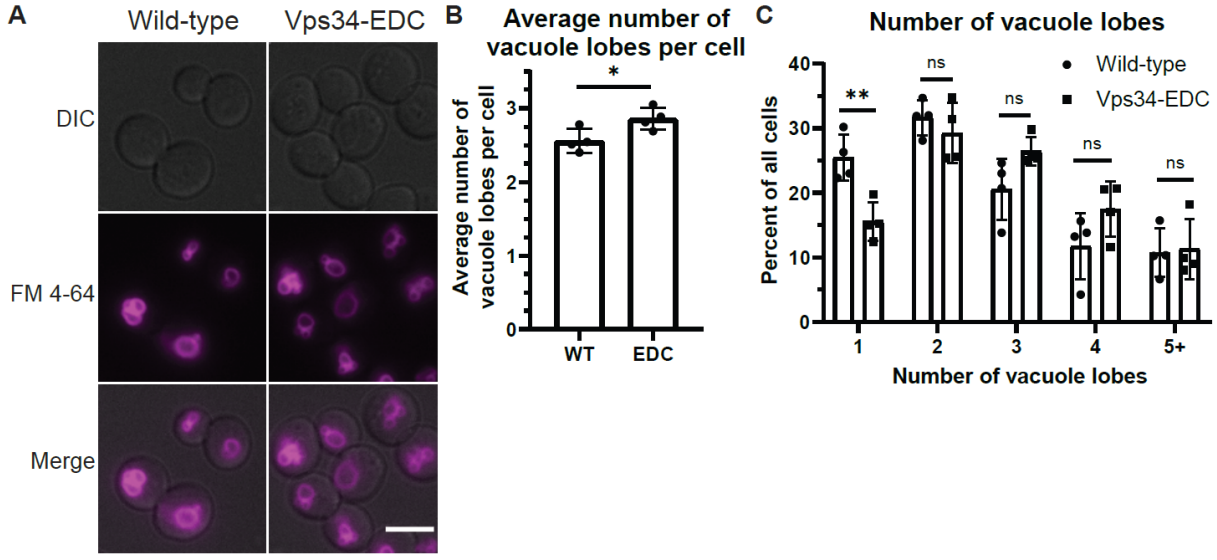

<u>Figure 29.</u> Hyperactive Vps34-EDC may lead to a modest decrease in homotypic vacuole fusion.

A-C) Hyperactive Vps34-EDC results in a 12% increase in the average number of vacuole lobes in a cell (B), which occurs primarily due to a decrease in the number of cells with 1 vacuole lobe (C). *vps34*Δ cells were transformed with pRS416-Vps34 or pRS416-Vps34-EDC. After labeling with FM 4-64, cells were chased at 24°C for 3 h before imaging. DIC, differential interference contrast. Scale bar: 5 μm. The number of vacuole lobes was counted by a scorer who was blinded to the genotype of the cells being quantified. Quantification of at least 100 cells per n, n=4. Error bars indicate standard deviation. Unpaired t-test (B). Two-way ANOVA and Dunnett's post-hoc test (C). ns=p>.05, *=p<.05, **=p<.01.

3.3 Conclusion

Most studies of PI lipids use knockdown, knockout, or drug inhibition of PI kinases to test whether a specific PI is essential for a pathway. However, this approach does not indicate whether a PI lipid is a key regulator of the pathway of interest. The ability to generate mutations that robustly elevate a PI lipid provides an effective tool to elucidate the regulatory roles of PI lipids. Previously, our lab generated hyperactive mutations in the PtdIns3P 5-kinase, Fab1, by screening for mutants that rescued Fab1 function in strains where key Fab1 activators were knocked out (Duex et al., 2006b; Lang et al., 2017). These mutants led to mechanistic insights into the regulation of Fab1 (Lang et al., 2017). In this study, instead of knocking out Vps34 regulators, we performed a screen based on rescuing growth of a hypomorphic Vps34 allele that was mutated near the active site of the enzyme. The mutants identified in this screen were concentrated near the active site of the kinase and most likely help favor an active conformation of the kinase but may not be regulatory sites on the native enzyme. These two different screening strategies appear to return mutations that provide insight into different aspects of PI kinase function and regulation. These differences should guide the design of future screens for hyperactive PI kinases. A screen that avoids crippling the active site of the kinase is more likely to yield mechanistic insights into the regulation of a PI kinase. When regulators of PI kinases are not known or when the sole goal of a hyperactive mutant is to determine downstream effects of elevating a PI lipid, a screening strategy based on a hypomorphic PI kinase allele is straightforward because catalytic site residues can be readily identified.

The major advantage of the Vps34-EDC mutant was that it enabled specific and direct testing of the downstream effects of elevating PtdIns3P. It should be noted that in these experiments, the Vps34-EDC plasmid is constitutively expressed and thus PtdIns3P is

constitutively elevated. This is in contrast with wild-type cells where stimulus-induced changes in phosphoinositides occur on the order of minutes (Duex et al., 2006a). Cells may respond differently to chronic versus acute elevation of phosphoinositides. We determined that elevation of PtdIns3P drives some pathways, including synthesis of PtdIns(3,5)P_2 during hyperosmotic shock, as well as retrograde transport of Atg27. These findings demonstrate that elevation of PtdIns3P drives some downstream processes and that in these cases, the PtdIns3P-dependent step is rate limiting. In contrast, hyperactive Vps34 does not affect ESCRT function, demonstrating that elevating PtdIns3P does not always increase the overall rate of a complex pathway. Much like ESCRT function, induction of autophagy is not accelerated by hyperactive Vps34, though, conversely, autophagic flux is lowered by hyperactive Vps34, in part by delaying disassembly of the autophagy machinery from the surface of mature autophagosomes as well as a delay in fusion of autophagosomes with the vacuole. These results provide evidence that PtdIns3P can also inhibit specific steps within a pathway. Thus, these studies suggest that stimulus-induced elevation of PtdIns3P can positively or negatively regulate some PtdIns3P-dependent membrane trafficking pathways and that phosphoinositide lipid are commonly rate-limiting in pathways where they are required. Moreover, these findings suggest that stimulus-induced elevation of PI lipids provides a way for stimuli to selectively regulate pathways.

3.4 Materials and Methods

3.4.1 Yeast strains, plasmids, and media

Yeast cultures were grown in yeast extract peptone dextrose (YEPD) containing 1% yeast extract, 2% peptone and 2% dextrose or synthetic complete (SC) media lacking the indicated amino acid(s) at 24°C unless specified. For nitrogen starvation, yeast strains were cultured in SD-N medium containing 0.19% yeast nitrogen base, 2% glucose, and vitamins and lacking

amino acids and ammonium sulfate (Formedium). Yeast strains and plasmids are listed in Tables S1 and 2, respectively.

3.4.2 Phosphoinositide lipid labeling and quantification

Yeast myo-3H-inositol labeling and total cellular phosphoinositide extraction, deacylation, and measurements were performed as described (Bonangelino et al., 2002; Duex et al., 2006a). Briefly, cells were grown in the appropriate SC media to mid-log phase, washed with SC media lacking inositol, and used to inoculate 5 mL of SC media lacking inositol and containing 50 µCi of myo-3H-inositol. Cells were grown for 16 h shaking at 24°C, harvested by centrifugation, and resuspended in 100 µL inositol-free media. For hyperosmotic shock, 100 µL of inositol-free media with 1.8 M NaCl was added to the sample for 10 min. For basal conditions, 100 µL of inositol-free media was added to the 100 µL sample. Cells were then killed via addition of ice-cold 4.5% perchloric acid. Cells were lysed using a mini-beadbeater for 2 min, then immediately put on ice for 2 min. This was repeated two more times for a total lysis time of 6 min. Cell extracts were centrifuged at 16,000 x g for 10 min at room temperature. Pellets were washed with 1 mL of 100 mM EDTA pH 8.0 then resuspended in 50 µL distilled deionized water (ddH_2O). Samples were deacylated with 1 mL methylamine reagent for 1 h at 55°C, then dried in a speed vac concentrator. Pellets were resuspended in 300 µL of ddH_2O, mixed with 300 µL of a 20:4:1 mixture of butanol/ethyl ether/formic acid ethyl ester, vortexed, and centrifuged for 2 min at 16,000 x g. The lower aqueous phase was then transferred to a fresh microcentrifuge tube. This sample extraction was repeated, and samples were dried in a speed vac concentrator. Dried samples were resuspended in 60 µL ddH_2O and analyzed by HPLC using a SAX anion exchange column. Buffer A (ddH_2O) and Buffer B (1 M $[NH_4]_2HPO_4$, pH 3.8) are used to generate the following gradients run at a 1 mL/min flow rate: 1% Buffer B for 5 min, 1–

20% Buffer B for 44 min, 20–50% Buffer B for 3.75 min, and 50% Buffer B for 8 min. To quantify scintillation counts from each sample, the raw counts in each peak were expressed as a percentage of total phosphatidylinositol-related species, calculated from summation of the counts of the five glycero-inositol peaks present in yeast (PI, PtdIns3P, PtdIns4P, PtdIns[3,5]P_2, and PtdIns[4,5]P_2). Background scintillation counts were calculated from adjacent regions and subtracted from all peaks.

3.4.3 Screen for hyperactive Vps34 mutants

Schematic of screen shown in Figure 20A. A pRS416-Vps34-K759D plasmid was gapped by digesting with XhoI restriction enzyme. The gapped plasmid was purified by agarose electrophoresis followed by DNA purification (Qiagen). Primers AM30 (5-GAATTCACTATTGTGGATGCCGTATCTTCG-3) and AM31 (5-GGGTAACGCCAGGGTTTTCC-3) were used to PCR amplify the gapped region along with approximately 100 bases upstream and downstream of the XhoI restriction sites using error-prone Taq DNA polymerase (Invitrogen). Gapped plasmid backbone and mutated PCR product were co-transformed into *vps34*Δ cells. Two days following co-transformation, colonies were replica plated to plates containing 10 nM rapamycin and grown at 33°C. From an estimated 12,000 colonies, mutant Vps34 plasmids were isolated from 59 single colonies that rescued growth on rapamycin at 33°C and amplified in E. coli. When mutant plasmids were retransformed into *vps34*Δ cells, 33 of the 59 plasmids rescued growth on rapamycin at 33°C. Sanger sequencing of those 33 plasmids revealed that 11 plasmids contained a mutation at the D759 locus. The 22 remaining independent mutants indicated 9 unique point mutations. Of those 9 mutations, changes at 5 of them elevated PtdIns3P levels.

3.4.4 Fluorescence microscopy

Yeast cells were grown in the appropriate SC media to mid-log phase. Live cell images were obtained on a DeltaVision Restoration system (Applied Precision) using an inverted epifluorescence microscope (IX-71; Olympus) with a charge-coupled device camera (Cool-SNAP HQ; Photometrics) and processed in FIJI. When vacuoles were visualized, cells were labeled with 12 μg FM 4-64 in 250 μl media for 1 h, then washed twice and grown in 5 ml fresh SC media for one doubling time (2-3 h; Vida and Emr, 1995).

3.4.5 Quantification of fluorescence microscopy images

Quantification of the number of vacuole lobes, the number of cells with Atg27-2xGFP visible on the vacuole, the number of GFP-Atg8 puncta, and the colocalization of GFP-Atg8 puncta with Atg18-RFP puncta was performed by a scorer who was blinded to the genotype of the cells being quantified. The amount of Envy-Vps34, Fab1-Envy, or Fig4-Envy that colocalized with the vacuole was measured using FIJI. Background fluorescence was subtracted using a 5.0 pixel rolling ball radius in the green channel and a 10.0 pixel rolling ball radius in the FM 4-64 channel. FM 4-64 images were thresholded such that pixels with signal present were set to 1 and pixels without signal present were set to 0 using the Otsu method. Total signal that colocalizes with the vacuole was calculated by multiplying the background subtracted green channel image by the FM 4-64 thresholded image and determining the integrated intensity of the resulting image. The total colocalized green signal was divided by the number of cells in the quantified images to give the green signal intensity on the vacuole per cell.

Colocalization of Atg27-2xGFP with FM 4-64, Sec7-mCherry, or Vps8-mCherry was measured using FIJI. Background fluorescence was subtracted using a 5.0 pixel rolling ball radius and

images were thresholded such that pixels with signal present were set to 1 and pixels without signal present were set to 0. The Otsu method was used, except for Vps8-mCherry where the Renyi Entropy method was used. Total Atg27-2xGFP signal was calculated by multiplying the background subtracted Atg27-2xGFP image by the Atg27-2xGFP thresholded image and determining the integrated intensity of the resulting image. The Atg27-2xGFP signal that colocalized with FM 4-64, Sec7-mCherry, or Vps8-mCherry was calculated by multiplying the Atg27-2xGFP thresholded image and the FM 4-64/Sec7-mCherry/Vps8-mCherry thresholded image. The resulting image was multiplied by the background subtracted Atg27-2xGFP image and integrated intensity of the resulting image was determined. Colocalized Atg27-2xGFP signal was divided by total Atg27-2xGFP signal to calculate percent overlap.

3.4.6 Western blot analysis

Yeast cells were grown in the appropriate SC media to mid-log phase. Before harvesting, cells were treated in the appropriate experiment-specific conditions. For Ypq1-GFP and Mup1-GFP degradation assays, cells were washed twice in lysine-free SC media before resuspending in lysine-free SC media or resuspended in SC media containing methionine, respectively (Zhu et al., 2017). For Atg8–PE and GFP-Atg8 assays, cells were shifted to nitrogen starvation media (-N) for autophagy induction. 1 OD of cells was harvested and 100 µL Urea lysis buffer was added (1% SDS, 8 M Urea, 10 mM Tris pH 6.8, 10 mM EDTA, 0.01% bromophenol blue, 0.2% β-mercaptoethanol, Roche complete protease inhibitor cocktail). ½ volume of 0.5 mm Zirconia glass beads were added and tubes were vortexed in a micro tube mixer for 10 min at 4°C. Supernatants were transferred to fresh tubes and samples were heated for 10 min at 75°C and run on an SDS polyacrylamide gel. Proteins were transferred to a nitrocellulose membrane at 60V for 16 h. Membranes were blocked in 5% milk before incubation with the indicated primary

antibody. Membranes were washed 3 times for 5 min in TBST, incubated in secondary antibodies, washed again, developed with ECL prime (GE Healthcare, Pgk1) or Clarity Max (Bio-Rad, other antibodies), imaged on a Bio-Rad ChemiDoc imager, and quantified using FIJI. For immunoblot analyses, the following antibodies were used: mouse anti-GFP (1:1,000; Roche), mouse anti-Myc (1:1,000; clone 9E10 EMD Millipore), mouse anti-Pgk1 (1:10,000; Invitrogen), mouse anti-Vph1 (1:1,000; Abcam), rabbit anti-Atg8 (described previously (Huang et al., 2000)), mouse anti-Dpm1 (1:5,000; ThermoFisher), mouse anti-HA (1;1,000; Covance, MMS-101P).

3.4.7 Analysis of Mup1-GFP degradation

Mup1-GFP levels were normalized to Pgk1. A linear mixed effects model was used to assess the degradation rate of Mup1-GFP. The logarithmic transformation of Mup1-GFP levels was modelled as a linear function of time and allowed to vary by genotype. Replicate-specific intercepts were included to account for residual correlation between protein levels within the same replicate. A 95% confidence interval of the genotype by time interaction was used to determine whether there were statistically significant differences between wild-type and hyperactive Vps34-EDC.

3.4.8 Hyperosmotic shock growth assay

Yeast cells were grown to mid-log phase in SC media and then diluted to equal concentrations. An equal volume of SC media or SC media with 1.8 M NaCl was added to the culture to begin the time-course. ODs were measured immediately following the addition of SC media or SC media with 1.8 M NaCl and then every 4 h for 24 h. The time zero OD measurement for each sample was normalized to 1. A natural logarithmic transformation was applied to the normalized ODs so that exponential growth is represented linearly.

3.4.9 Real-time quantitative PCR (RT-qPCR)

Yeast cells were cultured in the appropriate SC media to mid-log phase and then shifted to nitrogen starvation media (–N) for 30 min for autophagy induction. Cells were collected and flash frozen in liquid nitrogen. Total RNA was extracted using an RNA extraction kit (Clontech, Nucleo Spin RNA, 740955.250). Reverse transcription was carried out using the High-Capacity cDNA Reverse Transcription Kit (Applied Biosystems/Thermo Fisher Scientific, 4368814). For each sample, 1 μg RNA was used for cDNA synthesis. RT-qPCR was performed using the Radiant SYBR Green Lo-ROX qPCR kit (Alkali Scientific) in a CFX Connect (Bio-Rad, 1855201) real-time PCR machine. For all RT-qPCR experiments, melting curves were run after the PCR cycles to verify primer specificity. Relative gene expression was calculated using the $2^{-\Delta\Delta CT}$ method and normalized as indicated (Livak and Schmittgen, 2001).

3.4.10 Nitrogen starvation survival assay

Yeast cells were grown to mid-log phase in SC media. Equal numbers of cells were collected and rinsed twice in nitrogen starvation media before resuspending in nitrogen starvation media. Following 1 day and 14 days of nitrogen starvation, equal volumes of culture were serially diluted 1:5 and spotted on SC plates. Plates were imaged following 3 days of yeast growth.

3.5 Acknowledgements

We thank members of the Weisman and Klionsky laboratories for their insightful discussions. We thank Dr. Christopher Burd for the Atg27-2xGFP strain used to make yeast strains LWY19264, LWY19252, LWY19306, LWY19358, LWY19518, and LWY19521. We thank Dr. Ajit Joglekar for discussions of quantification of Atg27-2xGFP colocalization. We thank Dr. Ming Li for pRS416-Ypq1-GFP used to make pRS414-Ypq1-GFP. We thank Dr. Mara Duncan for pRS416-Mup1-GFP used to make pRS414-Mup1-GFP. We thank Joseph Dickens of Consulting for Statistics, Computing, and Analytics Research at the University of Michigan for his help performing statistical analysis on the degradation of Mup1-GFP. We thank Dr. Fulvio Reggiori for pRS416-Atg18-GFP.

This work was supported by NIH Grant R01-NS099340 and R01-GM062261 (to LSW), GM131919 (to DJK), mCubed 3.0, University of Michigan (to LSW), and an LSI Cubed Collaborative Grant from the Life Sciences Institute, University of Michigan (to NS and VL). NS was supported in part by NIGMS Grant T32-GM007315 and a Rackham Warner Lambert Fellowship from the Program in Cellular and Molecular Biology, University of Michigan.

3.6 Tables

Table 5. Yeast strains used in this study

Strain	Genotype	Source
LWY13700	*MATa, leu2,3-112, ura3-52, his3-Δ200, trp1-Δ901, lys2-801, suc2-Δ9, vps34Δ::KAN*	This study
LWY19264	*MATalpha, leu2,3-112, ura3-52, his3-Δ200, trp1-Δ901, lys2-801, suc2-Δ9, vps34Δ::KAN, Atg27-2xGFP::HIS3*	This study
LWY19252	*MATalpha, leu2,3-112, ura3-52, his3-Δ200, trp1-Δ901, lys2-801, suc2-Δ9, vps34Δ::KAN, Atg27-2xGFP::HIS3, snx4Δ::HYG*	This study
LWY19306	*MATa, leu2,3-112, ura3-52, his3-Δ200, trp1-Δ901, lys2-801, suc2-Δ9, vps34Δ::KAN, Atg27-2xGFP::HIS3, Sec7-mCherry::HYG*	This study
LWY19358	*MATa, leu2,3-112, ura3-52, his3-Δ200, trp1-Δ901, lys2-801, suc2-Δ9, vps34Δ::KAN, Atg27-2xGFP::HIS3, Vps8-mCherry::HYG*	This study
LWY19146	*MATalpha, leu2,3-112, ura3-52, his3-Δ200, trp1-Δ901, lys2-801, suc2-Δ9, vps34Δ::HYG*	This study
LWY19144	*MATa, leu2,3-112, ura3-52, his3-Δ200, trp1-Δ901, lys2-801, suc2-Δ9, vps34Δ::HYG, ymr1Δ::HIS3*	This study
LWY19450	*MATa, leu2,3-112, ura3-52, his3-Δ200, trp1-Δ901, lys2-801, suc2-Δ9, vps34Δ::HYG, Atg18-RFP::TRP1*	This study
LWY19453	*MATa, leu2,3-112, ura3-52, his3-Δ200, trp1-Δ901, lys2-*	This study

	801, suc2-Δ9, vps34Δ::HYG, Atg18-RFP::TRP1, vam3Δ::NAT	
LWY7235	*MATa, leu2,3-112, ura3-52, his3-Δ200, trp1-Δ901, lys2-801, suc2-Δ9*	(Bonangelino *et al.*, 1997)
LWY19518	*MATa, leu2,3-112, ura3-52, his3-Δ200, trp1-Δ901, lys2-801, suc2-Δ9, vps34Δ::KAN, Atg27-2xGFP::HIS3, Sec7-mCherry::HYG*	This study
LWY19521	*MATalpha, leu2,3-112, ura3-52, his3-Δ200, trp1-Δ901, lys2-801, suc2-Δ9, vps34Δ::KAN, Atg27-2xGFP::HIS3, Sec7-mCherry::HYG*, *vps35Δ::NAT*	This study
LWY19503	*MATalpha, leu2,3-112, ura3-52, his3-Δ200, trp1-Δ901, lys2-801, suc2-Δ9*, *vps35Δ::NAT*	This study

Table 6. **Yeast plasmids used in this study**

Plasmid	**Description**	**Source**
pRS416-Vps34	CEN, URA3	This study
pRS416-Vps34-R283E A287D	CEN, URA3	This study
pRS416-Vps34-Y501C	CEN, URA3	This study
pRS416-Vps34-EDC	CEN, URA3	This study
pRS414-Ypq1-GFP	CEN, TRP1	Subcloned from (Li *et al.*, 2015)
pRS414-Mup1-GFP	CEN, TRP1	Subcloned from (Lin *et al.*, 2008)
pRS414-GFP-Atg8	CEN, URA3	(Abeliovich *et al.*, 2003)
pRS414-pCup1-GFP-Atg8	CEN, TRP1	(Abeliovich *et al.*, 2003)
pRS413-GFP-Atg8	CEN, HIS3	Subcloned from (Abeliovich *et al.*, 2003)
pRS426-GFP-Vps34	2μ, URA3	This study
pRS425-Vps15-13xMyc	2μ, LEU2	This study
pRS416-Vps34-D275K	CEN, URA3	This study
pRS416-Vps34-R283E	CEN, URA3	This study
pRS416-Vps34-A287D	CEN, URA3	This study

pRS416-Vps34-N292D	CEN, URA3	This study
pRS416-Vps34-H322A	CEN, URA3	This study
pRS416-Vps34-E323D	CEN, URA3	This study
pRS416-Vps34-F761Y	CEN, URA3	This study
pRS416-Vps34-I863D	CEN, URA3	This study
pRS416-Vps34-D275K R283E A287D N292D	CEN, URA3	This study
pRS416-Vps34-D275K R283E A287D N292D H322A	CEN, URA3	This study
pRS416-Vps34-K759D	CEN, URA3	This study
pRS416-Vps34-E505G	CEN, URA3	This study
pRS416-Vps34-S506P	CEN, URA3	This study
pRS416-Vps34-D628V	CEN, URA3	This study
pRS416-Vps34-M642V	CEN, URA3	This study
pRS416-5xHA-Vps34	CEN, URA3	This study
pRS416-5xHA-Vps34-EDC	CEN, URA3	This study
pRS416-Envy-Vps34	CEN, URA3	This study
pRS416-Envy-Vps34-EDC	CEN, URA3	This study
pRS413-Vps34	CEN, HIS3	This study
pRS413-Vps34-EDC	CEN, HIS3	This study
pRS416-Fab1-Envy	CEN, URA3	This study
pRS413-Fig4-Envy	CEN, HIS3	This study
pRS416-GFP-Yck3	CEN, URA3	This study

pRS416-Atg18-GFP	CEN, URA3	(Rieter *et al.*, 2013)

3.7 References

Abeliovich, H., Zhang, C., Dunn, W.A., Jr., Shokat, K.M., and Klionsky, D.J. (2003). Chemical genetic analysis of Apg1 reveals a non-kinase role in the induction of autophagy. Mol Biol Cell 14, 477-490.

Araki, Y., Ku, W.C., Akioka, M., May, A.I., Hayashi, Y., Arisaka, F., Ishihama, Y., and Ohsumi, Y. (2013). Atg38 is required for autophagy-specific phosphatidylinositol 3-kinase complex integrity. J Cell Biol 203, 299-313.

Balla, T. (2013). Phosphoinositides: tiny lipids with giant impact on cell regulation. Physiol Rev 93, 1019-1137.

Barbet, N.C., Schneider, U., Helliwell, S.B., Stansfield, I., Tuite, M.F., and Hall, M.N. (1996). TOR controls translation initiation and early G1 progression in yeast. Mol Biol Cell 7, 25-42.

Bas, L., Papinski, D., Licheva, M., Torggler, R., Rohringer, S., Schuschnig, M., and Kraft, C. (2018). Reconstitution reveals Ykt6 as the autophagosomal SNARE in autophagosome-vacuole fusion. J Cell Biol.

Bonangelino, C.J., Catlett, N.L., and Weisman, L.S. (1997). Vac7p, a novel vacuolar protein, is required for normal vacuole inheritance and morphology. Mol Cell Biol 17, 6847-6858.

Bonangelino, C.J., Nau, J.J., Duex, J.E., Brinkman, M., Wurmser, A.E., Gary, J.D., Emr, S.D., and Weisman, L.S. (2002). Osmotic stress-induced increase of phosphatidylinositol 3,5-bisphosphate requires Vac14p, an activator of the lipid kinase Fab1p. J Cell Biol 156, 1015-1028.

Botelho, R.J., Efe, J.A., Teis, D., and Emr, S.D. (2008). Assembly of a Fab1 phosphoinositide kinase signaling complex requires the Fig4 phosphoinositide phosphatase. Mol Biol Cell 19, 4273-4286.

Burda, P., Padilla, S.M., Sarkar, S., and Emr, S.D. (2002). Retromer function in endosome-to-Golgi retrograde transport is regulated by the yeast Vps34 PtdIns 3-kinase. J Cell Sci 115, 3889-3900.

Cabrera, M., Nordmann, M., Perz, A., Schmedt, D., Gerondopoulos, A., Barr, F., Piehler, J., Engelbrecht-Vandre, S., and Ungermann, C. (2014). The Mon1-Ccz1 GEF activates the Rab7 GTPase Ypt7 via a longin-fold-Rab interface and association with PI3P-positive membranes. J Cell Sci 127, 1043-1051.

Cebollero, E., van der Vaart, A., Zhao, M., Rieter, E., Klionsky, D.J., Helms, J.B., and Reggiori, F. (2012). Phosphatidylinositol-3-phosphate clearance plays a key role in autophagosome completion. Curr Biol 22, 1545-1553.

Cheever, M.L., Sato, T.K., de Beer, T., Kutateladze, T.G., Emr, S.D., and Overduin, M. (2001). Phox domain interaction with PtdIns(3)P targets the Vam7 t-SNARE to vacuole membranes. Nat Cell Biol 3, 613-618.

Delorme-Axford, E., and Klionsky, D.J. (2018). Transcriptional and post-transcriptional regulation of autophagy in the yeast Saccharomyces cerevisiae. J Biol Chem 293, 5396-5403.

Dove, S.K., Cooke, F.T., Douglas, M.R., Sayers, L.G., Parker, P.J., and Michell, R.H. (1997). Osmotic stress activates phosphatidylinositol-3,5-bisphosphate synthesis. Nature 390, 187-192.

Dove, S.K., Piper, R.C., McEwen, R.K., Yu, J.W., King, M.C., Hughes, D.C., Thuring, J., Holmes, A.B., Cooke, F.T., Michell, R.H., et al. (2004). Svp1p defines a family of phosphatidylinositol 3,5-bisphosphate effectors. EMBO J 23, 1922-1933.

Duex, J.E., Nau, J.J., Kauffman, E.J., and Weisman, L.S. (2006a). Phosphoinositide 5-phosphatase Fig 4p is required for both acute rise and subsequent fall in stress-induced phosphatidylinositol 3,5-bisphosphate levels. Eukaryot Cell 5, 723-731.

Duex, J.E., Tang, F., and Weisman, L.S. (2006b). The Vac14p-Fig4p complex acts independently of Vac7p and couples PI3,5P2 synthesis and turnover. J Cell Biol 172, 693-704.

Fratti, R.A., and Wickner, W. (2007). Distinct targeting and fusion functions of the PX and SNARE domains of yeast vacuolar Vam7p. J Biol Chem 282, 13133-13138.

Gary, J.D., Sato, T.K., Stefan, C.J., Bonangelino, C.J., Weisman, L.S., and Emr, S.D. (2002). Regulation of Fab1 phosphatidylinositol 3-phosphate 5-kinase pathway by Vac7 protein and Fig4, a polyphosphoinositide phosphatase family member. Mol Biol Cell 13, 1238-1251.

Gary, J.D., Wurmser, A.E., Bonangelino, C.J., Weisman, L.S., and Emr, S.D. (1998). Fab1p is essential for PtdIns(3)P 5-kinase activity and the maintenance of vacuolar size and membrane homeostasis. J Cell Biol 143, 65-79.

Huang, W., Choi, W., Hu, W., Mi, N., Guo, Q., Ma, M., Liu, M., Tian, Y., Lu, P., Wang, F.L., et al. (2012). Crystal structure and biochemical analyses reveal Beclin 1 as a novel membrane binding protein. Cell Res 22, 473-489.

Huang, W.P., Scott, S.V., Kim, J., and Klionsky, D.J. (2000). The itinerary of a vesicle component, Aut7p/Cvt5p, terminates in the yeast vacuole via the autophagy/Cvt pathways. J Biol Chem 275, 5845-5851.

Ichimura, Y., Kirisako, T., Takao, T., Satomi, Y., Shimonishi, Y., Ishihara, N., Mizushima, N., Tanida, I., Kominami, E., Ohsumi, M., et al. (2000). A ubiquitin-like system mediates protein lipidation. Nature 408, 488-492.

Katzmann, D.J., Stefan, C.J., Babst, M., and Emr, S.D. (2003). Vps27 recruits ESCRT machinery to endosomes during MVB sorting. J Cell Biol 162, 413-423.

Kihara, A., Noda, T., Ishihara, N., and Ohsumi, Y. (2001). Two distinct Vps34 phosphatidylinositol 3-kinase complexes function in autophagy and carboxypeptidase Y sorting in Saccharomyces cerevisiae. J Cell Biol 152, 519-530.

Klionsky, D.J., Abdelmohsen, K., Abe, A., Abedin, M.J., Abeliovich, H., Acevedo Arozena, A., Adachi, H., Adams, C.M., Adams, P.D., Adeli, K., et al. (2016). Guidelines for the use and interpretation of assays for monitoring autophagy (3rd edition). Autophagy 12, 1-222.

Kotani, T., Kirisako, H., Koizumi, M., Ohsumi, Y., and Nakatogawa, H. (2018). The Atg2-Atg18 complex tethers pre-autophagosomal membranes to the endoplasmic reticulum for autophagosome formation. Proc Natl Acad Sci U S A 115, 10363-10368.

Lang, M.J., Strunk, B.S., Azad, N., Petersen, J.L., and Weisman, L.S. (2017). An intramolecular interaction within the lipid kinase Fab1 regulates cellular phosphatidylinositol 3,5-bisphosphate lipid levels. Mol Biol Cell.

Lawrence, G., Brown, C.C., Flood, B.A., Karunakaran, S., Cabrera, M., Nordmann, M., Ungermann, C., and Fratti, R.A. (2014). Dynamic association of the PI3P-interacting Mon1-Ccz1 GEF with vacuoles is controlled through its phosphorylation by the type 1 casein kinase Yck3. Mol Biol Cell 25, 1608-1619.

Li, M., Rong, Y., Chuang, Y.S., Peng, D., and Emr, S.D. (2015). Ubiquitin-dependent lysosomal membrane protein sorting and degradation. Mol Cell 57, 467-478.

Lin, C.H., MacGurn, J.A., Chu, T., Stefan, C.J., and Emr, S.D. (2008). Arrestin-related ubiquitin-ligase adaptors regulate endocytosis and protein turnover at the cell surface. Cell 135, 714-725.

Livak, K.J., and Schmittgen, T.D. (2001). Analysis of relative gene expression data using real-time quantitative PCR and the 2(-Delta Delta C(T)) Method. Methods 25, 402-408.

Ma, M., Burd, C.G., and Chi, R.J. (2017). Distinct complexes of yeast Snx4 family SNX-BARs mediate retrograde trafficking of Snc1 and Atg27. Traffic 18, 134-144.

Menant, A., Barbey, R., and Thomas, D. (2006). Substrate-mediated remodeling of methionine transport by multiple ubiquitin-dependent mechanisms in yeast cells. EMBO J 25, 4436-4447.

Nice, D.C., Sato, T.K., Stromhaug, P.E., Emr, S.D., and Klionsky, D.J. (2002). Cooperative binding of the cytoplasm to vacuole targeting pathway proteins, Cvt13 and Cvt20, to phosphatidylinositol 3-phosphate at the pre-autophagosomal structure is required for selective autophagy. J Biol Chem 277, 30198-30207.

Obara, K., Sekito, T., Niimi, K., and Ohsumi, Y. (2008). The Atg18-Atg2 complex is recruited to autophagic membranes via phosphatidylinositol 3-phosphate and exerts an essential function. J Biol Chem 283, 23972-23980.

Obara, K., Sekito, T., and Ohsumi, Y. (2006). Assortment of phosphatidylinositol 3-kinase complexes--Atg14p directs association of complex I to the pre-autophagosomal structure in Saccharomyces cerevisiae. Mol Biol Cell 17, 1527-1539.

Parrish, W.R., Stefan, C.J., and Emr, S.D. (2004). Essential role for the myotubularin-related phosphatase Ymr1p and the synaptojanin-like phosphatases Sjl2p and Sjl3p in regulation of phosphatidylinositol 3-phosphate in yeast. Mol Biol Cell 15, 3567-3579.

Rieter, E., Vinke, F., Bakula, D., Cebollero, E., Ungermann, C., Proikas-Cezanne, T., and Reggiori, F. (2013). Atg18 function in autophagy is regulated by specific sites within its beta-propeller. J Cell Sci 126, 593-604.

Rostislavleva, K., Soler, N., Ohashi, Y., Zhang, L., Pardon, E., Burke, J.E., Masson, G.R., Johnson, C., Steyaert, J., Ktistakis, N.T., et al. (2015). Structure and flexibility of the endosomal Vps34 complex reveals the basis of its function on membranes. Science 350, aac7365.

Schink, K.O., Tan, K.W., and Stenmark, H. (2016). Phosphoinositides in Control of Membrane Dynamics. Annu Rev Cell Dev Biol 32, 143-171.

Schu, P.V., Takegawa, K., Fry, M.J., Stack, J.H., Waterfield, M.D., and Emr, S.D. (1993). Phosphatidylinositol 3-kinase encoded by yeast VPS34 gene essential for protein sorting. Science 260, 88-91.

Seaman, M.N., Marcusson, E.G., Cereghino, J.L., and Emr, S.D. (1997). Endosome to Golgi retrieval of the vacuolar protein sorting receptor, Vps10p, requires the function of the VPS29, VPS30, and VPS35 gene products. J Cell Biol 137, 79-92.

Seaman, M.N., McCaffery, J.M., and Emr, S.D. (1998). A membrane coat complex essential for endosome-to-Golgi retrograde transport in yeast. J Cell Biol 142, 665-681.

Segarra, V.A., Boettner, D.R., and Lemmon, S.K. (2015). Atg27 tyrosine sorting motif is important for its trafficking and Atg9 localization. Traffic 16, 365-378.

Stack, J.H., Herman, P.K., Schu, P.V., and Emr, S.D. (1993). A membrane-associated complex containing the Vps15 protein kinase and the Vps34 PI 3-kinase is essential for protein sorting to the yeast lysosome-like vacuole. EMBO J 12, 2195-2204.

Stjepanovic, G., Baskaran, S., Lin, M.G., and Hurley, J.H. (2017). Vps34 Kinase Domain Dynamics Regulate the Autophagic PI 3-Kinase Complex. Mol Cell 67, 528-534 e523.
Strunk, B.S., Steinfeld, N., Lee, S., Jin, N., Munoz-Rivera, C., Meeks, G., Thomas, A., Akemann, C., Mapp, A.K., MacGurn, J.A., et al. (2020). Roles for a lipid phosphatase in the activation of its opposing lipid kinase. Mol Biol Cell 31, 1835-1845.
Sun, B., Chen, L., Cao, W., Roth, A.F., and Davis, N.G. (2004). The yeast casein kinase Yck3p is palmitoylated, then sorted to the vacuolar membrane with AP-3-dependent recognition of a YXXPhi adaptin sorting signal. Mol Biol Cell 15, 1397-1406.
Suzuki, S.W., and Emr, S.D. (2018). Membrane protein recycling from the vacuole/lysosome membrane. J Cell Biol.
Taylor, G.S., Maehama, T., and Dixon, J.E. (2000). Myotubularin, a protein tyrosine phosphatase mutated in myotubular myopathy, dephosphorylates the lipid second messenger, phosphatidylinositol 3-phosphate. Proc Natl Acad Sci U S A 97, 8910-8915.
Taylor, S.S., Shaw, A.S., Kannan, N., and Kornev, A.P. (2015). Integration of signaling in the kinome: Architecture and regulation of the alphaC Helix. Biochim Biophys Acta 1854, 1567-1574.
Teis, D., Saksena, S., and Emr, S.D. (2008). Ordered assembly of the ESCRT-III complex on endosomes is required to sequester cargo during MVB formation. Dev Cell 15, 578-589.
Valverde, D.P., Yu, S., Boggavarapu, V., Kumar, N., Lees, J.A., Walz, T., Reinisch, K.M., and Melia, T.J. (2019). ATG2 transports lipids to promote autophagosome biogenesis. J Cell Biol 218, 1787-1798.
Vida, T.A., and Emr, S.D. (1995). A new vital stain for visualizing vacuolar membrane dynamics and endocytosis in yeast. J Cell Biol 128, 779-792.
Yu, J.W., and Lemmon, M.A. (2001). All phox homology (PX) domains from Saccharomyces cerevisiae specifically recognize phosphatidylinositol 3-phosphate. J Biol Chem 276, 44179-44184.
Zhu, L., Jorgensen, J.R., Li, M., Chuang, Y.S., and Emr, S.D. (2017). ESCRTs function directly on the lysosome membrane to downregulate ubiquitinated lysosomal membrane proteins. Elife 6.

Chapter 4 : A Comprehensive Understanding of Selective Autophagy

(The chapter has been adapted from *Gatica, Lahiri and Klionsky, Nature Cell Biology, 2017*)

Macroautophagy, initially described as a non-selective nutrient recycling process, is essential for the removal of multiple cellular components. In the past three decades, selective autophagy has been characterized as a highly regulated and specific degradation pathway for the removal of unwanted cytosolic components and damaged and/or superfluous organelles. In this chapter, different types of selective autophagy are discussed, emphasizing the role of ligand receptors and scaffold proteins in providing cargo specificity, and unanswered questions in the field are highlighted.

4.1 Introduction

Autophagy is a highly conserved pathway in eukaryotes involving the cellular recycling of multiple cytoplasmic components during standard physiological conditions and different types of stress including starvation. Macroautophagy (hereafter autophagy), which can be either non-selective or selective, involves the sequestration of cytoplasm within double-membrane vesicles termed autophagosomes. Upon maturation, autophagosomes fuse with the vacuole (yeast and plants) or endosomes and lysosomes (metazoans) leading to degradation of their cargo by resident hydrolases. Cargo degradation produces molecular building blocks such as amino acids, which are subsequently recycled back into the cytoplasm for reuse (He and Klionsky, 2009) (Feng et al., 2014). Whereas non-selective autophagy, a cellular response to nutrient deprivation, typically involves random uptake of cytoplasm into phagophores, the precursors to autophagosomes, selective autophagy is responsible for specifically removing certain

components such as protein aggregates and damaged or superfluous organelles (Jin et al., 2013). Different studies have reported the selective autophagic degradation of several organelles including mitochondria (Ashrafi and Schwarz, 2013), peroxisomes (Hutchins et al., 1999), lysosomes (Hung et al., 2013), endoplasmic reticulum (ER) and the nucleus (Nakatogawa and Mochida, 2015) under various conditions. Furthermore, autophagy selectively degrades aggregation-prone misfolded proteins and protein microaggregates implicated in the pathology of various neurodegenerative diseases (Sarkar et al., 2009). In this chapter, I address the principal mechanisms of selective autophagy in yeast and mammals, with an emphasis on mitophagy, which is to date the best described type of selective autophagy.

4.2 Cytoplasm-to-vacuole targeting (Cvt) pathway

The Cvt pathway is a biosynthetic autophagy-related process specific to yeast, in which vacuolar enzymes are transported from the cytoplasm into the vacuole utilizing the autophagic machinery. Among the enzymes that utilize the Cvt pathway are Ape1, Ape4 and Ams1 (Lynch-Day and Klionsky, 2010). Ape1 is first synthesized in the cytoplasm as an inactive proenzyme (prApe1). Upon oligomerization, prApe1 is selectively recognized by the non-core autophagy-related (Atg) protein Atg19 that functions as a receptor for Ams1, prApe1 and Ape4 (Scott et al., 2001) (Leber et al., 2001). Once the prApe1-Atg19 or Cvt complex is formed, Atg19 binds to the scaffold protein Atg11, which in turn recruits the Cvt complex to the perivacuolar location termed the phagophore-assembly site (PAS) where autophagosomes and Cvt vesicles are formed in yeasts (Yorimitsu and Klionsky, 2005) (Shintani et al., 2002); interaction of Atg19 with Atg11 is facilitated by Hrr25-dependent phosphorylation of the receptor (Pfaffenwimmer et al., 2014). Upon reaching the PAS, Atg19 interacts with the ubiquitin-like protein Atg8 (Shintani et al., 2002). During autophagy and the Cvt pathway, Atg8 is covalently conjugated through its

C terminus to phosphatidylethanolamine (PE); thus, Atg8–PE is present on both the inner and outer membrane of forming autophagosomes (Ichimura et al., 2000) (Fig. 30a). Atg8 has been implicated in phagophore expansion and autophagosome size regulation (Xie et al., 2008). Thus, Atg19 binding to Atg8 tethers the Cvt complex to the Atg8–PE-conjugated sequestering vesicles. Once fully matured, Cvt vesicles fuse with the vacuole and deliver prApe1, which is then processed into its active form by resident hydrolases.

Using the Cvt pathway as a model for selective autophagy I can propose the following: while relying on the core autophagy machinery for phagophore membrane expansion and vesicle formation, cargo selectivity is achieved by a ligand receptor and a scaffold protein, roles taken by Atg19 and Atg11, respectively, in the Cvt pathway. Atg19 has a paralog, Atg34 (also phosphorylated by Hrr25), that functions as an Ams1 receptor during nitrogen starvation (Suzuki et al., 2010). Other types of selective autophagy in yeast such as mitophagy (Kanki et al., 2009) and pexophagy (Motley et al., 2012; Farre et al., 2008), also rely on Atg11 as a scaffold for cargo delivery to the PAS. However, a counterpart to Atg11 has yet to be discovered in mammals. Similarly, most types of selective autophagy require the binding of the cargo receptor to the core autophagy machinery. In the Cvt pathway, this process is illustrated by Atg19 binding to Atg8 through a specific WXXL motif found on the Atg19 C terminus, similar to that seen in SQSTM1/p6229 (Noda et al., 2008). This interaction is evolutionarily conserved as several proteins in yeasts and more complex eukaryotes contain Atg8-interacting motifs (AIM) or LC3-interacting regions (LIRs), respectively. The AIM or LIR provide selective binding to yeast Atg8 or one of the members of the LC3/GABARAP family of Atg8 mammalian homologs (Klionsky and Schulman, 2014). Recently, a specific type of LIR called GABARAP-interacting motif (GIM) has been proposed, showing enhanced specificity to GABARAP versus LC3 family

members (Rogov et al., 2017a). Multiple examples of scaffold and receptor proteins will be showcased as I discuss different types of selective autophagy.

4.3 Aggrephagy

The selective degradation of protein aggregates by autophagy is known as aggrephagy. Multiple aggregation-prone proteins such as amyloid-β (Pickford et al., 2008), HTT (huntingtin) (Ravikumar et al., 2004) and SNCA/α-synuclein (Winslow et al., 2010) are autophagy substrates. In yeast, Cue5 is a cargo receptor for the clearance of aggregation-prone poly-glutamine (polyQ)-containing proteins. Cue5 possesses a ubiquitin-binding CUE domain and an AIM, mediating the interaction between the ubiquitinated cargo and Atg8 (Lu et al., 2014a). Overexpression of TOLLIP, a Cue5 human homolog that also has a CUE domain, leads to the degradation of polyQ protein aggregates in human cell lines (Lu et al., 2014b) (Fig. 30b). Ubiquitination of substrates has been demonstrated as a key mediator in the recognition and degradation of these proteins by selective autophagy (Kim et al., 2008). At least three additional mammalian cargo receptors, SQSTM1 (Ichimura et al., 2008; Pankiv et al., 2007), NBR1 (Kirkin et al., 2009) and OPTN (Shen et al., 2015), act as ubiquitin binding proteins that mediate the interaction between ubiquitinated proteins and the core autophagy machinery. All three receptors possess LIRs and ubiquitin-binding domains, thus working as a bridge between the LC3/GABARAP family members and the ubiquitinated substrates (Pankiv et al., 2007; Lamark et al., 2009).

The nucleocytoplasmic shuttling protein WDFY3/ALFY has been proposed as a scaffold in aggrephagy (Filimonenko et al., 2010). While unable to directly interact with ubiquitinated substrates, WDFY3 binds the core autophagy protein ATG5, the cargo receptor SQSTM1 (Clausen et al., 2010), GABARAP subfamily members (Lystad et al., 2014), and

phosphatidylinositol-3-phosphate (Simonsen et al., 2004), a prominent lipid in the regulation of autophagosome membrane formation. WDFY3 depletion hinders the clearance of aggregated polyQ proteins. The latter observation, in conjunction with its high number of interacting partners, suggests that WDFY3 is an important scaffold protein in the SQSTM1-dependent degradation of ubiquitinated aggregates by selective autophagy.

The fact that ubiquitination plays an important role not only in substrate recognition and degradation by the ubiquitin-proteasome system (UPS), but also by selective autophagy, opens a set of questions regarding the hierarchy between these two degradation pathways. It has been proposed that protein aggregates that cannot be degraded by the UPS (e.g., due to size) may be cleared by autophagy (Verhoef et al., 2002; Korolchuk et al., 2010). At the same time, the Lys residues used for linkage, as well as the length and the nature of the ubiquitin chains, has been proposed as a mechanism to select which degradation pathway is chosen (Korolchuk et al., 2010). However, a recent paper by Lu et al. emphasizes the role of receptor oligomerization over the type of ubiquitination in selecting a degradation pathway (Lu et al., 2017). This finding agrees with data showing the importance of Cue5 and SQSTM1 oligomerization in their association with the phagophore (Korolchuk et al., 2010; Wurzer et al., 2015). Thus, both autophagy and the UPS provide dynamic alternatives to different cellular challenges.

Figure 30: The Cvt pathway, Aggrephagy and Pexophagy

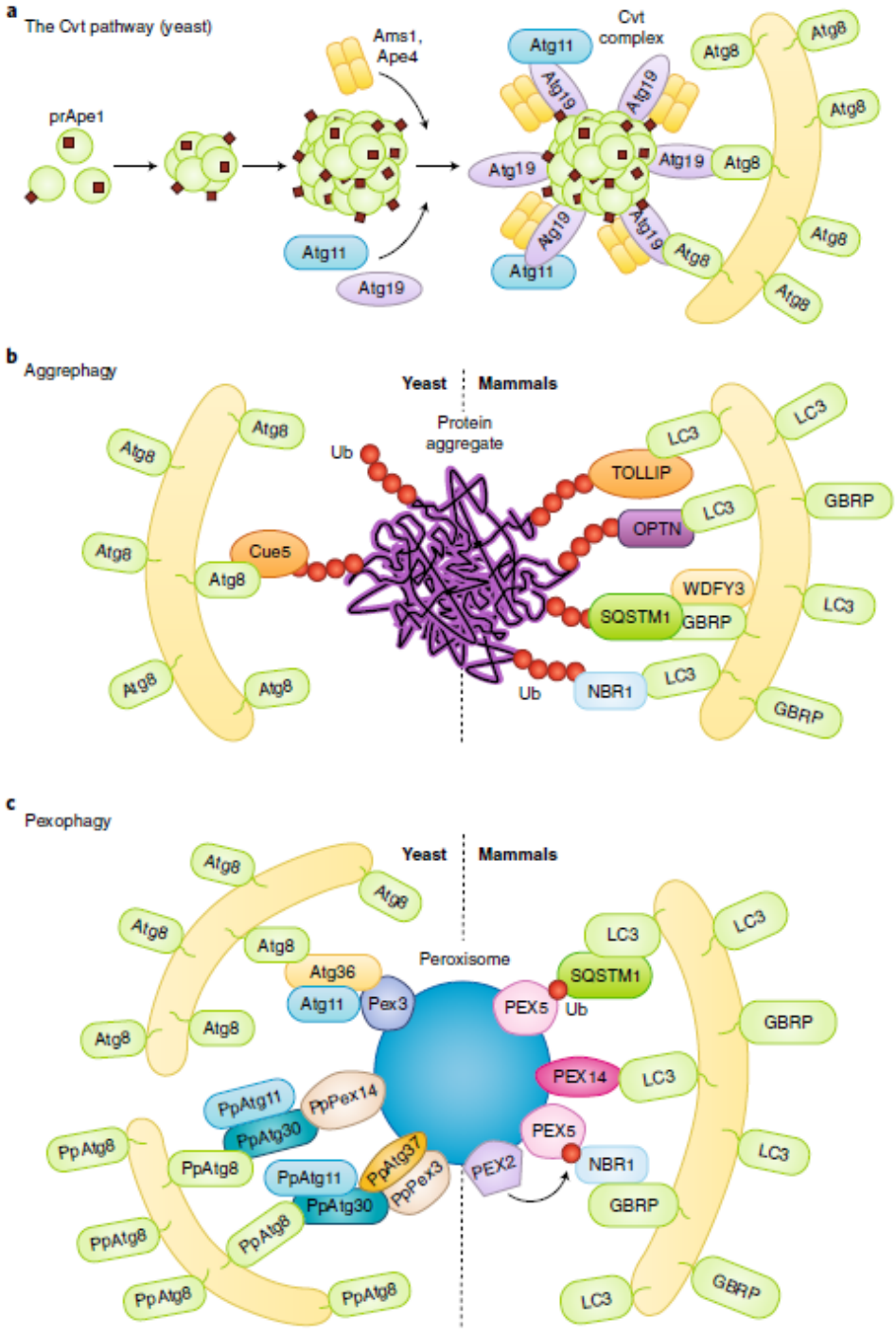

Figure 30. The Cvt pathway, Aggrephagy and Pexophagy.

a) In the yeast Cvt pathway prApe1, Ape4 and Ams1 are synthesized in the cytoplasm. prApe1 oligomerizes into dodecamers and subsequently higher order structures that are recognized by the receptor Atg19, which in turn binds the scaffold protein Atg11 forming the Cvt Complex. Ams1 and Apr4 also oligomerize and bind Atg19. Atg11 brings the Cvt Complex to the PAS where Atg19 binds Atg8–PE, tethering the Cvt complex to the phagophore.

b) In both yeast and mammalian aggrephagy, protein aggregates are ubiquitinated and subsequently recognized by cargo receptors. In yeast, Cue5 links the ubiquitinated aggregates to Atg8–PE. During mammalian aggrephagy, TOLLIP, SQSTM1, NBR1 and OPTN tether the ubiquitinated aggregates to the phagophore by binding LC3/GABARAP family members. WDFY3 has been described as a scaffold for SQSTM1-dependent degradation.

c) In *S. cerevisiae* pexophagy, Atg36 functions as a receptor linking peroxisomes to the phagophore by binding Pex3 and Atg8–PE. In *K. Phaffii/P. pastoris* pexophagy, PpAtg30 acts as a receptor by linking PpPex3 and PpPex14 to PpAtg8–PE. Atg11 functions as a scaffold for both *S. cerevisiae* and *K. Phaffii/P. pastoris.* The current model of mammalian pexophagy involves the E3-ubiquitin ligase PEX2-mediated mono-ubiquitination of PEX5, which in turn is recognized by receptors SQSTM1 and NBR1, tethering peroxisomes to the phagophore. PEX14 has also been reported to link peroxisomes to the phagophore by directly binding LC3 family members.

4.4 Pexophagy

Pexophagy is the selective removal of peroxisomes. Pexophagy has been mostly studied as a pathway for the removal of superfluous organelles in various fungi (Klionsky and Ohsumi, 1999). Incubating these fungi in oleic acid or methanol leads to peroxisome proliferation; following a shift to a preferred carbon source such as glucose, the excess peroxisomes are rapidly degraded through pexophagy (Hutchins et al., 1999; Klionsky and Ohsumi, 1999). Similar to other types of selective autophagy, cargo selectivity is provided by receptor proteins; in yeast this role is taken by PpAtg30 in *K. Phaffii/P. pastoris* (Farre et al., 2008) and Atg36 (Nazarko et al., 2009) in *S. cerevisiae*. Both Atg36 and PpAtg30 tether peroxisomes targeted for degradation to nascent phagophore membranes by linking Atg8 to peroxisomal membrane proteins, with Atg36 binding Pex3, and PpAtg30 binding both PpPex3 and PpPex14 (Motley et al., 2012; Farre et al., 2008). Phosphorylatable variants of the classical AIMs have been reported for both Atg36 and PpAtg30; however, disruption of these AIMs only delays pexophagy rather than abrogating it (Farre et al., 2013). As previously mentioned, Atg11 is required for pexophagy (Kim et al., 2001). PpAtg37, is an integral peroxisomal membrane protein specifically required for pexophagy in *K. Phaffii/P. pastoris*. During pexophagy, PpAtg37 is necessary for phagophore formation, because PpAtg37 null cells fail to recruit PpAtg11 to peroxisomes (Nazarko et al., 2014).

In contrast to yeast, no pexophagy-specific cargo receptor has been described in mammals. Thus, mammalian pexophagy relies on the ubiquitination of peroxisomal proteins and their recognition by SQSTM1 (Kim et al., 2008) and NBR1 (Deosaran et al., 2013). Initially, it was reported that PEX3 overexpression leads to peroxisome ubiquitination and pexophagy induction (Yamashita et al., 2014). However, this study failed to determine the specific

peroxisomal proteins targeted for ubiquitination—blocking PEX3 ubiquitination does not prevent pexophagy. Subsequently, two studies identified PEX5 mono-ubiquitination as the cargo signal for peroxisome degradation (Nordgren et al., 2015; Zhang et al., 2015). PEX5 is a cytosolic protein that shuttles between the peroxisomal membrane and the cytosol in a ubiquitin-dependent manner (Grou et al., 2009). The accumulation of mono-ubiquitinated PEX5 in the peroxisomal membrane, which was unable to shuttle back to the cytosol, triggers pexophagy (Nordgren et al., 2015). Furthermore, in response to reactive oxygen species (ROS), PEX5 is phosphorylated and subsequently mono-ubiquitinated, which leads to pexophagy induction in a SQSTM1-dependent manner (Zhang et al., 2015). A recent study has indicated that the peroxisomal E3-ubiquitin ligase PEX2 is responsible for PEX5 ubiquitination (Sargent et al., 2016). These data suggest a model in which mammalian pexophagy is dependent on the membrane accumulation of ubiquitinated peroxisomal proteins such as PEX5, which are recognized by the ubiquitin-binding receptors SQSTM1 and NBR1, that in turn link the target peroxisomes to LC3/GABARAP-bound sequestration membranes (Fig. 30c). However, this simple model fails to answer several questions: Mechanistically, how does PEX5 ubiquitination at a specific site determine whether the protein shuttles into the peroxisome or is directed to proteasomal degradation? Are there distinct mechanisms involving ROS and amino acid starvation-induced pexophagy? Regarding this last point, other studies have reported that the peroxisomal membrane protein PEX14, which acts a docking factor for PEX5, can directly interact with LC3-II under starvation conditions, outcompeting PEX5 (Hara-Kuge and Fujiki, 2008). This opens the possibility of different pathways being involved under different pexophagy-inducing stimuli. Finally, the human Atg37 ortholog ACBD5 has also been reported as an essential pexophagy factor (Nazarko et al., 2014).

4.5 Mitophagy

Mitophagy is the selective autophagic degradation of mitochondria. Mitophagy is a critical quality control process that eliminates damaged and/or superfluous mitochondria (Wang et al., 2013; Liu et al., 2014). Deficiencies in mitophagy have been linked to the development of several pathologies, including neurodegenerative disorders (Redmann et al., 2014) such as Parkinson disease (PD).

Mitochondria have multiple metabolic functions and also influence cell fate by regulating apoptosis. Consequently, mitochondrial damage leads to loss of metabolic homeostasis. Additionally, disruption of oxidative phosphorylation (OxPhos) in damaged mitochondria leads to excessive ROS generation (Kurihara et al., 2012). Mitochondria are high-maintenance organelles, and non-functioning/superfluous mitochondria become an energetic burden. Therefore, the regulation of mitochondrial quality and quantity is of paramount importance. Although mitochondria harbor some internal quality control machinery (Stotland and Gottlieb, 2015), the major contribution towards maintaining mitochondrial integrity comes from mitophagy, which functions in concert with the UPS to ensure mitochondrial homeostasis (Von Stockum et al., 2016).

4.5.1 Mitophagy in yeast

In fungi, mitophagy can be triggered by nitrogen starvation(Kanki and Klionsky, 2008) (Kanki et al., 2015; Aihara et al., 2014) or post-log phase growth in a non-fermentable medium. In yeast, selectivity is provided by the outer mitochondrial membrane (OMM) receptor Atg32 (Kanki et al., 2015), which links targeted mitochondria to the autophagic machinery (Kanki et al., 2009; Okamoto et al., 2009). The cytosolic N terminus of Atg32 interacts with Atg11. Ectopic targeting of the Atg32 N terminus to peroxisomes leads to pexophagy, underscoring the

function and sufficiency of Atg32 as an autophagy receptor (Kondo-Okamoto et al., 2012). The C terminus of Atg32 faces the intermembrane space, and its proteolytic processing by Yme1 may be required for efficient mitophagy (Wang et al., 2013). The interaction between Atg32 and Atg11 promotes the recruitment of mitochondria to the PAS for sequestration. Atg32 also orchestrates the subsequent expansion of the phagophore around the mitochondria through its interaction with Atg8 via the AIM in its cytosolic domain (Liu et al., 2014; Kondo-Okamoto et al., 2012). However, mutating the Atg32 AIM causes only a partial mitophagy defect, suggesting that the Atg32-Atg8 interaction increases mitophagy efficiency, but remains auxiliary (Kanki et al., 2015; Kondo-Okamoto et al., 2012; Aoki et al., 2011).

The expression of Atg32 can be influenced by oxidative stress and nutritional status. In *P. pastoris*, the Ume6-Sin3-Rpd3 complex, positively regulated by TOR, suppresses *ATG32* transcription (Aihara et al., 2014). During starvation, TOR is inactivated, promoting the synthesis of Atg32 and starvation-induced mitophagy. However, the upregulation of Atg32 expression is not by itself sufficient to induce mitophagy. Atg32 is activated by phosphorylation at residues Ser114 and Ser119 in its cytosolic domain, facilitating its interaction with Atg11(Aoki et al., 2011). Casein kinase 2 (CK2) has been proposed as the Atg32 Ser114 kinase (Kanki et al., 2013) as CK2 phosphorylates Atg32 in vitro but fails to phosphorylate $Atg32^{S114A}$. Similarly, CK2 temperature-sensitive mutants fail to phosphorylate Atg32 (Kanki et al., 2013). However, CK2 is a multitasking kinase, and its activation is independent of mitophagy-inducing stimuli (Kanki et al., 2015). Therefore, other signaling pathways may contribute to the temporal selectivity of CK2-mediated phosphorylation of Atg32. Two mitogen-activated protein kinase (MAPK) pathways have been implicated in mitophagy regulation in yeast (Mao et al., 2011). Hog1 is a MAPK in the Ssk1-Pbs2 pathway and Atg32 phosphorylation is suppressed in *hog1*Δ

cells. However, Hog1 does not phosphorylate Atg32 in vitro, suggesting an indirect regulation (Aoki et al., 2011). The Slt2 pathway plays a role in mitochondrial recruitment to the PAS (Mao et al., 2011). While further investigation is required to identify the signaling circuit regulating Atg32 phosphorylation, cooperative expression and activation of Atg32 highlights the multiple levels of regulation involved in mitophagy induction.

Because the dimensions of intact mitochondria are larger than that of autophagosomes, sequestration of damaged mitochondria might be facilitated by mitochondrial fission (Mao et al., 2013; Kanki et al., 2015). In *S. cerevisiae,* mitochondrial fission is mediated by several factors including Dnm1 and Fis1 (Mao et al., 2013). Deletion of either *DNM1* or *FIS1* significantly suppresses mitophagy (Abeliovich et al., 2013). Dnm1 interacts with Atg11, allowing the former to be recruited to mitochondria targeted for degradation. The proteins associated with the ER-mitochondrial encounter structure (ERMES) may play a role in modulating mitochondrial fission during mitophagy. Nevertheless, the exact mechanism of mitophagy-associated mitochondrial fission is unclear, and yet unidentified fission factors may be involved.

4.5.2 Mitophagy in mammals

Mitophagy in mammals is mechanistically more complex than in yeast and is induced by cellular and developmental cues. In mammalian cells the loss of mitochondrial membrane potential is a potent inducer of mitophagy (Ashrafi and Schwarz, 2013; Georgakopoulos et al., 2017). However, while the use of chemicals that target the electron transport chain or act as protonophores is a convenient and efficient way to study mitophagy, the acute dissipation of mitochondrial membrane potential precludes the study of subtle regulatory phenomenon. Furthermore, such severe mitochondrial damage might not be representative of the true pathophysiological triggers.

In mammals, mitophagy plays important physiological roles in development and cellular differentiation. Erythrocyte development requires the selective degradation of mitochondria in reticulocytes (Sandoval et al., 2008) and embryonic development in some organisms involves selective degradation of paternal mitochondria in the zygote (Wei et al., 2017). Hypoxia, which disrupts mitochondrial respiration, is another stimulus that promotes mitophagy in mammalian cells (Liu et al., 2014).

The PINK1-PRKN/PARK2/parkin pathway is the most extensively characterized mechanism effecting mitochondrial quality control in most mammalian cells. PINK1 is a Ser/Thr kinase with a C-terminal kinase domain and N-terminal mitochondrial targeting sequence (Nguyen et al., 2016), and PRKN/PARK2 is an E3-ubiquitin ligase (Durcan and Fon, 2015). Loss of mitochondrial integrity is usually accompanied by mitochondrial depolarization. PINK1, which requires the mitochondrial membrane potential for its inner mitochondrial membrane (IMM) import, acts as a depolarization sensor. In healthy mitochondria, PINK1 is imported into the matrix where it is cleaved by proteases and subsequently released back into the cytosol for degradation via the N-end rule pathway (Yamano and Youle, 2013). In compromised mitochondria, the loss of membrane potential prevents translocation, and PINK1 is stabilized on the OMM, leading to its activation by autophosphorylation (Narendra et al., 2010; Aerts et al., 2015). Active PINK1 phosphorylates several substrates including ubiquitin, MFN1 (mitofusin 1), MFN2 and PRKN/PARK2 (Gegg et al., 2010). Unphosphorylated PRKN/PARK2 is autoinhibited (Trempe et al., 2013); PINK1-mediated phosphorylation of PRKN/PARK2 (Kondapalli et al., 2012) leads to activation. PINK1 also phosphorylates available ubiquitin attached to OMM proteins at Ser65 generating phospho-ubiquitin (Koyano et al., 2014; Kane et al., 2014), which acts as a PRKN/PARK2 substrate. PRKN/PARK2 subsequently links phospho-

ubiquitin chains to OMM proteins, which possibly results in a feed-forward amplification loop recruiting more PRKN/PARK2. The phosphorylation of MFN2 by PINK1 might also play a role in PRKN/PARK2 recruitment (Chen and Dorn, 2013), possibly acting along with phospho-ubiquitin at the OMM. However, the role of MFN2 in PRKN/PARK2 recruitment is controversial (Pickrell and Youle, 2015).

The classic model for mitophagy involves the recognition of polyubiquitinated mitochondria by autophagy receptors SQSTM1 and OPTN which bind LC3 (Geisler et al., 2010). This interaction tethers damaged mitochondria to the expanding phagophore and promotes their subsequent sequestration within autophagosomes (Fig. 31a). Recent progress in the field suggests a complementary model where PINK1-mediated phosphorylation of ubiquitin, independent of PRKN/PARK2 activity, is sufficient to recruit the autophagy receptors CALCOCO2/NDP52 and OPTN and induce low-amplitude mitophagy (Lazarou et al., 2015). In this model CALCOCO2 and OPTN can successfully recruit ULK1 and facilitate mitophagy initiation upstream of LC3 binding (Lazarou et al., 2015). The importance of PRKN/PARK2-mediated ubiquitination is indicated by the fact that overexpression of the mitochondrial deubiquitinase USP30 inhibits mitophagy by promoting deubiquitination of PRKN/PARK2 substrates (Bingol et al., 2014).

Polyubiquitination also acts as a signal that promotes VCP/p97-mediated extraction of OMM proteins and their subsequent proteasomal degradation (Narendra et al., 2012), causing disruption of the OMM (Von Stockum et al., 2016; Wei et al., 2017). Recent findings suggest that OMM disintegration serves to expose the IMM protein PHB2 (prohibitin 2), which possesses a LIR and functions as a mitophagy receptor (Wei et al., 2017). PHB2 promotes mitophagy in a PINK1-PRKN/PARK2-dependent manner, and the selective removal of paternal

mitochondria in *C. elegans* embryos requires PHB2 function (Wei et al., 2017). The PINK1-PRKN/PARK2-dependent generation of mitochondria-derived vesicles (MDVs) (Sugiura et al., 2014; McLelland et al., 2016) is an alternative pathway to conventional PRKN/PARK2-dependent mitophagy. Limited and localized mitochondrial damage promotes MDV formation to ensure the selective removal of damaged portions of a mitochondrion instead of the entire organelle. It is possible that the PINK1-PRKN/PARK2 pathway switches between MDV formation and mitophagy depending upon the extent of mitochondrial damage.

PINK1 and PRKN/PARK2 are also involved in regulating the arrest of mitochondrial motility following mitochondrial damage (Wang et al., 2011). Mitochondria are transported via the kinesin KIF5 on microtubules. KIF5 binds mitochondria through the adaptor TRAK1-TRAK2 and the OMM protein RHOT1/Miro1 (Sheng and Cai, 2012). Upon induction of mitochondrial damage, RHOT1 is one of the earliest proteins to be degraded via PRKN/PARK2-mediated ubiquitination. The kinase LRRK2, which interacts with RHOT1, is also required for this degradation (Hsieh et al., 2016). The removal of RHOT1 halts mitochondrial motility and quarantines damaged mitochondria for degradation. In cells harboring mutations in PINK1, PRKN/PARK2 or LRRK2, RHOT1 degradation is inhibited, leading to continued motility of damaged mitochondria and delayed mitophagy.

Not all mammalian cell types express PARK2/PRKN and there exist several mitochondria-localized mitophagy receptors in mammalian cells. BNIP3L/Nix is one such mitophagy receptor and is involved in the selective elimination of mitochondria during the differentiation of reticulocytes into erythrocytes (Matsushima et al., 1998; Sandoval et al., 2008). BNIP3L localizes to the OMM and contains a LIR near its cytosolic N terminus (Novak et al., 2010), the activity of which may be regulated by phosphorylation (Rogov et al., 2017b).

However, mutations in the BNIP3L LIR only lead to a partial loss in mitophagy (Novak and Dikic, 2011). Another short motif has recently been reported to be indispensable for BNIP3L function (Zhang et al., 2012). While the exact mechanism by which BNIP3L mediates mitophagy remains unknown, reports suggest that BNIP3L may promote mitochondrial depolarization. This depolarization may result in PINK1-PRKN/PARK2 recruitment to mitochondria, activating mitophagy. BNIP3L might also work in concert with the related protein BNIP3 (Ni et al., 2015), which also possesses a LIR (Chourasia et al., 2015).

BNIP3L is also involved in hypoxia-induced mitophagy (Sowter et al., 2001), as is the LIR-containing OMM protein FUNDC1 (Liu et al., 2012). Mutations in the FUNDC1 LIR lead to loss of function. Similar to Atg32, FUNDC1 is regulated by reversible phosphorylation. Under normal conditions, FUNDC1 is phosphorylated by SRC kinase and CK2 (Chen et al., 2014), including the modification of one site in its LIR. Hypoxia promotes the dephosphorylation of these residues involving the phosphatase PGAM5. Hypoxia-induced mitophagy is particularly relevant to the pathobiology of tumors, and elucidating the role of BNIP3L and FUNDC1 in these contexts might be an important step towards therapeutic intervention (Palikaras et al., 2016) (Zhang et al., 2008).

In mammals, mitochondrial dynamics are regulated by the fission-promoting GTPase DNM1L/Drp1 and the profusion factors MFN1-MFN2 and OPA1(Shirihai et al., 2015; Bordi et al., 2017). Mitophagy induction is accompanied by a decrease in mitochondrial fusion and an increase in mitochondrial fission to facilitate degradation of damaged mitochondria (Ni et al., 2015). PINK1 activation promotes PRKN/PARK2-mediated degradation of MFN1-MFN2, consistent with the idea of reduced fusion (Gegg et al., 2010). The mitophagy receptor FUNDC1 is also involved in regulating mitochondrial dynamics during mitophagy. Whereas FUNDC1

binds to and recruits OPA1 to mitochondria under normal conditions, upon mitochondrial damage it preferentially recruits DNM1L, promoting fission (Chen et al., 2016). Like ERMES in yeast, mitochondria-associated membranes, are sites of ER-mitochondria contact in mammals, and have also been proposed to modulate mitophagy-related mitochondrial fission (Wu et al., 2016), although the mechanism remains unclear.

Whereas most selective autophagy receptors are proteins, recent evidence suggests that mitophagy may also be orchestrated by lipid receptors (Hamacher-Brady and Brady, 2016). Cardiolipin, a lipid unique to the mitochondria, may act as a mitophagy receptor in mammalian cortical neurons. Rotenone-induced mitochondrial damage causes a dramatic translocation of cardiolipin from the inner to the outer mitochondrial membrane (Chu et al., 2013), where it interacts with the LC3 N terminus. Inhibition of cardiolipin synthesis or translocation reduces the efficiency of mitophagy in these neurons (Chu et al., 2013). Cardiolipin was also recently reported to modulate mitophagy in *S. cerevisiae* (Shen et al., 2017), and ceramide has also been implicated as a mitophagy receptor in certain cancer cell lines (Sentelle et al., 2012).

Figure 31: Mitophagy, Reticulophagy and Nucleophagy

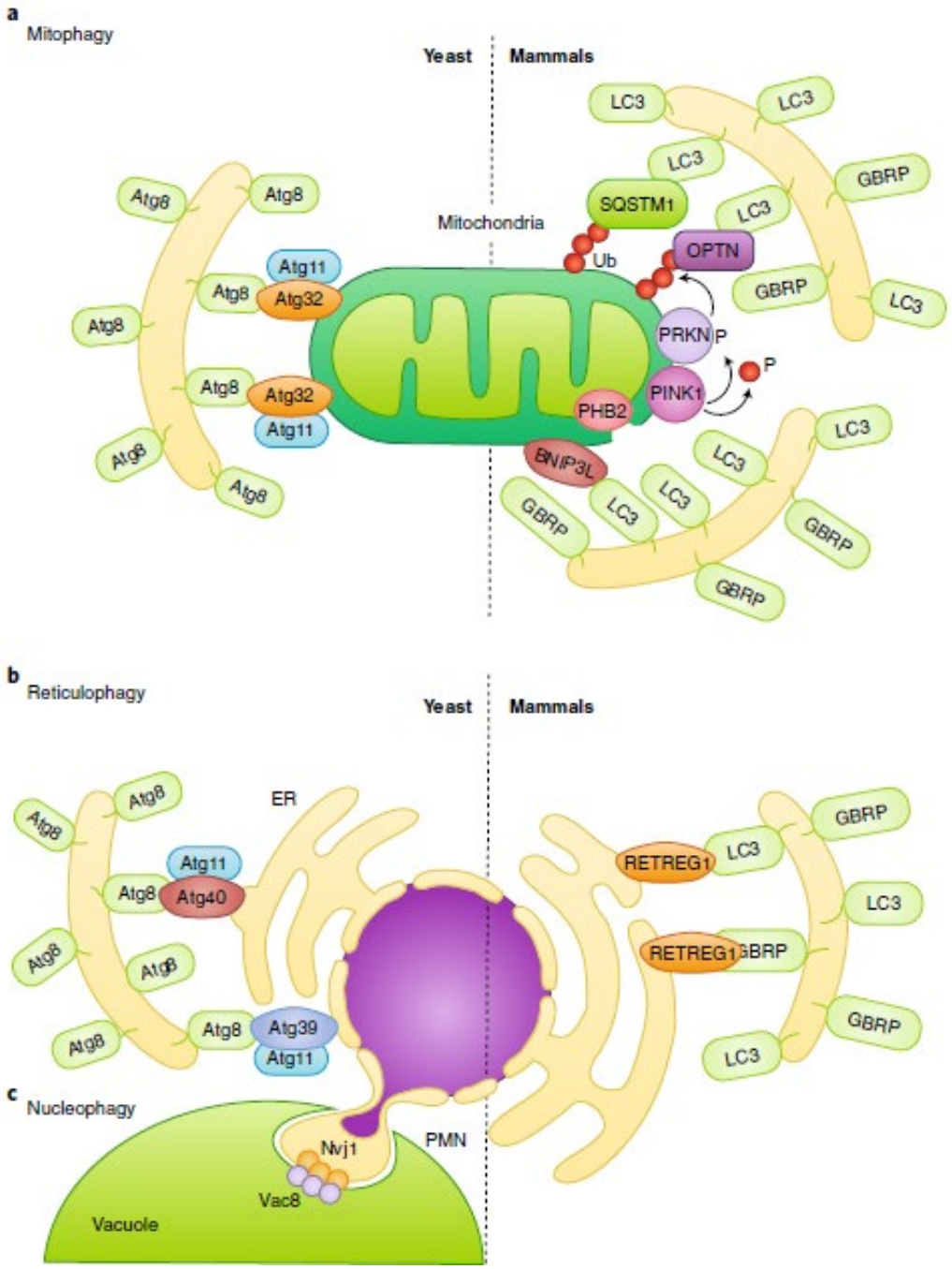

Figure 31. Mitophagy, Reticulophagy and Nucleophagy.

a) The yeast mitophagy receptor Atg32 links mitochondria to the phagophore by directly binding Atg8–PE; Atg11 functions as a scaffold. Several cargo receptors (not all shown) have been described for mammalian mitophagy. Mitochondria depolarization leads to PINK1 activation and phosphorylation of ubiquitin and PRKN, and OMM disruption exposes PHB2. Receptors link mitochondria targeted for degradation to the phagophore.

b) In yeast reticulophagy, Atg39 and Atg40 have been proposed as receptor proteins. Atg39 mediates the degradation of the perinuclear ER, and Atg40 the cytoplasmic ER. Both Atg39 and Atg40 link their respective ER sites to Atg8–PE-conjugated membranes for sequestration. Atg11 has been proposed as a scaffold protein for both Atg39 and Atg40-mediated reticulophagy. During mammalian reticulophagy, RETREG1/FAM134B tethers the cytoplasmic ER to LC3/GABARAP family members for membrane sequestration and degradation.

c) Because Atg39 specifically localizes to the perinuclear ER, Atg39-mediated degradation is also considered nucleophagy. During PMN, the nuclear envelope protein Nvj1 and vacuolar membrane protein Vac8 form nuclear-vacuolar junctions, which pinch off and engulf part of the nucleus inside the vacuole.

4.6 Reticulophagy

Reticulophagy describes the degradation of the ER by selective autophagy. Perturbation of ER function results in the accumulation of misfolded proteins and ER stress, which in turn triggers the unfolded protein response (UPR) and ER-associated degradation, in an effort to recover cellular homeostasis (Bravo et al., 2013). Autophagy is also activated by ER stress (Yorimitsu et al., 2006) as a means to control ER size and counterbalance the ER expansion after the UPR (Bernales et al., 2006; Schuck et al., 2014). Other stimuli such as rapamycin treatment and nutrient starvation also activate reticulophagy(Mochida et al., 2015) (Khaminets et al., 2015). Similar to other selective autophagy pathways, cargo receptors have been described for selective ER degradation. In yeast, starvation-induced reticulophagy is dependent on the cargo receptors Atg39 and Atg40; predicted transmembrane proteins that localize to the perinuclear and cytoplasmic ER, respectively. Consistent with their role as cargo receptors, Atg39 and Atg40 contain AIMs, and interact with both Atg8 and Atg11 (Mochida et al., 2015). In mammals, RETREG1/FAM134B is a reticulophagy cargo receptor protein, as well as an Atg40 functional homolog (Khaminets et al., 2015). Similar to Atg40, RETREG1 localizes to the cytoplasmic ER and interacts with LC3 and GABARAP family members through its LIR (Fig. 31b). Consistent with the reported role of reticulophagy in controlling ER size, RETREG1 overexpression increases ER fragmentation, whereas silencing of this protein results in ER expansion.

4.7 Nucleophagy

Nucleophagy has been described as the partial or bulk degradation of the nucleus by the vacuole/lysosome. Nucleophagy is closely related to reticulophagy because Atg39 localizes to, and mediates the degradation of, the perinuclear ER and nuclear envelope in yeast. However, to date no Atg39 functional homolog has been described in mammals and it is still unclear how

nucleophagy occurs in more complex eukaryotes. However, some studies have suggested selective autophagic degradation of chromatin (Changou et al., 2014) and the nuclear lamina (Dou et al., 2015) could play a role in preventing tumorigenesis.

Other types of nucleophagy termed piecemeal microautophagy of the nucleus (PMN) or micronucleophagy (Roberts et al., 2003), and late nucleophagy (Mijaljica et al., 2012) have been described in S. cerevisiae. During PMN the outer nuclear envelope protein Nvj1 interacts with the vacuolar membrane protein Vac8, forming nuclear-vacuolar junctions that pinch off parts of the nucleus, which are later engulfed and degraded by the vacuole (Roberts et al., 2003) (Fig. 31c). PMN is activated soon after nutrient starvation and depends on the core autophagic machinery (Kvam and Goldfarb, 2006) (Krick et al., 2008). In contrast, late nucleophagy occurs after prolonged starvation and is independent of Nvj1, Vac8 and some but not all core autophagy machinery (Mijaljica et al., 2012).

4.8 Lysophagy

Lysophagy is the selective degradation of damaged lysosomes by autophagy. Leakage of lysosomal enzymes into the cytosol due to lysosomal membrane rupture leads to lysosomal cell death (Aits and Jaattela, 2013). Therefore, the removal of damaged lysosomes is necessary to maintain cellular homeostasis. LGALS3 (galectin 3) binds to glycoproteins exposed upon lysosomal membrane damage and colocalizes with LC3, working as a key lysophagy marker (Maejima et al., 2013). Even though the specific mechanisms behind lysophagy are yet to be discovered, two independent reports have suggested a model in which damaged lysosomes are selectively degraded in a ubiquitin-SQSTM1-LC3-dependent manner (Hung et al., 2013; Maejima et al., 2013) (Fig. 32a). Thus, lysosome degradation appears analogous to other types of organelle-selective autophagy such as mitophagy and pexophagy. Still, many questions regarding

the specific ubiquitination targets and their regulation remain. At the same time, specific physiological conditions where lysophagy is triggered will need to be determined.

4.9 Xenophagy

Xenophagy is the collective term used for the selective autophagic degradation of intracellular pathogens including viruses, bacteria and fungi, which constitutes an important part of the immune response (Gomes and Dikic, 2014; Colombo et al., 2006). Once again, ubiquitination and cargo receptor binding play an important role in xenophagy. Following Salmonella typhimurium infection and release into the cytosol, bacterial proteins are rapidly ubiquitinated and recognized by the cargo receptors SQSTM1 (Zheng et al., 2009), CALCOCO2 (Thurston et al., 2009) and OPTN (Wild et al., 2011). CALCOCO2 binding to invading bacteria depends on lectin LGALS8 recruitment to damaged bacteria-containing vesicles (Thurston et al., 2012). All three receptors possess ubiquitin binding domains and LIRs, thus mediating the interaction between the ubiquitinated bacteria and LC3/GABARAP family members for phagophore sequestration (Thurston et al., 2009; Wild et al., 2011; Zheng et al., 2009) (Fig. 32b). Wild et al. showed that these three cargo receptors can bind to the same bacterium (Wild et al., 2011). However, individual silencing of SQSTM1, CALCOCO2 or OPTN is sufficient to increase S. typhimurium replication (Thurston et al., 2009; Wild et al., 2011; Zheng et al., 2009). This finding suggests that all three cargo receptors have individual roles in xenophagy that cannot be compensated by the other two. Although probably linked to their individual ability to recruit other autophagy-inducing factors, further studies will be necessary to determine the specific contributions of each cargo receptor. Additionally, finding the specific pathogen proteins that are ubiquitinated will prove indispensable to therapeutically counter the strategies that pathogens have evolved to avoid autophagy.

Figure 32: Lysophagy and Xenophagy

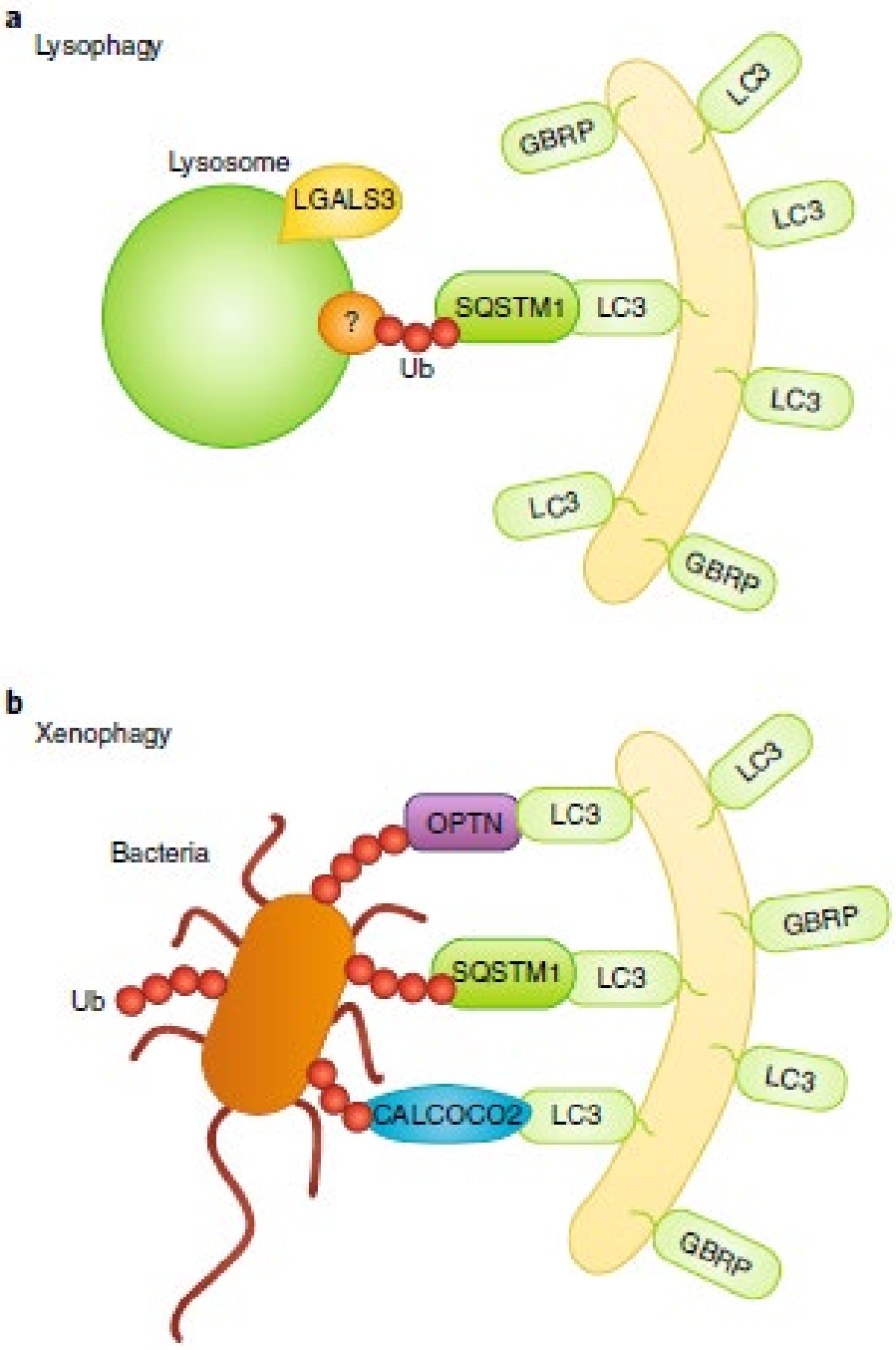

Figure 32. Lysophagy and Xenophagy.

a) During lysophagy, unknown lysosomal proteins are ubiquitinated and recognized by SQSTM1, which functions as a receptor, linking the damaged lysosomes with the LC3/GABARAP-conjugated sequestering membranes. LGALS3 binds to exposed lysosomal glycoproteins upon membrane rupture. A specific lysophagy mechanism remains to be elucidated.

b) In xenophagy, intracellular pathogens such as viruses and bacteria are recognized and ubiquitinated. SQSTM1, OPTN, CALCOCO2 and NBR1 have been described as receptor proteins.

4.10 Glycophagy

Glycophagy refers to the selective autophagy-mediated degradation of glycogen, the storage form of glucose in animal cells, by acid α-glucosidase within the lysosome (Delbridge et al., 2015). Glycophagy is distinct from cytosolic glycogen breakdown via glycogen phosphorylase, and these pathways likely have complementary roles in glycogen catabolism because they preferentially act on slightly different glycogen substrates (Ueno and Komatsu, 2017). The putative receptor for glycophagy is STBD1 (starch binding domain 1), which possesses a CBN20 glycan-binding domain (Zhu et al., 2014) as well as a LIR (Ueno and Komatsu, 2017). STBD1 localizes to glycogen particles and binds GABARAPL1 (Jiang et al., 2011) but not LC3B (Delbridge et al., 2015). Current evidence indicates an important role for glycophagy in cardiac and hepatic pathophysiology, and further mechanistic investigation of this process will be crucial for realizing the full scope of this pathway in carbohydrate metabolism.

4.11 Ferritinophagy

Ferritinophagy involves the degradation of the iron-sequestering protein ferritin (Kaur and Debnath, 2015). Iron is an essential component of various enzymes and proteins, making it indispensable for several cellular processes. However, free iron promotes ROS generation and is detrimental to the cell (Pantopoulos et al., 2012). Ferritin, consisting of multiple heavy chain (FTH1) and light chain (FTL) subunits, acts as a sink for iron when cellular iron levels are high. Conversely, when bioavailable iron levels are low, ferritin is mobilized by ferritinophagy to release iron (Kaur and Debnath, 2015).

Ferritinophagy was initially identified in atg5-/- MEF cells, which fail to degrade ferritin upon iron depletion (Asano et al., 2011). Selectivity during ferritinophagy is mediated by the receptor NCOA4 which specifically binds FTH1 and marks ferritin as an autophagic cargo (Mancias et al., 2014; Mancias et al., 2015). The level of NCOA4 is kept low in iron-replete conditions by the iron-dependent interaction between the HECT E3 ligase HERC2 and NCOA4, followed by the ubiquitination and proteasomal degradation of NCOA4 (Mancias et al., 2015). Upon iron-depletion NCOA4 is stabilized, which allows ferritin to be selectively degraded. NCOA4 does not contain a conventional LIR motif in contrast to other autophagy receptors (Kaur and Debnath, 2015). Therefore, how NCOA4 links its cargo to phagophores promises to be an intriguing question for the field.

4.12 Lipophagy

First discovered in hepatocytes and later in other cell types, lipophagy describes the selective degradation of lipid droplets (LD) by autophagy. In vivo and in vitro experiments have shown lipophagy occurs during basal and starvation conditions regulating cellular triglyceride content (Singh et al., 2009). Chaperone-mediated autophagy (CMA) has been proposed as a regulator of lipophagy. CMA would degrade the LD-associated PLIN (perilipin) proteins leading to lipophagy activation (Kaushik and Cuervo, 2015). While specific receptors for lipophagy have not been found, the metabolic implications associated with this process have highlighted new insights into energy utilization and possible therapeutic strategies for high-fat diet-induced pathologies. In *S. cerevisiae* lipid droplets are degraded in a process termed microlipophagy that depends on the core autophagy machinery, but not Atg11 (van Zutphen et al., 2014).

4.13 Conclusion and outstanding questions

Whereas selective autophagy occurs in different forms corresponding to various targets, there is a unifying principle: A receptor, that binds the cargo or that may be an integral part of the cargo as seen with Atg32, links the cargo to the autophagy machinery. Recent years have seen tremendous progress in understanding the mechanisms behind each of these selective processes; however, as I have highlighted here, there are still important unanswered questions. Exploring these queries will further our understanding of selective autophagy and may provide important clues for new therapeutic strategies.

4.14 References

Abeliovich, H., Zarei, M., Rigbolt, K.T., Youle, R.J., and Dengjel, J. (2013). Involvement of mitochondrial dynamics in the segregation of mitochondrial matrix proteins during stationary phase mitophagy. Nat Commun 4, 2789.

Aerts, L., Craessaerts, K., De Strooper, B., and Morais, V.A. (2015). PINK1 kinase catalytic activity is regulated by phosphorylation on serines 228 and 402. J Biol Chem 290, 2798-2811.

Aihara, M., Jin, X., Kurihara, Y., Yoshida, Y., Matsushima, Y., Oku, M., Hirota, Y., Saigusa, T., Aoki, Y., Uchiumi, T., et al. (2014). Tor and the Sin3-Rpd3 complex regulate expression of the mitophagy receptor protein Atg32 in yeast. J Cell Sci 127, 3184-3196.

Aits, S., and Jaattela, M. (2013). Lysosomal cell death at a glance. J Cell Sci 126, 1905-1912.

Aoki, Y., Kanki, T., Hirota, Y., Kurihara, Y., Saigusa, T., Uchiumi, T., and Kang, D. (2011). Phosphorylation of Serine 114 on Atg32 mediates mitophagy. Mol Biol Cell 22, 3206-3217.

Asano, T., Komatsu, M., Yamaguchi-Iwai, Y., Ishikawa, F., Mizushima, N., and Iwai, K. (2011). Distinct mechanisms of ferritin delivery to lysosomes in iron-depleted and iron-replete cells. Mol Cell Biol 31, 2040-2052.

Ashrafi, G., and Schwarz, T.L. (2013). The pathways of mitophagy for quality control and clearance of mitochondria. Cell Death Differ 20, 31-42.

Bernales, S., McDonald, K.L., and Walter, P. (2006). Autophagy counterbalances endoplasmic reticulum expansion during the unfolded protein response. PLoS Biol 4, e423.

Bingol, B., Tea, J.S., Phu, L., Reichelt, M., Bakalarski, C.E., Song, Q., Foreman, O., Kirkpatrick, D.S., and Sheng, M. (2014). The mitochondrial deubiquitinase USP30 opposes parkin-mediated mitophagy. Nature 510, 370-375.

Bordi, M., Nazio, F., and Campello, S. (2017). The Close Interconnection between Mitochondrial Dynamics and Mitophagy in Cancer. Front Oncol 7, 81.

Bravo, R., Parra, V., Gatica, D., Rodriguez, A.E., Torrealba, N., Paredes, F., Wang, Z.V., Zorzano, A., Hill, J.A., Jaimovich, E., et al. (2013). Endoplasmic reticulum and the unfolded protein response: dynamics and metabolic integration. Int Rev Cell Mol Biol 301, 215-290.

Changou, C.A., Chen, Y.R., Xing, L., Yen, Y., Chuang, F.Y., Cheng, R.H., Bold, R.J., Ann, D.K., and Kung, H.J. (2014). Arginine starvation-associated atypical cellular death involves mitochondrial dysfunction, nuclear DNA leakage, and chromatin autophagy. Proc Natl Acad Sci U S A 111, 14147-14152.

Chen, G., Han, Z., Feng, D., Chen, Y., Chen, L., Wu, H., Huang, L., Zhou, C., Cai, X., Fu, C., et al. (2014). A regulatory signaling loop comprising the PGAM5 phosphatase and CK2 controls receptor-mediated mitophagy. Mol Cell 54, 362-377.

Chen, M., Chen, Z., Wang, Y., Tan, Z., Zhu, C., Li, Y., Han, Z., Chen, L., Gao, R., Liu, L., et al. (2016). Mitophagy receptor FUNDC1 regulates mitochondrial dynamics and mitophagy. Autophagy 12, 689-702.

Chen, Y., and Dorn, G.W., 2nd (2013). PINK1-phosphorylated mitofusin 2 is a Parkin receptor for culling damaged mitochondria. Science 340, 471-475.

Chourasia, A.H., Boland, M.L., and Macleod, K.F. (2015). Mitophagy and cancer. Cancer Metab 3, 4.

Chu, C.T., Ji, J., Dagda, R.K., Jiang, J.F., Tyurina, Y.Y., Kapralov, A.A., Tyurin, V.A., Yanamala, N., Shrivastava, I.H., Mohammadyani, D., et al. (2013). Cardiolipin

externalization to the outer mitochondrial membrane acts as an elimination signal for mitophagy in neuronal cells. Nat Cell Biol 15, 1197-1205.
Clausen, T.H., Lamark, T., Isakson, P., Finley, K., Larsen, K.B., Brech, A., Overvatn, A., Stenmark, H., Bjorkoy, G., Simonsen, A., et al. (2010). p62/SQSTM1 and ALFY interact to facilitate the formation of p62 bodies/ALIS and their degradation by autophagy. Autophagy 6, 330-344.
Colombo, M.I., Gutierrez, M.G., and Romano, P.S. (2006). The two faces of autophagy: Coxiella and Mycobacterium. Autophagy 2, 162-164.
Delbridge, L.M., Mellor, K.M., Taylor, D.J., and Gottlieb, R.A. (2015). Myocardial autophagic energy stress responses--macroautophagy, mitophagy, and glycophagy. Am J Physiol Heart Circ Physiol 308, H1194-1204.
Deosaran, E., Larsen, K.B., Hua, R., Sargent, G., Wang, Y., Kim, S., Lamark, T., Jauregui, M., Law, K., Lippincott-Schwartz, J., et al. (2013). NBR1 acts as an autophagy receptor for peroxisomes. J Cell Sci 126, 939-952.
Dou, Z., Xu, C., Donahue, G., Shimi, T., Pan, J.A., Zhu, J., Ivanov, A., Capell, B.C., Drake, A.M., Shah, P.P., et al. (2015). Autophagy mediates degradation of nuclear lamina. Nature 527, 105-109.
Durcan, T.M., and Fon, E.A. (2015). The three 'P's of mitophagy: PARKIN, PINK1, and post-translational modifications. Genes Dev 29, 989-999.
Farre, J.C., Burkenroad, A., Burnett, S.F., and Subramani, S. (2013). Phosphorylation of mitophagy and pexophagy receptors coordinates their interaction with Atg8 and Atg11. EMBO Rep 14, 441-449.
Farre, J.C., Manjithaya, R., Mathewson, R.D., and Subramani, S. (2008). PpAtg30 tags peroxisomes for turnover by selective autophagy. Dev Cell 14, 365-376.
Feng, Y., He, D., Yao, Z., and Klionsky, D.J. (2014). The machinery of macroautophagy. Cell Res 24, 24-41.
Filimonenko, M., Isakson, P., Finley, K.D., Anderson, M., Jeong, H., Melia, T.J., Bartlett, B.J., Myers, K.M., Birkeland, H.C., Lamark, T., et al. (2010). The selective macroautophagic degradation of aggregated proteins requires the PI3P-binding protein Alfy. Mol Cell 38, 265-279.
Gegg, M.E., Cooper, J.M., Chau, K.Y., Rojo, M., Schapira, A.H., and Taanman, J.W. (2010). Mitofusin 1 and mitofusin 2 are ubiquitinated in a PINK1/parkin-dependent manner upon induction of mitophagy. Hum Mol Genet 19, 4861-4870.
Geisler, S., Holmstrom, K.M., Skujat, D., Fiesel, F.C., Rothfuss, O.C., Kahle, P.J., and Springer, W. (2010). PINK1/Parkin-mediated mitophagy is dependent on VDAC1 and p62/SQSTM1. Nat Cell Biol 12, 119-131.
Georgakopoulos, N.D., Wells, G., and Campanella, M. (2017). The pharmacological regulation of cellular mitophagy. Nat Chem Biol 13, 136-146.
Gomes, L.C., and Dikic, I. (2014). Autophagy in antimicrobial immunity. Mol Cell 54, 224-233.
Grou, C.P., Carvalho, A.F., Pinto, M.P., Alencastre, I.S., Rodrigues, T.A., Freitas, M.O., Francisco, T., Sa-Miranda, C., and Azevedo, J.E. (2009). The peroxisomal protein import machinery--a case report of transient ubiquitination with a new flavor. Cell Mol Life Sci 66, 254-262.
Hamacher-Brady, A., and Brady, N.R. (2016). Mitophagy programs: mechanisms and physiological implications of mitochondrial targeting by autophagy. Cell Mol Life Sci 73, 775-795.

Hara-Kuge, S., and Fujiki, Y. (2008). The peroxin Pex14p is involved in LC3-dependent degradation of mammalian peroxisomes. Exp Cell Res 314, 3531-3541.
He, C., and Klionsky, D.J. (2009). Regulation mechanisms and signaling pathways of autophagy. Annu Rev Genet 43, 67-93.
Hsieh, C.H., Shaltouki, A., Gonzalez, A.E., Bettencourt da Cruz, A., Burbulla, L.F., St Lawrence, E., Schule, B., Krainc, D., Palmer, T.D., and Wang, X. (2016). Functional Impairment in Miro Degradation and Mitophagy Is a Shared Feature in Familial and Sporadic Parkinson's Disease. Cell Stem Cell 19, 709-724.
Hung, Y.H., Chen, L.M., Yang, J.Y., and Yang, W.Y. (2013). Spatiotemporally controlled induction of autophagy-mediated lysosome turnover. Nat Commun 4, 2111.
Hutchins, M.U., Veenhuis, M., and Klionsky, D.J. (1999). Peroxisome degradation in Saccharomyces cerevisiae is dependent on machinery of macroautophagy and the Cvt pathway. J Cell Sci 112 (Pt 22), 4079-4087.
Ichimura, Y., Kirisako, T., Takao, T., Satomi, Y., Shimonishi, Y., Ishihara, N., Mizushima, N., Tanida, I., Kominami, E., Ohsumi, M., et al. (2000). A ubiquitin-like system mediates protein lipidation. Nature 408, 488-492.
Ichimura, Y., Kumanomidou, T., Sou, Y.S., Mizushima, T., Ezaki, J., Ueno, T., Kominami, E., Yamane, T., Tanaka, K., and Komatsu, M. (2008). Structural basis for sorting mechanism of p62 in selective autophagy. J Biol Chem 283, 22847-22857.
Jiang, S., Wells, C.D., and Roach, P.J. (2011). Starch-binding domain-containing protein 1 (Stbd1) and glycogen metabolism: Identification of the Atg8 family interacting motif (AIM) in Stbd1 required for interaction with GABARAPL1. Biochem Biophys Res Commun 413, 420-425.
Jin, M., Liu, X., and Klionsky, D.J. (2013). SnapShot: Selective autophagy. Cell 152, 368-368 e362.
Kane, L.A., Lazarou, M., Fogel, A.I., Li, Y., Yamano, K., Sarraf, S.A., Banerjee, S., and Youle, R.J. (2014). PINK1 phosphorylates ubiquitin to activate Parkin E3 ubiquitin ligase activity. J Cell Biol 205, 143-153.
Kanki, T., Furukawa, K., and Yamashita, S. (2015). Mitophagy in yeast: Molecular mechanisms and physiological role. Biochim Biophys Acta 1853, 2756-2765.
Kanki, T., and Klionsky, D.J. (2008). Mitophagy in yeast occurs through a selective mechanism. J Biol Chem 283, 32386-32393.
Kanki, T., Kurihara, Y., Jin, X., Goda, T., Ono, Y., Aihara, M., Hirota, Y., Saigusa, T., Aoki, Y., Uchiumi, T., et al. (2013). Casein kinase 2 is essential for mitophagy. EMBO Rep 14, 788-794.
Kanki, T., Wang, K., Cao, Y., Baba, M., and Klionsky, D.J. (2009). Atg32 is a mitochondrial protein that confers selectivity during mitophagy. Dev Cell 17, 98-109.
Kaur, J., and Debnath, J. (2015). Autophagy at the crossroads of catabolism and anabolism. Nat Rev Mol Cell Biol 16, 461-472.
Kaushik, S., and Cuervo, A.M. (2015). Degradation of lipid droplet-associated proteins by chaperone-mediated autophagy facilitates lipolysis. Nat Cell Biol 17, 759-770.
Khaminets, A., Heinrich, T., Mari, M., Grumati, P., Huebner, A.K., Akutsu, M., Liebmann, L., Stolz, A., Nietzsche, S., Koch, N., et al. (2015). Regulation of endoplasmic reticulum turnover by selective autophagy. Nature 522, 354-358.

Kim, J., Kamada, Y., Stromhaug, P.E., Guan, J., Hefner-Gravink, A., Baba, M., Scott, S.V., Ohsumi, Y., Dunn, W.A., Jr., and Klionsky, D.J. (2001). Cvt9/Gsa9 functions in sequestering selective cytosolic cargo destined for the vacuole. J Cell Biol 153, 381-396.

Kim, P.K., Hailey, D.W., Mullen, R.T., and Lippincott-Schwartz, J. (2008). Ubiquitin signals autophagic degradation of cytosolic proteins and peroxisomes. Proc Natl Acad Sci U S A 105, 20567-20574.

Kirkin, V., Lamark, T., Sou, Y.S., Bjorkoy, G., Nunn, J.L., Bruun, J.A., Shvets, E., McEwan, D.G., Clausen, T.H., Wild, P., et al. (2009). A role for NBR1 in autophagosomal degradation of ubiquitinated substrates. Mol Cell 33, 505-516.

Klionsky, D.J., and Ohsumi, Y. (1999). Vacuolar import of proteins and organelles from the cytoplasm. Annu Rev Cell Dev Biol 15, 1-32.

Klionsky, D.J., and Schulman, B.A. (2014). Dynamic regulation of macroautophagy by distinctive ubiquitin-like proteins. Nat Struct Mol Biol 21, 336-345.

Kondapalli, C., Kazlauskaite, A., Zhang, N., Woodroof, H.I., Campbell, D.G., Gourlay, R., Burchell, L., Walden, H., Macartney, T.J., Deak, M., et al. (2012). PINK1 is activated by mitochondrial membrane potential depolarization and stimulates Parkin E3 ligase activity by phosphorylating Serine 65. Open Biol 2, 120080.

Kondo-Okamoto, N., Noda, N.N., Suzuki, S.W., Nakatogawa, H., Takahashi, I., Matsunami, M., Hashimoto, A., Inagaki, F., Ohsumi, Y., and Okamoto, K. (2012). Autophagy-related protein 32 acts as autophagic degron and directly initiates mitophagy. J Biol Chem 287, 10631-10638.

Korolchuk, V.I., Menzies, F.M., and Rubinsztein, D.C. (2010). Mechanisms of cross-talk between the ubiquitin-proteasome and autophagy-lysosome systems. FEBS Lett 584, 1393-1398.

Koyano, F., Okatsu, K., Kosako, H., Tamura, Y., Go, E., Kimura, M., Kimura, Y., Tsuchiya, H., Yoshihara, H., Hirokawa, T., et al. (2014). Ubiquitin is phosphorylated by PINK1 to activate parkin. Nature 510, 162-166.

Krick, R., Muehe, Y., Prick, T., Bremer, S., Schlotterhose, P., Eskelinen, E.L., Millen, J., Goldfarb, D.S., and Thumm, M. (2008). Piecemeal microautophagy of the nucleus requires the core macroautophagy genes. Mol Biol Cell 19, 4492-4505.

Kurihara, Y., Kanki, T., Aoki, Y., Hirota, Y., Saigusa, T., Uchiumi, T., and Kang, D. (2012). Mitophagy plays an essential role in reducing mitochondrial production of reactive oxygen species and mutation of mitochondrial DNA by maintaining mitochondrial quantity and quality in yeast. J Biol Chem 287, 3265-3272.

Kvam, E., and Goldfarb, D.S. (2006). Structure and function of nucleus-vacuole junctions: outer-nuclear-membrane targeting of Nvj1p and a role in tryptophan uptake. J Cell Sci 119, 3622-3633.

Lamark, T., Kirkin, V., Dikic, I., and Johansen, T. (2009). NBR1 and p62 as cargo receptors for selective autophagy of ubiquitinated targets. Cell Cycle 8, 1986-1990.

Lazarou, M., Sliter, D.A., Kane, L.A., Sarraf, S.A., Wang, C., Burman, J.L., Sideris, D.P., Fogel, A.I., and Youle, R.J. (2015). The ubiquitin kinase PINK1 recruits autophagy receptors to induce mitophagy. Nature 524, 309-314.

Leber, R., Silles, E., Sandoval, I.V., and Mazon, M.J. (2001). Yol082p, a novel CVT protein involved in the selective targeting of aminopeptidase I to the yeast vacuole. J Biol Chem 276, 29210-29217.

Liu, L., Feng, D., Chen, G., Chen, M., Zheng, Q., Song, P., Ma, Q., Zhu, C., Wang, R., Qi, W., et al. (2012). Mitochondrial outer-membrane protein FUNDC1 mediates hypoxia-induced mitophagy in mammalian cells. Nat Cell Biol 14, 177-185.

Liu, L., Sakakibara, K., Chen, Q., and Okamoto, K. (2014). Receptor-mediated mitophagy in yeast and mammalian systems. Cell Res 24, 787-795.

Lu, K., den Brave, F., and Jentsch, S. (2017). Receptor oligomerization guides pathway choice between proteasomal and autophagic degradation. Nat Cell Biol 19, 732-739.

Lu, K., Psakhye, I., and Jentsch, S. (2014a). Autophagic clearance of polyQ proteins mediated by ubiquitin-Atg8 adaptors of the conserved CUET protein family. Cell 158, 549-563.

Lu, K., Psakhye, I., and Jentsch, S. (2014b). A new class of ubiquitin-Atg8 receptors involved in selective autophagy and polyQ protein clearance. Autophagy 10, 2381-2382.

Lynch-Day, M.A., and Klionsky, D.J. (2010). The Cvt pathway as a model for selective autophagy. FEBS Lett 584, 1359-1366.

Lystad, A.H., Ichimura, Y., Takagi, K., Yang, Y., Pankiv, S., Kanegae, Y., Kageyama, S., Suzuki, M., Saito, I., Mizushima, T., et al. (2014). Structural determinants in GABARAP required for the selective binding and recruitment of ALFY to LC3B-positive structures. EMBO Rep 15, 557-565.

Maejima, I., Takahashi, A., Omori, H., Kimura, T., Takabatake, Y., Saitoh, T., Yamamoto, A., Hamasaki, M., Noda, T., Isaka, Y., et al. (2013). Autophagy sequesters damaged lysosomes to control lysosomal biogenesis and kidney injury. EMBO J 32, 2336-2347.

Mancias, J.D., Pontano Vaites, L., Nissim, S., Biancur, D.E., Kim, A.J., Wang, X., Liu, Y., Goessling, W., Kimmelman, A.C., and Harper, J.W. (2015). Ferritinophagy via NCOA4 is required for erythropoiesis and is regulated by iron dependent HERC2-mediated proteolysis. Elife 4.

Mancias, J.D., Wang, X., Gygi, S.P., Harper, J.W., and Kimmelman, A.C. (2014). Quantitative proteomics identifies NCOA4 as the cargo receptor mediating ferritinophagy. Nature 509, 105-109.

Mao, K., Wang, K., Liu, X., and Klionsky, D.J. (2013). The scaffold protein Atg11 recruits fission machinery to drive selective mitochondria degradation by autophagy. Dev Cell 26, 9-18.

Mao, K., Wang, K., Zhao, M., Xu, T., and Klionsky, D.J. (2011). Two MAPK-signaling pathways are required for mitophagy in Saccharomyces cerevisiae. J Cell Biol 193, 755-767.

Matsushima, M., Fujiwara, T., Takahashi, E., Minaguchi, T., Eguchi, Y., Tsujimoto, Y., Suzumori, K., and Nakamura, Y. (1998). Isolation, mapping, and functional analysis of a novel human cDNA (BNIP3L) encoding a protein homologous to human NIP3. Genes Chromosomes Cancer 21, 230-235.

McLelland, G.L., Lee, S.A., McBride, H.M., and Fon, E.A. (2016). Syntaxin-17 delivers PINK1/parkin-dependent mitochondrial vesicles to the endolysosomal system. J Cell Biol 214, 275-291.

Mijaljica, D., Prescott, M., and Devenish, R.J. (2012). A late form of nucleophagy in Saccharomyces cerevisiae. PLoS One 7, e40013.

Mochida, K., Oikawa, Y., Kimura, Y., Kirisako, H., Hirano, H., Ohsumi, Y., and Nakatogawa, H. (2015). Receptor-mediated selective autophagy degrades the endoplasmic reticulum and the nucleus. Nature 522, 359-362.

Motley, A.M., Nuttall, J.M., and Hettema, E.H. (2012). Pex3-anchored Atg36 tags peroxisomes for degradation in Saccharomyces cerevisiae. EMBO J 31, 2852-2868.

Nakatogawa, H., and Mochida, K. (2015). Reticulophagy and nucleophagy: New findings and unsolved issues. Autophagy 11, 2377-2378.
Narendra, D., Walker, J.E., and Youle, R. (2012). Mitochondrial quality control mediated by PINK1 and Parkin: links to parkinsonism. Cold Spring Harb Perspect Biol 4.
Narendra, D.P., Jin, S.M., Tanaka, A., Suen, D.F., Gautier, C.A., Shen, J., Cookson, M.R., and Youle, R.J. (2010). PINK1 is selectively stabilized on impaired mitochondria to activate Parkin. PLoS Biol 8, e1000298.
Nazarko, T.Y., Farre, J.C., and Subramani, S. (2009). Peroxisome size provides insights into the function of autophagy-related proteins. Mol Biol Cell 20, 3828-3839.
Nazarko, T.Y., Ozeki, K., Till, A., Ramakrishnan, G., Lotfi, P., Yan, M., and Subramani, S. (2014). Peroxisomal Atg37 binds Atg30 or palmitoyl-CoA to regulate phagophore formation during pexophagy. J Cell Biol 204, 541-557.
Nguyen, T.N., Padman, B.S., and Lazarou, M. (2016). Deciphering the Molecular Signals of PINK1/Parkin Mitophagy. Trends Cell Biol 26, 733-744.
Ni, H.M., Williams, J.A., and Ding, W.X. (2015). Mitochondrial dynamics and mitochondrial quality control. Redox Biol 4, 6-13.
Noda, N.N., Kumeta, H., Nakatogawa, H., Satoo, K., Adachi, W., Ishii, J., Fujioka, Y., Ohsumi, Y., and Inagaki, F. (2008). Structural basis of target recognition by Atg8/LC3 during selective autophagy. Genes Cells 13, 1211-1218.
Nordgren, M., Francisco, T., Lismont, C., Hennebel, L., Brees, C., Wang, B., Van Veldhoven, P.P., Azevedo, J.E., and Fransen, M. (2015). Export-deficient monoubiquitinated PEX5 triggers peroxisome removal in SV40 large T antigen-transformed mouse embryonic fibroblasts. Autophagy 11, 1326-1340.
Novak, I., and Dikic, I. (2011). Autophagy receptors in developmental clearance of mitochondria. Autophagy 7, 301-303.
Novak, I., Kirkin, V., McEwan, D.G., Zhang, J., Wild, P., Rozenknop, A., Rogov, V., Lohr, F., Popovic, D., Occhipinti, A., et al. (2010). Nix is a selective autophagy receptor for mitochondrial clearance. EMBO Rep 11, 45-51.
Okamoto, K., Kondo-Okamoto, N., and Ohsumi, Y. (2009). Mitochondria-anchored receptor Atg32 mediates degradation of mitochondria via selective autophagy. Dev Cell 17, 87-97.
Palikaras, K., Lionaki, E., and Tavernarakis, N. (2016). Mitophagy: In sickness and in health. Mol Cell Oncol 3, e1056332.
Pankiv, S., Clausen, T.H., Lamark, T., Brech, A., Bruun, J.A., Outzen, H., Overvatn, A., Bjorkoy, G., and Johansen, T. (2007). p62/SQSTM1 binds directly to Atg8/LC3 to facilitate degradation of ubiquitinated protein aggregates by autophagy. J Biol Chem 282, 24131-24145.
Pantopoulos, K., Porwal, S.K., Tartakoff, A., and Devireddy, L. (2012). Mechanisms of mammalian iron homeostasis. Biochemistry 51, 5705-5724.
Pfaffenwimmer, T., Reiter, W., Brach, T., Nogellova, V., Papinski, D., Schuschnig, M., Abert, C., Ammerer, G., Martens, S., and Kraft, C. (2014). Hrr25 kinase promotes selective autophagy by phosphorylating the cargo receptor Atg19. EMBO Rep 15, 862-870.
Pickford, F., Masliah, E., Britschgi, M., Lucin, K., Narasimhan, R., Jaeger, P.A., Small, S., Spencer, B., Rockenstein, E., Levine, B., et al. (2008). The autophagy-related protein beclin 1 shows reduced expression in early Alzheimer disease and regulates amyloid beta accumulation in mice. J Clin Invest 118, 2190-2199.

Pickrell, A.M., and Youle, R.J. (2015). The roles of PINK1, parkin, and mitochondrial fidelity in Parkinson's disease. Neuron 85, 257-273.
Ravikumar, B., Vacher, C., Berger, Z., Davies, J.E., Luo, S., Oroz, L.G., Scaravilli, F., Easton, D.F., Duden, R., O'Kane, C.J., et al. (2004). Inhibition of mTOR induces autophagy and reduces toxicity of polyglutamine expansions in fly and mouse models of Huntington disease. Nat Genet 36, 585-595.
Redmann, M., Dodson, M., Boyer-Guittaut, M., Darley-Usmar, V., and Zhang, J. (2014). Mitophagy mechanisms and role in human diseases. Int J Biochem Cell Biol 53, 127-133.
Roberts, P., Moshitch-Moshkovitz, S., Kvam, E., O'Toole, E., Winey, M., and Goldfarb, D.S. (2003). Piecemeal microautophagy of nucleus in Saccharomyces cerevisiae. Mol Biol Cell 14, 129-141.
Rogov, V.V., Stolz, A., Ravichandran, A.C., Rios-Szwed, D.O., Suzuki, H., Kniss, A., Lohr, F., Wakatsuki, S., Dotsch, V., Dikic, I., et al. (2017a). Structural and functional analysis of the GABARAP interaction motif (GIM). EMBO Rep 18, 1382-1396.
Rogov, V.V., Suzuki, H., Marinkovic, M., Lang, V., Kato, R., Kawasaki, M., Buljubasic, M., Sprung, M., Rogova, N., Wakatsuki, S., et al. (2017b). Phosphorylation of the mitochondrial autophagy receptor Nix enhances its interaction with LC3 proteins. Sci Rep 7, 1131.
Sandoval, H., Thiagarajan, P., Dasgupta, S.K., Schumacher, A., Prchal, J.T., Chen, M., and Wang, J. (2008). Essential role for Nix in autophagic maturation of erythroid cells. Nature 454, 232-235.
Sargent, G., van Zutphen, T., Shatseva, T., Zhang, L., Di Giovanni, V., Bandsma, R., and Kim, P.K. (2016). PEX2 is the E3 ubiquitin ligase required for pexophagy during starvation. J Cell Biol 214, 677-690.
Sarkar, S., Ravikumar, B., and Rubinsztein, D.C. (2009). Autophagic clearance of aggregate-prone proteins associated with neurodegeneration. Methods Enzymol 453, 83-110.
Schuck, S., Gallagher, C.M., and Walter, P. (2014). ER-phagy mediates selective degradation of endoplasmic reticulum independently of the core autophagy machinery. J Cell Sci 127, 4078-4088.
Scott, S.V., Guan, J., Hutchins, M.U., Kim, J., and Klionsky, D.J. (2001). Cvt19 is a receptor for the cytoplasm-to-vacuole targeting pathway. Mol Cell 7, 1131-1141.
Sentelle, R.D., Senkal, C.E., Jiang, W., Ponnusamy, S., Gencer, S., Selvam, S.P., Ramshesh, V.K., Peterson, Y.K., Lemasters, J.J., Szulc, Z.M., et al. (2012). Ceramide targets autophagosomes to mitochondria and induces lethal mitophagy. Nat Chem Biol 8, 831-838.
Shen, W.C., Li, H.Y., Chen, G.C., Chern, Y., and Tu, P.H. (2015). Mutations in the ubiquitin-binding domain of OPTN/optineurin interfere with autophagy-mediated degradation of misfolded proteins by a dominant-negative mechanism. Autophagy 11, 685-700.
Shen, Z., Li, Y., Gasparski, A.N., Abeliovich, H., and Greenberg, M.L. (2017). Cardiolipin Regulates Mitophagy through the Protein Kinase C Pathway. J Biol Chem 292, 2916-2923.
Sheng, Z.H., and Cai, Q. (2012). Mitochondrial transport in neurons: impact on synaptic homeostasis and neurodegeneration. Nat Rev Neurosci 13, 77-93.
Shintani, T., Huang, W.P., Stromhaug, P.E., and Klionsky, D.J. (2002). Mechanism of cargo selection in the cytoplasm to vacuole targeting pathway. Dev Cell 3, 825-837.
Shirihai, O.S., Song, M., and Dorn, G.W., 2nd (2015). How mitochondrial dynamism orchestrates mitophagy. Circ Res 116, 1835-1849.
Simonsen, A., Birkeland, H.C., Gillooly, D.J., Mizushima, N., Kuma, A., Yoshimori, T., Slagsvold, T., Brech, A., and Stenmark, H. (2004). Alfy, a novel FYVE-domain-containing

protein associated with protein granules and autophagic membranes. J Cell Sci 117, 4239-4251.
Singh, R., Kaushik, S., Wang, Y., Xiang, Y., Novak, I., Komatsu, M., Tanaka, K., Cuervo, A.M., and Czaja, M.J. (2009). Autophagy regulates lipid metabolism. Nature 458, 1131-1135.
Sowter, H.M., Ratcliffe, P.J., Watson, P., Greenberg, A.H., and Harris, A.L. (2001). HIF-1-dependent regulation of hypoxic induction of the cell death factors BNIP3 and NIX in human tumors. Cancer Res 61, 6669-6673.
Stotland, A., and Gottlieb, R.A. (2015). Mitochondrial quality control: Easy come, easy go. Biochim Biophys Acta 1853, 2802-2811.
Sugiura, A., McLelland, G.L., Fon, E.A., and McBride, H.M. (2014). A new pathway for mitochondrial quality control: mitochondrial-derived vesicles. EMBO J 33, 2142-2156.
Suzuki, K., Kondo, C., Morimoto, M., and Ohsumi, Y. (2010). Selective transport of alpha-mannosidase by autophagic pathways: identification of a novel receptor, Atg34p. J Biol Chem 285, 30019-30025.
Thurston, T.L., Ryzhakov, G., Bloor, S., von Muhlinen, N., and Randow, F. (2009). The TBK1 adaptor and autophagy receptor NDP52 restricts the proliferation of ubiquitin-coated bacteria. Nat Immunol 10, 1215-1221.
Thurston, T.L., Wandel, M.P., von Muhlinen, N., Foeglein, A., and Randow, F. (2012). Galectin 8 targets damaged vesicles for autophagy to defend cells against bacterial invasion. Nature 482, 414-418.
Trempe, J.F., Sauve, V., Grenier, K., Seirafi, M., Tang, M.Y., Menade, M., Al-Abdul-Wahid, S., Krett, J., Wong, K., Kozlov, G., et al. (2013). Structure of parkin reveals mechanisms for ubiquitin ligase activation. Science 340, 1451-1455.
Ueno, T., and Komatsu, M. (2017). Autophagy in the liver: functions in health and disease. Nat Rev Gastroenterol Hepatol 14, 170-184.
van Zutphen, T., Todde, V., de Boer, R., Kreim, M., Hofbauer, H.F., Wolinski, H., Veenhuis, M., van der Klei, I.J., and Kohlwein, S.D. (2014). Lipid droplet autophagy in the yeast Saccharomyces cerevisiae. Mol Biol Cell 25, 290-301.
Verhoef, L.G., Lindsten, K., Masucci, M.G., and Dantuma, N.P. (2002). Aggregate formation inhibits proteasomal degradation of polyglutamine proteins. Hum Mol Genet 11, 2689-2700.
Von Stockum, S., Nardin, A., Schrepfer, E., and Ziviani, E. (2016). Mitochondrial dynamics and mitophagy in Parkinson's disease: A fly point of view. Neurobiol Dis 90, 58-67.
Wang, K., Jin, M., Liu, X., and Klionsky, D.J. (2013). Proteolytic processing of Atg32 by the mitochondrial i-AAA protease Yme1 regulates mitophagy. Autophagy 9, 1828-1836.
Wang, X., Winter, D., Ashrafi, G., Schlehe, J., Wong, Y.L., Selkoe, D., Rice, S., Steen, J., LaVoie, M.J., and Schwarz, T.L. (2011). PINK1 and Parkin target Miro for phosphorylation and degradation to arrest mitochondrial motility. Cell 147, 893-906.
Wei, Y., Chiang, W.C., Sumpter, R., Jr., Mishra, P., and Levine, B. (2017). Prohibitin 2 Is an Inner Mitochondrial Membrane Mitophagy Receptor. Cell 168, 224-238 e210.
Wild, P., Farhan, H., McEwan, D.G., Wagner, S., Rogov, V.V., Brady, N.R., Richter, B., Korac, J., Waidmann, O., Choudhary, C., et al. (2011). Phosphorylation of the autophagy receptor optineurin restricts Salmonella growth. Science 333, 228-233.
Winslow, A.R., Chen, C.W., Corrochano, S., Acevedo-Arozena, A., Gordon, D.E., Peden, A.A., Lichtenberg, M., Menzies, F.M., Ravikumar, B., Imarisio, S., et al. (2010). alpha-Synuclein impairs macroautophagy: implications for Parkinson's disease. J Cell Biol 190, 1023-1037.

Wu, W., Lin, C., Wu, K., Jiang, L., Wang, X., Li, W., Zhuang, H., Zhang, X., Chen, H., Li, S., et al. (2016). FUNDC1 regulates mitochondrial dynamics at the ER-mitochondrial contact site under hypoxic conditions. EMBO J 35, 1368-1384.

Wurzer, B., Zaffagnini, G., Fracchiolla, D., Turco, E., Abert, C., Romanov, J., and Martens, S. (2015). Oligomerization of p62 allows for selection of ubiquitinated cargo and isolation membrane during selective autophagy. Elife 4, e08941.

Xie, Z., Nair, U., and Klionsky, D.J. (2008). Atg8 controls phagophore expansion during autophagosome formation. Mol Biol Cell 19, 3290-3298.

Yamano, K., and Youle, R.J. (2013). PINK1 is degraded through the N-end rule pathway. Autophagy 9, 1758-1769.

Yamashita, S., Abe, K., Tatemichi, Y., and Fujiki, Y. (2014). The membrane peroxin PEX3 induces peroxisome-ubiquitination-linked pexophagy. Autophagy 10, 1549-1564.

Yorimitsu, T., and Klionsky, D.J. (2005). Atg11 links cargo to the vesicle-forming machinery in the cytoplasm to vacuole targeting pathway. Mol Biol Cell 16, 1593-1605.

Yorimitsu, T., Nair, U., Yang, Z., and Klionsky, D.J. (2006). Endoplasmic reticulum stress triggers autophagy. J Biol Chem 281, 30299-30304.

Zhang, H., Bosch-Marce, M., Shimoda, L.A., Tan, Y.S., Baek, J.H., Wesley, J.B., Gonzalez, F.J., and Semenza, G.L. (2008). Mitochondrial autophagy is an HIF-1-dependent adaptive metabolic response to hypoxia. J Biol Chem 283, 10892-10903.

Zhang, J., Loyd, M.R., Randall, M.S., Waddell, M.B., Kriwacki, R.W., and Ney, P.A. (2012). A short linear motif in BNIP3L (NIX) mediates mitochondrial clearance in reticulocytes. Autophagy 8, 1325-1332.

Zhang, J., Tripathi, D.N., Jing, J., Alexander, A., Kim, J., Powell, R.T., Dere, R., Tait-Mulder, J., Lee, J.H., Paull, T.T., et al. (2015). ATM functions at the peroxisome to induce pexophagy in response to ROS. Nat Cell Biol 17, 1259-1269.

Zheng, Y.T., Shahnazari, S., Brech, A., Lamark, T., Johansen, T., and Brumell, J.H. (2009). The adaptor protein p62/SQSTM1 targets invading bacteria to the autophagy pathway. J Immunol 183, 5909-5916.

Chapter 5: Outlook

(Includes excerpts from *Ariosa, Lahiri et al., BBA: Molecular Basis of Disease, 2021*)

Research in the field of autophagy has exploded over the last decade and great progress has been made towards understanding the basic mechanisms of autophagy as well as the implications of autophagy in physiology and pathology. But this was not always the case. After the term "autophagy" was coined by Christian de Duve in 1963, to explain observations of cytoplasmic material in lysosomes, the field remained in dormancy until Yoshinori Ohsumi and Daniel Klionsky started probing and identifying the molecular mechanisms of the process in the mid-1990s (Yang and Klionsky, 2010). This led to what can be compared to a renaissance – the number of discoveries related to autophagy has increased exponentially post-2005. The huge wealth of basic discoveries in the field and their impact on human health has now been universally recognized with the Nobel Prize for Physiology and Medicine being awarded to the field in 2016. But why is autophagy so relevant? The answer is simple: autophagy participates in just about everything (Klionsky, 2020).

To begin with, autophagy is highly conserved among eukaryotes, indicating that the functional value that this pathway provides is critical for all eukaryotic cells. Even yeast cells, simple organisms with scarce requirements and no tantrums, growing in nutrient-rich medium cannot sporulate if they are autophagy-deficient (Ohsumi, 2014). In mammals, the loss of autophagy is more debilitating – it is embryonic lethal. Pioneering studies from the late Beth Levine and Noboru Mizushima's laboratories showed that autophagy is essential for fetal development in mice and autophagy-deficient mice do not survive beyond embryonic pre-

implantation. Indeed, autophagy is upregulated early in development, and may be critical for the embryonic genome activation process by mediating the removal of maternal factors (Mizushima and Levine, 2010; Mizushima and Levine, 2020). Selective autophagy of the mitochondria – mitophagy – is critical for organismal developmental processes such as the degradation of paternal mitochondria in zygotes (Wei et al., 2017) as well as in cellular differentiation such as the degradation of mitochondria in erythrocytes (Rodger et al., 2018). Mitophagy is also critical for removing damaged mitochondria in neurons and perturbations in this process are risk factors for the development of neurodegenerative disorders such as Parkinson disease (Malpartida et al., 2021).

However, the link between autophagy and disease is not quite linear. For example, xenophagy – the selective elimination of pathogens by autophagy – is intended to be anti-pathogenic but several pathogens can hijack the system for their proliferation (Chaudhary and Miller, 2019; Kimmey and Stallings, 2016). However, no other disease has a more nuanced relationship with autophagy than cancer. Autophagy has both tumor-promoting and tumor-inhibiting roles. Briefly, in normal cells autophagy promotes metabolic homeostasis, proteostasis and genome maintenance which prevents tumor initiation. However, within tumors, autophagy helps cancer cells survive nutrient-deprived, hypoxic, crowded environments by acting as a secondary source of nutrients and essential metabolites (White, 2015). Indeed, autophagy is not only upregulated in the tumor cells themselves but also in the tumor-associated tissue (such as fibroblasts, also known as cancer-associated fibroblasts), contributing to tumor growth (Sousa et al., 2016). But systemic targeting of autophagy in cancer patients in not a possibility as research from Eileen White's group has demonstrated. Upon tumor transplantation and concomitant autophagy inhibition, mice with systemic autophagy deficiency do not support tumor growth

unlike wild-type mice but die regardless due to infection (potentially due to the lack of xenophagy) and neurodegeneration (potentially due to the lack of mitophagy). This necessitates the need for understanding the mechanisms that regulate autophagy.

In this body of work, I have tried to further the understanding of autophagy regulation at the post-transcriptional and post-translational levels. My research has focused on two critical proteins involved in phagophore formation and autophagy initiation – Atg1 (ULK1 in mammals) and Vps34 (PIK3C3/VPS34 in mammals). The details of the investigations are provided in the respective chapters and while basic research on these proteins and their expression and regulation continue, I would like to highlight some of the exciting pre-clinical work that is currently underway that target these proteins for therapeutically altering autophagy in cancer.

ULK1 inhibition is a potent mechanism to block autophagy and the small-molecule kinase inhibitor SBI-0206965 was identified as a selective ULK1 inhibitor that could effectively promote cell death when used in concert with MTOR inhibition (Egan et al., 2015). Subsequently, the compound was identified to be a potent inhibitor of AMPK, another positive regulator of autophagy (Dite et al., 2018). In several independent pre-clinical studies that have followed, SBI-0206965 has been demonstrated to promote tumor suppression. In non-small cell lung cancer, ULK1 promotes tumor survival by modulating both autophagy and apoptosis and the administration of SBI-0206965 sensitizes non-small cell lung cancer to cisplatin (Tang et al., 2017). In glioblastoma, increased autophagy through AMPK and ULK1 activation promotes resistance to temozolomide therapy; however, co-treatment with SBI-0206965 and high dose temozolomide promotes apoptosis (Zheng et al., 2021). A similar effect is seen in clear cell renal cell carcinoma, where ULK1 overexpression plays a protective role via autophagy upregulation (Lu et al., 2018).

Due to its critical role in phagophore nucleation, PIK3C3/VPS34 is an attractive target for autophagy inhibition. Inhibition of PIK3C3/VPS34 leads to the accumulation of autophagy substrates (Dowdle et al., 2014). Two potent PIK3C3/VPS34 inhibitors, SB02024 and SAR405, have demonstrated pre-clinical promise in cancer therapy. SB02024, developed by the Karolinska Institute and Spirit Biosciences, reduces autophagy flux *in vitro* and the growth of breast cancer cell line-derived xenografts *in vivo*. Furthermore, co-administration with SB02024 increases the efficacy of the FDA-approved breast cancer drug sunitinib in monolayer cultures or multicellular spheroids of two breast cancer lines: MCF-7 and MDA-MB-231 (Dyczynski et al., 2018). SAR405, developed by Sanofi, is another highly potent inhibitor of PIK3C3/VPS34 that promotes reduction in autophagy flux (Ronan et al., 2014) and has shown promise in the treatment of osteosarcoma when combined with celecoxib (Zhou et al., 2018). SAR405 was also successful in increasing the sensitivity of head and neck squamous cell carcinoma cells to cisplatin in a xenograft model (New et al., 2017). Both SB02024 and SAR405 have the potential of bolstering the potency of immune checkpoint inhibitors by blocking autophagy flux. In murine models of melanoma and colorectal cancer blocking autophagy with either of these PIK3C3/VPS34 inhibitors leads to better infiltration of immune cells, including natural killer cells and $CD8^+$ T-lymphocytes (Noman et al., 2020). Another PIK3C3/VPS34 inhibitor, VPS34-IN-1, suppresses the expansion of cancer stem cell in a mouse model of hepatocellular carcinoma but its effect regarding the regulation of autophagy is still unclear (Bago et al., 2014; Liu et al., 2020).

The ULK1-ULK2 and PIK3C3/VPS34 complexes are critical inducers of both non-selective and selective autophagy. While extensive research has shed considerable light on the activation of the ULK1-ULK2 and the PIK3C3/VPS34 complexes downstream of nutrient-

deprivation, research on the mechanisms of induction of selective forms of autophagy that may occur independently of starvation is still in its infancy in terms of mechanistic clarity. During starvation-induced non-selective autophagy, several cellular sensors (such as MTORC1, AMPK and PRKA/PKA in mammals) respond to changes in the status of key cellular metabolites. During selective autophagy, the response is initiated either by organellar damage or dysfunction (mitophagy, reticulophagy, etc.) or due to the scarcity of a particular metabolite (ferritinophagy to replenish iron stores, glycophagy to provide glucose, lipophagy to break down lipids) rather than general metabolic scarcity. While the latter may seem to lend more easily to induction mechanisms like those in non-selective autophagy, that might not always be the case.

Whereas glycophagy and lipophagy are often induced in response to starvation, what promotes the sequestration of branched glycogen particles and lipid droplets (LDs) is poorly understood. For example, STBD1 is identified as a glycophagy receptor that binds LC3 but the mechanism of STBD1 activation is unclear. Similarly, LDs are thought to be engulfed due to the formation of autophagosomes around them, with the LDs themselves serving as a point of origin. Once again, how upstream autophagy inducers like ULK1-ULK2 and PIK3C3/VPS34 are recruited and activated in this context is poorly understood. For ferritinophagy, where iron limitation is the autophagic trigger, these regulatory mechanisms are virtually unexplored. While our knowledge regarding the mechanisms of ULK1-ULK2 recruitment and autophagy activation during mitophagy is slightly better, how autophagy is induced in response to such diverse stresses remains an outstanding question. Do different stresses activate autophagy via completely distinct mechanisms? Or is there a certain amount of overlap between these different activation processes? It is even intriguing, although it might seem slightly fanciful, to speculate on a unified mechanism that sets off the cascade downstream of different stress situations.

If it is indeed a conserved activation mechanism, it is likely to be mediated by a handful of metabolites. I would speculate that these small molecules could be lipids. This is not only because the process of autophagosome formation is inherently a process involving lipid dynamics, but also because lipids are increasingly being recognized as potent signaling molecules. Indeed, the formation of the autophagosome requires the signaling lipid PtdIns3P generated by PIK3C3/Vps34. This lipid is generated at ER-peripheral sites (in mammalian cells; and the vacuole-peripheral phagophore assembly site or PAS in yeast) during autophagy and can directly regulate the selective autophagic process of reticulophagy by downstream lipid signaling. In fact, because the mitochondria and the ER are connected via contact sites (ERMES) this could indirectly influence mitophagy induction as well. Indeed, cardiolipin has now been recognized as a receptor for mitophagy highlighting the important role of lipid signaling in selective autophagy. Finally, the generation of autophagosomes around LDs requires extensive LD lipid remodeling by the Rab GTPases, which are likely activated downstream of lipid signaling events. Therefore, it would not be entirely incredulous that a set of lipid signals could be a unified regulator of non-selective and selective autophagic processes.

Focusing on autophagic mechanisms and their implications in health and disease is important, but it is equally important to investigate the origins of the process because history can be very instructive. It is interesting to note that whereas autophagy is conserved across eukaryotes, the pathway is absent in prokaryotes, underlining the possibility that the evolutionary development of this pathway may be inextricably linked to the evolution of eukaryotic life. Indeed, the very core of the autophagy process relies on the presence of intracellular membranes and intracellular membrane trafficking, both of which evolved with eukaryogenesis. However, how such a complex pathway may have evolved suddenly is an intriguing question. Comparative

genomic analysis is now telling us that while autophagy as a pathway is absent in prokaryotes, distant homologs of autophagy-related proteins are indeed present, especially in cyanobacteria and archaea. A curious correlation also exists in eukaryotes between the emergence of mitochondrial protein import machinery (MPIM) and the development of the autophagy pathway – ancestral eukaryotes with more developed MPIM also express more autophagy pathway components. This has led researchers to speculate that autophagy may have initially evolved as a mitochondrial quality control mechanism. Indeed, while genes encoding core non-selective autophagy components are more conserved across eukaryotic species, those encoding selective autophagy proteins, including receptors and adaptors are more variable indicating the possibility that they may have evolved independently several times in different organisms (Zhang et al., 2021).

While we have begun unravelling the secrets behind the process of *de novo* autophagosome formation *in situ*, a plethora of questions remain – most pertinent are those relating to the mechanics of phagophore formation and autophagosome trafficking. While we partially understand the role of autophagy in development, a deeper analysis of its regulation in time and space is required for a more comprehensive understanding. While we understand the role of autophagy in various pathologies, more detailed mechanistic understanding is required to develop therapeutic interventions targeting autophagy for these indications. The horizon is rich with possibilities and, as an autophagy researcher, I am excited to see what intriguing discoveries the future has in store for the field.

References

Bago, R., Malik, N., Munson, M.J., Prescott, A.R., Davies, P., Sommer, E., Shpiro, N., Ward, R., Cross, D., Ganley, I.G., et al. (2014). Characterization of VPS34-IN1, a selective inhibitor of Vps34, reveals that the phosphatidylinositol 3-phosphate-binding SGK3 protein kinase is a downstream target of class III phosphoinositide 3-kinase. Biochem J 463, 413-427.

Chaudhary, A., and Miller, S.I. (2019). Xenophagy: Pathogen-Containing Vacuoles Are Hard to Digest. Curr Biol 29, R1086-R1088.

Dite, T.A., Langendorf, C.G., Hoque, A., Galic, S., Rebello, R.J., Ovens, A.J., Lindqvist, L.M., Ngoei, K.R.W., Ling, N.X.Y., Furic, L., et al. (2018). AMP-activated protein kinase selectively inhibited by the type II inhibitor SBI-0206965. J Biol Chem 293, 8874-8885.

Dowdle, W.E., Nyfeler, B., Nagel, J., Elling, R.A., Liu, S., Triantafellow, E., Menon, S., Wang, Z., Honda, A., Pardee, G., et al. (2014). Selective VPS34 inhibitor blocks autophagy and uncovers a role for NCOA4 in ferritin degradation and iron homeostasis in vivo. Nat Cell Biol 16, 1069-1079.

Dyczynski, M., Yu, Y., Otrocka, M., Parpal, S., Braga, T., Henley, A.B., Zazzi, H., Lerner, M., Wennerberg, K., Viklund, J., et al. (2018). Targeting autophagy by small molecule inhibitors of vacuolar protein sorting 34 (Vps34) improves the sensitivity of breast cancer cells to Sunitinib. Cancer Lett 435, 32-43.

Egan, D.F., Chun, M.G., Vamos, M., Zou, H., Rong, J., Miller, C.J., Lou, H.J., Raveendra-Panickar, D., Yang, C.C., Sheffler, D.J., et al. (2015). Small Molecule Inhibition of the Autophagy Kinase ULK1 and Identification of ULK1 Substrates. Mol Cell 59, 285-297.

Kimmey, J.M., and Stallings, C.L. (2016). Bacterial Pathogens versus Autophagy: Implications for Therapeutic Interventions. Trends Mol Med 22, 1060-1076.

Klionsky, D.J. (2020). Autophagy participates in, well, just about everything. Cell Death Differ 27, 831-832.

Liu, F., Wu, X., Qian, Y., Jiang, X., Wang, Y., and Gao, J. (2020). PIK3C3 regulates the expansion of liver CSCs and PIK3C3 inhibition counteracts liver cancer stem cell activity induced by PI3K inhibitor. Cell Death Dis 11, 427.

Lu, J., Zhu, L., Zheng, L.P., Cui, Q., Zhu, H.H., Zhao, H., Shen, Z.J., Dong, H.Y., Chen, S.S., Wu, W.Z., et al. (2018). Overexpression of ULK1 Represents a Potential Diagnostic Marker for Clear Cell Renal Carcinoma and the Antitumor Effects of SBI-0206965. EBioMedicine 34, 85-93.

Malpartida, A.B., Williamson, M., Narendra, D.P., Wade-Martins, R., and Ryan, B.J. (2021). Mitochondrial Dysfunction and Mitophagy in Parkinson's Disease: From Mechanism to Therapy. Trends Biochem Sci 46, 329-343.

Mizushima, N., and Levine, B. (2010). Autophagy in mammalian development and differentiation. Nat Cell Biol 12, 823-830.

Mizushima, N., and Levine, B. (2020). Autophagy in Human Diseases. N Engl J Med 383, 1564-1576.

New, J., Arnold, L., Ananth, M., Alvi, S., Thornton, M., Werner, L., Tawfik, O., Dai, H., Shnayder, Y., Kakarala, K., et al. (2017). Secretory Autophagy in Cancer-Associated Fibroblasts Promotes Head and Neck Cancer Progression and Offers a Novel Therapeutic Target. Cancer Res 77, 6679-6691.

Noman, M.Z., Parpal, S., Van Moer, K., Xiao, M., Yu, Y., Viklund, J., De Milito, A., Hasmim, M., Andersson, M., Amaravadi, R.K., et al. (2020). Inhibition of Vps34 reprograms cold into hot inflamed tumors and improves anti-PD-1/PD-L1 immunotherapy. Sci Adv 6, eaax7881.
Ohsumi, Y. (2014). Historical landmarks of autophagy research. Cell Res 24, 9-23.
Rodger, C.E., McWilliams, T.G., and Ganley, I.G. (2018). Mammalian mitophagy - from in vitro molecules to in vivo models. FEBS J 285, 1185-1202.
Ronan, B., Flamand, O., Vescovi, L., Dureuil, C., Durand, L., Fassy, F., Bachelot, M.F., Lamberton, A., Mathieu, M., Bertrand, T., et al. (2014). A highly potent and selective Vps34 inhibitor alters vesicle trafficking and autophagy. Nat Chem Biol 10, 1013-1019.
Sousa, C.M., Biancur, D.E., Wang, X., Halbrook, C.J., Sherman, M.H., Zhang, L., Kremer, D., Hwang, R.F., Witkiewicz, A.K., Ying, H., et al. (2016). Pancreatic stellate cells support tumour metabolism through autophagic alanine secretion. Nature 536, 479-483.
Tang, F., Hu, P., Yang, Z., Xue, C., Gong, J., Sun, S., Shi, L., Zhang, S., Li, Z., Yang, C., et al. (2017). SBI0206965, a novel inhibitor of Ulk1, suppresses non-small cell lung cancer cell growth by modulating both autophagy and apoptosis pathways. Oncol Rep 37, 3449-3458.
Wei, Y., Chiang, W.C., Sumpter, R., Jr., Mishra, P., and Levine, B. (2017). Prohibitin 2 Is an Inner Mitochondrial Membrane Mitophagy Receptor. Cell 168, 224-238 e210.
White, E. (2015). The role for autophagy in cancer. J Clin Invest 125, 42-46.
Yang, Z., and Klionsky, D.J. (2010). Eaten alive: a history of macroautophagy. Nat Cell Biol 12, 814-822.
Zhang, S., Hama, Y., and Mizushima, N. (2021). The evolution of autophagy proteins - diversification in eukaryotes and potential ancestors in prokaryotes. J Cell Sci 134.
Zheng, Y., Liu, L., Wang, Y., Xiao, S., Mai, R., Zhu, Z., and Cao, Y. (2021). Glioblastoma stem cell (GSC)-derived PD-L1-containing exosomes activates AMPK/ULK1 pathway mediated autophagy to increase temozolomide-resistance in glioblastoma. Cell Biosci 11, 63.
Zhou, P., Li, Y., Li, B., Zhang, M., Xu, C., Liu, F., Bian, L., Liu, Y., Yao, Y., and Li, D. (2018). Autophagy inhibition enhances celecoxib-induced apoptosis in osteosarcoma. Cell Cycle 17, 997-1006.

****